

学位論文

**Measurement of longitudinal
double spin asymmetries
in the single-inclusive hadron
quasi-real photoproduction at high- p_T
by a muon beam for the study
of gluon polarisation in nucleon**

核子中のグルーオン偏極度の研究のための
ミュオンビームを用いた
高横方向運動量領域における仮想光生成による
ハドロンの縦方向二重スピン非対称度の測定

December, 2015

Graduate School of Science and Engineering
Yamagata University

Hiroki MATSUDA

Abstract

The COMPASS experiment at CERN has studied properties of a nucleon and hadrons since 2002. One of the main goals in COMPASS is determination of gluon spin contribution, ΔG , to the nucleon. COMPASS has performed several analyses and showed that the contribution is compatible with zero.

ΔG can be studied by using the Photon Gluon Fusion (PGF) process where a photon interacts with a gluon of the nucleon by exchanging a quark and produces a quark-antiquark pair. Two types of methods are employed in COMPASS: an Open Charm method and a High- p_T hadron method. In the Open Charm method, an event is marked as a PGF event if charmed hadrons are detected in the final state. On the other hand, in the High- p_T method, events are selected if hadrons with large transverse momenta are detected in the final state. In both methods, the gluon polarisation $\Delta G/G$ is evaluated by comparing Monte Carlo simulations. The former method has no physical background and weak dependence on Monte Carlo simulation. On the other hand, quite lower statistics than the latter method. Data to be analysed by the latter method has large statistics, but the large physical background and strong Monte Carlo model dependence.

I developed a new method, namely single-inclusive hadron method, in which longitudinal double spin asymmetries for single-inclusive hadron production are measured and ΔG is evaluated by comparing theoretically calculated asymmetries. Data was taken with 160 GeV/c or 200 GeV/c polarised muon beam impinging on polarised ${}^6\text{LiD}$ or NH_3 solid targets.

An asymmetry was calculated by a second order weighted method which allowed to minimise uncertainties. I calculated asymmetries for deuteron and proton and their uncertainties, respectively. The uncertainties were evaluated, confirming that smaller systematic uncertainty than statistical one exists. The comparisons between the observed and theoretically calculated asymmetries indicate that ΔG is positive in a range of a gluon momentum fraction to the nucleon x_g , $0.05 < x_g < 0.2$.

概要

CERN で行われている COMPASS 実験では核子やハドロンの性質についての研究が 2002 年から現在に至るまで精力的に行われている。COMPASS の研究の中で注力しているひとつが、 ΔG と呼ばれるグルーオンスピンの核子スピンへの寄与の決定である。これまで COMPASS ではいくつかの解析を行っており、いずれの結果も ΔG はほぼゼロと矛盾しないというものであった。

ΔG は、光子と核子からのグルーオンがクォークを介して相互作用しクォーク・反クォーク対を生成する光子グルーオン融合 (PGF) 過程を含んだイベントを解析することで得られる。COMPASS では 2 つの方法で解析が行われてきた。ひとつは Open Charm 法で、チャームクォークを含む中間子が生成されたイベントを PGF 過程が含まれているイベントとして解析する手法である。もうひとつは High- p_T 法で、高横方向運動量 (p_T) を持つハドロンの対が生成されるイベントを PGF 過程が含まれるイベントとして解析する手法である。前者の手法は物理的バックグラウンドが少なく、さらにモンテカルロシミュレーションでのモデル依存性が小さい。一方、後者の手法に比べ解析に用いられるデータの統計数が圧倒的に少ないという特徴を持つ。後者の手法においてデータの統計数は圧倒的に多いものの、物理的バックグラウンドが大きくモンテカルロシミュレーションでのモデル依存性が強い。いずれの手法も実験値をモンテカルロシミュレーションと比較することで ΔG の寄与を決定する。

この論文では、single-inclusive hadron 法という新しい手法を開発し解析を行った。これは仮想光子を通じた反応により生成された $0.7 < p_T < 4 \text{ GeV}/c$ 領域でのハドロンの縦方向二重スピン非対称度を測定し理論計算と比較してグルーオンスピンの寄与を評価する手法である。解析では $160 \text{ GeV}/c$ または $200 \text{ GeV}/c$ の偏極ミューオンビームと ^6LiD または NH_3 の固体偏極標的を用いて測定されたデータを用いた。

非対称度は誤差を抑制できる second order weighted 法で計算された。重陽子および陽子に対する非対称度を計算し、さらにそれら非対称度の誤差を評価した。その結果、系統誤差は統計誤差にくらべて小さいことが確認され、どちらの非対称度も誤差の範囲内でほぼゼロであった。この非対称度と理論から計算された非対称度との比較は、核子の運動量に対するグルーオン運動量の比 x_g が $0.05 < x_g < 0.2$ の領域に於いて ΔG は正であることを示唆している。

Contents

Contents	i
List of Figures	iii
List of Tables	v
1. Introduction	1
2. Theory	3
2.1. The QCD-improved quark parton model	10
2.2. DGLAP equation	10
2.3. Sum rules	13
2.4. Fragmentation	15
2.5. JSV framework	16
2.6. Accessing to gluon polarisation	24
2.6.1. Photon Gluon Fusion	24
2.6.2. Proton-Proton scattering	30
3. COMPASS setup	33
3.1. Beam	34
3.2. Target	38
3.3. Spectrometers	41
3.4. VSAT	44
3.4.1. Scintillating Fibre Detectors	44
3.4.2. Silicon Microstrip Detectors	44
3.5. SAT	45
3.5.1. Micromegas	45
3.5.2. GEM	45
3.6. LAT	46
3.6.1. Drift Chamber	46
3.6.2. Multi Wire Proportional Chamber	47
3.6.3. Straw tube	47
3.6.4. RICH Wall	48
3.7. Particle identification	49
3.7.1. RICH	49
3.7.2. Muon Wall	51
3.7.3. Hadron Calorimeter	54
3.7.4. Electromagnetic Calorimeter	55
3.8. Trigger	58
3.9. Data acquisition	61
3.10. Data reconstruction	62

4. Data analysis	66
4.1. Data input	66
4.2. Data selection	67
4.2.1. Event selection	67
4.2.2. Hadron selection	69
4.3. Method for asymmetry calculation	74
4.3.1. The first order method	74
4.3.2. The first order weighted method	75
4.3.3. The second order method	76
4.3.4. The second order weighted method	78
4.4. Dilution factor	81
4.5. Data grouping	82
4.6. Asymmetry calculation	83
5. Results and discussion	85
5.1. Systematic studies	85
5.1.1. Multiplicative uncertainties	85
5.1.2. Reproducible false asymmetry	86
5.1.3. Fake configuration asymmetry	86
5.1.4. Top-Bottom and Left-Right asymmetry	87
5.1.5. The estimation of the systematic uncertainty via a <i>pulls</i> method	87
5.1.6. Summary of systematic study	88
5.2. Results	89
6. Conclusion	95
7. Future prospects	96
A. Derivations	98
A.1. The derivation of the first order method	98
A.2. The derivation of uncertainty in the second order weighted method	99
A.3. Optimised histogram bin	101
B. Kinematic distribution	102
C. Tables and plots for asymmetries	115
C.1. Tables	115
C.2. Plots	119
Bibliography	123

List of Figures

2.1. DIS process	3
2.2. Kinematics of polarised deep-inelastic scattering	5
2.3. Virtual photon-nucleon scattering	6
2.4. The proton and deuteron structure function F_2 as a function of Q^2 for bins of fixed x_{Bj}	9
2.5. A_1 and g_1 of deuteron and proton	11
2.6. Results for the COMPASS NLO QCD fit to g_1 world data	12
2.7. Decomposition of the single-inclusive cross section for quasi-photoproduction of a hadron h into direct and resolved subprocesses	17
2.8. The hard scattering process in two systems	18
2.9. Comparison of the theoretical calculations and measured data	24
2.10. Ratios of the various PYTHIA subprocesses in the final high- p_T sample	27
2.11. Gluon polarisations obtained at LO accuracy, in COMPASS, SMC, and HERMES as a function of x_g	29
2.12. Selected lowest-order Feynman diagrams for elementary processes with gluons in the initial state in p - p collisions	30
2.13. A_{LL} measured by STAR and PHENIX at RHIC	32
3.1. COMPASS reference system	34
3.2. CERN aerial view and accelerator complex	35
3.3. A schematic view of CERN SPS M2 beam line	36
3.4. Layout of the beam momentum station for the COMPASS muon beam	36
3.5. the COMPASS CEDAR detector	37
3.6. Side views of the COMPASS polarised target system with SMC and OD magnet	40
3.7. The schematic picture of filed rotation and microwave reversal	42
3.8. Schematic view of COMPASS experiment	42
3.9. Top views of the COMPASS setup with muon and hadron beam	43
3.10. Schematic view of a COMPASS straw detector (type X)	48
3.11. Cross section of a Mini Drift Tube module and front view of an X -plane on the Rich Wall detector	49
3.12. Resolution of the reconstructed Cherenkov ring for pions as a function of the track angle	50
3.13. Principle and artistic view of RICH-1	50
3.14. Cross section of the RICH-1 photon detector	51
3.15. PID efficiency versus polar angle for a sample of Ks from ϕ -decay	52
3.16. Cross section of a MDT module for MW1	52
3.17. Schematic cross sectional side view of MW2	53
3.18. The layout of the tubes in a double layer of MW2 planes	54
3.19. The schematic front view of ECAL1	56
3.20. Schematic view of the LASER monitoring system for ECAL1	56
3.21. Configuration of ECAL2	57
3.22. Schematic view of the trigger system	58
3.23. Schematic layout of the veto system	61
3.24. The general architecture of the DAQ system	62
4.1. Vertex position distribution along the Z -axis for the two- and three- target cells	68
4.2. The beam momentum distribution	69

4.3.	Trigger by trigger y distribution for each year	70
4.4.	Relative momentum resolution as a function of track momentum	71
4.5.	Dilution factors for ${}^6\text{LiD}$ and NH_3 as a function of x_{Bj}	82
4.6.	Schematic pictures of consecutive and global grouping	82
5.1.	Fake configuration grouping. Arrows indicate the direction of the target polarisation	87
5.2.	The <i>pulls</i> distribution for hadron charge integrated asymmetries for the deuteron at a single bin	88
5.3.	$x\Delta g(x_g, \mu^2 = 3)$ of GRSV and DSSV14.	90
5.4.	Comparison of DSS07 and DSS14	91
5.5.	Comparison between theoretical asymmetries for hadron and pion production using DSS07 fragmentation functions	92
5.6.	Comparison with measured asymmetries and calculated ones for deuteron target	93
5.7.	Comparison with measured asymmetries and calculated ones for proton target	94
7.1.	The theoretical calculations for the longitudinal double spin asymmetry in COMPASS kinematics	97
B.1.	The number of events period by period in each year	103
B.2.	The number of hadrons period by period in each year	104
B.3.	Q^2 distributions in each year and target	105
B.4.	x_{Bj} distributions in each year and target	106
B.5.	y distributions in each year and target	107
B.6.	W distributions in each year	108
B.7.	Multiplicity distributions in each year	109
B.8.	z distributions in each year and target	110
B.9.	p_T distributions in each year and target	111
B.10.	θ_{hadron} distributions in each year and target	112
B.11.	η_{CMS} distributions in each year and target	113
B.12.	Q^2-p_T distributions in each year and target	114
C.1.	A_R for deuteron and proton targets	119
C.2.	Fake configuration asymmetries for deuteron and proton	119
C.3.	Top-Bottom asymmetries for the deuteron and the proton	120
C.4.	Left-Right asymmetries for deuteron and proton	120
C.5.	Asymmetries for positive and negative hadrons	121
C.6.	Asymmetries for deuteron and proton	122

List of Tables

2.1. The values of coefficient functions	15
3.1. A summary of COMPASS data taking	33
3.2. Trigger component	60
3.3. Trigger rate for each trigger in 2004 run	60
3.4. Description of the variables used by extended likelihood method	64
4.1. Periods list used in this analysis for each year	67
4.2. Statistics of event selection	72
4.3. Statistics of hadron selection	73
4.4. The parameters for Monte Carlo simulation of the uncertainties	80
4.5. The ratios of uncertainties to the one of the first order method	80
4.6. Microwave configurations for all periods	83
5.1. Summary of the multiplicative systematic uncertainties	85
C.1. The ratios of the systematic uncertainty to the statistical one for A_{LL}^d	115
C.2. The ratios of the systematic uncertainty to the statistical one for A_{LL}^p	116
C.3. Values of A_{LL}^d	117
C.4. Values of A_{LL}^p	118

1. Introduction

Deep inelastic scattering (DIS) of a lepton and a nucleon revealed that the nucleon is not an elementary particle: it is made of elementary particles, namely quarks. DIS experiments in 1960's observed the existence of scaling: the structure functions depend only on the variable x_{Bj} , not Q^2 [1]. This observation revealed presence of point-like constituents in the nucleon and led to the parton picture [2]. This gave firm evidence of existence of the quarks, which was anticipated in the quark model [3, 4]. In quark model, the nucleon is made up of three quarks, called valence quarks, with fractional electric charge ($1/3$ or $2/3$ of the elementary charge) and $\frac{1}{2}$ spin. According to the Quantum Chromodynamics (QCD) that is the theory of the strong interaction of hadrons, the valence quarks are bonded by gluons, which are the gauge bosons intermediating strong force and having spin 1, and are surrounded by sea quark pairs, which are created by a gluon and annihilate into a gluon.

In the quark model, the nucleon spin $1/2$ is the sum of the valence quarks spin, like nucleon charge (e.g. proton charge is $+2/3 + 2/3 - 1/3 = 1$ since it's made of two u quarks and one d quark). In 1988 European Muon Collaboration (EMC) [5] performing DIS measurements at CERN observed that the quark spin contribution $\Delta\Sigma$ to the nucleon spin was about 10 %, which is known as a “spin crisis” or a “spin puzzle” [6]. Relativistic quark model predicted that $\Delta\Sigma$ contributes about 60 % and the rest comes from quark orbital angular moment. Today the quark spin contribution is converged from a dozen vigorous experiments to be about 30 %.

In the framework of the QCD improved parton model [7, 8], the spin of the nucleon can be decomposed into

$$\frac{1}{2} = \frac{1}{2}\Delta\Sigma + \Delta G + L_q + L_g \quad (1.1)$$

where $\Delta\Sigma$ is the contributions of the quark spins, ΔG is the contributions of the gluon spin, and L_q, L_g are the orbital angular momenta of the quarks and the gluons in the nucleon [9]. Thus, the large remaining contribution was considered to come from the gluon spin and the angular momenta of quarks and gluons. It was expected that the gluon spin have a potentially very large contribution ($\Delta G \geq 2$) [10]. This suggestion sparked a vigorous and ambitious program to measure Δg [8]. Since the beginning of the twenty-first century, many experiments in the world have started to measure the gluon polarisation with different experimental setups. The latest global analysis based on the data from the DIS experiments and the RHIC experiments shows that the gluon spin contribution in the proton is nonzero [11].

Deeply Virtual Compton Scattering (DVCS) can provide an experimental tool to access the quark total angular momentum with in a framework of the Generalised Parton Distributions (GPDs). In order to obtain a size of the quark “orbital angular momentum”, it is needed to subtract the value of the “quark spin contribution” measured in the polarised DIS experiments from the quark total angular momentum.

The means of decomposition of the nucleon spin also give vigorous discussion. At the moment, several ways are proposed and are derived from two different decompositions: Jaffe-Manohar (JM) [12] and Ji [13] decompositions. A main difference comes from “gauge” chosen in the prescriptions. The JM decomposition is defined in Eq. (1.1), whereas the Ji decomposition is defined as

$$\frac{1}{2} = \frac{1}{2}\Delta\Sigma + L_q + J_g \quad (1.2)$$

where J_g is the total angular momentum of the gluons. In Ji decomposition, the gluon spin contribution can not be split into the spin and the orbital angular momentum part.

The gluon spin contribution ΔG is defined in JM decomposition, and in this thesis JM decomposition is employed. Details about decomposition problems, which have been already solved, are quite well summarised in Refs. [9, 14].

The COMPASS experiment [15] at CERN analysed ΔG using the high- p_T hadron production [16, 17] and D meson production [18, 19]. The method used in the analyses have large systematic uncertainty originating from the simulation model. Thus, a new approach was proposed that ΔG is evaluated by comparing an observed and a theoretical asymmetry for single-inclusive hadron production [20, 21]. The availability of the theoretical calculation was verified by comparing the observed and the calculated unpolarised cross sections for single-inclusive hadron production [22, 23]. This analysis is a continuation of the analyses of the longitudinal double spin asymmetry and the unpolarised cross section for single-inclusive hadron production [20, 21, 22].

In this thesis, the observable related to the gluon spin contribution to the nucleon spin has been studied using a challenging method described in Chapt. 4. Before that, not only theoretical basis of this analysis but also ones of the nucleon structure, and the quark model are discussed in Chapt. 2. The COMPASS experiment setup is described in Chapt. 3. The results are presented and discussed in Chapt. 5.

2. Theory

Deep inelastic scattering (DIS) gives vital hints for the partonic structure of the nucleon. An incoming lepton interacts with a nucleon by a virtual photon, then only scattered lepton is measured. The process $\ell N \rightarrow \ell' X$ is shown in Fig. 2.1. The lepton of four-momentum k

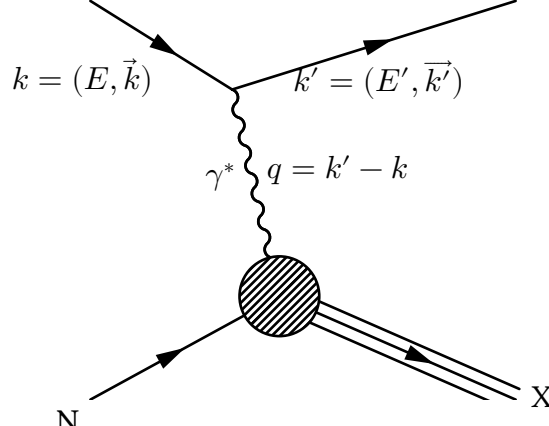


Figure 2.1: Deep Inelastic Scattering (DIS) process.

scatters from the nucleon target at rest at an angle θ and with k' . Following kinematic variables are defined:

$$q^2 = (k - k')^2 \stackrel{\text{lab.}}{=} -4EE' \sin^2 \frac{\theta}{2}, \quad (2.1)$$

$$P \cdot q \stackrel{\text{lab.}}{=} M(E - E') = E\nu, \quad (2.2)$$

$$P \cdot k \stackrel{\text{lab.}}{=} ME, \quad (2.3)$$

$$(2.4)$$

where k , k' , and $P = (M, \vec{0})$ are the four-momenta of the incoming lepton, the scattered lepton, and the target nucleon, respectively. The important variables are defined as follows:

$$Q^2 = -q^2, \quad (2.5)$$

$$x_{Bj} = \frac{-q^2 \stackrel{\text{lab.}}{=} Q^2}{2P \cdot q \stackrel{\text{lab.}}{=} 2M\nu}, \quad (2.6)$$

$$y = \frac{P \cdot q \stackrel{\text{lab.}}{=} \nu}{P \cdot k \stackrel{\text{lab.}}{=} E}. \quad (2.7)$$

x_{Bj} is well known as Bjorken variable [1]. Other variables of the scattering process are the centre of mass energy \sqrt{s} , and the invariant mass of the hadronic final state W ,

$$s = (k + P)^2 = \frac{Q^2}{x_{Bj}y} + M^2, \quad (2.8)$$

$$W^2 = (q + P)^2 = \frac{1 - x_{Bj}}{x_{Bj}} Q^2 + M^2. \quad (2.9)$$

Here, there is no clear definition of the DIS region. Empirically, $W \gg 2 \text{ GeV}$ region is called the DIS region since there is no clear resonance state above the range.

Born cross section for inclusive inelastic scattering of the charged lepton from the nucleon $\ell' N \rightarrow \ell' X$ can be written as

$$\frac{d^2\sigma}{d\Omega dE'} = \frac{\alpha^2}{q^4} \frac{E'}{E} L_{\mu\nu} W^{\mu\nu}, \quad (2.10)$$

where $L_{\mu\nu}$ is the leptonic tensor, $W^{\mu\nu}$ is the hadronic tensor, and α is the fine-structure constant.

The first tensor, *i.e.* leptonic tensor, is well known from QED and defined as

$$L_{\mu\nu}(s, k; k') = \sum_{s'} \overline{[\bar{u}(k', s') \gamma_\mu u(k, s)]} [\bar{u}(k', s') \gamma_\nu u(k, s)] = L_{\mu\nu}^{(S)} + iL_{\mu\nu}^{(A)}, \quad (2.11)$$

where $s = (0, \vec{s})$ is the polarisation vector of the lepton in its rest frame. One can split the leptonic tensor into two parts: symmetric part and asymmetric part as follows

$$L_{\mu\nu}^{(S)} = 2(k_\mu k'_\nu + k'_\mu k_\nu) - 2g_{\mu\nu}(k \cdot k' - m^2), \quad (2.12)$$

$$L_{\mu\nu}^{(A)} = 2m\epsilon_{\mu\nu\alpha\beta} s^\alpha q^\beta, \quad (2.13)$$

where m is the lepton mass, $g_{\mu\nu}$ is the metric tensor, and $\epsilon_{\mu\nu\alpha\beta}$ is the Levi-Civita symbol.

Similarly, the second tensor, *i.e.* hadronic tensor, contains the unknown non-perturbative structure of the nucleon and is defined as

$$W^{\mu\nu}(S, P; q) = \frac{1}{2\pi} \int d^4\xi e^{iq\xi} \langle P, S | J^\mu(0) | X \rangle \langle X | J^\nu(0) | P, S \rangle (2\pi)^4 \delta^4(P + q - p_X) \quad (2.14)$$

$$= W^{\mu\nu(S)}(P; q) + iW^{\mu\nu(A)}(S, P; q) \quad (2.15)$$

and symmetric and asymmetric parts are

$$\frac{1}{2} W^{\mu\nu(S)}(P; q) = - \left(g^{\mu\nu} - \frac{q^\mu q^\nu}{q^2} \right) F_1 + \left(P^\mu - \frac{P \cdot q}{q^2} q^\mu \right) \left(P^\nu - \frac{P \cdot q}{q^2} q^\nu \right) \frac{F_2}{P \cdot q}, \quad (2.16)$$

$$\frac{1}{2} W^{\mu\nu(A)}(P; q) = -i\epsilon^{\mu\nu\alpha\beta} q_\alpha \left(\frac{M S_\beta}{P \cdot q} (g_1 + g_2) - \frac{M (S \cdot q) P_\beta}{P \cdot q} g_2 \right) \quad (2.17)$$

where F_1 , F_2 , g_1 , and g_2 are the dimensionless structure functions, S is the nucleon's polarisation vector, and p_X is the total momentum of the final hadronic state X . Eq. (2.10) can be expressed by other kinematic variables;

$$\frac{d^2}{d\Omega dE'} = \frac{E'}{M\nu} \frac{d^3}{dx dy d\phi}. \quad (2.18)$$

The differential cross section is then given by

$$\frac{d^3\sigma}{dx dy d\phi} = \frac{\alpha^2 y}{Q^4} \frac{1}{2} \left(L_{\mu\nu}^{(S)} W^{\mu\nu(S)} - L_{\mu\nu}^{(A)} W^{\mu\nu(A)} \right). \quad (2.19)$$

The term $L_{\mu\nu}^{(S)} W^{\mu\nu(S)}$ corresponds to the spin-averaged part and the one $L_{\mu\nu}^{(A)} W^{\mu\nu(A)}$ corresponds to the spin-dependent part. Since the lepton and the nucleon polarisation vectors are involved in the latter term, spin-dependent effects can only occur if both the lepton and the hadron are polarised.

The spin-dependent cross sections are further subdivided into the longitudinal and transverse part:

$$\frac{d^3\sigma}{dx dy d\phi} = \frac{d^3\bar{\sigma}}{dx dy d\phi} - h_\ell \cos \beta \frac{d^3\Delta\sigma_{\parallel}}{dx dy d\phi} - h_\ell \sin \beta \cos \phi \frac{d^3\Delta\sigma_{\perp}}{dx dy d\phi}, \quad (2.20)$$

where $h_\ell = \pm 1$ is the helicity for the incident lepton, $\bar{\sigma}$ is the spin-averaged cross section, and σ_{\parallel} and σ_{\perp} are the cross sections for longitudinal and transverse orientation of the target spin. The exact forms of these cross sections are

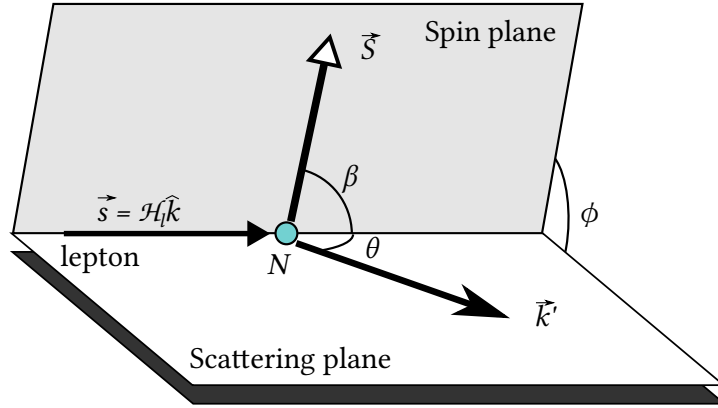


Figure 2.2: Kinematics of polarised deep-inelastic scattering [24].

$$\frac{d^3\bar{\sigma}}{dx dy d\phi} = \frac{4\alpha^2}{Q^2} \left[\frac{y}{2} F_1 + \frac{1}{2xy} \left(1 - y - \frac{y^2\gamma^2}{4} \right) F_2 \right], \quad (2.21)$$

$$\frac{d^3\Delta\sigma_{\parallel}}{dx dy d\phi} = \frac{4\alpha^2}{Q^2} \left[\left(1 - \frac{y}{2} - \frac{y^2\gamma^2}{4} \right) g_1 - \frac{y}{2} \gamma^2 g_2 \right], \text{ and} \quad (2.22)$$

$$\frac{d^3\Delta\sigma_{\perp}}{dx dy d\phi} = \frac{4\alpha^2}{Q^2} \left[\gamma \sqrt{1 - y - \frac{y^2\gamma^2}{4}} \left(\frac{y}{2} g_1 + g_2 \right) \right]. \quad (2.23)$$

The measurements for proton and deuteron structure function F_2^p and F_2^d are shown in Fig. 2.4. The kinematic factor $\gamma^2 = \frac{Q^2}{\nu^2} = \frac{4x^2 M^2}{Q^2}$ goes to zero as $Q^2 \rightarrow \infty$. The angle between the lepton momentum and the target spin is $0 \leq \beta \leq \pi$, whereas the azimuthal angle between the scattering plane and the plane containing the lepton and the target spins is $0 \leq \phi \leq 2\pi$ in Fig. 2.2. If the target is polarised longitudinally ($\beta = 0^\circ$), the structure function g_1 can be studied. On the other hand, one can study the combination $\frac{y}{2}g_1 + g_2$ when the target has the transverse polarisation ($\beta = 90^\circ$). Note that σ_{\perp} is suppressed by the factor γ since $\gamma = \frac{Q}{E_y}$.

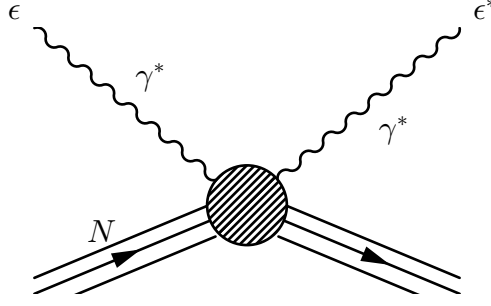


Figure 2.3: Virtual photon-nucleon scattering

It is worth to introduce the virtual photon-nucleon cross section (shown in Fig. 2.3) with the structure functions. First of all, let's define the virtual photon flux by the Hand convention [25]:

$$K \equiv \frac{W^2 - M^2}{2M} = \nu - \frac{Q^2}{2M}. \quad (2.24)$$

The optical theorem relates the hadronic structure tensor to the imaginary part of the forward virtual Compton scattering amplitude [7, 26, 27]. The helicity amplitude can be expressed as

$$A(h, H; h', H') = \epsilon_{h'}^{\mu*} \epsilon_h^\nu T_{\mu\nu}, \quad (2.25)$$

where ϵ and ϵ^* are the polarisation vectors of the virtual photons. Here h (h') and H (H') are the virtual photon and the nucleon helicity in the initial (final) state, respectively.

The cross sections of this process are defined as follows:

$$\sigma_{\frac{3}{2}}^T = \frac{4\pi^2\alpha}{MK} A(+1, +\frac{1}{2}; +1, +\frac{1}{2}) = \frac{4\pi^2\alpha}{MK} [F_1 - g_1 + (\kappa - 1)g_2], \quad (2.26)$$

$$\sigma_{\frac{1}{2}}^T = \frac{4\pi^2\alpha}{MK} A(+1, -\frac{1}{2}; +1, -\frac{1}{2}) = \frac{4\pi^2\alpha}{MK} [F_1 + g_1 - (\kappa - 1)g_2], \quad (2.27)$$

$$\sigma_{\frac{1}{2}}^{TL} = \frac{4\pi^2\alpha}{MK} A(+1, -\frac{1}{2}; 0, +\frac{1}{2}) = \frac{4\pi^2\alpha}{MK} \sqrt{\kappa - 1} (g_1 + g_2), \quad (2.28)$$

$$\sigma_{\frac{1}{2}}^L = \frac{4\pi^2\alpha}{MK} A(0, +\frac{1}{2}; 0, +\frac{1}{2}) = \frac{4\pi^2\alpha}{MK} \left(-F_1 + \frac{\kappa}{2x} F_2 \right) \quad (2.29)$$

where $\kappa = 1 + \frac{4x^2 M^2}{Q^2} = 1 + \frac{Q^2}{\nu^2} = 1 + \gamma^2$. The subscript is the total spin of the photon-nucleon system and the superscript shows the polarisation of the photon in the initial and the final states. The single superscript L or T means there is no polarisation flip between the initial and the final states.

The total absorption cross sections of longitudinally and transversely polarised photons are defined as

$$\sigma^L = \sigma_{\frac{1}{2}}^L = \frac{4\pi^2\alpha}{MK} \left[-F_1 + (1 + \gamma^2) \frac{F_2}{2x} \right], \quad (2.30)$$

$$\sigma^T = \frac{1}{2} \left(\sigma_{\frac{1}{2}}^T + \sigma_{\frac{3}{2}}^T \right) = \frac{4\pi^2\alpha}{MK} F_1. \quad (2.31)$$

The ratio of these cross sections becomes

$$R = (1 + \gamma^2) \frac{F_2}{2xF_1} - 1 . \quad (2.32)$$

Now one can define the longitudinal structure function, F_L as

$$F_L = F_2 (1 + \gamma^2) - 2xF_1 . \quad (2.33)$$

From these equations above, one can write the following relations:

$$R = \frac{F_L}{2xF_1} , \quad (2.34)$$

$$F_1 = \frac{F_2 (1 + \gamma^2)}{2x (1 + R)} . \quad (2.35)$$

Observable double-spin asymmetries in longitudinally polarised lepton, and longitudinally or transversely polarised target systems are defined as follows:

$$A_{\parallel} (x, Q^2) = \frac{\Delta\sigma_{\parallel}}{\bar{\sigma}} = \frac{\sigma^{\rightarrow\leftarrow} - \sigma^{\rightarrow\Rightarrow}}{\sigma^{\rightarrow\leftarrow} + \sigma^{\rightarrow\Rightarrow}} , \quad (2.36)$$

$$A_{\perp} (x, Q^2) = \frac{\Delta\sigma_{\perp}}{\bar{\sigma}} = \frac{\sigma^{\rightarrow\uparrow} - \sigma^{\rightarrow\Downarrow}}{\sigma^{\rightarrow\uparrow} + \sigma^{\rightarrow\Downarrow}} . \quad (2.37)$$

Here the narrow arrow (\rightarrow) represents the longitudinal polarisation of photon along to momentum direction and the wide arrows (\Rightarrow , \leftarrow , \uparrow , \Downarrow) indicates the nucleon spin direction: \Rightarrow (\leftarrow) is parallel (anti-parallel) to the incoming photon direction, and \uparrow (\Downarrow) is perpendicular to the incoming photon direction.

The parallel and perpendicular asymmetries strongly depend on E or y so that the observed asymmetries with different incident energies cannot be compared directly. Therefore, it is customary to express the lepton asymmetries in terms of the virtual photon asymmetries:

$$A_1 = \frac{\sigma_{\frac{1}{2}}^T - \sigma_{\frac{3}{2}}^T}{\sigma_{\frac{1}{2}}^T + \sigma_{\frac{3}{2}}^T} = \frac{\sigma_{\frac{1}{2}}^T - \sigma_{\frac{3}{2}}^T}{2\sigma^T} , \quad (2.38)$$

$$A_2 = \frac{\sigma_{\frac{1}{2}}^{TL}}{\sigma_{\frac{1}{2}}^T + \sigma_{\frac{3}{2}}^T} = \frac{\sigma_{\frac{1}{2}}^{TL}}{2\sigma^T} . \quad (2.39)$$

These asymmetries are valid for the spin $\frac{1}{2}$ target. The asymmetries A_1 and A_2 for a spin one target are as follows:

$$A_1 = \frac{3}{2} \frac{\sigma_0^T - \sigma_2^T}{\sigma_0^T + \sigma_1^T + \sigma_2^T} = \frac{\sigma_0^T - \sigma_2^T}{2\sigma^T} , \quad A_2 = \frac{3}{2} \frac{\sigma_0^T + \sigma_2^T}{\sigma_0^T + \sigma_1^T + \sigma_2^T} = \frac{\sigma_0^T + \sigma_2^T}{2\sigma^T} . \quad (2.40)$$

σ_J^T is the virtual photon-deuteron absorption cross section for a total spin projection J in the photon direction. σ_J^{TL} results from the interference between transverse and longitudinal amplitudes for $J = 0, 1$, and $\sigma^T = (\sigma_0^T + \sigma_1^T + \sigma_2^T)/3$ is the total transverse photo-absorption cross section.

A_1 and A_2 fulfil positivity constraints:

$$0 \leq |A_1| \leq 1 \quad \text{and} \quad |A_2| \leq \sqrt{R}. \quad (2.41)$$

From Eq. (2.41), A_1 and A_2 are directly related to the spin-dependent structure functions g_1 and g_2 :

$$A_1 = \frac{g_1 - \gamma^2 g_2}{F_1}, \quad A_2 = \gamma \frac{g_1 + g_2}{F_1}. \quad (2.42)$$

Conversely, the structure functions g_1 and g_2 are expressed in terms of A_1 and A_2 that are measured by experiments:

$$g_1 = \frac{F_1}{(1 + \gamma^2)} (A_1 + \gamma A_2), \quad g_2 = \frac{F_1}{(1 + \gamma^2)} \left(-A_1 + \frac{1}{\gamma} A_2 \right). \quad (2.43)$$

The latest A_1 and g_1 for deuteron and proton are shown in Fig. 2.5.

Similarly, A_{\parallel} and A_{\perp} are also expressed:

$$A_{\parallel} = D (A_1 + \eta A_2), \quad A_{\perp} = d (A_2 - \xi A_1). \quad (2.44)$$

where D is the depolarisation factor that describes the polarisation transfer from the incident lepton to the virtual photon, and other factors are defined as follows:

$$D = \frac{y(2-y) \left(1 + \frac{\gamma^2 y}{2}\right)}{(1 + \gamma^2) y^2 + 2 \left(1 - y - \frac{\gamma^2 y^2}{4}\right) (1 + R)}, \quad (2.45)$$

$$d = \frac{\sqrt{1 - y - \frac{y^2 \gamma^2}{4}}}{1 - \frac{y}{2}} D, \quad (2.46)$$

$$\eta = \gamma \frac{1 - y - \frac{\gamma^2 y^2}{4}}{\left(1 - \frac{y}{2}\right) \left(1 + \frac{\gamma^2 y}{2}\right)}, \quad (2.47)$$

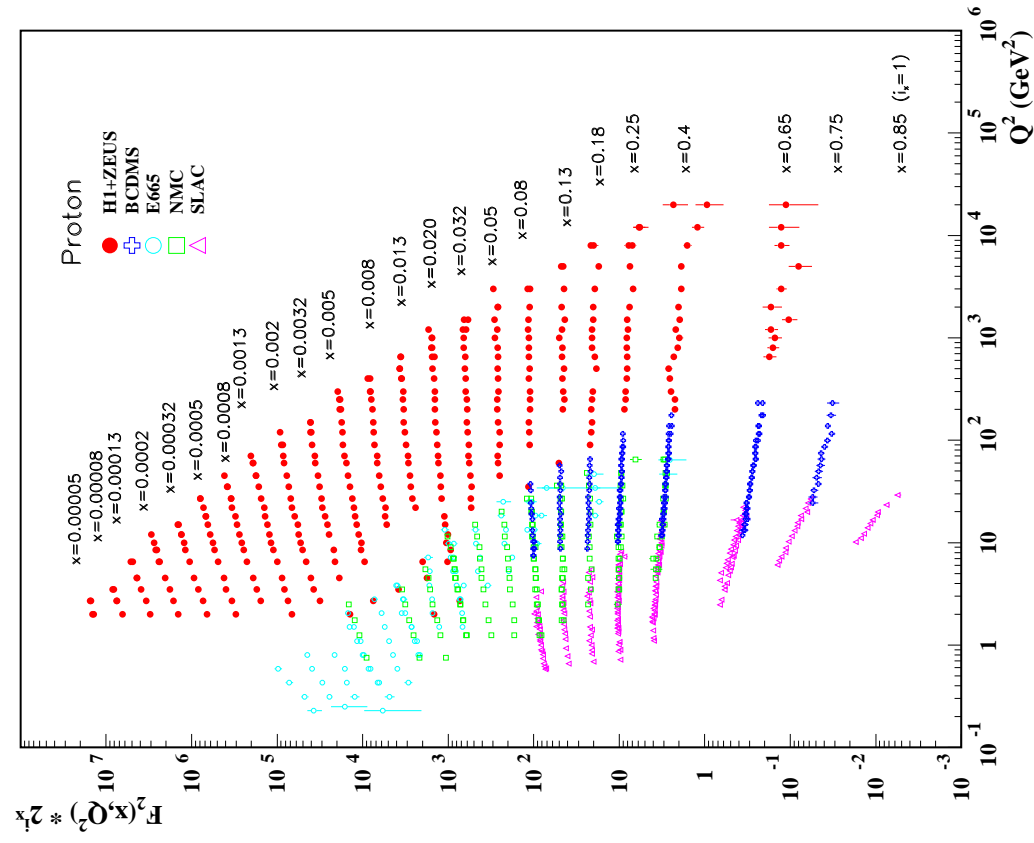
$$\xi = \gamma \frac{1 - \frac{y}{2}}{1 + \frac{\gamma^2 y}{2}}. \quad (2.48)$$

In the real condition of the COMPASS experiment, η is of the order 10^{-4} . Thus, it was found that A_2 is significantly smaller than \sqrt{R} [28,29]. Therefore, A_1 and g_1 are rewritten as follows:

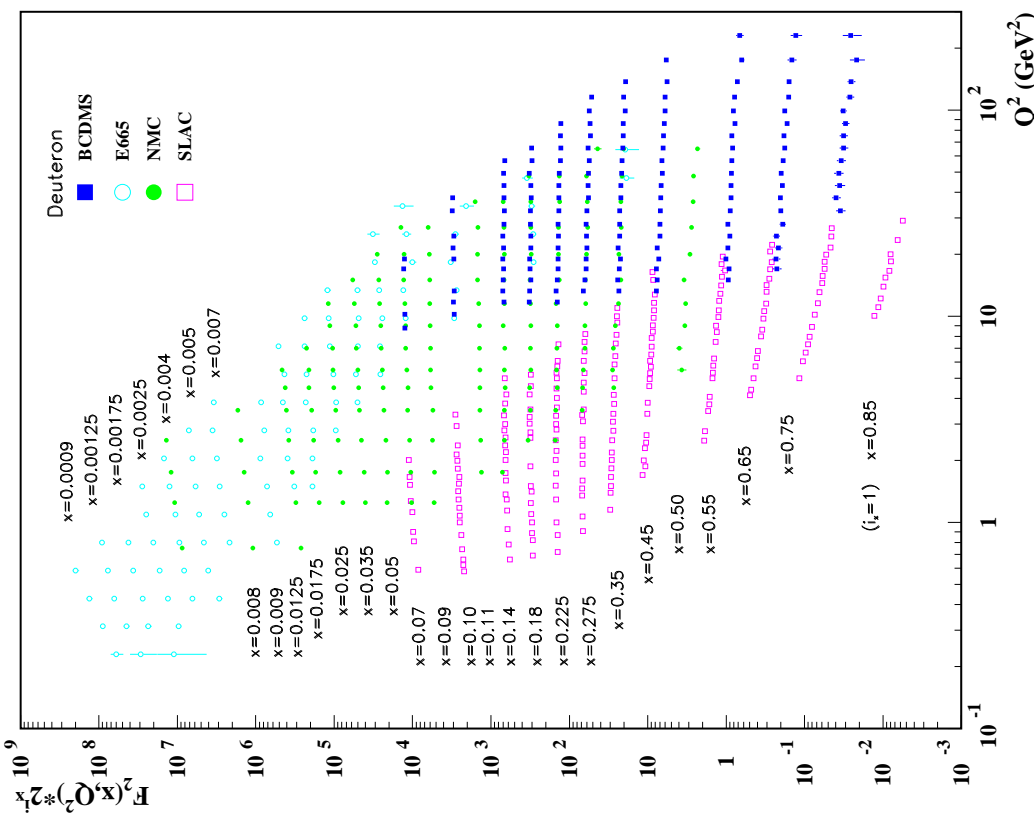
$$A_1 \simeq \frac{A_{\parallel}}{D}, \quad (2.49)$$

$$g_1 \simeq \frac{F_1}{1 + \gamma^2} \frac{A_{\parallel}}{D} = \frac{F_2}{2x(1 + R)} \frac{A_{\parallel}}{D}. \quad (2.50)$$

F_w and R are parameterised by data measured by the other experiments, one can easily access to the structure function g_1 by measuring A_{\parallel} .



(a) The proton structure functions F_2^p measured in electromagnetic scattering of electrons and positrons on protons (collider experiments H1 and ZEUS), and for electrons (SLAC) and muons (BCDMS, E665, NMC) on a fixed target, as a function of Q^2 for bins of fixed x_{Bj} [30, p.303].



(b) The deuteron structure functions F_2^d measured in electromagnetic scattering of electrons (SLAC) and muons (BCDMS, E665, NMC) on a fixed target, as a function of Q^2 for bins of fixed x_{Bj} [30, p.304].

Figure 2.4: The proton and deuteron structure function F_2 as a function of Q^2 for bins of fixed x_{Bj} . Both F_2 was multiplied by 2^{i_x} as the number of x bin in the range $i_x = 1$ to $i_x = 24(29)$.

COMPASS has measured A_1 and g_1 with the polarised deuteron and proton targets with the polarised muon beam [31, 32, 33]. The recent COMPASS results of g_1^p and g_1^d are shown in Fig. 2.6. Thanks to higher lepton energy and high statistics, g_1 can cover wider kinematic range and have smaller uncertainties than others.

2.1. The QCD-improved quark parton model

The quark parton model gives us a picture which the nucleon is made up of partons, namely quarks and gluons. The structure functions $F_1(x)$ and $g_1(x)$ are expressed in terms of the quark distributions $q^+(x)$ and $q^-(x)$ as follows:

$$F_1(x) = \frac{1}{2} \sum_q e_q^2 [q^+(x) + q^-(x)] \equiv \frac{1}{2} \sum_q e_q^2 q(x), \quad (2.51)$$

$$g_1(x) = \frac{1}{2} \sum_q e_q^2 [q^+(x) - q^-(x)] \equiv \frac{1}{2} \sum_q e_q^2 \Delta q(x). \quad (2.52)$$

$q(x)$ is the spin-averaged quark distribution, *i.e.* probability of finding quark q with a nucleon momentum fraction x . Δq is the spin-dependent quark distribution. The $+$ and $-$ in superscript express quark spin is parallel or anti-parallel to that of the spin of the target nucleon. Electric charge of the quark with flavour q is denoted by e_q .

2.2. DGLAP equation

According to QCD, partons radiate other partons: quarks and gluons radiate a gluon, which can be absorbed by other parton. Moreover, a quark and an anti-quark can annihilate into a gluon.

Probability to radiate a parton j with momentum zp from a parton i with momentum p is described by the splitting function, $P_{ij}(z)$, where i and j are a quark or a gluon ($i, j = q, g$). In the process $\gamma^*q \rightarrow qg$ the integration over the gluon phase space results in a logarithmic Q^2 dependence of the cross section. This Q^2 dependence can be absorbed into the definition of the parton distribution functions $q(x, Q^2)$ and gluon distribution function $g(x, Q^2)$. This leads to DGLAP¹ evolution equations [36, 37, 38, 39]².

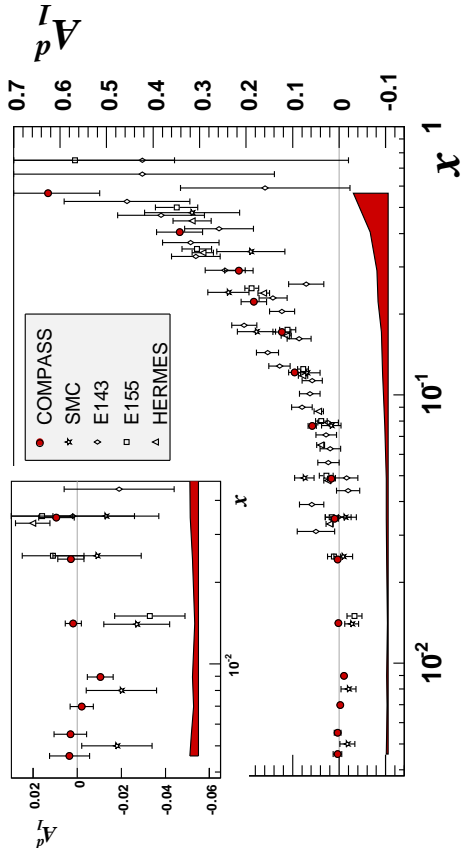
The flavour singlet combination, *i.e.* the sum of all quark distribution functions is defined as

$$\Delta\Sigma(x, Q^2) = \sum_{i=1}^{n_f} \Delta q_i(x, Q^2). \quad (2.53)$$

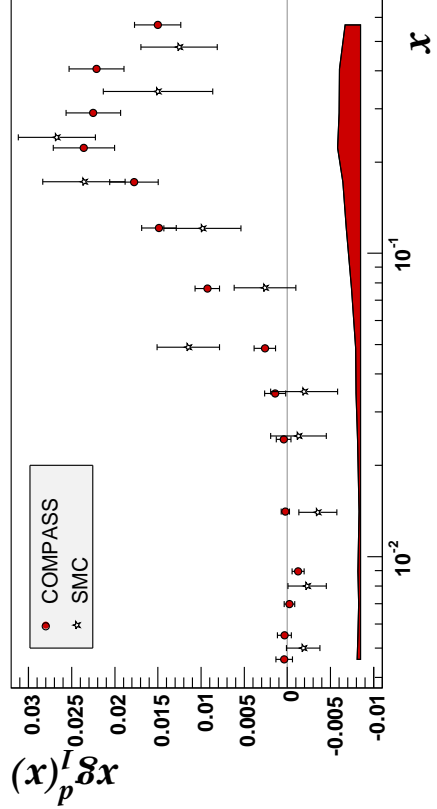
Flavour-nonsinglet combinations, Δq^{NS} is

¹Acronym of Dokshitzer-Gribov-Lipatov-Altarelli-Parisi

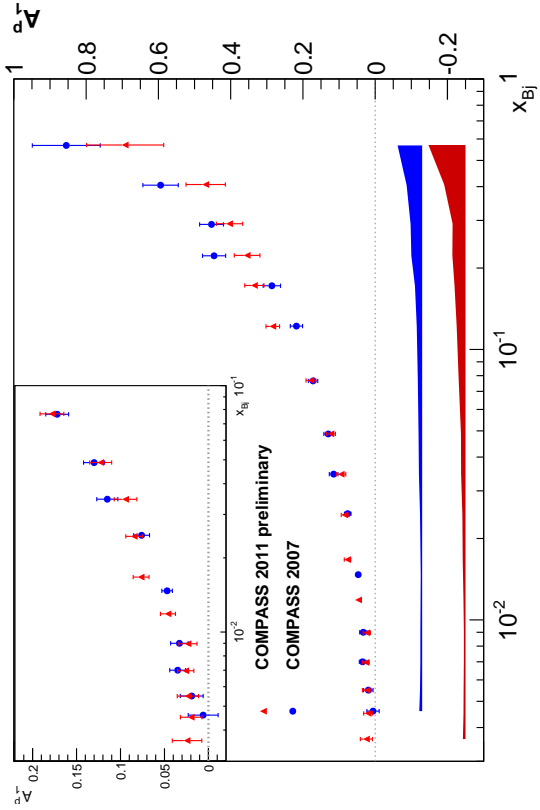
²Until 1990s, it is called Altarelli-Parisi (AP) equations



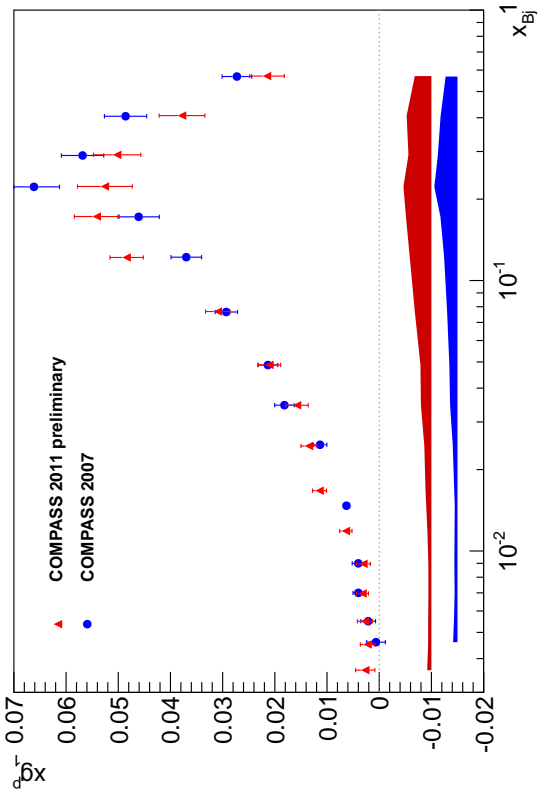
(a) The asymmetry $A_1^d(x)$ measured in COMPASS, SMC, HERMES, SLAC E143, and E155 at $Q^2 > 1$ (GeV/c^2).



(b) Values of $xg_1^d(x)$ measured in COMPASS and SMC.

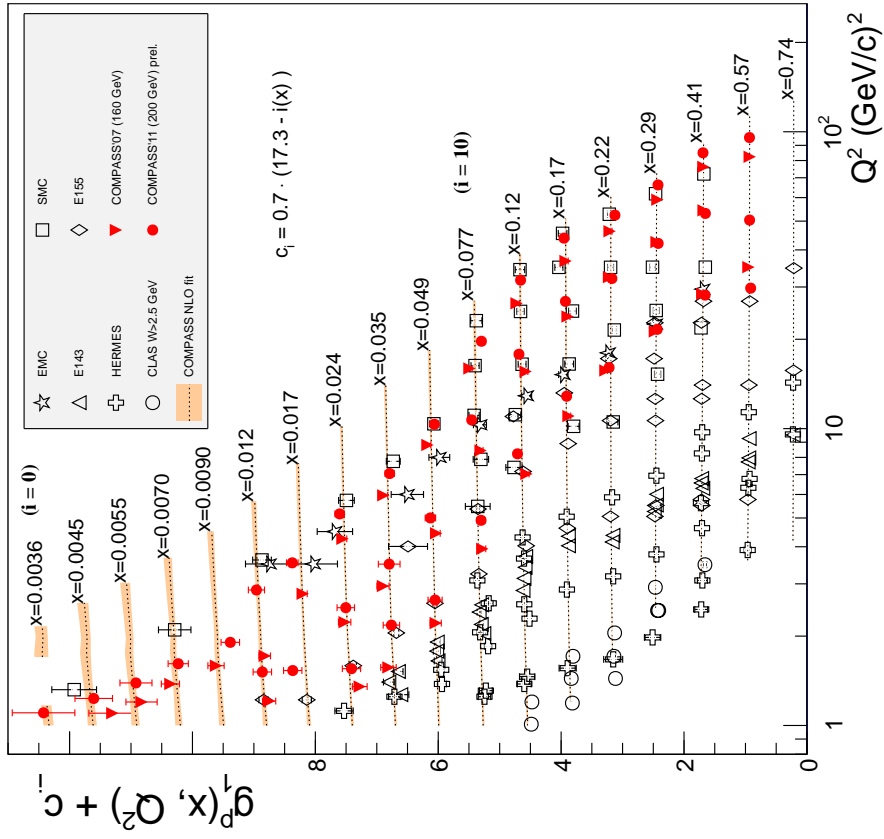


(c) The asymmetry $A_1^p(x)$ measured in COMPASS.

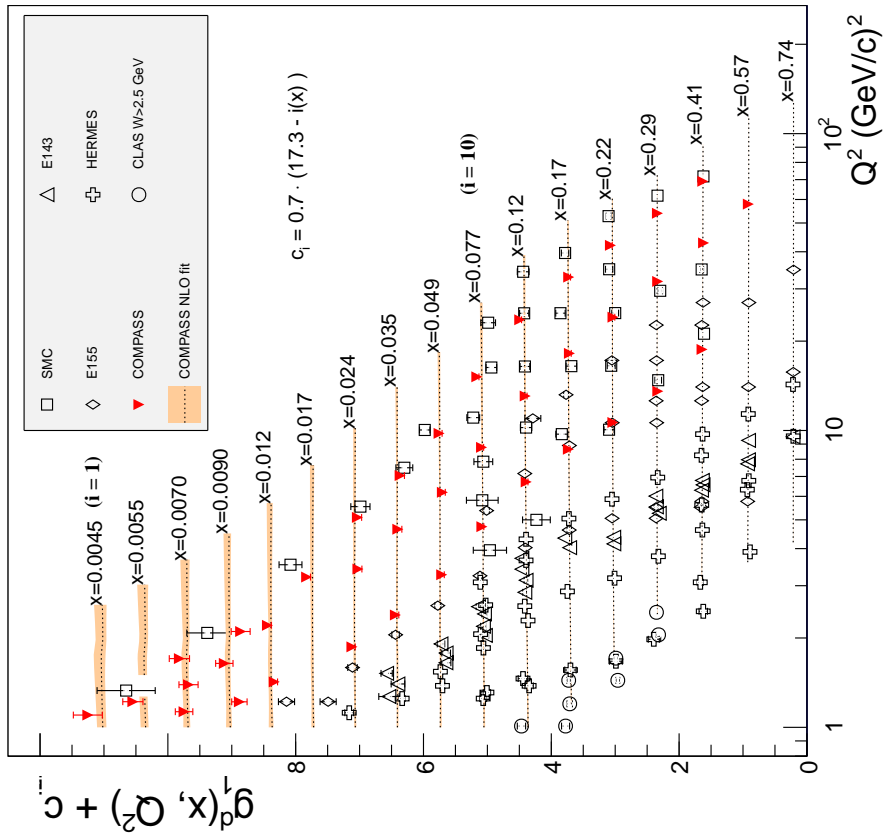


(d) Values of $xg_1^p(x)$ measured in COMPASS.

Figure 2.5: A_1 and g_1 of deuteron and proton [33, 34].



(a) g_1 for deuteron



(b) g_1 for proton

Figure 2.6: Results for the COMPASS NLO QCD fit to g_1 world data, proton (left) and deuteron (right). The curves are given by Q^2 at several values of x_{Bj} , and are compared to the data. The orange band represents the envelope of the different parametrisations including statistical and systematic errors [33, 35].

$$\Delta q^{\text{NS}}(x, Q^2) = \sum_{i=1}^{n_f} \left(\frac{e_i^2}{\langle e^2 \rangle} - 1 \right) \Delta q_i(x, Q^2), \quad (2.54)$$

$$\langle e^2 \rangle = \sum_{i=1}^{n_f} \frac{e_i^2}{n_f} \quad (2.55)$$

with n_f is the number of active flavours.

The DGLAP equations are given as:

$$\frac{d}{d \ln Q^2} \Delta q^{\text{NS}} = \frac{\alpha_s}{2\pi} \Delta P_{qq}^{\text{NS}} \otimes \Delta q^{\text{NS}}, \quad (2.56)$$

$$\frac{d}{d \ln Q^2} \begin{pmatrix} \Delta \Sigma \\ \Delta g \end{pmatrix} = \frac{\alpha_s}{2\pi} \begin{pmatrix} \Delta P_{qq}^{\text{S}} & 2n_f \Delta P_{qg}^{\text{S}} \\ \Delta P_{gq}^{\text{S}} & \Delta P_{gg}^{\text{S}} \end{pmatrix} \otimes \begin{pmatrix} \Delta \Sigma \\ \Delta g \end{pmatrix}, \quad (2.57)$$

where α_s is the strong coupling constant, Δg is the spin-dependent gluon distribution, and $\Delta P_{ab} = P_{a^+b^+} - P_{a^+b^-}$ and the operator \otimes are defined as

$$(a \otimes b)(x) \equiv \int_x^1 \frac{dy}{y} a\left(\frac{x}{y}\right) b(y). \quad (2.58)$$

Δq^{NS} evolves independently from gluons.

2.3. Sum rules

In the leading-order, the first moment of g_1 is related to the total quark helicity contribution to the nucleon spin:

$$\Gamma_1 \equiv \int_0^1 g_1(x) dx = \frac{1}{2} \sum_q^{n_f} e_q^2 \int_0^1 dx \Delta q(x). \quad (2.59)$$

Assuming that $n_f = 3$, one can rewrite Eq. (2.59) of the proton as follows:

$$\Gamma_1^{\text{p}} = \frac{1}{2} \left(\frac{4}{9} \Delta u + \frac{1}{9} \Delta d + \frac{1}{9} \Delta s \right) \quad (2.60)$$

$$= \frac{1}{12} (\Delta u - \Delta d) + \frac{1}{36} (\Delta u + \Delta d - 2\Delta s) + \frac{1}{9} (\Delta u + \Delta d + \Delta s) \quad (2.61)$$

$$= \frac{1}{12} a_3 + \frac{1}{36} a_8 + \frac{1}{9} a_0, \quad (2.62)$$

where

$$a_3 = \Delta u - \Delta d, \quad (2.63)$$

$$a_8 = \Delta u + \Delta d - 2\Delta s, \quad (2.64)$$

$$a_0 = \Delta u + \Delta d + \Delta s. \quad (2.65)$$

For the neutron case, Γ_1^n is obtained from the first momentum of proton using the isospin symmetry. Thus, the Γ_1 for the proton and the neutron are written as

$$\Gamma_1^{p(n)} = \pm \frac{1}{12}a_3 + \frac{1}{36}a_8 + \frac{1}{9}a_0. \quad (2.66)$$

The terms a_0 , a_3 , and a_8 are given by following equations [7]:

$$\langle P, S | \bar{q}\gamma_\mu\gamma_5q | P, S \rangle = 2MS_\mu\Delta q, \quad (2.67)$$

$$\langle P, S | J_{5\mu}^i | P, S \rangle = MS_\mu a_i, \quad i = 1, 2, \dots, 8, \quad (2.68)$$

$$\langle P, S | J_{5\mu}^0 | P, S \rangle = 2MS_\mu a_0, \quad (2.69)$$

where S_μ is the spin vector of proton and $|P, S\rangle$ is proton states with momentum P_μ and spin S_μ . The flavour-singlet axial-vector current $J_{5\mu}^0$ is defined as

$$J_{5\mu}^0 = \bar{\psi}\gamma_\mu\gamma_5\psi \quad \text{with} \quad \psi = \begin{pmatrix} \psi_u \\ \psi_d \\ \psi_s \end{pmatrix}. \quad (2.70)$$

Similarly, the octet of axial-vector currents $J_{5\mu}^i$ is defined as

$$J_{5\mu}^i = \bar{\psi}\gamma_\mu\gamma_5\frac{\lambda_i}{2}\psi \quad \text{with} \quad i = 1, 2, \dots, 8. \quad (2.71)$$

The matrices λ_i are Gell-Mann matrices and the γ_μ are the gamma matrices (Dirac matrices).

In the naïve quark-parton model, a_0 is identical to $\Delta\Sigma$ that expresses the total fraction of the spin of the nucleon carried by the quark. The axial charges a_3 and a_8 are measured with the weak β -decay of the neutron and the spin-1/2 hyperons (Σ^\pm , Σ^0 , Λ , Ξ^- , and Ξ^0) in the SU_3 baryon octet. Now one can define the Bjorken sum rule

$$\Gamma_1^p - \Gamma_1^n = \frac{1}{6}a_3. \quad (2.72)$$

Ellis and Jaffe [40] assumed that the strange quarks are not polarised, $\Delta s \equiv 0$, leading to $a_0 = a_8$ and thus

$$\Gamma_1^{p,n} = \frac{5}{36}a_0 \pm \frac{1}{12}a_3 \quad (2.73)$$

which is known as Ellis-Jaffe sum rules.

The structure functions can be evolved with Q^2 by DGLAP equations. The sum rules can be also rewritten with coefficient functions:

$$\Gamma_1^{p,n}(Q^2) = \frac{1}{12} \left[\pm a_3 + \frac{1}{3}a_8 \right] C^{\text{NS}}(Q^2) + \frac{1}{9}a_0 C^{\text{S}}(Q^2) \quad (2.74)$$

for Ellis-Jaffe sum rule, and

$$\Gamma_1^p(Q^2) - \Gamma_1^n(Q^2) = \frac{1}{6} a_3 C^{\text{NS}}(Q^2) \quad (2.75)$$

for Bjorken sum rule.

The singlet and non-singlet coefficient functions, C^{S} and C^{NS} , can be expanded into a power series of α_s/π :

$$C^{\text{S,NS}} = 1 + c_1^{\text{S,NS}} \left(\frac{\alpha_s}{\pi} \right) + c_2^{\text{S,NS}} \left(\frac{\alpha_s}{\pi} \right)^2 + c_3^{\text{S,NS}} \left(\frac{\alpha_s}{\pi} \right)^3 + \dots \quad (2.76)$$

The actual values of c_i are shown in Tab. 2.1. Note that $C_1^{\text{S,NS}}$ is identical to 1.

Table 2.1: The values of coefficient functions, $c_i^{\text{S,NS}}$, with a different number of active flavours [41].

n_f	singlet		non-singlet	
	c_2	c_3	c_2	c_3
3	-0.549 59	-4.447 25	-3.583 33	-20.215 27
4	1.081 53	4.874 23	-3.250 00	-13.850 26
5	2.978 45	13.071 03	-2.916 67	-7.840 19
6	5.279 32	20.730 34	-2.583 33	-2.185 06

Calculations in Ref. [41] used the $\overline{\text{MS}}$ -scheme [42]. In general the result depends on the renormalisation scheme.

2.4. Fragmentation

In the previous sections, we have discussed the inclusive measurement of DIS, where only scattered muon is detected. In order to get more insight into the nucleon's constituents, it is very useful to consider semi-inclusive experiments where hadrons are detected in coincidence with the scattered muon. This allows, *e.g.* to separate the distributions of quarks with different flavours in the nucleon [43].

To describe such process a set of two variables, *i.e.* x_{Bj} and Q^2 , is not sufficient, an additional one is needed. The variable usually used is an energy fraction of the virtual photon energy carried by the hadron

$$z = \frac{E_h}{\nu} . \quad (2.77)$$

Alternatively, one can use Feynman x ,

$$x_F = \frac{p_L^{\text{c.m.}}}{p_{L,\text{max}}^{\text{c.m.}}} \approx \frac{2p_L^{\text{c.m.}}}{W} , \quad (2.78)$$

where $p_L^{c.m.}$ is the longitudinal momentum of the hadron and $p_{L,max}^{c.m.} \approx W/2$ is the maximum allowed p_L in the virtual photon-nucleon centre of the mass system. The region $x_F < 0$ selects preferably hadrons from the target fragmentation region, which originate from the target remnant. Hadrons that originate from the struck quark are produced mostly at $x_F > 0$, which is called the current region.

According to QCD, the quarks are confined, and one cannot pick up each of them; free quark does not exist. Thus the struck quark and the target remnant have to form colour neutral final state hadrons. This process of hadronisation cannot be described by pQCD but is parametrised in the form of fragmentation functions. This means that the hard process can be calculated using pQCD and the soft part, namely the fragmentation, is parametrised independently.

The semi-inclusive measurement of the hadrons in the current region allows one to obtain information about the struck quark since its flavour and direction are correlated to the identity and the direction of the leading hadron.

The cross section for the production of a hadron h can be written in leading order QCD as

$$\sigma^h \propto \sum_f e_f^2 q_f(x, Q^2) D_f^h(z, Q^2) \quad (2.79)$$

where $D_f^h(z, Q^2)$ is the fragmentation function. The fragmentation function gives the probability density that a struck quark of flavour f , probed at a scale Q^2 , fragments into a hadron h carrying a fraction z of the virtual photon energy. One of the most recent parametrisations of parton-to-pion fragmentation functions (DSS14) is presented in Ref. [44].

2.5. JSV framework

In this section, the theoretical framework of this analysis is described, which is referred as “JSV framework” [45].

One considers photoproduction of a single-inclusive hadron shown in Fig. 2.7: $lN \rightarrow l'hX$. The lepton l is longitudinally polarised and the target nucleon N is also polarised longitudinally. Their directions are either parallel or antiparallel to each other.

JSV framework is based on a collinear pQCD framework in NLO. There are two contributions to the cross section: “direct” part where the virtual photon directly interacts with the parton b and “resolved” part where the partonic component of the virtual photon interacts with the parton b . In an experiment, one can only measure the sum of the “direct” and “resolved” cross section:

$$d\sigma = d\sigma_{\text{direct}} + d\sigma_{\text{resolved}}. \quad (2.80)$$

The spin-averaged (unpolarised) and differential (polarised) cross sections for this process are written as follows:

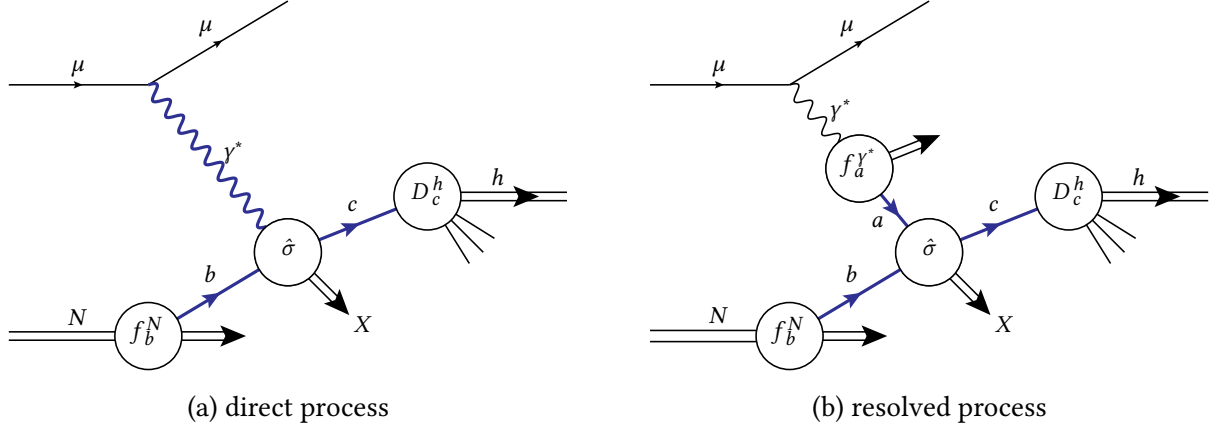


Figure 2.7: Decomposition of the single-inclusive cross section for quasi-photoproduction of a hadron h into direct (*left*) and resolved (*right*) subprocesses, taken from Ref. [46]. In the resolved process, the photon exhibits a hadronic structure in the framework of QCD. The internal wavy line represents the photon γ^* and the solid lines do partons $\{a, b, c\} = \{q, \bar{q}, g\}$. The central blob describes a hard scattering cross section $\hat{\sigma}$. The peripheral blobs describe the non-perturbative objects: parton distributions of the nucleon $f_{b/N}$, and photon f_{a/γ^*} , and fragmentation functions of the observed hadron $D_{c/h}$.

$$d\sigma \equiv \frac{1}{2} [d\sigma_{++} + d\sigma_{+-}] \quad (2.81)$$

$$= \sum_{a,b,c} \int dx_a dx_b dz_c f_{a/\ell}(x_a, \mu_f) f_{b/N}(x_b, \mu_f) \times d\hat{\sigma}_{ab \rightarrow cX}(S, x_a, x_b, P_h/z_c, \mu_r, \mu_f, \mu'_f) D_{c/h}(z_c, \mu'_f), \quad (2.82)$$

$$d\Delta\sigma \equiv \frac{1}{2} [d\sigma_{++} - d\sigma_{+-}] \quad (2.83)$$

$$= \sum_{a,b,c} \int dx_a dx_b dz_c \Delta f_{a/\ell}(x_a, \mu_f) \Delta f_{b/N}(x_b, \mu_f) \times d\Delta\hat{\sigma}_{ab \rightarrow cX}(S, x_a, x_b, P_h/z_c, \mu_r, \mu_f, \mu'_f) D_{c/h}(z_c, \mu'_f). \quad (2.84)$$

subscripts ++ and +-

the helicities of the lepton and nucleon: the lepton helicity is fixed and only the nucleon one is changed.

x_a

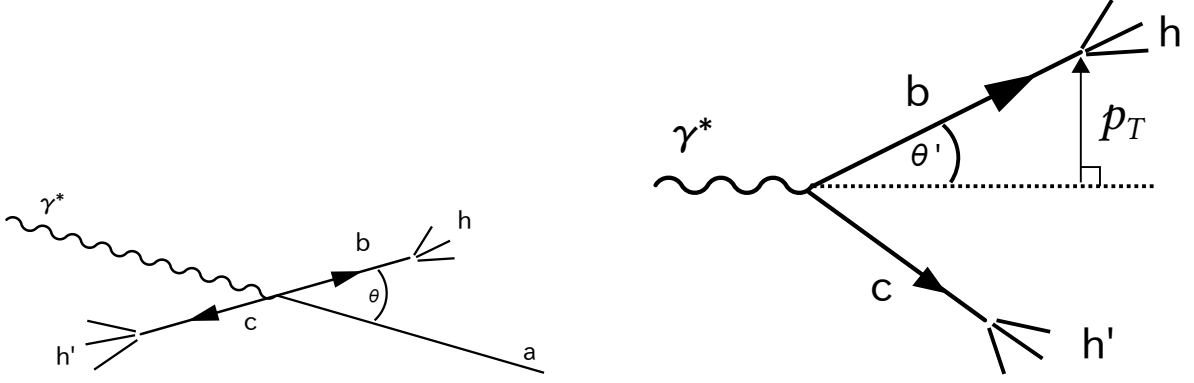
the momentum fraction of the parton a taken from the virtual photon in the resolved process. In the direct process, it is identical to x_γ .

x_b

the momentum fraction of the parton b taken from the nucleon

$d\Delta\hat{\sigma}_{ab \rightarrow cX}$

the hard-scattering cross section of $a + b \rightarrow c + X$



(a) The hard scattering process in the centre of mass system of the photon γ and the parton a . Scattered partons b and c fragment into hadrons h and h' to be measured.

(b) The hard scattering process in the laboratory system. Partons with large scattering angle at c.m.s have large transverse momenta with respect to the virtual photon.

Figure 2.8: The hard scattering process in two systems: the centre of mass system of the photon and the parton, and the laboratory system.

S
the lepton-nucleon centre of mass system energy

P
the momentum of the hadron h

μ_f and μ'_f
the factorisation scales for the initial and final states

μ_r
the renormalisation scale.

Choosing the transverse momentum of hadron with respect to p_T as scales guarantees that the observed hadrons are fragmented from partons which are interacted by the virtual photon and the parton. The scattering process in the photon-parton centre of mass system shown in Fig. 2.8. In this system, the produced partons are emitted back-to-back. After the Lorentz boost to the laboratory system, they can still have large transverse momenta with respect to the virtual photon direction [47]. Collinear partons of the incident virtual photon and the incident parton have small scattering angle at centre of mass system, resulting in small transverse momenta in the laboratory system. Thus, the most natural scale for the theoretical calculation is p_T , which varies between 1/2 to 2 in order to investigate the scale dependence:

$$\mu = \mu_r = \mu_{fi} = \mu_{ff} = p_T \quad (2.85)$$

Fig. 2.9 shows the comparison of the theoretical cross sections with various order (LO, NLO, and resummed) and the measured cross section. The sum in Eqs. (2.81) and (2.83) runs over all partonic channels.

The parton density in the lepton l can be rewritten as

$$\Delta f_{a/\ell}(x_a, \mu_f) = \int_{x_a}^1 \frac{dy}{y} \Delta P_{\gamma\ell}(y) \Delta f_{a/\gamma} \left(x_\gamma = \frac{x_a}{y}, \mu_f \right). \quad (2.86)$$

$\Delta P_{\gamma\ell}(y)$ is the spin-dependent Weizsäcker-Williams “equivalent photon” spectrum [48] that describes the collinear emission of a photon with low virtuality Q^2 less than some upper limit Q_{\max}^2 (determined by the experimental conditions) by a lepton of mass m_ℓ [45].

$$\Delta P_{\gamma\ell}(y) = \frac{\alpha_e}{2\pi} \left\{ \left[\frac{1 - (1-y)^2}{y} \right] \ln \frac{Q_{\max}^2(1-y)}{m_\ell^2 y^2} + 2m_\ell^2 y^2 \left(\frac{1}{Q_{\max}^2} - \frac{1-y}{m_\ell^2 y^2} \right) \right\} \quad (2.87)$$

$\Delta f_{a/\gamma}$ is process dependent. For the direct photon contribution, the parton a is identified as the photon. Thus $\Delta f_{a/\gamma}$ is

$$\Delta f_{a/\gamma} = \delta(1 - x_\gamma). \quad (2.88)$$

On the other hand, for the resolved process, $\Delta f_{a/\gamma}$ is the parton density of a circularly polarised photon. As this is completely unknown experimentally so far, one must consider it in the numeric calculations. According to Ref. [45], it is sufficient to only use the two extreme cases that $\Delta f_{a/\gamma} = f_{a/\gamma}$ (maximal case, $\Delta f_{a/\gamma}$ is identical to $f_{a/\gamma}$) and $\Delta f_{a/\gamma} = 0$ (minimal case).

The longitudinal double spin asymmetry to be measured in experiments is defined with the unpolarised and polarised cross sections as

$$A_{LL} \equiv \frac{d\Delta\sigma}{d\sigma} = \frac{d\sigma_{++} - d\sigma_{+-}}{d\sigma_{++} + d\sigma_{+-}}. \quad (2.89)$$

In fixed target experiments, p_T of the produced hadron is relatively small comparing the square root of the centre of mass energy, so that the variable $x_T = 2p_T/\sqrt{S}$ is relatively large. This means that the initial photon and parton have just enough energy to produce the high- p_T partons fragmenting into hadrons. Relatively little phase space is available for additional radiation of partons. It is essential to take the large logarithms to all orders in the strong coupling, a technique known as “threshold resummation” [49], into account. The calculation of cross sections with resummation technique for $pp \rightarrow hX$ and $pp \rightarrow h_1 h_2 X$ had been carried out and observed the substantial effects [50, 51].

The rapidity-dependent unpolarised cross section for the single hadron production $\ell N \rightarrow \ell' h^\pm X$ is written as

$$\frac{p_T^3 d\sigma}{dp_T d\eta} = \sum_{a,b,c} \int_{x_\ell^{\min}}^1 dx_\ell \int_{x_n^{\min}}^1 dx_n \int_x^1 dz \frac{\hat{x}_T^4 z^2}{8\nu} f_{a/\ell}(x_\ell, \mu_{fi}) f_{b/N}(x_n, \mu_{fi}) D_{h/c}(z, \mu_{ff}) \frac{\hat{s} d\hat{\sigma}_{ab \rightarrow cX}}{d\nu d\omega} \quad (2.90)$$

where the rapidity η , the factorisation scales, μ_{fi} and μ_{ff} , parton distributions, $f_{a/\ell}$ and $f_{b/N}$, the fragmentation function, $D_{h/c}$, and the partonic hard scattering cross section, $\hat{\sigma}_{ab \rightarrow cX}$. Typically the factorisation scales are chosen to be equal, $\mu_r = \mu_{fi} = \mu_{ff} = p_T$. $\hat{x}_T, x_\ell^{\min}, x_n^{\min}$, and x are defined by

$$\hat{x}_T = \frac{x_T}{z\sqrt{x_\ell x_n}}, \quad (2.91)$$

$$x_\ell^{\min} = \frac{x_T e^\eta}{2 - x_T e^{-\eta}}, \quad (2.92)$$

$$x_n^{\min} = \frac{x_T e^{-\eta}}{2 - \frac{x_T}{x_\ell} e^\eta}, \quad (2.93)$$

$$x = \frac{x_T \cosh \hat{\eta}}{\sqrt{x_n x_\ell}}, \quad (2.94)$$

$$\nu = 1 - \frac{\hat{x}_T}{2} e^{-\hat{\eta}}, \quad (2.95)$$

where $\hat{\eta} = \eta + \frac{1}{2} \ln(x_n/x_\ell)$.

Other variables are also defined:

$$w = \frac{1}{\nu} \frac{\hat{x}_T}{2} e^{\hat{\eta}}, \quad (2.96)$$

$$\hat{s} = x_n x_\ell s, \quad (2.97)$$

$$\hat{t} = (p_a - p_c)^2 = -\frac{\hat{s} \hat{x}_T e^{-\hat{\eta}}}{2}, \quad (2.98)$$

$$\hat{u} = (p_b - p_c)^2 = -\frac{\hat{s} \hat{x}_T e^{\hat{\eta}}}{2}, \quad (2.99)$$

and

$$s_4 = \hat{s} + \hat{t} + \hat{u} = \hat{s} \nu (1 - w) = \hat{s} \left[1 - \hat{x}_T \frac{1}{2} (e^{\hat{\eta}} + e^{-\hat{\eta}}) \right] = \hat{s} (1 - \hat{x}_T \cosh \hat{\eta}). \quad (2.100)$$

Note that \hat{s} , \hat{t} , and \hat{u} are the Mandelstam variables and s_4 is square of the invariant mass of the unobserved partonic final state.

The partonic hard scattering functions $\hat{\sigma}_{ab \rightarrow cX}$ can be evaluated with pQCD and be written as an expansion in the strong coupling constant $\alpha_s(\mu_r)$:

$$\hat{\sigma}_{ab \rightarrow cX}(\nu, w) = \hat{\sigma}_{ab \rightarrow cX}^{(0)}(\nu, w) + \alpha_s(\mu_r) \hat{\sigma}_{ab \rightarrow cX}^{(1)}(\nu, w) + \mathcal{O}(\alpha_s^2). \quad (2.101)$$

In the unpolarised case, the splitting function is given by

$$P_{\gamma\ell}(y) = \frac{\alpha}{2\pi} \left[\frac{1 + (1 - y^2)}{y} \ln \frac{Q_{\max}^2 (1 - y)}{m_\ell^2 y^2} + 2m_\ell^2 y \left(\frac{1}{Q_{\max}^2} - \frac{1 - y}{m_\ell^2 y^2} \right) \right] \quad (2.102)$$

and describes the collinear emission of a quasi-real photon with momentum fraction y off a lepton ℓ of mass m_ℓ ³. The virtuality of the radiated photon is restricted to be less than Q_{\max}^2 , which is in turn constrained by the experimental setup.

³The definitions of unpolarised and polarised splitting functions look similar but are not identical, see Ref. [48].

There are two basic partonic subprocesses in LO: photon-gluon fusion ($\gamma g \rightarrow q\bar{q}$) and Compton scattering ($\gamma q \rightarrow qg$). For each process, either of the final-state partons may hadronise into the observed hadron. As the processes are partly electromagnetic and partly due to the strong interaction, their cross sections are proportional to $\alpha\alpha_s(\mu_r)$. In addition to that, the photon also exhibits a hadronic structure in the framework of QCD, which is described by the resolved process. Unlike hadronic parton distributions, photonic densities may be decomposed into a purely perturbatively calculable “pointlike” contribution and a nonperturbative “hadronlike” part. While the pointlike contribution dominates at large momentum fractions x_γ , the latter dominates in the low- to mid- x_γ region and may be estimated via the vector-meson-dominance model.

At the lowest order, the possible resolved subprocesses $a + b \rightarrow c + d$, which represents the parton a and b interacts and the parton c and d are observed in the final state, are following:

$$\begin{aligned} qq' \rightarrow qq', \quad q\bar{q}' \rightarrow q\bar{q}', \quad q\bar{q} \rightarrow q'\bar{q}', \quad qq \rightarrow qq, \quad q\bar{q} \rightarrow q\bar{q} \\ q\bar{q} \rightarrow gg, \quad gq \rightarrow qg, \quad qg \rightarrow gq, \quad gg \rightarrow gg, \quad gg \rightarrow q\bar{q}. \end{aligned} \quad (2.103)$$

Each of these is a pure QCD process and, therefore, has a cross section quadratic in $\alpha_s(\mu_r)$. However, as the photon parton distributions are formally of order $\alpha/\alpha_s(\mu_f)$, the perturbative expansion of the direct and resolved contributions starts at the same order of α_s . The hard scattering cross section at leading order, where one has $2 \rightarrow 2$ kinematics, $w \equiv 1$, $\hat{\sigma}_{ab \rightarrow cX}^{(0)}$ can be written as

$$\frac{\hat{s}d\hat{\sigma}_{ab \rightarrow cX}^{(0)}}{d\nu dw} = \frac{\hat{s}d\hat{\sigma}_{ab \rightarrow cd}^{(0)}(\nu)}{d\nu} \delta(1-w). \quad (2.104)$$

On the other hand, the one at NLO have been computed and can be cast into the form

$$\frac{\hat{s}d\hat{\sigma}_{ab \rightarrow cX}^{(1)}}{d\nu dw} = A(\nu)\delta(1-w) + B(\nu)\left(\frac{\ln(1-w)}{1-w}\right)_+ + C(\nu)\left(\frac{1}{1-w}\right)_+ + F(\nu, w). \quad (2.105)$$

Here the “+”-distribution represented with the subscript + is defined as

$$f_+(x) \equiv f(x) - \delta(1-x) \int_0^1 dw f(w). \quad (2.106)$$

If a function $g(x)$ is a smooth function as $x \rightarrow 1$, then

$$\int_0^1 dw f(w) \left[g(w) \right]_+ = \int_0^1 dw \left[f(w) - f(1) \right] g(w). \quad (2.107)$$

The terms, $B(\nu)\left(\frac{\ln(1-w)}{1-w}\right)_+$ and $C(\nu)\left(\frac{1}{1-w}\right)_+$, are traced back to soft gluon emission. Moreover, these “+”-distributions yield large logarithmic first order corrections close to the threshold and will show up in all higher order corrections. For example, in the k -th order the cross section $d\hat{\sigma}_{ab \rightarrow cX}^{(k)}/d\nu dw$ contains logarithms of the form $\alpha_s^k \left[\frac{\ln^{2k-1}(1-w)}{1-w} \right]_+$ and subleading terms with fewer logarithms. Depending on kinematics, these logarithmic terms have to be resummed order by order.

The numerical calculation of Eq. (2.90) is extremely hard since one has to take care of the convolutions. Hence, the Mellin transform is employed, which can transform the convolutions of components into the products of corresponding Mellin- N moments. The “+”-distributions are also transformed into simple forms: powers of logarithms, $\ln N$. This logarithmic behaviour converges as $1/N^4$ or faster at large N in the moment space.

The single hadron cross section depends on two kinematic variables, p_T and η . If one integrates it over η , it depends only on p_T^2 . This transformation makes the calculation of Mellin moments simple since it can be factorised in terms of moments of parton distributions, fragmentation functions, and partonic cross sections. After resummation, the resummed cross section can be given by inverting the Mellin expression.

On the other hand, the calculation of η -depended cross section has to use different techniques. One of the methods to do is to apply the Mellin transform only to the fragmentation functions and resummed cross sections. By including fragmentation functions, the integrand for the inverse Mellin transform falls off fast enough.

The actual procedures are following:

1. taking Mellin moments only of the product of fragmentation functions and the resummed partonic cross sections,
2. performing Mellin inverse, and
3. convoluting the result with the parton distributions in x space.

The first procedure: Mellin transformation To be specific, starting from Eq. (2.90), one considers only the last integral and take moments in x^2

$$\int_0^1 dx^2 (x^2)^{N-1} \int_x^1 dz \frac{\hat{x}_T^4 z^2}{8\nu} D_{h/c}(z, \mu_{ff}) \frac{\hat{s} d\hat{\sigma}_{ab \rightarrow cX}}{d\nu dw} \equiv D_{h/c}^{2N+3}(\mu_{ff}) \tilde{w}^{2N}(\hat{\eta}) . \quad (2.108)$$

Here x is the lower bound of the z integral. The Mellin moments of fragmentation function and the hard scattering function are defined as

$$D_{h/c}^N(\mu_{ff}) = \int_0^1 dz z^{N-1} D_{h/c}(z, \mu_{ff}) , \quad (2.109)$$

$$\tilde{w}^N(\hat{\eta}) = 2 \int_0^1 d\frac{s_4}{\hat{s}} \left(1 - \frac{s_4}{\hat{s}}\right)^{N-1} \frac{\hat{x}_T^4 z^2}{8\nu} \frac{\hat{s} d\hat{\sigma}_{ab \rightarrow cX}}{d\nu dw} . \quad (2.110)$$

The second and third procedures: Mellin inverse and convolution One can get the cross section by taking Mellin inverse of Eq. (2.110) and convoluting with the parton distributions:

$$\frac{p_T^3 d\sigma}{dp_T d\eta} = \sum_{a,b,c} \int_0^1 dx_\ell \int_0^1 dx_n f_{a/\ell}(x_\ell, \mu_{fi}) f_{b/N}(x_n, \mu_{fi}) \int_C \frac{dN}{2\pi i} (x^2)^{-N} D_{h/c}^{2N+3}(\mu_{ff}) \tilde{w}^{2N}(\hat{\eta}) . \quad (2.111)$$

Eqs. (2.90) and (2.111) are mathematically equivalent. However, the former is much suitable from a computational point of view since the moments of the fragmentation functions tame the large- N behaviour of the \tilde{w}^{2N} so that the Mellin integral converges rapidly. The latter, however, contains “+”-distributions with any power of a logarithm, which makes carrying out a convolution over z very difficult.

The resummed cross section in momentum space factorises into functions since in Mellin space the phase space including the constraint of energy conservation also factorises.

$$\tilde{w}_{ab \rightarrow cd}^{\text{resum}, N}(\hat{\eta}) = \Delta_a^{N_a}(\hat{s}, \mu_{fi}) \Delta_b^{N_b}(\hat{s}, \mu_{fi}) \Delta_c^N(\hat{s}, \mu_{ff}) J_d^N(\hat{s}) \text{Tr} \left\{ H S_N^\dagger S S_N \right\}_{ab \rightarrow cd} \quad (2.112)$$

The functions (Δ_a , Δ_b , Δ_c , and J_d) describe soft-gluon emissions off these partons (a , b , c , and d). H is the hard scattering part, and S is the soft function. S represents the contributions by soft gluon emitted at wide angles and resummed by the exponentials.

Finally, one can get the resummed cross section:

$$\begin{aligned} \frac{p_T^3 d\sigma^{\text{matched}}}{dp_T d\eta} &= \sum_{a,b,c} \int_0^1 dx_\ell \int_0^1 dx_n f_{a/\ell}(x_\ell, \mu_{fi}) f_{b/N}(x_n, \mu_{fi}) \\ &\quad \times \int_C \frac{dN}{2\pi i} (x^2)^{-N} D_{h/c}^{2N+3}(\mu_{ff}) [\tilde{w}^{\text{resum}, 2N}(\hat{\eta}) - \tilde{w}^{\text{resum}, 2N}(\hat{\eta})|_{\text{first-order}}] \\ &\quad + \frac{p_T^3 d\sigma^{\text{NLO}}}{dp_T d\eta}. \end{aligned} \quad (2.113)$$

Matching resummed cross section to the NLO one is needed to make use of the fixed-order theoretical calculation available. This is performed by expanding the partonic cross sections to the first nontrivial order in α_s , subtracting the expanded result from the resummed one, and adding the full NLO cross section. This procedure avoids any double counting of perturbative terms. The authors of Ref. [49] compared the resummed cross section of the single-inclusive hadron production for deuteron target to measured data at COMPASS [23]. The input parameters for theoretical calculation are following:

- $\sqrt{s} = 17.4 \text{ GeV}/c$
- $0.2 \leq y \leq 0.8$
- $Q_{\text{max}}^2 = 0.1 (\text{GeV}/c)^2$
- $0.2 \leq z \leq 0.8$
- $10 \leq \theta \leq 120 \text{ mrad}$ (*i.e.* $2.38 \geq \eta \geq -0.1$ in the lepton-nucleon centre of mass system)
- CTEQ6M5 [52] for the parton distribution functions for the nucleon
- GRS [53] for the parton distribution functions of the photon
- DSS [54] for the fragmentation functions

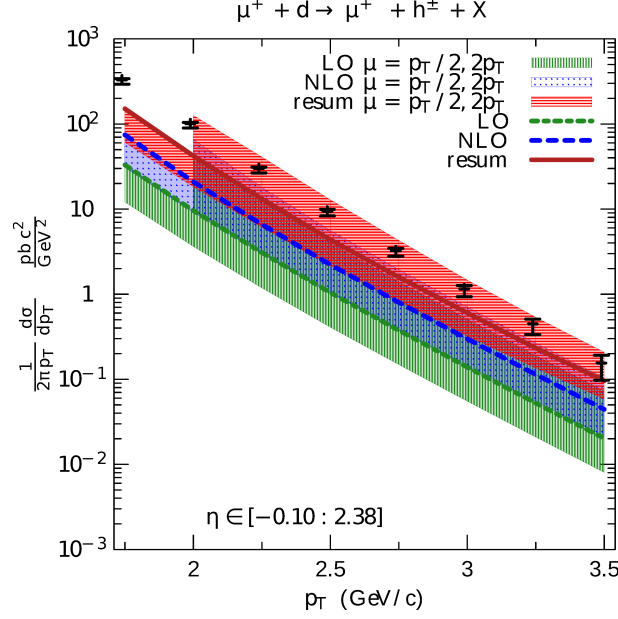


Figure 2.9: Comparison of the theoretical calculations and measured data, taken from Ref. [49]. Shaded areas represent the systematic errors. The error bars on the measured data are the square root of the quadratic sums of the statistic and the systematic uncertainties. And there is the 10 % normalisation uncertainty due to the luminosity determination.

The LO cross section is far below the data about a factor of 10. Even though NLO correction applied, which enhances by a factor of 2, there is still a sizeable difference. The resummed cross section agrees with the data within the (admittedly, large) systematic uncertainty.

The longitudinal double spin asymmetry is calculated using Eq. (2.89). As described above, cross sections can be split into direct and resolved part:

$$A_{LL} = \frac{d\Delta\sigma_{\text{direct}} + d\Delta\sigma_{\text{resolved}}}{d\sigma_{\text{direct}} + d\sigma_{\text{resolved}}}. \quad (2.114)$$

One can calculate A_{LL} with only changing polarised gluon distribution function. By integrating Δg over x_g at the given scale, ΔG is estimated. Then comparing χ^2 of the observed and the calculated A_{LL} , one can evaluate ΔG . This method is called single-inclusive hadron method and is named after the longitudinal double spin asymmetry for single-inclusive hadron production.

2.6. Accessing to gluon polarisation

In the previous section, A_{LL} method and its framework are discussed. In this section, ΔG analyses in COMPASS are described.

2.6.1. Photon Gluon Fusion

Direct measurements of the ΔG are based on the selection of pQCD processes where a gluon from a nucleon undergoes an interaction. In the lepton-nucleon scattering the interesting process is the Photon Gluon Fusion (PGF). Two methods to identify an event as the PGF

one are mostly employed: Open Charm Production and High- p_T Hadron Production. Comparing to both the methods, the single-inclusive hadron method is rather indirect since other subprocesses are considered altogether.

Open Charm Production Due to the large mass of the charm quark ($m_c = 1.5 \text{ GeV}/c^2$) its production via the fragmentation of light quarks as well as interaction of a virtual photon with an intrinsic charm quark in the nucleon is strongly suppressed. Therefore, it can be produced only in the hard scattering process. The PGF is the lowest order pQCD process where the charm quarks are produced. Thus, selection of charmed mesons in the final state suppresses completely other contributions to the cross section.

Spin-dependent cross section asymmetry for the $\gamma N \rightarrow c\bar{c}X$ process is related to the gluon polarisation in the following way:

$$A^{\text{experiment}} = (fP_b P_t) \times \frac{S}{S+B} A_{c\bar{c}}^{\mu N} + (fP_b P_t) \times \frac{B}{S+B} \hat{A}_{\text{bg}} \quad (2.115)$$

where P_b is the beam polarisation, P_t is the target polarisation, and f is the dilution factor accounting for the fraction of polarisable nucleons in the target material. The $\frac{S}{S+B}$ is another diluting factor with S and B being the number of signal and background events in the studied open charm sample. The background consists of those non-charm events that passed selections used to obtain the open charm sample. The resulting asymmetry \hat{A}^{BG} is assumed to be equal zero.

$A_{c\bar{c}}^{\mu N}$ is given by

$$A_{c\bar{c}}^{\mu N} = D \times A_{c\bar{c}}^{\gamma^* N} \approx D \times \langle \hat{a}_{LL}^{\gamma^* g} \rangle \frac{\Delta G}{G} (\langle x_g \rangle) \quad \text{with} \quad \hat{a}_{LL}^{\gamma^* g} = \frac{\Delta \hat{\sigma}_{\gamma^* g \rightarrow c\bar{c}}}{\hat{\sigma}_{\gamma^* g \rightarrow c\bar{c}}} \quad (2.116)$$

where D is the depolarisation factor defined in Eq. (2.45). The partonic cross section $\hat{\sigma}$ is calculated at LO [55]. Eqs. (2.115) and (2.116) allow one to extract $\Delta G/G$.

Similar to this LO extraction, the asymmetry via NLO extraction also can be defined as

$$A_{c\bar{c}}^{\mu N, \text{NLO}} = D \left(a_{LL}^{\gamma^* g} \frac{\Delta G}{G} + a_{LL}^{\gamma^* q} A_1 \right), \quad (2.117)$$

where

$$a_{LL}^{\gamma^* g} = \frac{\Delta \hat{\sigma}_{\gamma^* g \rightarrow c\bar{c}}^{\text{LO}} + \Delta \hat{\sigma}_{\gamma^* g \rightarrow c\bar{c}}^{\text{NLO}} + \Delta \hat{\sigma}_{\gamma^* g \rightarrow c\bar{c}g}^{\text{NLO}}}{\hat{\sigma}_{\gamma^* g \rightarrow c\bar{c}}^{\text{LO}} + \hat{\sigma}_{\gamma^* g \rightarrow c\bar{c}}^{\text{NLO}} + \hat{\sigma}_{\gamma^* g \rightarrow c\bar{c}g}^{\text{NLO}}}, \quad (2.118)$$

$$a_{LL}^{\gamma^* q} = \frac{\Delta \hat{\sigma}_{\gamma^* q \rightarrow c\bar{c}}^{\text{NLO}}}{\hat{\sigma}_{\gamma^* q \rightarrow c\bar{c}}^{\text{NLO}}}, \quad (2.119)$$

$$A_1 \approx \frac{g_1}{F_1} = \frac{\sum_q e_q^2 \Delta q}{\sum_q e_q^2 q}. \quad (2.120)$$

Eq. (2.115) is still valid in the NLO-QCD approximation. The only difference is that the signal S contains open charm mesons originating from non-PGF processes ($S = S^g + S^q$). The proper method to extract $\Delta G/G$ and A_{bg} simultaneously is discussed in Ref. [56].

The measurement of the gluon polarisation based on tagging of the PGF events via the charmed hadrons that contains charm quarks was for the first time implemented in the COMPASS experiment. Two main channels of the open charm production were considered. The first one is the channel with D^0 meson in the final state identified as a $K\pi$ pair of invariant mass in the mass window around known mass of D^0 . The second one is the channel with D^* meson that decays into D^0 and a slow pion. $D^*(2010)^+ \rightarrow D^0\pi_s^+ \rightarrow (K^-\pi^+, K^-\pi^+\pi^0, K^-\pi^+\pi^+\pi^-)\pi_s^+$ or $D^0 \rightarrow K^-\pi^+$ (the subscript “s” refers to “slow”).

Virtual photon cross section asymmetries, $A^{\gamma N \rightarrow D^0 X}$, and the gluon polarisation $\langle \Delta G/G \rangle$ are extracted from these open charm events. In LO, the result obtained from the data collected in 2002–2007 years with the polarised deuteron and proton target at COMPASS [19] is

$$\frac{\Delta G^{\text{LO}}}{G} = -0.06 \pm 0.21 (\text{stat.}) \pm 0.08 (\text{syst.}) \quad (2.121)$$

at the average fraction of nucleon momentum carried by the gluon $\langle x_G \rangle \approx 0.11$ and at average scale $\mu^2 \approx 13 (\text{GeV}/c)^2$. In the NLO analysis, the result is

$$\frac{\Delta G^{\text{NLO}}}{G} = -0.13 \pm 0.15 (\text{stat.}) \pm 0.15 (\text{syst.}) \quad (2.122)$$

at the scale $\mu^2 \approx 13 (\text{GeV}/c)^2$ and $\langle x_G \rangle \approx 0.20$. Details of the extraction of $\Delta G/G$ at NLO can be found in Refs. [56, 57].

High- p_T hadron production The method using open charm production is a clean method since there is no intrinsic charm quark in the nucleon in the COMPASS kinematics. A weak point, however, is quite lower statistics than the method using high- p_T hadron production to be described here.

A selection of high- p_T hadron pairs will result in a sample of events produced by perturbative processes, where mostly light quarks (u, d, and s) and gluons are involved. Thus in addition to the PGF, two other processes contribute to the cross section in the LO pQCD⁴. These are the Leading Process (LP, $\gamma + q \rightarrow q$) and QCD-Compton (QCDC, $\gamma + q \rightarrow q + g$) process. As all three processes contribute to the cross section the expression for the cross section spin asymmetry is following:

$$A^{\gamma N \rightarrow hhX} = A_{LL}^{2h} = R^{\text{PGF}} \langle \hat{a}_{LL}^{\text{PGF}} \rangle \frac{\Delta G}{G}(\bar{x}_G) + R^{\text{QCDC}} \langle \hat{a}_{LL}^{\text{QCDC}} \rangle A_1^{\text{LO}}(\bar{x}_c) + R^{\text{LP}} \langle \hat{a}_{LL}^{\text{LP}} \rangle A_1^{\text{LO}}(\bar{x}_{Bj}) \quad (2.123)$$

where x_c is the momentum fraction of parton in the QCDC process, \hat{a}_{LL}^i are the partonic cross section asymmetries⁵ for the given process i , R^i is the fraction of the process i , and $A_1^{\text{LO}} \equiv \sum_f e_f^2 \Delta q_f / \sum_f e_f^2 q_f$ is the photon-nucleon asymmetry at leading order. Moreover, \bar{x}_{Bj} , \bar{x}_c , and \bar{x}_G mean the average value of x_{Bj} , x_c , and x_G in the sample, respectively.

There are two possibilities to estimate A_1^{LO} . The first one is to use the parameters of unpolarised and polarised quark distribution functions evaluated from the global analyses. The

⁴That is, indeed, the weakness of this method.

⁵also called as *analysing power*.

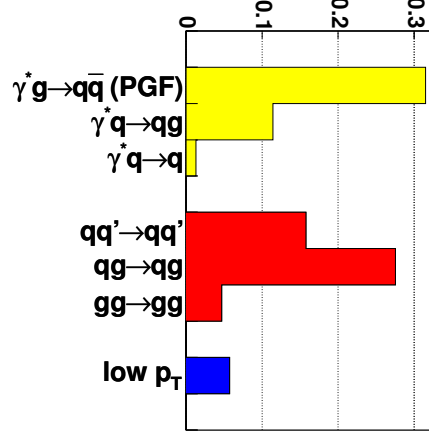


Figure 2.10: Ratios of the various PYTHIA subprocesses in the final high- p_T sample [16]. PGF process contributes approximately 30%. The second highest contribution is the resolved photon process $qg \rightarrow qq$.

second option is to use directly the inclusive measured asymmetry A_1 . The second option was selected in the latest analyses since for the determination of PDFs assumptions on the shape of ΔG and G as a function of x are needed and this could lead to a bias of extracted $\Delta G/G$.

First of all, it was assumed that the inclusive measured asymmetry $A_{LL}^{\text{incl.}} \approx DA_1$ contains only the LP contribution. With such assumption, one can obtain A_1 at LO as

$$A_1^{\text{LO}} \equiv \frac{\sum_f e_f^2 \Delta q_f}{\sum_f e_f^2 q_f} \approx A_1. \quad (2.124)$$

Thus, the equation for A_{LL}^{2h} can be re-written as

$$A_{LL}^{2h} \approx R^{\text{PGF}} \langle \hat{a}_{LL}^{\text{PGF}} \rangle \frac{\Delta G}{G}(\bar{x}_G) + R^{\text{QCDC}} \langle \hat{a}_{LL}^{\text{QCDC}} \rangle A_1(\bar{x}_C) + R^{\text{LP}} \langle \hat{a}_{LL}^{\text{LP}} \rangle A_1(\bar{x}_{Bj}). \quad (2.125)$$

Similar to Eq. (2.125), the inclusive asymmetry can be decomposed as

$$\begin{aligned} A_1(x_{Bj}) &\approx A_{LL}^{\text{incl.}}(x_{Bj}) \\ &= R^{\text{PGF, incl.}} \langle \hat{a}_{LL}^{\text{PGF, incl.}} \rangle \frac{\Delta G}{G}(\bar{x}_G) \\ &\quad + R^{\text{QCDC, incl.}} \langle \hat{a}_{LL}^{\text{QCDC, incl.}} \rangle A_1^{\text{LO}}(\bar{x}_C) \\ &\quad + R^{\text{LP, incl.}} \langle \hat{a}_{LL}^{\text{LP, incl.}} \rangle A_1^{\text{LO}}(\bar{x}_{Bj}). \end{aligned} \quad (2.126)$$

$$(2.127)$$

The superscript “incl.” emphasises the fact that the kinematic phase space is different from A_{LL}^{2h} case.

Eq. (2.127) can be re-written for $A_1(x_{Bj})$ and $A_1(x_C)$ with the fact $D = \hat{a}_{LL}^{\text{LP, incl.}}$ and introduce the equation for A_1 measured at $\bar{x}_{Bj} = \bar{x}_C$,

$$A_1(x_{Bj}) = A_1^{\text{LO}}(\bar{x}_{Bj})R^{\text{LP, incl.}} + A_1^{\text{LO}}(\bar{x}_C)R^{\text{QCDC, incl.}} \frac{\langle \hat{a}_{LL}^{\text{QCDC, incl.}} \rangle}{D} + \frac{\Delta G}{G}(\bar{x}_G)R^{\text{PGF, incl.}} \frac{\langle \hat{a}_{LL}^{\text{PGF, incl.}} \rangle}{D}, \quad (2.128)$$

$$A_1(x_C) = A_1^{\text{LO}}(\bar{x}_C)R^{\text{LP, incl.}} + A_1^{\text{LO}}(\bar{x}'_C)R^{\text{QCDC, incl.}} \frac{\langle \hat{a}_{LL}^{\text{QCDC, incl.}} \rangle}{D} + \frac{\Delta G}{G}(\bar{x}'_G)R^{\text{PGF, incl.}} \frac{\langle \hat{a}_{LL}^{\text{PGF, incl.}} \rangle}{D}. \quad (2.129)$$

with x'_C and x'_G being fractions of nucleon momentum carried by the struck parton for sample measured at $\bar{x}_{Bj} = \bar{x}_C$.

Now one has three equations (Eqs. (2.125), (2.128), and (2.129)) and three unknown variables ($\Delta G/G$, $A_1^{\text{LO}}(x_{Bj})$, and $A_1^{\text{LO}}(x_C)$). After combining the equations and neglecting small terms (the fractions R^{PGF} and R^{QCDC} are much smaller for the inclusive sample than for the high- p_T sample), the formula for A_{LL}^{2h} leads

$$A_{LL}^{2h} = R^{\text{PGF}} \langle \hat{a}_{LL}^{\text{PGF}} \rangle \frac{\Delta G}{G}(\bar{x}_G) \quad (2.130)$$

$$+ \frac{R^{\text{LP}}}{R^{\text{LP, incl.}}} D \left(A_1(\bar{x}_{Bj}) - A_1(\bar{x}_C) \frac{\langle \hat{a}_{LL}^{\text{QCDC}} \rangle}{D} \frac{R^{\text{QCDC, incl.}}}{R^{\text{LP, incl.}}} - R^{\text{PGF, incl.}} \frac{\Delta G}{G}(\bar{x}_G) \right) \quad (2.131)$$

$$+ \frac{R^{\text{QCDC}}}{R^{\text{LP, incl.}}} \langle \hat{a}_{LL}^{\text{QCDC}} \rangle \left(A_1(\bar{x}_C) - A_1(\bar{x}'_C) \frac{\langle \hat{a}_{LL}^{\text{QCDC}} \rangle}{D} \frac{R^{\text{QCDC, incl.}}}{R^{\text{LP, incl.}}} - R^{\text{PGF, incl.}} \frac{\Delta G}{G}(\bar{x}'_G) \right). \quad (2.132)$$

Since the terms $\Delta G/G$ are present in Eq. (2.132) at two different x_G values (denoted as x_G and x'_G), the extraction of $\Delta G/G$ requires a new definition of average x_G . The final formula for the gluon polarisation reads now

$$\frac{\Delta G}{G}(x_G^{\text{avg.}}) = \frac{A_{LL}^{2h}(\bar{x}) - A^{\text{corr.}}}{\lambda}, \quad (2.133)$$

$$A^{\text{corr.}} = A_1(\bar{x}_{Bj})D \frac{R^{\text{LP}}}{R^{\text{LP, incl.}}} + A_1(\bar{x}_C)\beta_1 + A_1(\bar{x}'_C)\beta_2 \quad (2.134)$$

Details can be found in Ref. [58]. The \bar{x}'_C is assumed to be equal to \bar{x}_C . A possible impact of \bar{x}'_C being different from \bar{x}_C is taken into account in the systematic error estimation. All the input variables like \hat{a}_{LL} or R are estimated using Neural Networks. In order not to introduce a bias in $\Delta G/G$ extraction, one has to take into account the fact that the average x and y are different for inclusive and high- p_T samples. In case of a proposed weighted method of $\Delta G/G$ extraction this requirement is automatically fulfilled since the fractions and analysing powers are estimated on the event-by-event basis.

Recently, a new method is developed, namely *all- p_T* method [59, 60]. This method is originated in high- p_T method and asymmetries are simultaneously extracted in order to reduce or eliminate a few systematic sources presented in the high- p_T analyses. The simultaneous extraction of asymmetries has been already introduced in the COMPASS open-charm analysis [19].

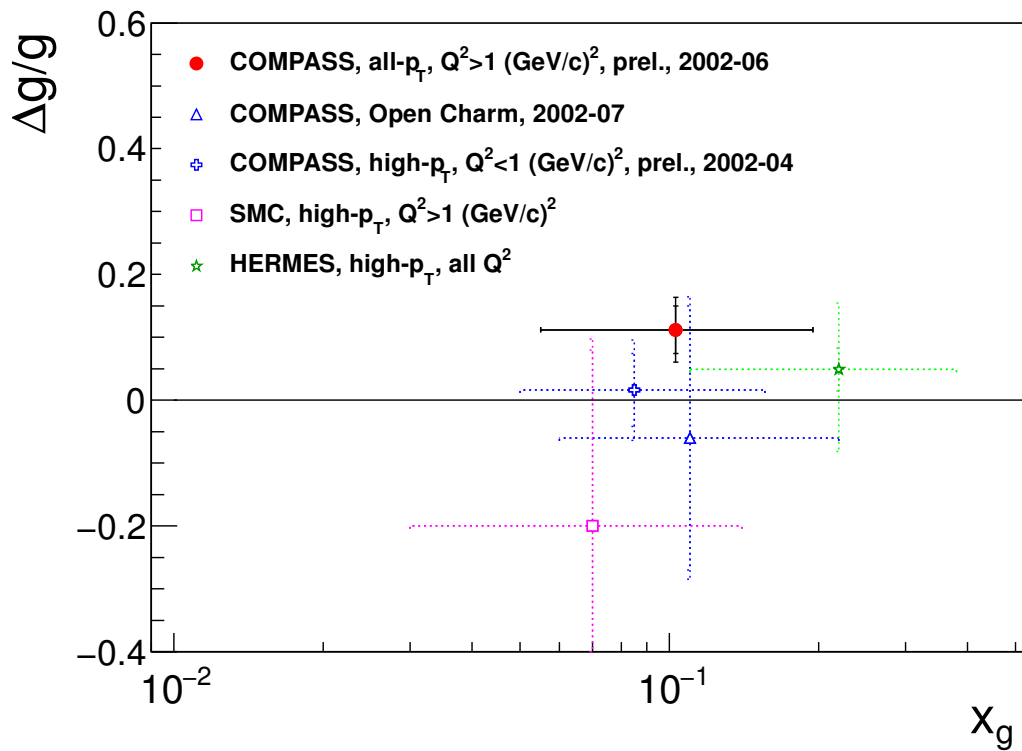


Figure 2.11: Gluon polarisations obtained at LO accuracy, in COMPASS [17, 19], SMC [61], and HERMES [62] as a function of x_g , taken from Ref. [59]. The data point with a closed red circle is the latest result of COMPASS.

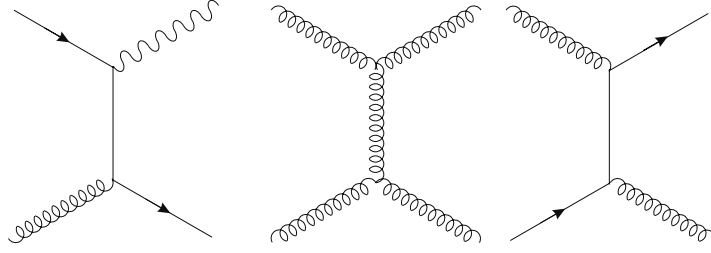


Figure 2.12: Selected lowest-order Feynman diagrams for elementary processes with gluons in the initial state in p - p collisions: quark-gluon Compton process with prompt photon production (*left*), gluon-gluon (*centre*), and gluon-quark (*right*) scattering for jet production [66].

The global gluon polarisation results are shown in Fig. 2.11. Gluon polarisations are either positive or negative with large uncertainties. $\langle x_g \rangle$ range is also limited around $\langle x_g \rangle \approx 0.1$. The latest COMPASS result shows a clear positive data with smaller uncertainty, indicating the positive gluon polarisation.

2.6.2. Proton-Proton scattering

Studies of the polarised proton-proton scattering are performed at Brookhaven National Laboratory (U.S.A.) by experiments at the RHIC accelerator [63], STAR [64] and PHENIX [65]. Polarised proton beams collide at the centre of mass energy $\sqrt{s} = 200$ GeV, which was upgraded to 500 GeV from 2009 and to 510 GeV from 2012. Extraction of the gluon polarisation in the proton-proton interactions is performed using the processes shown in Fig. 2.12. The leftmost diagram presents a prompt photon production while the two others show the jet production processes. The main advantage of the studies performed with pp interactions is that they provide a large number of events with gluon interactions, a disadvantage is a sizable background. As an example, for the prompt photon channel the background comes mostly from the decay of $\pi^0 \rightarrow \gamma\gamma$, while for the jet channels from the quark-quark interactions.

The protons are polarised at the polarised proton source. After passing the 3-step acceleration, they are injected and then accelerated in the two rings of the RHIC. The proton spin orientations inside the rings are usually vertical. However, before the interaction the spins are rotated to the longitudinal direction. To overcome the protons depolarisation during the acceleration dedicated superconducting magnets called Siberian Snakes [67] that are installed on the accelerator ring. The magnetic field in the Snakes flips the protons spins leading to compensation of the depolarisation effects. The beam polarisation of the proton beam has been improved over the years; 45 % in 2004, and 56 % in 2009.

STAR is a detector that is optimised for the charged particles tracking and identification. It is also well suited for the jet reconstruction. PHENIX specialises in the lepton and photon registration and has an excellent capability to detect π^0 's in the mid-rapidity region.

For a selected final state, the observable measured in the experiment is the cross section asymmetry for parallel (σ^{++}) and antiparallel (σ^{+-}) directions of the two proton beam polarisations

$$A_{LL}^{\text{experiment}} = \frac{1}{P_1 P_2} \frac{\sigma^{++} - \sigma^{+-}}{\sigma^{++} + \sigma^{+-}}, \quad (2.135)$$

where P_1 and P_2 are the beams polarisations.

The A_{LL}^q cross section asymmetry for a given partonic reaction q can be expressed in the LO pQCD as

$$A_{LL}^q = \frac{\Delta q_1}{q_1} \frac{\Delta q_2}{q_2} \hat{a}_{LL}^i . \quad (2.136)$$

The $\Delta q/q$ factors are the ratios of the spin dependent to spin-averaged parton density functions. When in the process there is a gluon interaction, corresponding $\Delta q/q$ equals to $\Delta G/G$. The parton density functions are obtained from the QCD fits to the results of DIS experiments. The partonic cross section asymmetry \hat{a}_{LL}^i can be calculated for each process in pQCD.

The experimental asymmetry $A_{LL}^{\text{experiment}}$ is a sum of all A_{LL}^i , for reactions leading to a given final hadronic state. The asymmetries in the sum should be taken with weights corresponding to a fraction of a particular reaction in the studied sample. Disentangling the $\Delta G/G$ from this sum is a complex and challenging task. Therefore, another method was elaborated. Different scenarios of ΔG distribution are assumed and the corresponding expected experimental double spin asymmetries for a production of a given final state are calculated. They are then compared to the data.

In Fig. 2.13, selected results of the measured A_{LL} asymmetries as a function of p_T from PHENIX and STAR are compared to various theoretical predictions. The curves correspond to theoretical predictions obtained for different parametrisations of $\Delta G(x_g)$, resulting in different values of the first moment of Δg . PHENIX collaboration released the result $\Delta g(x_g)|_{0.05}^{0.2} = 0.06_{-0.15}^{+0.11}$ [68] using asymmetries for productions of π^0 and η in the range $0.05 < x < 0.2$. STAR collaboration published the longitudinal double spin asymmetries A_{LL} for the jet production, which provide evidence at the 3σ level for positive gluon polarisation in the x_g region $x_g > 0.05$ [69].

Traditionally, in COMPASS the gluon polarisation analyses are performed by using either the High- p_T or the Open Charm method. Both the method has large biases to extract ΔG , resulting in large uncertainties. In order to reduce biases, the method used in the RHIC experiments is introduced to the COMPASS analysis.

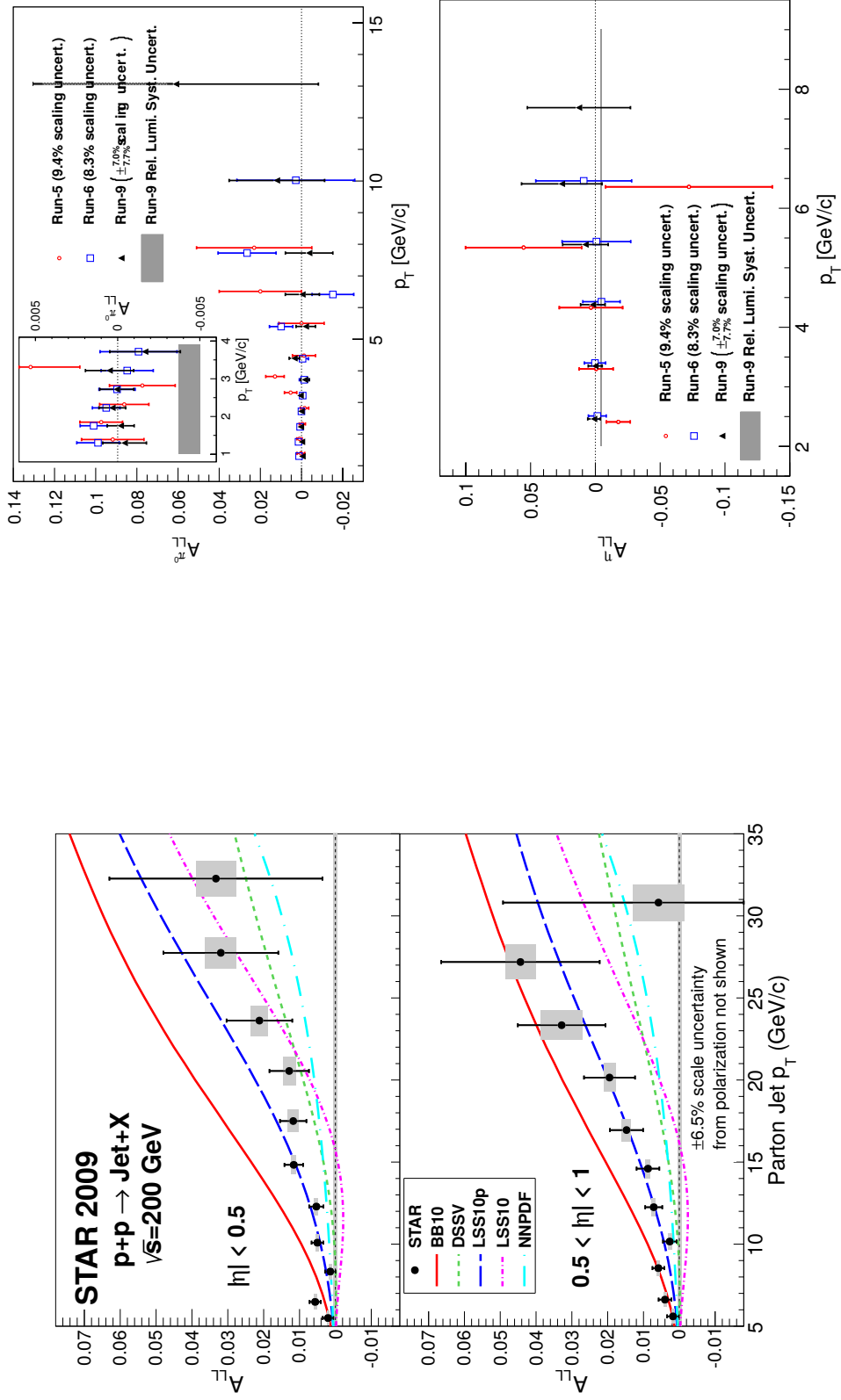


Figure 2.13: A_{LL} measured by STAR (left) and PHENIX (right) at RHIC [68, 69].

Table 3.1: A summary of COMPASS data taking

Year	Target	E_{beam}	Detail
2002	${}^6\text{LiD}$	160	Longitudinal/transverse mode
2003	${}^6\text{LiD}$	160	Longitudinal/transverse mode
2004	${}^6\text{LiD}$	160	Longitudinal/transverse mode
2005			Shutdown & upgrade
2006	${}^6\text{LiD}$	160	Longitudinal mode
2007	NH_3	160	Longitudinal/transverse mode
2008			Hadron physics
2009			Hadron physics
2010	NH_3	160	Transverse mode
2011	NH_3	200	Longitudinal mode
2012	Solid material, Liq. H_2		Hadron physics, DVCS test run, and SIDIS
2013			Shutdown & upgrade
2014	NH_3	190	Drell-Yan
2015	NH_3	190	Drell-Yan
2016	Liq. H_2		DVCS
2017	Liq. H_2		DVCS

3. COMPASS setup

COMPASS experiment has been studying the nucleon structure at CERN in Switzerland and France. CERN approved the COMPASS experiment in 1998 and a technical run was performed in 2001. Since 2002 data taking has been performed. COMPASS updated their apparatuses during the shutdown of the accelerators in 2005. After the shutdown of the accelerators, COMPASS-II started with new physics programmes to explore nucleon structure in 2014 [70].

CERN SPS accelerator can deliver two kinds of beams: muon and hadron. With the hadron beam, COMPASS has studied three issues: (1) physics of charmed hadrons (2) spectroscopy of light quark systems and glueballs, and (3) an investigation of the hadron structure of unstable particles using Primakoff reactions. COMPASS has also studied issues with the muon beam: (1) measurement of gluon polarisation, (2) measurements of structure functions for the proton and neutron, (3) measurements of $\Lambda(\bar{\Lambda})$ polarisation, and (4) studies of transverse spin distribution functions [71].

The measurement of gluon polarisation is the flagship measurement in COMPASS since the contribution of quarks' polarisation was obtained at that time by the SMC experiment and other experiments. It was thought that quite a large gluon polarisation via the axial anomaly masked the quark spin contributions and explained its smallness [10]. Data were taken from 2002 to 2004 and 2006 to 2012 in COMPASS. The experimental setup can be varied for the various proposed physics programmes. The spectrometers also are updated and improved year by year. The summary of data taking is shown in Tab. 3.1.

There are two kinds of targets: polarised and unpolarised fixed targets. The unpolarised solid targets, which are made of metals such as Pb, Ni, etc. and liquid hydrogen target, are used for the hadron spectroscopy with the hadron beam.

For the muon beam program, two kinds of materials are used as the polarised target, which is

described in Sec. 3.2 in detail. The spin direction of the polarised target is either longitudinal or transverse. In the longitudinal spin mode, the spin direction is parallel or anti-parallel to the beam polarisation direction. In contrast, the polarisation direction of the transverse spin mode is perpendicular to the beam direction.

COMPASS reference system The official COMPASS reference system is defined as follows and is shown in Fig. 3.1.

Z-axis the nominal beam direction

X-axis the direction pointing to the left side facing to the Z-axis

Y-axis the vertical direction pointing upwards

ϕ the azimuthal angle ($-\pi < \phi < \pi$)

θ the polar angle ($-\pi < \theta < \pi$)

There are also special frames for detectors and wires of wire chambers.

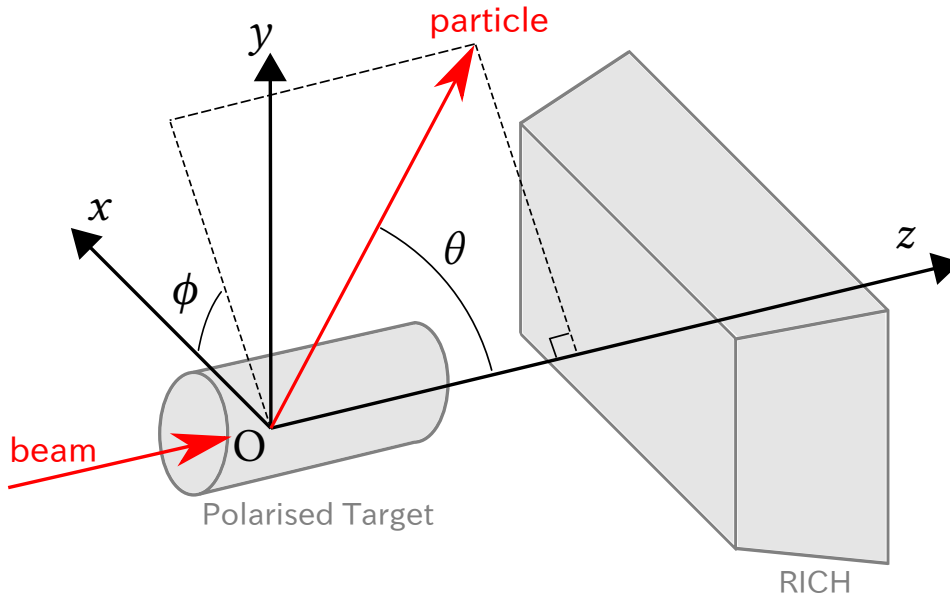


Figure 3.1: COMPASS reference system. The origin O is defined inside the polarised target. The topviews of the COMPASS setup are shown in Fig. 3.9 and details are described in Sec. 3.3.

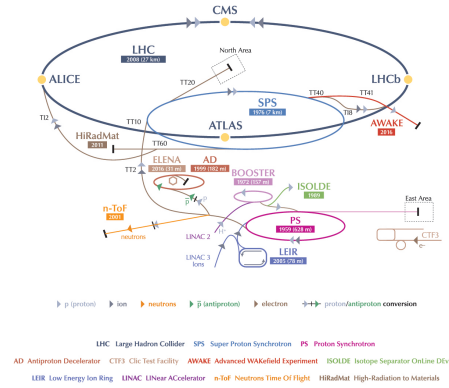
3.1. Beam

The polarised muon beam is provided by CERN SPS facility, which is able to provide high-intensity positively charged muon beam, high intensity hadron (mainly proton or pion, positive or negative) beams and lower-intensity negative muon beam. Normally, the positive muon beam is employed for the muon program. On the other hand, the negative beam is used for special data taking [72]. The data to be analysed in this thesis were taken with the positive muon beam.

A proton beam accelerated by the PS and the SPS up to 400 GeV/c (see Fig. 3.2b) impinges on a Beryllium target with 500 mm thickness. Created pions with up to 225 GeV/c are transported along a 600 m path, in which pions decay into muons and muon neutrinos. On the other hand, other hadrons are absorbed by nine movable absorbers made of Beryllium. Due to the parity violation of the pion decay, the muon is naturally polarised. The muon polarisation depends on the ratio of the muon momentum to the pion one. As the ratio is 0.57 the polarisation is 100 %, whereas the polarisation is -100 % with the ratio 1. Basically one can compute the beam polarisation analytically using the pion beam momentum. As the pion beam contains other hadron components, however, a tiny correction is required. The achieved polarisation of the positive muon is $(80 \pm 4)\%$ [35, 73]. This corresponds to the ratio 0.92, in 2004 run and the muon flux was 2×10^8 per SPS cycle due to the guidelines of radiation protection. The spot size at the COMPASS target is $8 \text{ mm} \times 8 \text{ mm}$ ($\sigma_x \times \sigma_y$).



(a) Aerial View of the CERN
© CERN/used under CC BY SA.



(b) The CERN accelerator complex © CERN.

Figure 3.2: CERN aerial view and accelerator complex

The measurement of muon momentum is done by Beam Momentum Station (BMS). BMS consists of six detectors and four of them (BM01–BM04) has been used in the EMC experiment and are scintillator hodoscopes with horizontal strips. Each hodoscope is made up of 64 elements with 5 mm height and 20 mm length along the beam. In the central region, the strips are horizontally divided into several elements for the muon flux not to exceed $1 \times 10^7 \text{ s}^{-1}$ at maximum. Remaining two detectors (BM05 and BM06), which are scintillating fibre hodoscopes, were added to deal with the high beam intensity and the multiple-hit environment. This increases the overall beam detection efficiency.

The simulation of beam tracks has been carried out to parameterise the momentum dependence of the track coordinates in these six detectors. These parameters are used to calculate the momentum of each muon track within 1 % precision. The reconstruction efficiency is approximately 93 %. The efficiency and purity of BMS are further improved by the information of tracking detectors located in front of the target. The extrapolated track and actual BMS hits are used to select among beam track candidates. If there are not enough hits to reconstruct the momentum, a rescue algorithm is used.

The hadron beams are provided by moving nine absorbers out of the beam axis and loading the configuration for the beam optics. Up to 225 GeV/c, the beamline operation is same as one

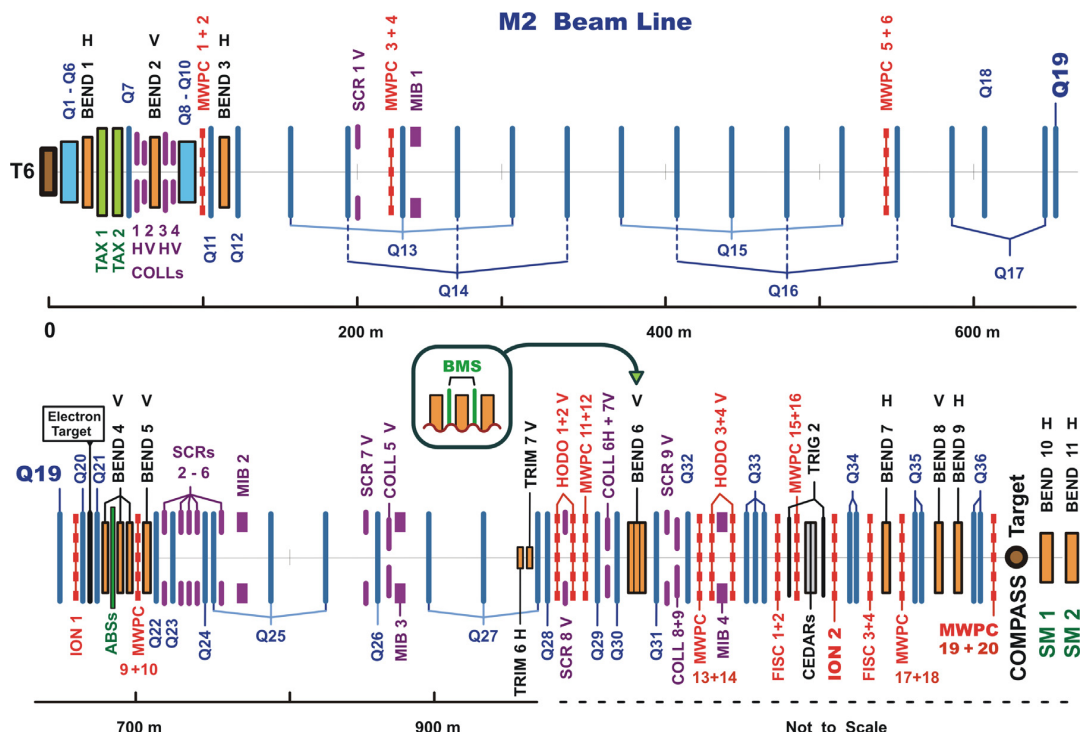


Figure 3.3: A schematic view of CERN SPS M2 beam line [70].

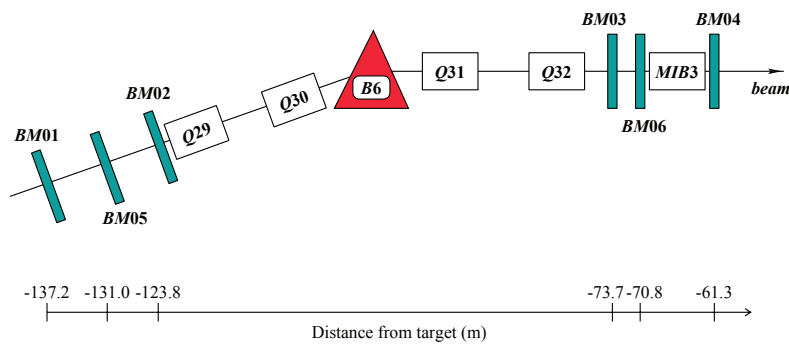
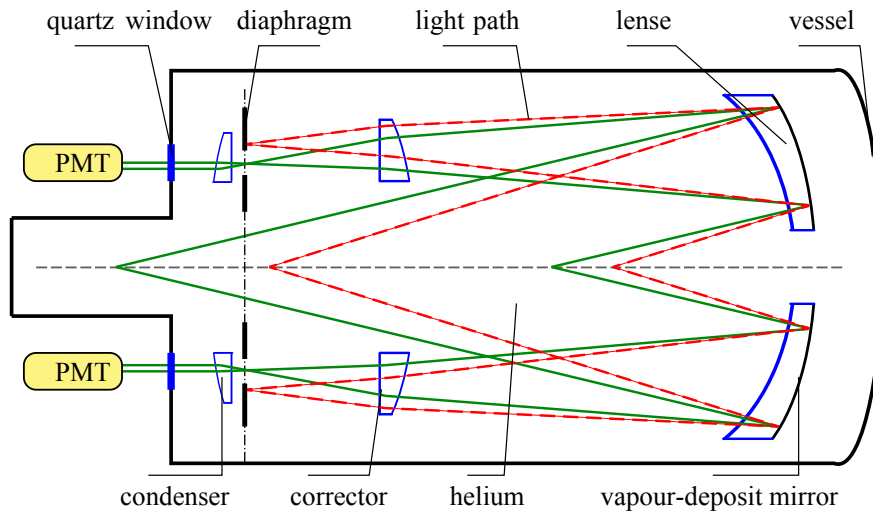


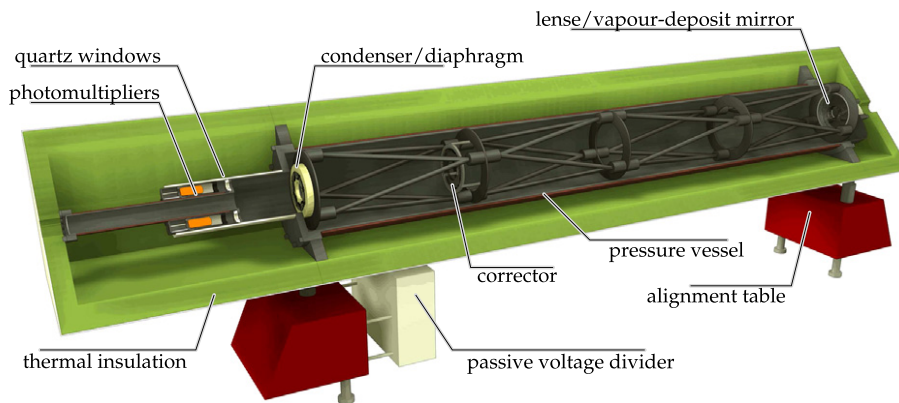
Figure 3.4: Layout of the beam momentum station for the COMPASS muon beam [15].

for the muon beam. By using different optics, 280 GeV/c hadron beam is available. The hadron beam contains several types of hadron: pion, kaon, proton, etc.

For identifying each particle, Čerenkov Differential with Achromatic Ring focus (CEDAR) is employed, which make use of Cherenkov radiation. Two particles with the same momentum and different masses radiate Cherenkov lights at different angles, making rings with different radii. Two CEDAR detectors are installed 30 m before the COMPASS target region. They were designed to provide fast beam particle identification at high rates for particle momenta up to 300 GeV/c [74].



(a) The basic principle of a CEDAR counter. Two particles with the same momentum but with different masses (here full and dashed lines) radiate Cherenkov photons at different angles, resulting in rings with different radii. A diaphragm selects the rings from the required particle type [70].



(b) A cut through one of the CEDAR detectors.

Figure 3.5: the COMPASS CEDAR detector [70].

Negative beams are mainly composed of pions while for momenta larger than 150 GeV/c the positive beam have a dominant proton component. In both cases, kaons and electrons may be present at a level of a few percent, depending on the energy chosen. For example, the positive hadron beam with 190 GeV/c momenta consists of 24 % of pion, 1.4 % of kaon, and

74.6 % proton, whereas the negative one with 190 GeV/ c momenta is composed of 96.8 % of pion, 2.4 % of kaon, and 0.8 % of antiproton.

For the purpose of the calibration of electromagnetic calorimeters, the 40 GeV/ c electron beam can be provided. 100 GeV/ c negative hadron beam contains electrons at about 10 %. A 5 mm thick lead plate, which is equivalent to 90 % of a radiation length, is moved into the beam-line. By the lead plate, hadrons are absorbed, and electrons deposit energy about 60 GeV/ c . The electron flux is a few thousands per spill.

3.2. Target

One of unique aspects in the COMPASS experiment is the polarised target. The polarised target system mainly consists of a dilution refrigerator and a magnet. With high magnetic field and extremely low temperature, the spin direction of the nucleon aligns to the direction of magnetic field. The polarisation of electron reaches almost 100 % at 1 K and 1 T. On the other hand, nucleon has only 0.1 % under the same condition. Thus, Dynamic Nuclear Polarisation (DNP) [75] technique is used, which requires microwave field and the material containing free radicals in order to obtain high polarisation of the nucleon. The density of free radicals is of the order of 10^{-4} – 10^{-3} per nucleus. The polarisation of electron is transferred to the nucleon polarisation by the microwave field.

The COMPASS polarised target system is the largest system in the world: the target volume is about 1000 cm³, and the diameter of the solenoid magnet is about 1 m. The side views of the target systems are shown in Fig. 3.6.

The observed asymmetry is the physical asymmetry multiplied by the beam polarisation, the target polarisation and a dilution factor. The dilution factor is the ratio of the number of the polarisable nucleons in the target to the number of all nucleons in the target. The polarisation and dilution factor of the target are essential parameters to the statistical significance of the asymmetry. Material ⁶LiD is used for the deuteron target, of which system is considered as ⁴He + ²D. Thus the dilution factor becomes 50 % in naïve picture and the deuteron polarisation is 50 %.

For the proton target, NH₃ is employed. Its polarisation is about 90 %, however, the dilution factor is 0.18 in naïve picture. The actual dilution factors depend on the kinematics, and are typically 0.4 for ⁶LiD and 0.16 for NH₃ (see Sec. 4.4 in detail).

Dilution cryostat In order to achieve low temperature below 1 K for large volume (≈ 1 cm³) under external heat by the beam, a ³He/⁴He dilution refrigerator is employed. It can achieve high cooling power and maintain temperatures between 100 m K to 300 m K when the electron spins absorb microwave powers of 40 mW to 400 mW during the polarisation build-up [76].

The cryostat is placed in upstream side vertically, and is filled with liquid helium from the gas/liquid phase separator in Fig. 3.6a. The cold gas from the separator cools down the outer and inner vertical and horizontal thermal screens around the dilution refrigerator at nominal temperatures of 80 K and 4 K, respectively. The incoming ³He gas is also cooled with the cold gas from the separator. Three needle valves control ⁴He flow to fill the ⁴He evaporator with the liquid helium and to cool the microwave cavity. Two needle valves control ³He flow to optimise the target temperature and the cooling power. The nominal operation temperatures of the cavity and the ⁴He evaporator are 3 K and 1.5 K, respectively.

Magnet Not only low temperature but also strong and homogeneous magnetic field is mandatory to achieve the high polarisation. A superconducting solenoid magnet producing 2.5 T magnetic field along the beam direction is employed. Until 2004, the magnet used at the SMC experiment was employed, which is referred as SMC magnet in this thesis. 10 or more correction coils are mounted to give an axial homogeneity better than 20 ppm in a volume 1500 mm long, and 50 mm in diameter [77]. The transverse holding field of 0.42 T, which is used for the transverse spin measurements, is produced by a superconducting dipole coil and deviates at most by 10 % from its nominal value inside the target volume. To reduce systematic effects, the magnetic field is reversed periodically⁶ during measurements, which is called “field rotation” or “spin reversal”. The magnet system automatically operated, making the spin reversal in about 33 min [78].

In 2005, the target system was completely replaced with new one, which was originally designed in the COMPASS proposal. The new solenoid magnet, which is called Oxford (OD) magnet, has the acceptance ± 180 mrad. Comparing to the SMC magnet, the acceptance is twice or more larger due to the large bore diameter. The relative intrinsic field uniformity was tuned to within $\pm 3 \times 10^{-5}$ over the useful volume of the target cells (130 cm total length, $\varnothing 4$ cm). A fully automated control system for the handling of the cryogenics and a fast safety system designed to trigger the heaters in case of a quench were implemented. After installing the magnet in its final position in the COMPASS hall, new optimisations of the shim coil currents were performed to account for the presence of the large SM1 dipole magnet yoke. A final relative field uniformity of $\pm 4 \times 10^{-5}$ was achieved, valid for operation at both field orientations. A dipole coil of OD magnet generates 0.6 T field.

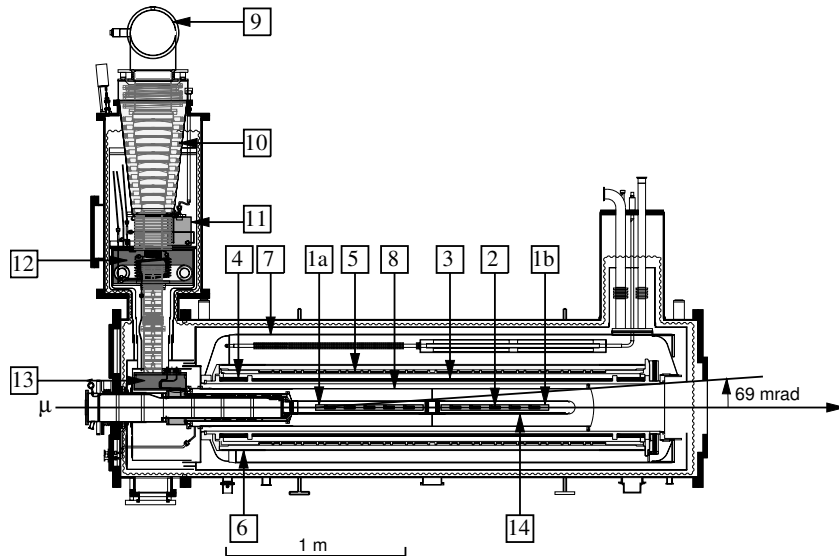
Further upgrades of the OD magnet was performed in 2013 for the COMPASS-II Drell-Yan measurement. A repair of the trim coil (G2), an exchange of current leads which are used in the LHC superconducting magnet, and an installation of a power source and its control system which are also employed by the LHC were the most important tasks. Upgrades on the cryogenics of the magnet system were also performed: an enlargement of a contact surface to improve heat exchange by liquid nitrogen, an installation of the cryocooler, an exchange of conducting wires having low thermal conductivity, etc.

Target cells There are two cells called the upstream cell and the downstream cell, whose length is 60 cm each. There is a 10 cm gap between the cells and a microwave stopper is placed there. The cells are polarised in opposite direction each other. The microwave cavity surrounds the target cells.

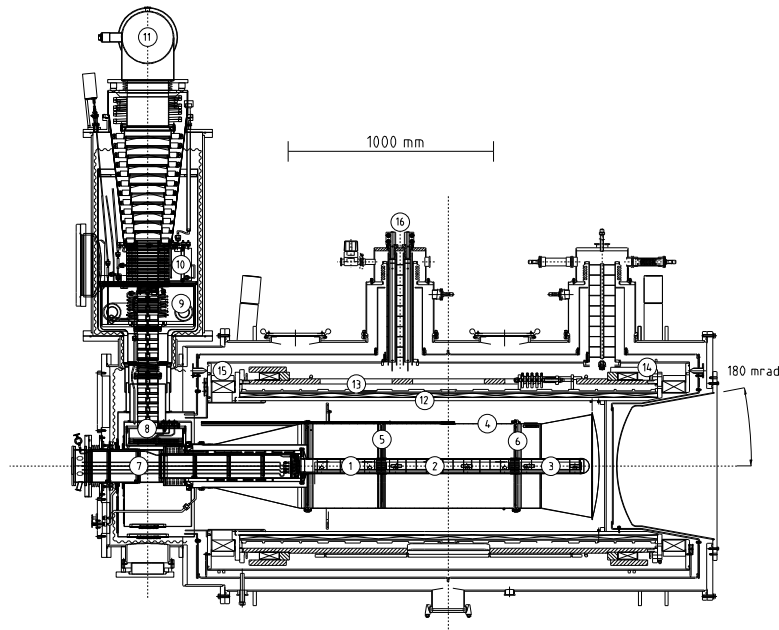
Since 2006, the target cell was upgraded from two cells to three cells: the longer (60 cm) cell in the centre and the two shorter (30 cm) cells in the outer. The direction of polarisation for the central cell is always opposite to the ones for two outer cells. The field rotation, which is performed every 8 hours, could largely reduce a false asymmetry originating from the variation of the spectrometer acceptance.

Microwave system The target material is polarised via DNP, obtained by irradiating the paramagnetic centres with microwaves at frequencies of 70.2 GHz to 70.3 GHz at 2.5 T and a temperature of about 200 mK. The microwave field is generated with two Extended Interaction Oscillator (EIO) tubes. An additional modulation of the microwave frequency of about 5 MHz

⁶every 8 hours, every half a day, or every several weeks. This depends on year-by-year.



(a) Side view of the polarised target in the COMPASS SMC magnet having used until 2004: (1a) upstream target cell, (1b) downstream target cell, (2) 10 NMR coils inside target material, (3) solenoid coil, (4) compensation coil, (5) 16 correction coils, (6) dipole coil, (7) liquid helium vessel for the magnet, (8) microwave cavity, (9) ^3He pumping port, (10) ^3He pre-cooler, (11) separator, (12) evaporator, (13) sill, and (14) mixing chamber. The two halves of the microwave cavity are separated by a thin microwave stopper [79].



(b) Side view of the polarised target in the COMPASS OD magnet having used since 2006: (1) upstream target cell, (2) midstream target cell, (3) downstream target cell, (4) microwave cavity, (5) upstream microwave stopper, (6) downstream microwave stopper, (7) target holder, (8) still or ^3He evaporator, (9) ^4He evaporator, (10) ^4He liquid/gas separator, (11) ^3He pumping port, (12) solenoid coil, (13) correction coils, (14) dipole coil, (15) solenoid compensation coil, and (16) magnet current leads [80].

Figure 3.6: Side views of the COMPASS polarised target system with SMC and OD magnet. The muon beam traverses from left to right.

helps to enhance the polarisation. A deuteron polarisation $|P_t| > 40\%$ is reached within 24 hours in a 2.5 T field with a ^3He flow of 80 mmol/s to 120 mmol/s in the dilution refrigerator.

NMR system The polarisation of the target is measured by NMR [81]. There are five NMR coils in the each target cell for the two cells system and three and four coils in the upstream and downstream cells, and the midstream cell for the three cells system. The coils are made of the Cu – Ni tube with wall thickness of 0.1 mm to reduce extra material in the target and are placed on the outer surface of the target cells.

Since the integral of an NMR signal, *i.e.* *area* is proportional to the target polarisation at thermal equilibrium (TE), the enhanced polarisation by DNP P_e is obtained by the measured area:

$$P_e = C \times \frac{P_{\text{TE}}}{A_{\text{TE}}} \times A_{\text{DNP}} \quad (3.1)$$

where C is the correction factor taking the different TE calibration results for the two magnetic field directions into account, A_{TE} is the area at TE at known temperature around 1 K with the polarisation P_{TE} , and A_{DNP} is the areunit at DNP. Since the TE signals of the deuteron and the proton with about 0.05 % and 0.1 % polarisation at 1 K are small, A_{TE} have large uncertainty. Therefore, the area is evaluated as a function of the inverse of the temperature by measuring the NMR TE signals at several temperature and fitting with a linear function.

The uncertainty of the target polarisation is summarised in Ref. [81]. The main source is the TE calibration about 90 %. This is due to uncertainties of the temperature measurement, the fitting with a linear function, the fitting to the background NMR signal. The other contributions are the field polarity due to the field rotation, the NMR signal shifting, the signal skew, hardware nonlinearity, etc.

Field rotation The maximum polarisation difference between the upstream and downstream cells $|P_{t,\text{up}} - P_{t,\text{down}}| > 100\%$ is reached in five days. The proton polarisations $|P_t| > 90\%$ are reached in 36 hours with continuous microwave pumping. The frequency modulation that clearly helps in building polarisation in ^6LiD has only small about 2 % effect to the final polarisation value of deuteron.

A microwave frequency f_+ , which enhances the positive polarisation via DNP, is irradiated in a upstream cell. On the other hand, a microwave frequency f_- , which enhances the negative polarisation, is irradiated in a downstream cell. Whenever field rotation is performed, the polarisation in the upstream cell is always positive; in the downstream cell, it is negative. Thus this could be the one of sources for the systematic uncertainty. In order to reduce possible origins of the uncertainty, microwave reversal that swaps microwave frequencies among target cells is performed once or twice in a data taking year.

The schematic picture of filed rotation and microwave reversal is shown in Fig. 3.7. This clearly indicates that only field rotation is not sufficient to eliminate systematic effects since microwave frequencies are unchanged during field rotation.

3.3. Spectrometers

An overview and topviews of the COMPASS setup are depicted in Figs. 3.8, 3.9a, and 3.9b. The aims of setup are large angle and momentum acceptance, precise kinematic reconstruct-

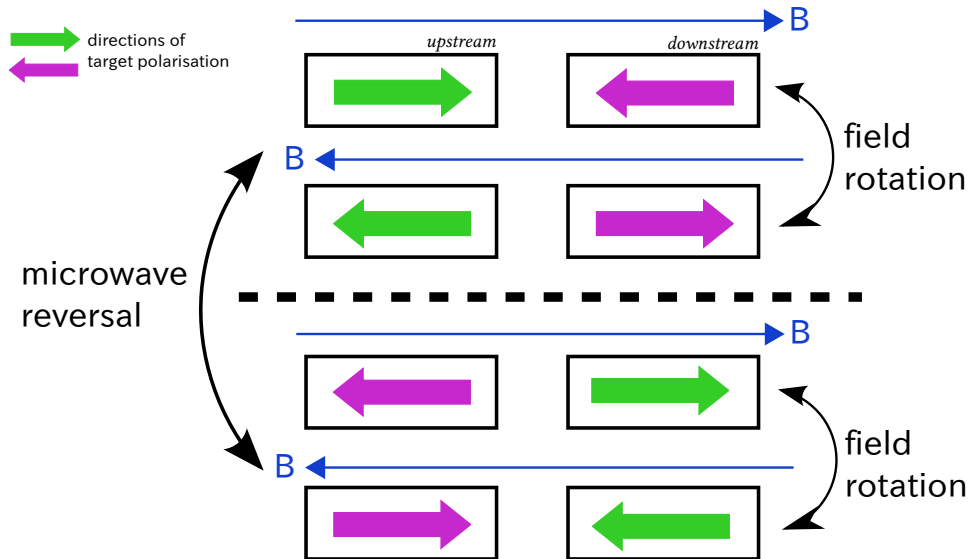


Figure 3.7: The schematic picture of field rotation and microwave reversal. As explained above, for the three target cell setting the polarisation direction of the midstream cell in three cells is always opposite to the upstream and the downstream cells. In order to achieve the parallel (anti-parallel) polarisations denoted by green (magenta) arrows, the microwave f_+ (f_-) is irradiated.

tion with particle identification and good mass reconstruction [15]. There are the large angle spectrometers (LAS) and the small angle spectrometers (SAS), which are set in the upstream part and the downstream part respectively.

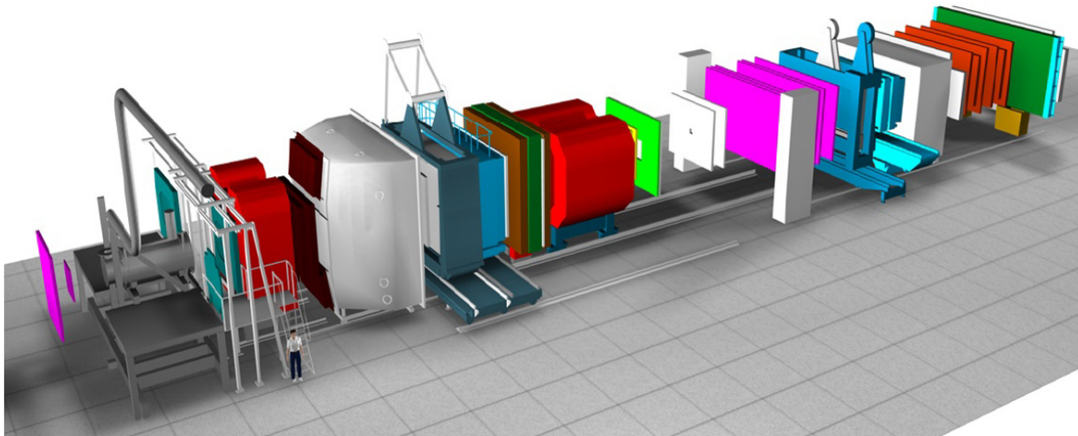
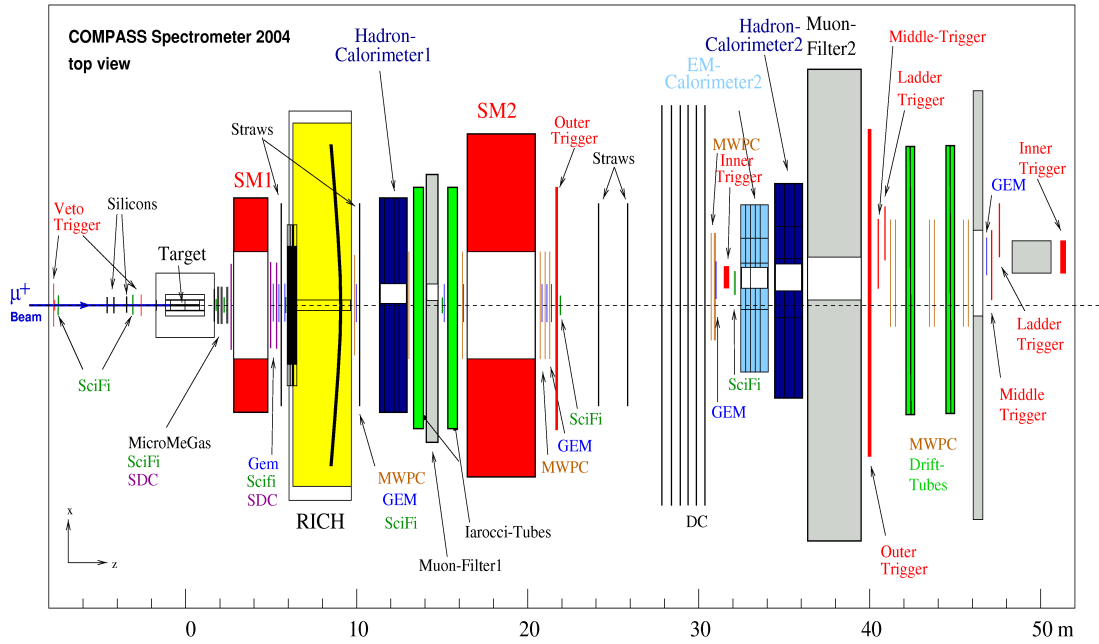
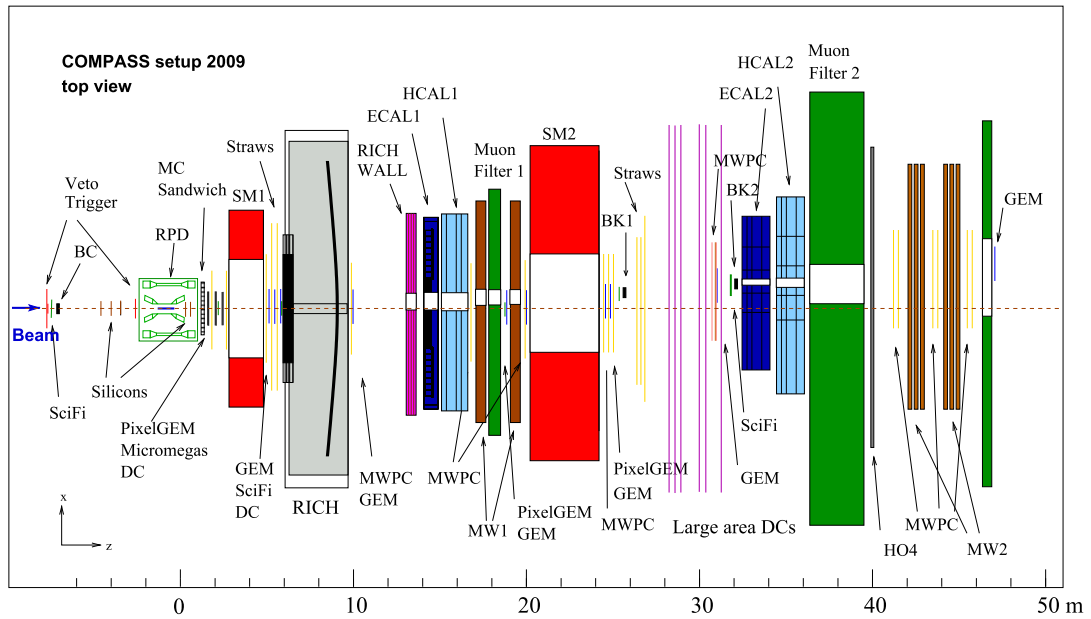


Figure 3.8: Schematic view of the COMPASS experiment. Most spectrometers are used in both muon and hadron programmes. Some additional detectors are installed and/or uninstalled according to the programme. The overall length including the target and the last trigger is over 50 m.

The aim of the LAS is certainly to have ± 180 mrad acceptance. “ ± 180 mrad” comes from a diameter of the solenoid magnet surrounding the polarised target (see Fig. 3.6). There is a dipole magnet, called SM1, to bend charged particles for the momentum measurement. The



(a) The COMPASS setup with muon beam used until 2004.



(b) The COMPASS setup with hadron beam. DC4, ECAL1, upgrade RICH, and Rich Wall are part of apparatus that is common to both muon and hadron physics programmes since 2006.

Figure 3.9: Top views of the COMPASS setup with muon and hadron beam [15,70].

SM1 magnet is followed by a RICH detector with large transverse dimensions to match the LAS acceptance requirement, which is used to identify charged hadrons with momenta ranging from a few GeV/c to $43 \text{ GeV}/c$. The energy of charged hadron is measured by the Hadron CALorimeter1 (HCAL1) which is located in next to RICH. On the other hand, the energy measurement of photons and neutral pions is done by an electromagnetic calorimeter, called ECAL1. It has a large hole in the centre to match the SAS acceptance. Hit information is

also used as a trigger formation. Between those detectors, there are other detectors to detect muon's tracks.

The SAS is located in the downstream part and detects particles having small angles (30 mrad) and large momentum (5 GeV/ c or higher). There is also a dipole magnet, called SM2 which is in the downstream side. All other spectrometers are set around SM2. The basic setup is as same as the LAS: dipole magnet, calorimeters, and trackers.

There are many tracking detectors with different types to cover a wide kinematic range. They are grouped by the following.

Very Small Area Trackers (VSAT) These trackers have the smallest detection area like 4 cm to 12 cm while having high flux capabilities and excellent space or time resolutions.

Small Area Trackers (SAT) These trackers have high space resolution and minimum material budget. COMPASS have used GEM (Gas Electron Multiplier) stations and Microegas (MICRO-Mesh Gaseous Structure) stations.

Large Area Trackers (LAT) These trackers have a good spatial resolution and cover the large area. There are drift chambers (DC), MultiWire Proportional Chamber (MWPC), and straw drift tubes in COMPASS.

3.4. VSAT

VSAT are required to have an excellent time or position resolution to identify tracks. COMPASS has used scintillating fibre and silicon microstrip detectors.

3.4.1. Scintillating Fibre Detectors

The purpose of scintillating fibre (SciFi) detectors in the COMPASS experiment is to provide tracking of the incoming and scattered beam particles as well as of all other charged reaction products in and very near the centre of the primary beam [15].

There are eight SciFi detectors in total, which are placed in upstream and downstream of the target, more upstream of the target and more downstream of the SM2 magnet as a pair. Each detector has several fibre layers with approximately hundred channels in each projection. In total, there are more than 2500 PMT channels for about 8000 fibres. The scintillating light is guided by clear fibres (0.5 m and 3 m) and detected by 16-channel multi-anode PMTs (Hamamatsu H6568) [82]. Each station consists of at least two projections (vertically (Y) and horizontally (X)). Three stations have an additional inclined ($\sim 45^\circ$) projection (U). Kurary SCSF-78MJ is chosen as fibre material for all SciFi stations [82].

R.M.S.s of spatial resolution are 130 μm , 170 μm , and 210 μm respectively. On the other hand, observed R.M.S.s of time resolution are between 350 ps and 450 ps for the centre region of the various planes.

3.4.2. Silicon Microstrip Detectors

Silicon microstrip detectors are another constituent of VSAT, which are used for the detection of the incoming muon beam track. They are needed to stand for high radiation dose and have an excellent and time resolution.

The silicon wafer was initially designed and developed for the HERA-B experiment [15, 83]. It is made of two kinds of wafers: n-type and p-type. They are placed perpendicularly, which allows to obtain two dimensional position information. Each wafer has about thousand readout strips and is cooled down by nitrogen gas with the front-end chips. Silicon station is made up of two detectors. In a similar way to SciFi detectors, one detector is rotated by 5° around the beam axis, which provides two-dimensional planes (U , V) [84].

The observed spatial resolutions are $8\ \mu\text{m}$ for the p-side and $11\ \mu\text{m}$ for the n-side respectively. The observed time, on the other hand, is $2.5\ \text{ns}$ in average.

3.5. SAT

SAT cover at the radial distance of $2.5\ \text{cm}$ to $20\ \text{cm}$ and are consisted from Micromegas and GEM detectors.

3.5.1. Micromegas

Micromegas stands for Micro-MESH Gaseous Structure and has similar structures with wire chambers. There are three stations of Micromegas detectors with four planes (X , Y , U , V) between the solenoid magnet and SM1 magnet. COMPASS is the first experiment using Micromegas detectors [15, 85, 86, 87].

The Micromegas detector is based on a parallel plate electrode structure and a set of parallel microstrips for readout. There are two gaseous regions that are separated by a metallic micromesh: the conversion gap where the ionisation occurs and the amplification gap where an electron avalanche occurs. $\text{Ne}/\text{C}_2\text{H}_6/\text{CF}_4$ is used as the ionising gas, whose ratio is 80:10:10 to optimise for a good resolution. It also minimises the discharge rate to 0.03 discharges per detector and beam spill [87].

The active area is $40 \times 40\ \text{cm}^2$ with $5\ \text{cm}$ dead zone in diameter. In order to reduce the amount of material inside detectors, the readout boards are located in $35\ \text{cm}$ away by readout strips.

A Micromegas station consists of two identical detectors, which are mounted on with rotating by 90° each other to measure two-dimensional position. In some stations, detectors are rotating by $+45^\circ$ and -45° to have U -plane and V -plane. Observed time resolution is $9.3\ \text{ns}$ and the efficiency is close to 97%. Spatial resolution is $90\ \mu\text{m}$ which is evaluated by calculating residuals of position between reconstructed position using 11 Micromegas and position at the 12th Micromegas.

3.5.2. GEM

COMPASS is the first high-luminosity particle physics experiment to employ gaseous micropattern detectors with amplification in GEM foils only [15, 88]. GEM consists of thin Polyimide foil with Cu cladding, which have numbers of tiny holes ($10^4\ \text{holes}/\text{cm}^2$, $\varnothing 70\ \mu\text{m}$). As same amplification mechanism as Micromegas, the electric avalanche occurs and then numbers of electrons are created. After passing the last GEM foil, the electron cloud induces a fast signal on the readout anode, which has two-dimensions.

The gas mixture used is Ar/CO_2 (70/30) since it has large drift velocity, low diffusion, non-flammability and non-polymerising properties.

The active area of GEM is $31 \times 31 \text{ cm}^2$, and the deactivated area is 5 cm in the centre. Its area can be activated remotely in low-intensity beam so that the detector is aligned using beam tracks. The amount of material in one detector is 0.4 % of a radiation length in the centre and 0.7 % on the periphery to avoid spoiling the mass resolution of the spectrometer.

The spatial resolution of all GEM planes is 70 μm on average, which includes a contribution of overlapping clusters of about 20 μm : The extraction of time information is achieved by the analogue readout method. The three point signals are measured in time. Knowing the detector response to a minimum ionising particle, the hit time can be determined from the ratio of the three measured amplitudes [15]. By this method, the observed time resolution results in 12 ns.

3.6. LAT

There are three kinds of trackers as mentioned above: DC, MWPC and straw. We will introduce DC at first.

3.6.1. Drift Chamber

Several identical Drift Chambers are installed. One is in the upstream of the SM1 magnet, and two chambers are in the downstream of the magnet. They have $180 \times 270 \text{ cm}^2$ active area to cover the acceptance fully. DC has eight layers of wires with four different inclinations: vertical (x), horizontal (y), $+20^\circ$ (U) and -20° (V). The angle between U and V is with respect to vertical direction. Each layer has 176 sensitive wires with $\varnothing 20 \mu\text{m}$, 177 potential wires with $\varnothing 100 \mu\text{m}$. It is enclosed by two Mylar® cathode foils with 25 μm thickness coated with 10 μm graphite. During operation, their voltages are kept by -1700 V , 0 V , and -1700 V in cathode foils, sensitive wires and potential wires respectively. The radiation length is 0.32 % in total.

Ar/C₂H₆/CF₄ (45/45/10) is employed as the gas mixture since it meets several requirements for the Drift Chamber: good spatial resolution, linear RT relation, fast, good efficiency, and large HV plateau. The measured gain is 2×10^4 at 1800 V, whereas full efficiency is obtained at 1600 V. At normal operations, the mean layer efficiency is 95 % or higher. The inefficiency comes from the pile-up at high rates.

The spatial resolution of a single wire layer is 270 μm at nominal operations. The resulting resolutions of one DC are 110 μm at X direction and 170 μm for Y direction.

A large drift chamber (DC4) has been working since 2006 in LAS, which is behind the SM1 magnet. The basic design is as same as DCs already used, whereas the size is enlarged to cover the angular acceptance in the downstream of the SM1 magnet. Temperature variations cause the chamber frame to deform, resulting in the instability. Therefore, a water cooling system is installed. The external dimensions are $294 \times 254 \times 17 \text{ cm}^3$ and the active area is $248 \times 208 \text{ cm}^2$. As well as other DCs, DC4 has eight layers of wires with four different inclinations: two vertical layers (X and X'), two horizontal layers (Y and Y'), two inclined (10° with respect to vertical axis) layers (U and U') and two inclined ($\text{arg } -10$ with respect to vertical axis) layers (V and V'). The layer configuration along the beam is $UU'VV'XX'YY'$. Every layer with same orientations is staggered by 4 mm, which is corresponding to the half of the cell dimension. Each layer has 256 active wires of gold plated tungsten ($\varnothing 20 \mu\text{m}$) and 257 potential wires of beryllium ($\varnothing 100 \mu\text{m}$). In addition to those wires, two nylon wires per plane are fixed perpendicularly to those wires. Two active wires are separated by 8 mm. Each layer is splitted by Mylar® cathode foils at a distance 4 mm from wires. This configuration makes the drift cells of $8 \times 8 \text{ mm}^2$. During operation, active wires are grounded while Mylar® foils

and potential wires are kept by -1700 V. The central dead zone is deactivated during normal operation. However, it is activated only for detector alignment purposes with low-intensity beam operation.

The gas mixture used is $\text{Ar}/\text{C}_2\text{H}_6/\text{CF}_4$ (45/45/10) so that it ensure fast charge collection and preserves a good spatial resolution. Full efficiency is obtained with approximately 1750 V HV supplement, and its gain value is close to 10^4 . With hadron beam intensity ($5 \times 10^6 \text{ s}^{-1}$), the efficiencies of whole eight planes are in the range of 95 % to 97 %. The position resolution for a single plane is 226 μm in the central region, which corresponds to about one-tenth of the total detector area.

3.6.2. Multi Wire Propotional Chamber

The tracking of particles at large radial distances to the beam in the SAS is mainly based on a system of MWPCs. A total of 34 wire layers, corresponding to about 25 000 detector channels, is installed and operated since the year 2001. All layers are characterised by a wire length of about 1 m, a wire diameter of 20 mm, a wire pitch of 2 mm and an anode/cathode gap of 8 mm.

COMPASS use three types of MWPC: A, A* and B. Type-A and type-A* stations are almost identical: the number of layers, planes, and dead zone are different. Type-B stations are composed of two detectors with inclined wire layers with opposite orientations, fixed together; only three layers, one vertical and two tilted, are read out. All wire layers are enclosed from both sides by 10 mm thick graphite coated Mylars® cathode foils, to provide field symmetry and to enclose the detector gas. A central dead zone of 16–22 mm diameter, depending on the location of the chamber along the beam axis, was realised by removing the graphite coating from the foils. The total thickness of each type are 0.2 %, 0.3 %, and 0.3 % for type-A, type-A*, and type-B, respectively. The summary of characteristics for each type can be found in Table 8 in Ref. [15].

The gas mixture of $\text{Ar}/\text{CO}_2/\text{CF}_4$ (74/6/20) is employed. CF_4 is quite important since it does not give excessive dead time at high environment. The gain is between 3.5×10^4 and 4×10^4 at 4250 V.

The observed spatial resolution of the single layer at one MWPC is 1.6 mm. The efficiencies for all MWPCs during the 2004 data taking exceed 98 % on average.

3.6.3. Straw tube

Straw tube chamber [89] is used for particles with large scattering angle (15 to 200 mrad) in the downstream of SM1 magnet. A straw tube consists of 40 μm thickness Kapton® loaded by carbon and 12 μm thickness alminised Kapton®. There is an anode wire with $\varnothing 30 \mu\text{m}$ in the centre. The gas is supplied through the end-plug and gas-manifold.

There are 15 detectors with 12440 tubes in total. One detector consists of two staggered layers to resolve left-right ambiguities. One station consists of three detectors in order to measure three-dimensional of particle trajectory, and each detector is aligned to horizontally, vertically and rotated by 10° with respect to the vertical detector. The detectors with vertical and inclined straws are of the same type (called type X) while the ones with horizontal straws have a slightly different geometry (type Y). The type X detector is presented in Fig. 3.10. The thickness of one detector is 40 mm; 0.2 % radiation length. $\text{Ar}/\text{CO}_2/\text{CF}_4$ (74/6/20) is used as gas mixture. The typical gain under 1950 V HV is 6×10^4 .

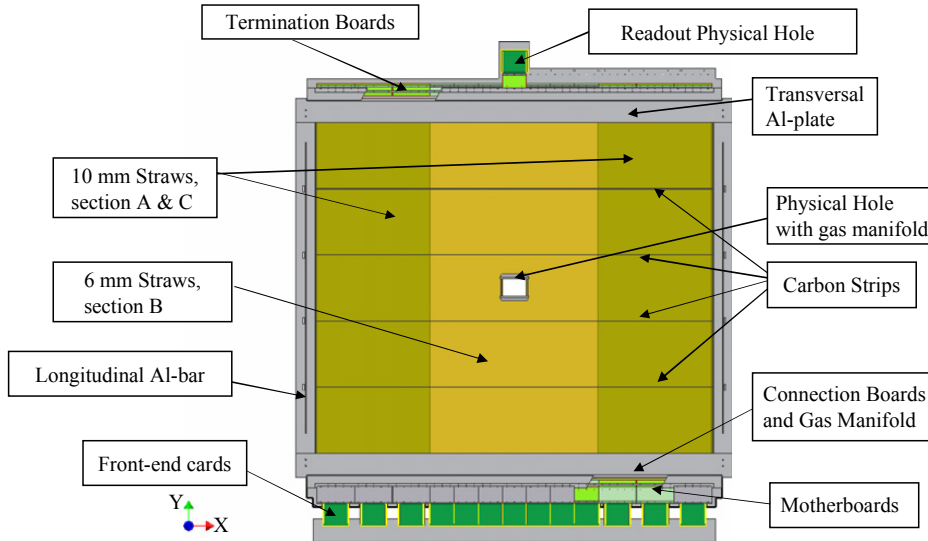


Figure 3.10: Schematic view of a COMPASS straw detector (type X) [89].

The relative elongation of the straw tube is observed by about 3.5×10^{-5} for 1% humidity change. This can result in increasing tension on the frame or bending straws. To keep the humidity constant, each straw station is surrounded by a N_2 gas, which is enclosed by 12 mm thin aluminised Mylar® foils.

The mechanical wire position is measured to be $170 \mu\text{m}$ by a triple stereo imaging X-ray scanner [90]. This information is used in the offline analysis as the correction, and reduces the uncertainty of the mechanical wire position to $60 \mu\text{m}$. With this information and drift time information, the resolution of a given straw tube can be determined. The mean value of the resolution is $270 \mu\text{m}$ for one straw layer under normal beam condition.

3.6.4. RICH Wall

The Rich Wall detector has been working since 2006, which is located between RICH detector and ECAL1. The purpose of the building it is to improve the tracking accuracy at large angles ($150 < \theta < 300 \text{ mrad}$). As a consequence, this also results in the improvement of the reconstruction of Cherenkov ring in RICH detector since RICH Wall provides the additional track points for large angle particle trajectories. The basic structure is as same as Muon Wall 1 (see Sec. 3.7.2); it consists of a vast number of Mini Drift Tubes (MDTs) shown in Fig. 3.11.

An MDT module is made of aluminum comb with eight cells, which is covered on the top by stainless steel foil. Gold plated tungsten wires with $\varnothing 50 \mu\text{m}$ is in the centre of each cell. They are thermally glued to plastic spacers to provide electrostatic stability. A plastic envelope covers the aluminum comb with 1 mm thickness.

RICH Wall consists of eight planes. Two planes are grouped, making four groups in total. Each plane in one group is staggered by 2.5 mm. There are two groups aligned vertically and two groups aligned horizontally, which are called X-planes and Y-planes respectively. X-plane consists of 2×25 long MDT modules and 2×12 short modules to avoid the paths of the beam and scattered muons. Similarly, Y-plane consists of 2×20 long MDT modules and 2×6 short modules.

The gas mixture used is Ar/CO_2 (70/30) and shows no ageing effect. The HV of 2050 V

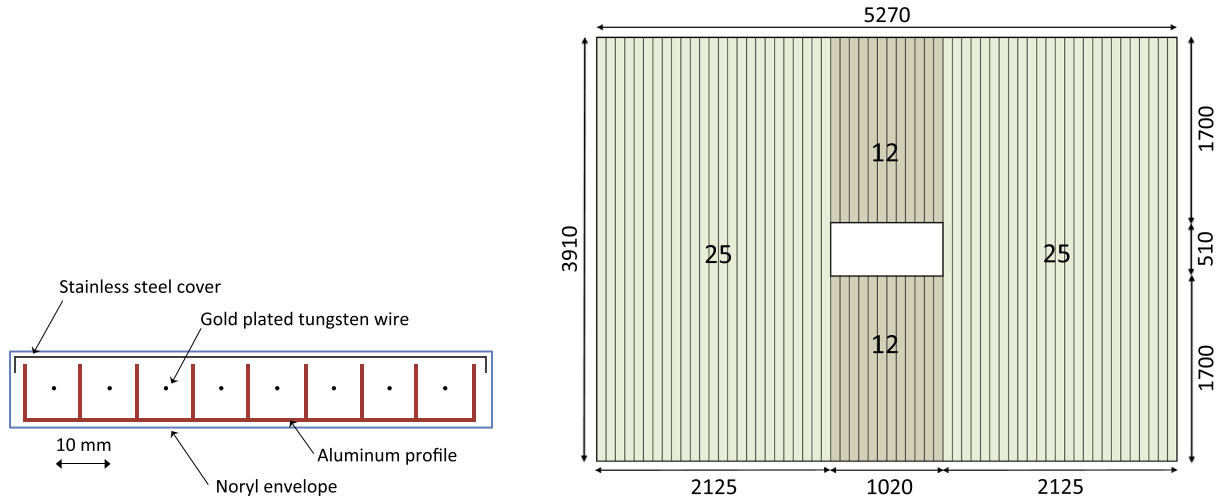


Figure 3.11: Cross section of a Mini Drift Tube module (*left*) and front view of an X -plane on the Rich Wall detector (*right*). The large-size numbers correspond to the number of MDT modules in each sector, the small numbers indicate the dimensions in units of mm [70].

is supplied during operation. Ageing tests performed with this gas mixture have shown no degradation effects for incident charges of up to 1 C/cm of anode wire length.

The obtained resolution of a single plane is of the order of 1.0 mm. The efficiency of the detector is 90 % to 91 % for a single plane. The beneficial effect for RICH ring reconstruction is shown in Fig. 3.12. In large angle region, the reconstruction is improved by 20 % on average.

3.7. Particl identification

3.7.1. RICH

Ring Imaging Cherenkov detector (RICH) is located just after SM1 magnet [91]. RICH has the large acceptance: $\varnothing 250$ mrad in the horizontal plane and ± 180 mrad in the vertical plane. C_4F_{10} gas is used as a radiator gas, which has low chromaticity.

Cherenkov light is reflected by UV mirrors and then the light is detected by Photon Detectors (PD) shown in Fig. 3.14. This photocathode detector is firstly developed by CERN RD26 collaboration, and later optimised for ALICE HMPID [92] and COMPASS RICH. The severe tolerances for the MWPC parameters are imposed. The required precision for an anode-cathode gap is 50 μm and the anode wire mechanical tension is within 5 % of the nominal values.

Handling of CsI layer is also strongly imposed. Its surface should be never exposed to air since CsI has high deliquescence and water vapour decreases the quantum efficiency. A dedicated glove boxes and monitoring system are developed and build. The PD consists of MWPC with CsI photocathodes [93]. The Cherenkov light is converted into photoelectron by CsI photocathode. Its photoelectron results in electron avalanche, which generates a signal at wires in MWPC.

The gain during normal operation is up to 5×10^4 . The electrical stability has been improved since 2001: it was 25 % in 2002, 75 % in 2002 and 97 % in 2003 and 2004. The achieved resolution allows pions and kaons separation at 2.5σ level up to 43 GeV/c [91].

Upgrades of RICH had been done in 2005 and has been working since 2006 data taking.

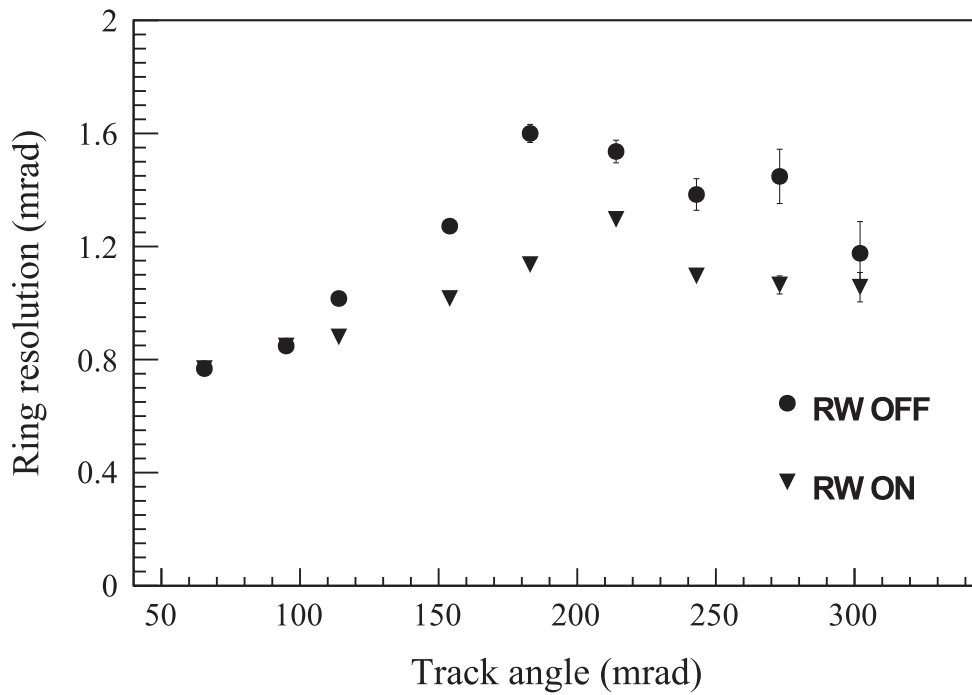


Figure 3.12: Resolution of the reconstructed Cherenkov ring for pions as a function of the track angle. The two different trends in the curve below and above ≈ 175 mrad are due to the different RICH-1 photon detector types [70].

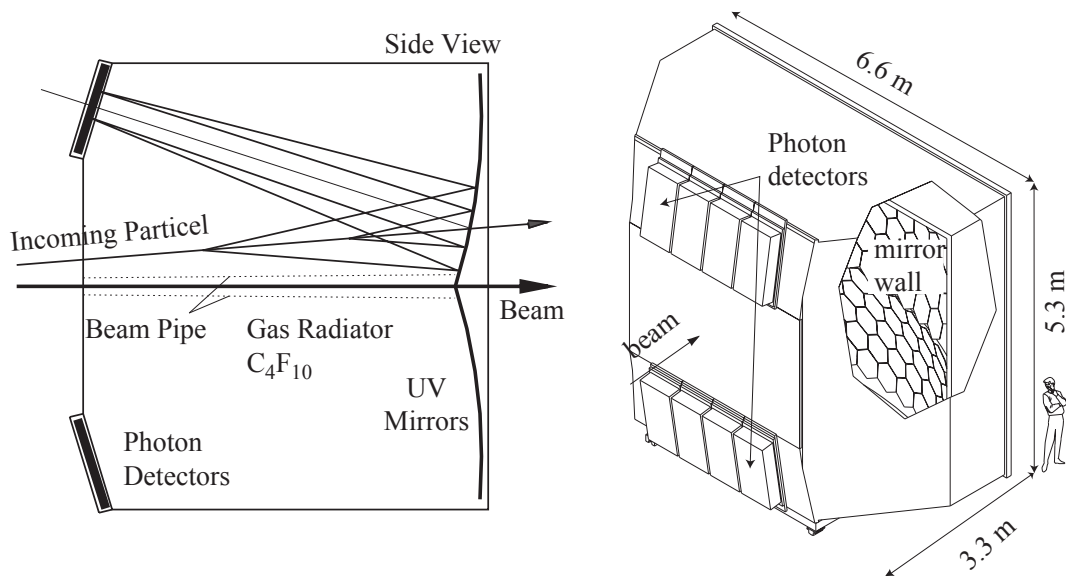


Figure 3.13: Principle and artistic view of RICH-1 [15].

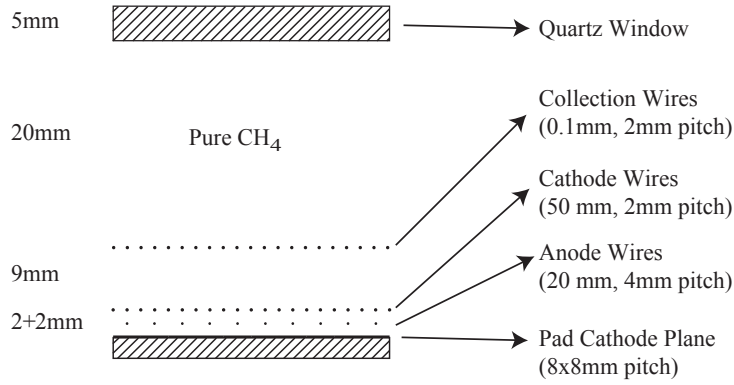


Figure 3.14: Cross section of the RICH-1 photon detector [15].

There were two major limitations: MWPC operation gain and non-negligible dead time ($3.5 \mu\text{s}$). Details can be found in Refs. [94, 95, 96].

For the sake of minimising the cost, two different technologies were chosen. In the peripheral regions that cover 75 % of the photodetection surface, where the level of the uncorrelated background is small, the MWPC/CsI photon detectors were kept. However, their front-end electronics were replaced by a new system that was based on the 128 channel APV25 chip. The new system provides two major improvements. First, it reduces the effective time window from $3 \mu\text{s}$ to 4400 ns and decreases the dead-time losses of the readout system to values close to 5 %. Second, the APV25 chip performs a triple sampling of the MWPC signal, resulting in a much improved time resolution and an increase in the signal-to-background ratio from 0.35 with the old system to 2.13 with the new one.

The central region of RICH-1, which covers 25 % of the photodetection surface, is instrumented with a detection system based on MultiAnode PhotoMultiplier Tubes (MAPMTs). The MAPMTs are coupled to individual telescopes of fused silica lenses that consist of a prismatic field lens followed by a concentrator lens, thereby enlarging the effective active area of the photon detectors by a factor of seven. The effective pad size that results from the MAPMT pixel size and the lens telescope magnification is about $12 \text{ mm} \times 12 \text{ mm}$. The new system detects about four times more Cherenkov photons than the old one and reaches values as high as 60 photons per ring. The MAPMT detectors are intrinsically fast and have time resolutions better than 1 ns. They are coupled to a readout system based on the MAD4 high sensitivity amplifier/discriminators and the standard COMPASS F1 TDCs.

The resolutions for pions and kaons separation at 2.5σ is up to $43 \text{ GeV}/c$ before upgrades, which is improved to $45 \text{ GeV}/c$ after upgrades. No efficiency reduction is observed for particle scattered at small angles of which images are formed in a photon detection area where the photon flux is extremely high (up to $1 \text{ MHz}/\text{channel}$). The comparison of efficiencies before and after upgrades is shown in Fig. 3.15.

3.7.2. Muon Wall

In order to identify muons, two detector systems are installed in LAS and SAS. Each of them is made up of a hadron absorber made of iron (Muon Filter 1) or concrete (Muon Filter 2), and tracking station. In LAS, Muon Wall 1 (MW1) is placed, and Muon Wall 2 (MW2) is placed in SAS. They are not an identical system but have same functions.

MW1 consists of numbers of gaseous wire detector, which is called Mini Drift Tube (MDT) [97,

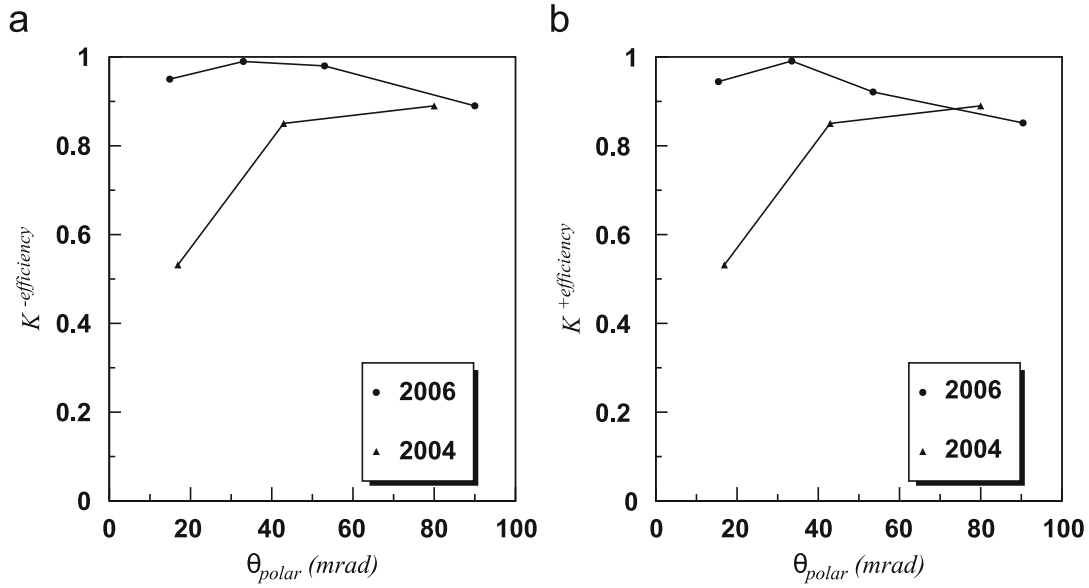


Figure 3.15: PID efficiency versus polar angle for a sample of Ks from ϕ -decay; ϕ -decay events are selected using the kinematic reconstruction; (a) K^- , (b) K^+ [96]

98]. A modified version of MDT optimised for COMPASS is used in proportional mode, which are presented in Fig. 3.16. This makes MDT stand with high-rate background conditions.

A basic element of MDT is made of an aluminium comb with eight cells, stainless steel foil cover on top, gold plated tungsten wires in the centre of cell and ABS plastic sleeve as an insulator. Ar/CO₂ (70/30) is used since it has no ageing effects, fast drifting time (below 150 ns), non-flammable property, and cheapness. MW1 has eight layers and each four layers is separated by 60 cm thick iron absorber. MDTs are placed horizontally and vertically so that one can get muon tracks. The MW1 system provides a measurement of up to eight points per track in each projection with the coordinate accuracy of $10/\sqrt{12}$ mm typical for the 10 mm wire pitch. The obtained efficiency is typically 91 % and there is no large time variation in 2002, 2003 and 2004.

MW2 consists of two identical stations of layers of drift tubes. Each of the two stations

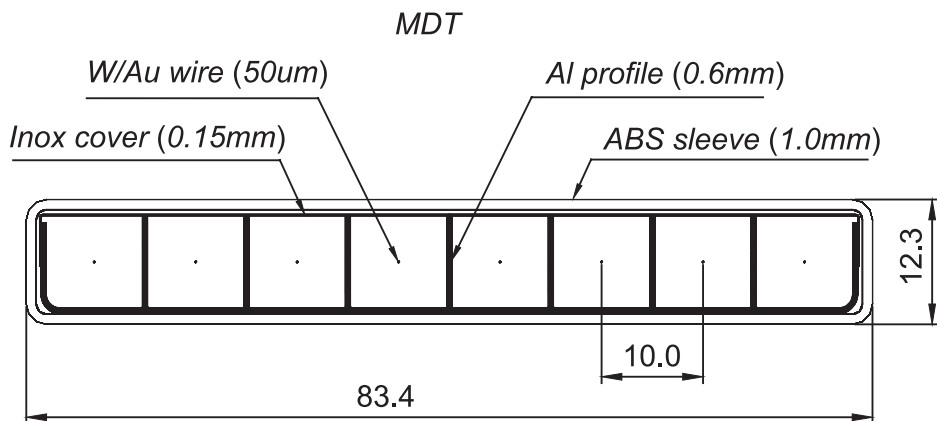


Figure 3.16: Cross section of a MDT module for MW1; all dimensions (except for the wires) are given in millimetres [15].

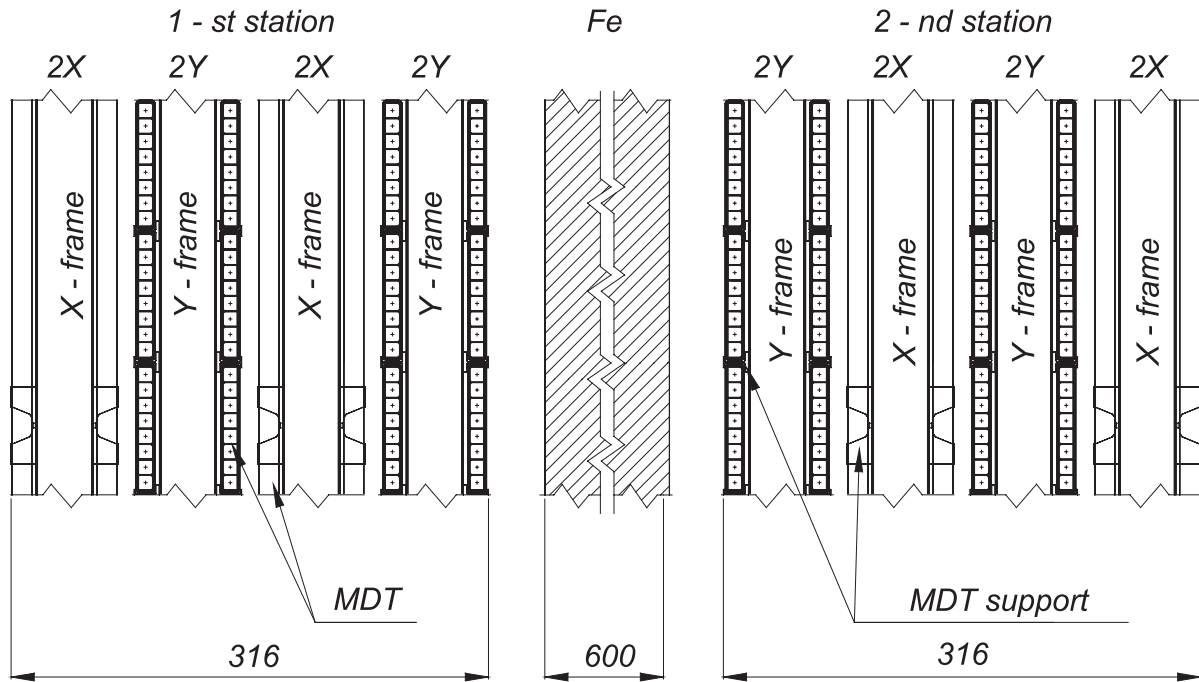


Figure 3.17: Schematic cross sectional side view of MW2; all dimensions are given in millimetres. Vertically only part (255 mm) of the stations are shown [15].

of six layers grouped into double layers, each mounted on a separate steel frame. The three double layers have vertical, horizontal and inclined (at -15° with respect to the vertical) tubes, respectively.

The basic structure of drift tube was originally designed in DØ experiment [99]. The schematic view of a double layer is shown in Fig. 3.18. Like Straw tube, numbers of drift tubes with tungsten anode wire of $\varnothing 50 \mu\text{m}$ in the centre made a layer of MW2. Each tube is inserted into guide holes in the both sides of a frame and fixed with a clamp. This feature allows to replace damaged or malfunctioning tubes quite easily. In total 1680 tubes are used in MW2.

Ar/CH_4 (75/25) is used as gas mixture since it is known for saturated and rather fast drifting time, wide working plateau, and stable performance against radiation ageing. The actual drifting time is obtained $\sim 240 \text{ ns}$ at +3 kV HV.

The spatial resolution is determined by the intrinsic detector resolution and the track fitting error. Thus, Y planes have worse resolution since the projection measurement is less reductant in this region. The structure of residual on single MW2 layer has two gaussians with a same mean: the “core” gaussian with σ of 0.53 mm (0.94 mm for Y planes) which amounts to 79 % to 91 % of the entries and the “halo” gaussian with σ of 2.0 mm and 4.8 mm. This spread mainly comes from irregular spacing of the tubes. Whereas, the obtained drift velocity is between 5.8 cm/ μs and 6.2 cm/ μs .

The tracking efficiency for single plane averaged both over all wires and the wires length varies from 81 % to 84 %. Taking into account of the ratio of the inner diameter of the tube to the pitch, 83 % corresponds to 96 % drift tube efficiency.

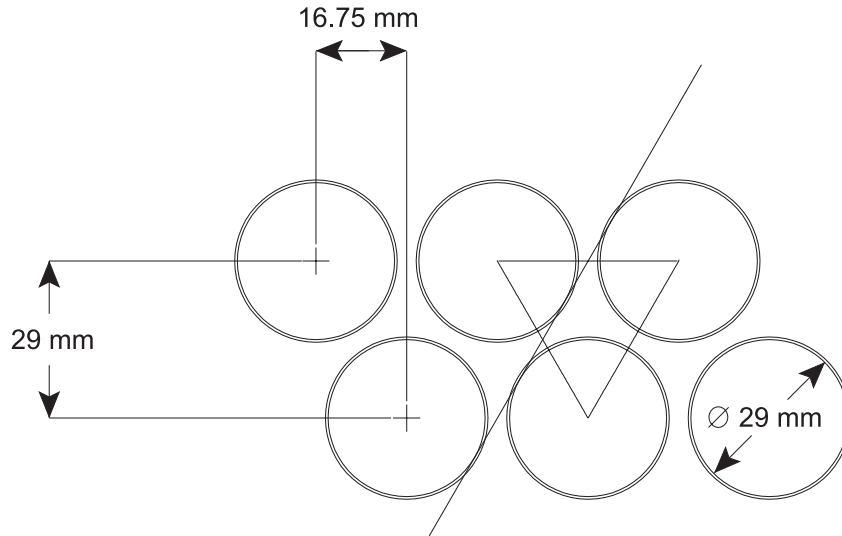


Figure 3.18: The layout of the tubes in a double layer of MW2 planes. Dimensions in mm. An imaginary equilateral triangle formed by centres of three adjacent tubes and a common tangent to their interior are shown [15].

3.7.3. Hadron Calorimeter

Hadron CALorimeter 1 (HCAL1) is located before MW1. It consists of 480 segmented modules. Each module has 40 layers of 20 mm iron plate and 5 mm scintillator, which amounts to 4.8 nuclear interaction length. It can measure hadrons having energy in 10 GeV to 100 GeV. Those particles are almost fully absorbed.

28 modules are horizontally placed, and 20 modules are vertically placed. Twelve modules (8 + 4) in the centre are removed to pass the beam and scattered muons. The overall surface of HCAL1 is $4.2 \times 3 \text{ m}^2$ and the useful surface is 10.8 m^2 .

The energy resolution depends on the qualities of scintillators, light guides, and PMTs. The scintillator is made of polystyrene, P-terphenyl (1.5 %) and POP (1,4-Bis-[2-(5-phenyloxazolyl)-benzene]) (0.04 %), which is molded under pressure. The emitted light is collected by a light guide. Typically an MIP deposits energy enough to produce 4–6 photoelectrons at PMT. PMT (FEU-84-3 PMT) has multi-sodium photocathodes with 0.18–0.26 quantum efficiencies at 460 nm.

The basic characteristics were measured at the CERN X5 beamline with various energies (10 GeV to 100 GeV). The energy resolution were parameterised by $\sigma(E)/E = (59.4 \pm 2.9)\% / \sqrt{(E) \oplus (7.6 \pm 0.4)\%}$. The e/π ratio, which is calculated from the positions of electron and pion ADC spectrum is 1.2 ± 0.1 . The spatial resolutions are $\sigma_{x,y} = 14 \pm 2 \text{ mm}$.

The monitoring system for PMT stabilities is installed and continuously checked. The light of single LED is distributed over 480 modules by optical fibres. The relativistic stability is controlled to 2 %. The efficiency of HCAL1 includes the efficiency of the cluster search and the energy reconstruction. The obtained efficiency for particles with momenta above $5 \text{ GeV}/c$ is almost close to 100 %.

Hadron CALorimeter 2 (HCAL2) is located before Muon Filter2 that is made of concrete blocks and absorbs hadrons. Similar to HCAL1, HCAL2 consists of modules (20×10 matrix). Each module is sandwich calorimeter of 25 mm steel plate and 5 mm scintillator sheet with 36 layers. Their modules had been used in NA12 experiment [100], but readout system (light

collection and HV bases for PMs) has been modified. The thickness is five nuclear interaction length for pion and seven for proton. 8×6 modules in the central region has 40 layers instead of 36 layers.

HCAL2 also has a light monitoring system. A light of not single LED but a group of LEDs fed to the PMs through fibre light guides. This system is used for amplification adjustment and control.

The characteristics were measured in the CERN X5 test beam facilities using a matrix of 5×5 modules. The obtained energy resolution is $\sigma(E)/E = (66\%/\sqrt{(E)} \oplus 5)\%$. The uniformity of calorimeter response was found to be better than 2%. The efficiency for hadrons is close to 100%.

3.7.4. Electromagnetic Calorimeter

ECAL1 and ECAL2 are the electromagnetic calorimeters, where the photons emitted during the interaction and decay photons are detected. Until 2004, there is only ECAL2 in SAS part. In the upgrades, new ECAL2 calorimeter was installed in LAS part, which extends the acceptance for photon detection to large angles. The ECAL2 calorimeter was also upgraded with radiation-hard Shashlik modules in its central region and with fully pipelined electronics. For both calorimeters, the calibration procedure and the monitoring of the individual modules were significantly improved.

ECAL1 is installed between HCAL1 and RICH WALL. It consists of 1500 lead glass modules. A width is 3.97 m and the height is 2.86 m. There is a centre hole for the beam and scattered muons, whose size is $1.07 \times 0.61 \text{ m}^2$.

The schematic front view of the structure of modules is presented in Fig. 3.19. There are three parts: GAMS, Mainz and OLGA. The GAMS modules are in the innermost part and arranged in a 44×24 matrix with its central 28×16 array left empty. Above and below this central part, two 22×13 matrices of "MAINZ" modules are installed, which contain in total 572 lead glass modules. In order to compensate for the small difference between one MAINZ module and four GAMS modules in size, 1.6 mm vertical gap has been left. The two outermost parts of ECAL1 consist of two matrices of 8×20 large size "OLGA" modules. One OLGA module has the size of nearly four MAINZ modules.

The Cherenkov light is detected by several types of PMT. Its analogue signals are processed by the following electronics; signal shaper and sampling ADC (SADC). In the offline event reconstruction, the SADC information is used to extract the amplitude and the time of a signal relative to the trigger time. The achieved time resolution for photons with energies larger than $1 \text{ GeV}/c$ is about 1 ns.

Module calibration is done once or twice per data taking using $15 \text{ GeV}/c$ electron beam without the SM1 magnetic field. The calibration is performed by comparing the sum of the charges of the module and its neighbouring modules with incident electron energy. To determine the HV setting for all modules, several iterations are needed.

The controls of the light collection efficiency and the photomultiplier gains are performed with the LASER system, which is shown in Fig. 3.20. A light from single laser feeds into each module through optical fibres uniformly and measures signals. They are used to correct the responses of all modules on a run-by-run basis.

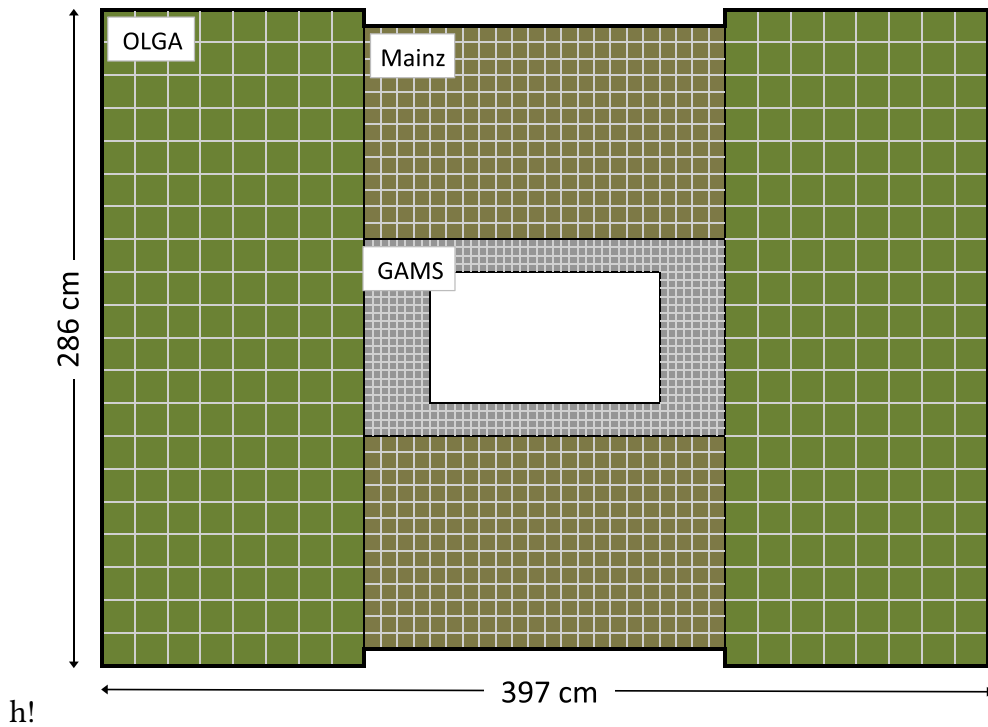


Figure 3.19: The schematic front view of ECAL1. The central area is equipped with GAMS modules. The MAINZ modules are installed above and below the GAMS area. The OLGA modules cover the outer left and right regions [70].

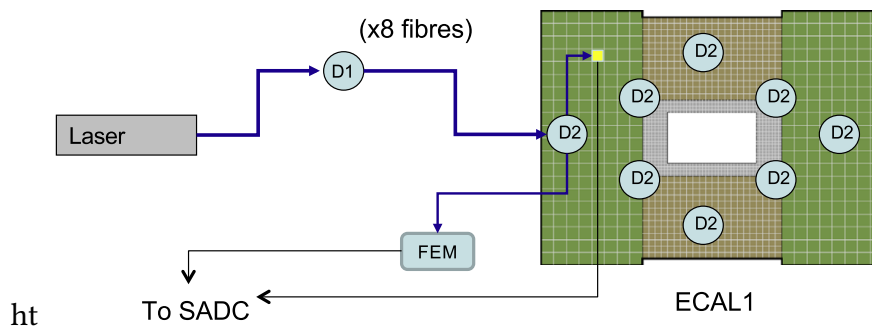


Figure 3.20: Schematic view of the LASER monitoring system for ECAL1. The laser beam is distributed to the ECAL1 modules using one primary (D1) and eight secondary (D2) light diffusion spheres. For clarity, only one of the eight primary fibres dispatching the light to D2, only one of the secondary 1500 fibres transmitting it to the LG modules, and only one of the eight front-end-monitoring (FEM) modules are explicitly shown [70].

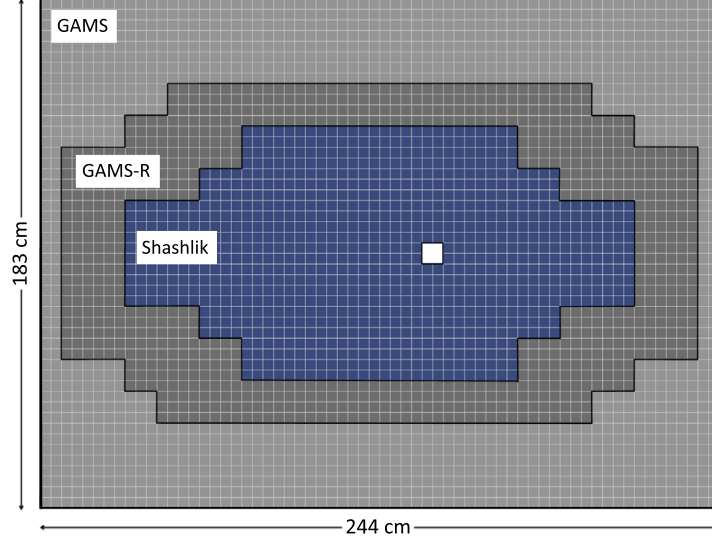


Figure 3.21: Configuration of ECAL2. The outer and intermediate regions are equipped with GAMS and radiation-hardened GAMS modules respectively. The inner region is equipped with Shashlik sampling modules. The transverse sizes of all three types of modules are identical. The central hole of 2×2 modules can be seen as a white spot [70].

ECAL2 is placed before HCAL2 in SAS. It consists of 2972 (64×48 matrix) lead glass modules with $38 \times 38 \times 450 \text{ mm}^3$ dimensions, which corresponds to 16 radiation length. They had been used in GAMS-4000 spectrometer [101, 102].

High energy gamma ray or electron develops an electromagnetic shower. The electron and positron from a shower emit Cherenkov light on the way through the glass. Cherenkov light is proportional to the energy deposited in each counter. PMT measures the intensity of the light.

The basic calibration scheme is as same as ECAL2: For module calibrations, 40 GeV/c electron beam is used and for time stability calibration is performed by LED. The electron beam calibration correct the HV setting in each module and the information from the monitoring system is used for the correction of drifts at individual modules on a spill-by-spill basis. The energy resolution is $\sigma E/E = 5.5/\sqrt{(E)} \oplus 1.5\%$ and the spatial one for horizontal axis is $\sigma(x) = 6/\sqrt{(E)} \oplus 0.5 \text{ mm}$.

After upgrades, ECAL2 consists of 3068 (64×48 matrix) calorimeter modules of three different types, all with the same transverse dimensions ($3.83 \times 3.83 \text{ cm}^2$), which is shown in Fig. 3.21. With its dimensions of $2.44 \times 1.83 \text{ m}^2$, ECAL2 covers angular ranges between 1.3 mrad and 39 mrad in the horizontal plane and between 1.3 mrad and 29 mrad in the vertical plane. In both planes, the angular ranges are slightly larger than the corresponding angular ranges of both ECAL1 and the hadron calorimeter HCAL1. Accordingly, the peripheral rows and columns of ECAL2 are not used; for the corresponding ECAL2 angles the photons from the target are either detected in ECAL1 or absorbed in HCAL1. ECAL2 is installed on a motorised platform allowing movements in both horizontal and vertical directions.

The outermost part is equipped with 1332 identical modules with ECAL1. The intermediate part is filled with 848 radiation-hardened modules (GAMS-R). The innermost part is equipped with 888 Shashlik type modules, which has 39 cm long and are composed of 154 double layers,

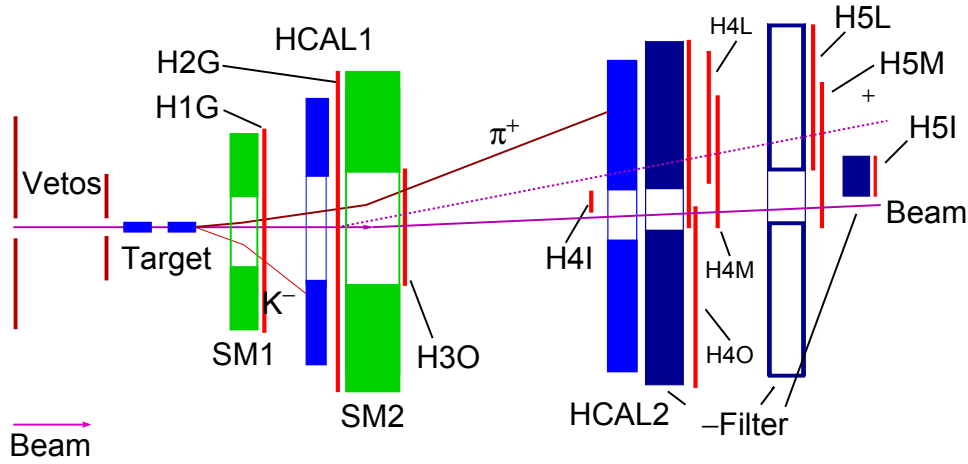


Figure 3.22: Schematic view of the trigger system. The most upstream veto is not shown [15].

each consisting for a 0.8 mm that lead plate and of a 1.55 mm thick scintillator plate.

The different ECAL2 modules have identical transverse dimensions, but different radiation hardness properties. Calculations have shown that the modules located closest to the beam would stand radiation does corresponding to several years of data taking for GAMS and GAMS-R, and nearly 20 years for Shashlik without significant degradation of their response at the COMPASS nominal hadron beam intensity and duty cycle.

The signals from PMTs are sent to shapers and then Mezzanine sampling ADC (MSADC) systems, which was upgraded. The information from the MSADCs is also used to calculate the time for each event. The time resolution for ECAL2 is 1 ns or better for energies higher than $2 \text{ GeV}/c$.

3.8. Trigger

The trigger system has to serve several purposes: to select event candidates in a high rate environment with a decision time below 500 ns and minimum dead time, to provide an event time reference and generate strobes for gating some of the analogue-to-digital converters, and to trigger the readout of detectors and front-end electronics. The trigger system is based on fast hodoscope signals, energy deposits in calorimeters, and a veto system. Depending on the incident beam —muons or hadrons— and on the kinematics of the reactions different elements are combined to form the trigger signal.

The COMPASS setup for the muon beam is designed for an as large kinematic acceptance in Q^2 as possible ranging from $Q^2 \approx 0$ to the maximum allowed by kinematics. Events with $Q^2 > 0.5 (\text{GeV}/c)^2$ are mainly triggered by using the scattered muon information. The muons are measured in two horizontal scintillator hodoscopes in order to determine the projection of the muon scattering angle η in the non-bending plane, and to check its compatibility with the target position (vertical target pointing). A veto system is added to the trigger system to suppress events due to halo muons.

At low Q^2 , in the quasi-real photon regime, the muon scattering angles are close to zero, so that target pointing does not work any longer. These events are selected by measuring the energy loss with two vertical scintillator hodoscopes using the bending of the muon track in the spectrometer magnets. At these small angles, there are several background processes such

as elastic scattering off target electrons, elastic and quasi-elastic radiative scattering off target nuclei, and beam halo contributing to the scattered muon signal. The trigger system requires energy clusters in the hadronic calorimeter, which are absent in the background processes. Thus, the quasi-real photon trigger consists of two parts, a trigger on the energy loss by measuring the deflection of the scattered muon in the two spectrometer magnets, and a calorimetric trigger selecting hadron energy clusters above a threshold. The location of the components of the trigger system in the COMPASS experiment is shown schematically in Fig. 3.22.

For deep inelastic scattering reactions, the trigger system is based mainly on hodoscope signals that rely on the information on scattered muons alone. The trigger is fired when the signal of two hodoscopes, which are made of slabs of fast scintillators, are in coincidence and that the trajectory of the hit slabs points to the target. The hodoscopes in coincidence are following.

- H4L and H5L for the Ladder Trigger (LT), which covers low values of Q^2 in the DIS regime.
- H4M and H5M for the Middle Trigger (MT), which extends the kinematic coverage up to few Q^2 (GeV/c)².
- H3O and H4O for the Outer Trigger (OT), which significantly contributes to measuring values of Q^2 up to 30 (GeV/c)².

Those three sub-triggers constitute the purely inclusive trigger component of the trigger system.

A second component of the trigger system is provided by hodoscope signals combined with a calorimetric condition. This is the case for the Inner Trigger (IT), which requires the coincidence of H4I with H5I and an energy deposit beyond the one expected of a single muon in one of the two hadronic calorimeters to reduce background triggers due to elastic or quasi-elastic scattering. This sub-trigger covers almost the same kinematic domain as the LT in the DIS regime. The LAS Trigger (LAST), which requires also an energy deposit in the calorimeters in addition to the coincidence between H1G and H2G hodoscopes contributes significantly in measuring events with Q^2 above 30 (GeV/c)² and up to 100 (GeV/c)². The semi-inclusive trigger component of the trigger system is made up those sub-triggers.

Finally, a standalone calorimeter signal can trigger the data acquisition when the scattered muon escapes the hodoscope-based trigger acceptance. This is particularly interesting at very large Q^2 (in the absence of the LAST). In this case, the energy deposit must be well beyond the one expected by a single muon.

In 2010 and for the 2011 data taking with a muon beam of 200 GeV/c , the additional hodoscope system (LAST) was added to better cover the large values of Q^2 , H1G was installed before SM1 and H2G after SM2. H4O was also updated in 2010 to shrink the inner hole about 20 cm in Salève side.

Many triggers are fired by muons that did not interact with the target due to the sizeable beam emittance and the halo. The beam cross section at the target is 7 mm for the Gaussian core. The halo is included in the muon beam by 25 %, which consists for “near halo” and “far halo”. Those events are rejected by several veto systems. The first veto (Veto 1) is installed at -800 cm and the second veto (Veto 2)⁷ is at -300 cm. There are the new veto hodoscopes called

⁷In 2006, Veto 2 was upgraded.

Table 3.2: Trigger component [35]

		Target pointing	Energy loss of the scattered μ	Low energy deposit in calorimeters	High energy deposit in calorimeters
inclusive	incMT	✓	✓		
	OT	✓			
	LT		✓		
semi-inclusive	IT		✓	✓	
	MT	✓	✓	✓	
	LAST	✓		✓	
calorimetric	CT				✓

Table 3.3: Trigger rate for each trigger in 2004 run [15]

	Trigger rates (/spill)
Inner (with calorimeter trigger)	14 000
Ladder (with calorimeter trigger)	7000
Middle (without calorimeter trigger)	18 000
Outer (without calorimeter trigger)	9500
Calorimeter (stand-alone)	22 000

Veto 1', which is part of Veto 1. With these two systems, beam particles passing through the $\varnothing 4$ cm holes in one of them are vetoed. These systems are fully efficient for tracks with 8 mrad. Thus, the third system (Veto BL) with $\varnothing 10$ cm is installed at -2000 cm. Each veto hodoscope is segmented, which consists of smaller elements with better time resolutions for an off-axis beam region and larger elements for an outside region. Schematic layout of COMPASS veto system is shown in Fig. 3.23.

A drawback of the veto system is the dead time associated with it. It is calculated by the product of the rate of the system and the duration of the time gate during which the veto prohibits a trigger signal. The losses due to the dead time of full veto system (Veto 1 + Veto 2 + Veto BL) are 21 % at nominal beam intensity, whereas the ones of subsample veto system (Veto1 + Veto BL) are 6 %. The full veto system is only applied to the middle and the outer triggers. The subsample veto system is applied to the ladder trigger. The ladder hodoscopes overlap with the calorimeters so that a halo muon may traverse both HCAL2 and hodoscopes. If the muon deposits energy enough to the threshold, no one can distinguish the real event from the halo event: this is why the subsample veto system is required for the ladder trigger. No veto system is applied to the inner trigger if both hodoscope signals and calorimeter signals coincide.

The trigger rates in 2004 are shown in Tab. 3.3. The efficiencies for all hodoscope trigger systems are above 99 % for the inner and the ladder systems, >96 % for the middle system and >97 % for the outer system by means of using the stand alone calorimeter trigger system. The one for the calorimeter trigger system is about 90 % at $\nu \approx 40$ GeV.

The time resolution achieved 500 ps for the inner and ladder system, 1 ns for the outer system due to its large elements and 2 ns for the stand-alone calorimeter trigger system. The efficiency of the veto system is estimated to be about 99 %.

For the hadron physics program, the more complicated trigger system is used. Details can

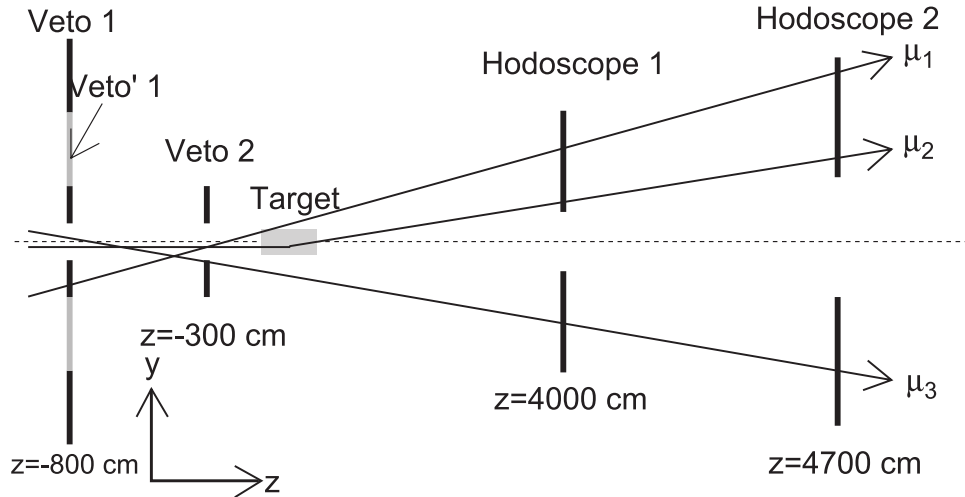


Figure 3.23: Schematic layout of the veto system. The tracks μ_1 and μ_3 are vetoed, whereas the track μ_2 fulfils the inclusive trigger condition [15].

be found in Section 7 of Ref. [70].

3.9. Data acquisition

The vast number of 250 000 detector channels and the total amount of up to 580 TB data recorded per year demanded to follow new directions in the design of the data acquisition scheme. In order to cope with the high particle fluxes of $2 \times 10^8 \mu/\text{spill}$ of 4.8 s, a typical event size of 35 kB, trigger rates of about 10 kHz for the muon beam, and a design value of 100 kHz triggers for the hadron beam, a pipelined and nearly dead-time free readout scheme has been adopted. An overview of the data flow is given in Fig. 3.24. The preamplifiers and discriminators are located close to the detectors. The connection of the detector channels depends on the detector type and is described in the corresponding detector chapters. The data are constantly digitised and buffered, where possible directly at the detector front-end electronics, in custom-designed TDC or ADC modules. The synchronisation of the digitising and readout units is performed by the TCS. Upon arrival of the trigger signal, the data are transferred via fast links to readout-driver modules named CATCH and GeSiCA. These modules also distribute the trigger signals to the front ends and initialise them during the system startup. The readout-driver modules combine the data from up to 16 front-end cards and transmit these sub-events via optical S-LINK [103] at a maximum throughput of 160 MB s^{-1} to readout buffers. The data arriving from each link are stored in 512 MB spill buffer cards. Data from readout modules serving low occupancy detectors are combined by S-LINK multiplexer modules (SMUX) before transmission through the S-LINK. In 2004, the total data transmitted during the spill to the readout buffers corresponded to 230 MB s^{-1} .

The electronics components discussed above, apart from the S-LINK, have been developed specially for COMPASS while the final event building system is based on high-performance PCs and standard Gigabit Ethernet components. The event building takes place during the on- and off-spill time, resulting in an average data rate of 70 MB s^{-1} . These data are recorded on tape remotely at the CERN central data recording facility located in the computer centre.

The architecture of the data acquisition system is very flexible and expandable to handle the

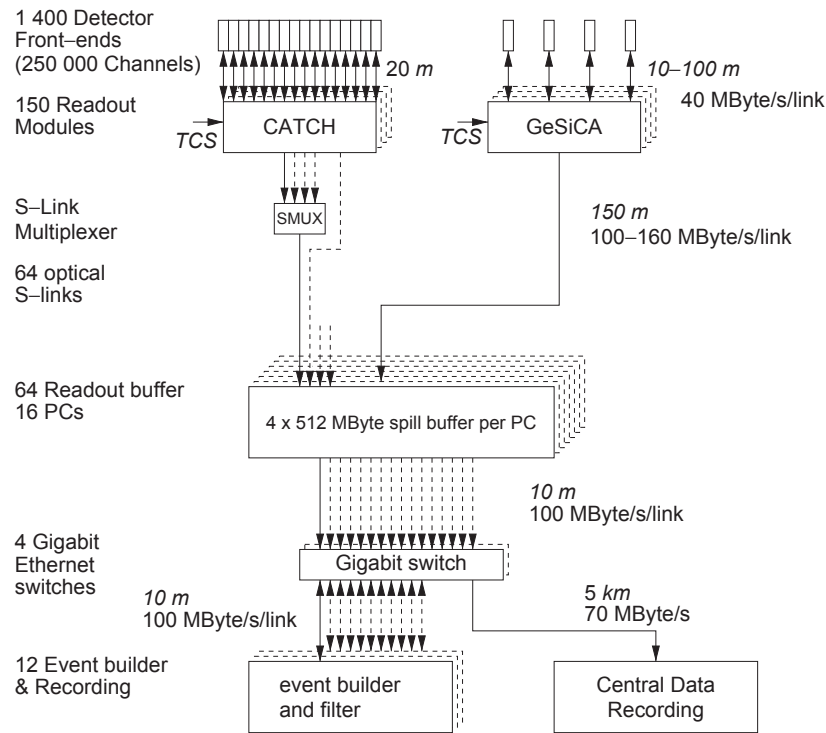


Figure 3.24: The general architecture of the DAQ system. Digitised data from the detector front ends are combined with the readout modules named CATCH and GeSiCA close to the detectors. The storage of the data during the spill and the event building is performed locally. The data are recorded at the CERN computer centre [15].

modifications and upgrades during the lifetime of the experiment. New detectors can simply be added by including the COMPASS standardised readout-driver modules and readout-buffer PCs while higher rates can be processed by adding more event builders and utilising online filter capabilities.

The data taking period containing 200 spills in maximum is called a *run*. A data acquisition lasts until the target and the detectors conditions change. Its span is called *period*, which is typically a week or several weeks. The period is referred to as a week number of a year with prefix W (W24, W35, W49, etc) or serial numbering of periods (P1A, P1B, P2A, etc). The former style was introduced from 2006, and the latter was used until 2003. During data taking, any information like detector problems, DAQ program failures, etc is recorded in the electronic logbook, which are used for the data quality studies.

3.10. Data reconstruction

The total amount of data during data taking is 350 TB per year (at that time in 2006)⁸. The required CPU power for the reconstruction of the events is estimated to 200 k SPECint2000

⁸In 2014 the number of files on CASTOR is 59 million; 83 million for the CMS experiment, and 63 million for the ATLAS experiment. Whereas the total size of files is 14 PB; 31 PB for the ATLAS experiment, and 19 PB for the ALICE experiment. In total there are 270 million files for a total of 90 PB of data on CASTOR. Details can

units⁹, which are provided by 200 Linux Dual-CPU PCs (at that time in 2006). The event reconstruction is performed by CORAL (COmpass Reconstruction and AnaLysis) [105], which is a object oriented program and written in C++.

By comparing read data with Monte Carlo data, reconstructed tracks, clusters, vertices and particle IDs are stored in mini Data Summary Trees (mDST) files. Those files are analysed by the dedicated software called PHAST (PHysics Analysis Software Tool). PHAST can filter an event by user-specified codes and output filtered mDST files but also ROOT files that contain histograms, vertex information, TTree, etc. Details are well described in Section 10 in Ref. [15].

The particle identification The particle identification (PID) is performed inside CORAL by a package called RICHONE [106], which uses the extended likelihood method [107, 108]. The expected Cherenkov emission angle Θ_M for a particle of mass M is computed from the Cherenkov equation:

$$\cos \Theta_M = \frac{1}{n\beta} = \frac{\sqrt{p^2 + M^2}}{np} \quad (3.2)$$

where the particle momentum p provided by CORAL and the refractive index n of the radiator provided by RICH data themselves

The refractive index depends on many parameters; the purity of the gas, the atmospheric pressure, the local temperature, etc. However, it does not depend on the time, so the measurement of the refractive index from the data is necessary. The estimation is performed by (1) computing the refractive indices from data with Eq. (3.2) assuming the π mass, (2) fitting to it distribution with Gaussian, and (3) obtaining the mean values of Gaussian fit. Another method can be used that employs distributions of θ for selected Cherenkov rings or for identified particles, resulting in a cleaner peak. However, the obtained refractive index suffer from biases due to the selection of the sample. Thus, the refractive index estimated by the π mass hypothesis is employed.

The extended likelihood function for each mass hypothesis M is written as

$$\mathcal{L}_M = \exp[-(S_M + B)] \prod_{j=1}^N s_M(\theta_j, \varphi_j) + b, \quad (3.3)$$

$$s_M(\theta_j, \varphi_j) = \frac{S_0}{\sigma_{\theta_j} \sqrt{2\pi}} \exp \left[-\frac{1}{2} \frac{(\theta_j - \Theta_M)^2}{\sigma_{\theta_j}^2} \varepsilon_D(\theta_j, \varphi_j) \right] \quad (3.4)$$

where the variables are listed in Tab. 3.4.

\mathcal{L}_M is computed for mass hypotheses (π , K, p, e, μ) and the background hypothesis. In order to compute the \mathcal{L}_M for the background hypothesis, it is assumed that $s_M(\theta_j, \varphi_j)$ be zero in Eq. (3.3).

In the first order of approximation, the maximum of all the likelihood values corresponds to the best mass hypothesis. In order to improve the identification purity, it is required that the ratios of \mathcal{L} with respect to the background hypothesis $\mathcal{L}_{\text{back}}$ and to the second highest likelihood $\mathcal{L}_{2\text{nd}}$ be above certain thresholds, which depend on analysis-by-analysis. The former

be found in Ref. [104].

⁹www.spec.org/cpu2000

Table 3.4: Description of the variables used by extended likelihood method

Variable	Description
j	the j -th detected photon
N	the number of detected photons
θ_j	the polar angle for j -th photon
φ_j	the azimuthal angle for j -th photon
Θ_M	the expected Cherenkov emission angle for a particle of mass M and momentum p
σ_{θ_j}	the single-photon resolution, calibrated on data
$\varepsilon_D(\theta_j, \varphi_j)$	the photon probability to reach the RICH photon detectors
b	the background hypothesis for the origin of a single reconstructed photon
$s_M(\theta_j, \varphi_j)$	the signal hypothesis for the origin of a single reconstructed photon
S_M	the expected number of signal photons, obtained by integrating s_M over θ up to 70 mrad (the maximum Cherenkov angle allowed by the RICH)
S_0	the expected number of photons from the Frank-Tamm law: $S_0 \equiv N_0 \sin^2 \Theta_M$
N_0	the number of photons at saturation: $N_{\beta \rightarrow 1} / \sin^2 \Theta_{M, \beta \rightarrow 1}$
B	the expected number of background photons, obtained by integrating b over θ up to 70 mrad

ratio $\mathcal{L}/\mathcal{L}_{\text{back}}$ gives the quality of the separation between a mass hypothesis and background hypothesis. The letter ratio $\mathcal{L}/\mathcal{L}_{\text{2nd}}$ indicates the distinction between two different mass hypotheses.

4. Data analysis

The longitudinal double spin asymmetry A_{LL} to be measured in the current study is the asymmetry in the photoproduction of the single-inclusive hadron. In the COMPASS setup the spin direction of the initial lepton beam is fixed, the polarisation of target nucleon is changed.

A_{LL} is defined as

$$A_{LL} = \frac{1}{fP_bP_t} A_{raw}, \quad (4.1)$$

$$A_{raw} = \frac{\sigma_{\leftarrow}^{\rightarrow} - \sigma_{\rightarrow}^{\rightarrow}}{\sigma_{\leftarrow}^{\rightarrow} + \sigma_{\rightarrow}^{\rightarrow}} \quad (4.2)$$

where the dilution factor f that describes the number of polarisable nucleons in the target, lepton beam polarisation P_b , target polarisation P_t , and cross section σ . The narrow arrow (\rightarrow) indicates the direction of the lepton beam polarisation, and the wide arrows (\Rightarrow and \Leftarrow) do the direction of the target polarisation.

There are two or three target cells (see Sec. 3.2), and the direction of the target polarisation is opposite each other. For three cells configuration, the upstream and downstream cells have the same orientation, but the midstream cell has the opposite one. In order to keep the consistency between two and three cells settings, the upstream and the downstream are called “the upstream” and the midstream is called “the downstream” for three cells one. Thus $\sigma_{\leftarrow}^{\rightarrow}$ and $\sigma_{\rightarrow}^{\rightarrow}$ can be written as σ_u and σ_d , respectively:

$$A_{raw} = \frac{\sigma_u - \sigma_d}{\sigma_u + \sigma_d}. \quad (4.3)$$

The analysis procedure is following:

1. Data selection of the reconstructed data
2. Asymmetry calculations from selected data
3. Asymmetry merging

In the following subsections, details are described.

4.1. Data input

Data to be analysed in this analysis were taken in 2002, 2003, 2004, 2006, 2007, and 2011. The track reconstruction (see Sec. 3.10) had been performed on the raw data, and the reconstructed data are stored on tape media at CERN¹⁰. All periods used in this analysis are summarised in Tab. 4.1. The periods P2G+ and P2G− are split from the period P2G since a configuration mixed up with different microwave setups. All mDST files of the first and the second production on W35 in 2006 was produced with bad alignment files. Still in the latest production there are some small problems. Thus, this period is excluded from this analysis.

The selection of runs for the analysis is based on general criteria, like a minimum number of spills per run, a maximum number of detector planes that were marked by a shift crew as having problems, etc. Other rejection criteria are as follows:

¹⁰This management system is called CERN Advanced STORage manager (CASTOR) [109].

Table 4.1: Periods list used in this analysis for each year

Year	Periods
2002	P1C, P2A, P2D, P2E, P2F, P2G+, P2G—
2003	P1A, P1B, P1C, P1D, P1E, P1F, P1I, P1J
2004	W22, W23, W26, W27, W28, W29, W30, W31, W32, W37, W38, W39, W40
2006	W32, W33, W34, W36, W37, W40, W41, W42, W43, W44, W45, W46
2007	W32, W33, W34, W35, W36, W37, W38, W44, W45
2011	W25, W27, W30, W31, W32, W33, W34, W36, W38, W39, W41, W43

- some mDST files are corrupted for unknown reason, they are removed from analysis: 7 runs in 2003, 1 run in 2006 and 2011, respectively. The statistical impact for this removal is negligible (9 out of 7048 runs).
- For the end of 2004 data and whole 2006 data, the incorrect factor for the magnetic field of the SM2 magnet was used in the data reconstruction, causing incorrect particles momenta. In order to fix it, a re-calculation algorithm is applied at the stage of the PHAST data processing.
- In 2006, some runs were taken with 2.5 T or 1.8 T magnetic field of solenoid magnet: normal operation underwent with 1 T. This larger field resulted in the decrease of efficiency for Micromegas since it had still magnetic materials in the structure in 2006 run. The number of runs to be rejected is 116 out of 1262 runs.

On the spill-by-spill basis, it is required that certain observables have stable values: if not, a spill is marked as problematic. These observables are, for example, the number of primary vertices, the number of tracks per event, and the number of tracks per vertex. The spills that do not fulfil requirements are discarded.

4.2. Data selection

4.2.1. Event selection

The analysis starts from the following event selection:

1. event has a primary vertex¹¹ which contains a beam track,
2. event has the incoming muon and the scattered muon,
3. two or more outgoing charged particles (including the scattered muon) are in the primary vertex,
4. the primary vertex is in target region,
5. the incoming muon trajectory is crossing all target cells,
6. the momentum of the incoming muon is in range and momentum uncertainty is in range,

¹¹A vertex is the place where particles collide. It is also called Interaction Point (IP).

7. $0.1 < y < 0.9$,
8. $Q^2 < 1 \text{ (GeV/c)}^2$,
9. the maximum value of the hadron transverse momentum p_T in all the hadrons in the event exceeds 0.7 GeV/c .

In the reconstruction one or more vertices can be marked as “a primary vertex”, one has to select “the true primary vertex” by counting the number of outgoing particles as the more energy a particle has, the more outgoing particles are created. If the number of outgoing particles equals with some primary vertices, the vertex that has the minimum χ^2 is selected as the primary. Here χ^2 is the sum of the square of the difference between the fitted track position and the hit position divided by the square of the hit position uncertainty and stored in a mDST file. Vertex position distribution on Z -axis is shown in Fig. 4.1.

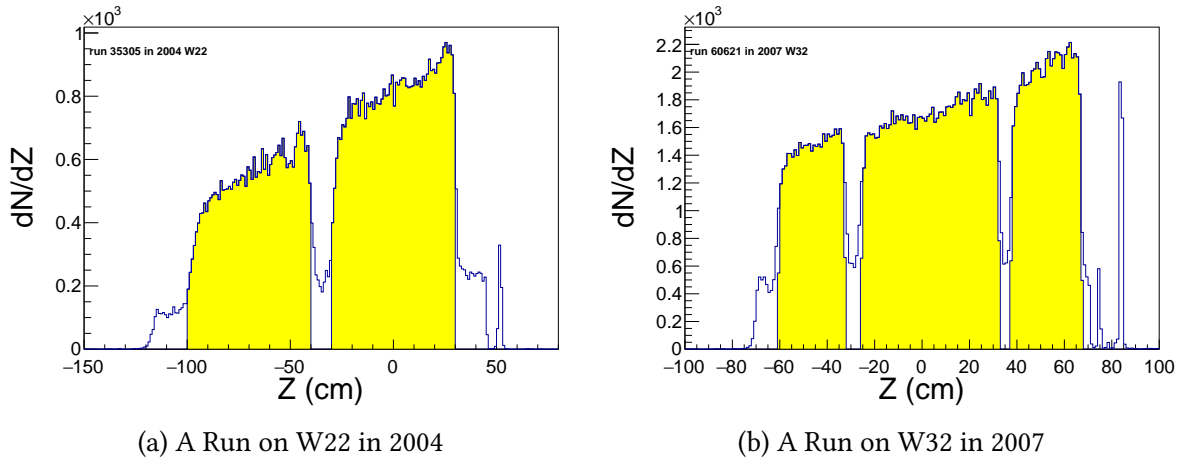


Figure 4.1: Vertex position distribution along Z -axis for the two- and the three- target cells. The peaks around 50 cm (left) and 85 cm (right) shows the Mylar window of target system. The events on filling areas (yellow highlighting) are used for further analysis.

The incoming muon trajectory should pass through all the target cells to ensure an equal flux on them. Also, a momentum of the incoming muon lies with a range, which depends on the beam centre momentum. Specifically, it is $185 < P_b < 215 \text{ GeV/c}$ only for 2011 data and $140 < P_b < 180 \text{ GeV/c}$ for the other years. Beam Momentum Station (BMS) measures the momentum of the beam on event by event. If BMS fails the measurement its momentum is to be set as the centre values of the beam without uncertainty $\sigma_{|q|/p}$. Therefore, those events are removed by applying $0.5 \times 10^{-9} < \sigma_{|q|/p}^2 < 20 \times 10^{-9} \text{ (c/GeV)}^2$. The beam momentum distribution with and without $\sigma_{|q|/p}^2$ cut is shown in Fig. 4.2.

The energy fraction y of the virtual photon to the incoming muon is larger than 0.1 as the difficulty of handling an event in the reconstruction. Moreover, y should be smaller than 0.9 since the radiative correction affects strongly. As the photoproduction is discussed in this analysis Q^2 should be smaller than 1 (GeV/c)^2 .

Finally, the maximum value of transverse momentum p_T for outgoing charged particles with respect to the virtual photon direction in an event exceeds 0.7 GeV/c for the sake of the reduction of event statistics to be processed in the next step.

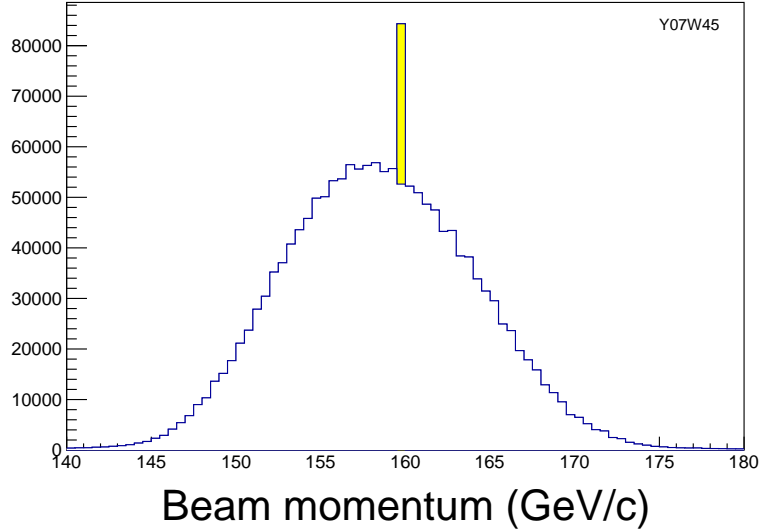


Figure 4.2: The beam momentum distribution. Events cut by $\sigma_{|q|/p}^2$ selection are shown by yellow highlighted region.

4.2.2. Hadron selection

After the event selection, hadron by hadron selection starts. The following list shows the summary of hadron selection.

1. triggered by either IT, MT, LT, CT, or iMT,
2. each outgoing particle is not confirmed as muon,
3. the hadron does not cross solenoid magnet vessel,
4. $p_T > 0.7 \text{ GeV}/c$,
5. $0.2 < z < 0.8$,
6. $0.01 < \theta_{\text{hadron}} < 0.12$,
7. the hadron is not electron,
8. $Z_{\text{last}} > 350 \text{ cm}$,
9. $2.4 > \eta_{\text{CMS}} > 0.45$ for 2002, 2003, and 2004,
 $2.4 > \eta_{\text{CMS}} > -0.1$ for 2006, 2007, and 2011.

Either InnerTrigger (IT), MiddleTrigger (MT), LadderTrigger (LT), CalorimeterTrigger (CT), or inclusiveMiddleTrigger (iMT) is fired on the event¹². The y distributions for each trigger are shown in Fig. 4.3. The almost events are triggered by IT and its peak is around 0.3. The second most events are triggered by LT and its peak is around 0.6. As CT is introduced from 2004, there is no events triggered by it.

¹²This may be done at the event selection naturally. However, it was performed in the hadron selection for a technical reason.

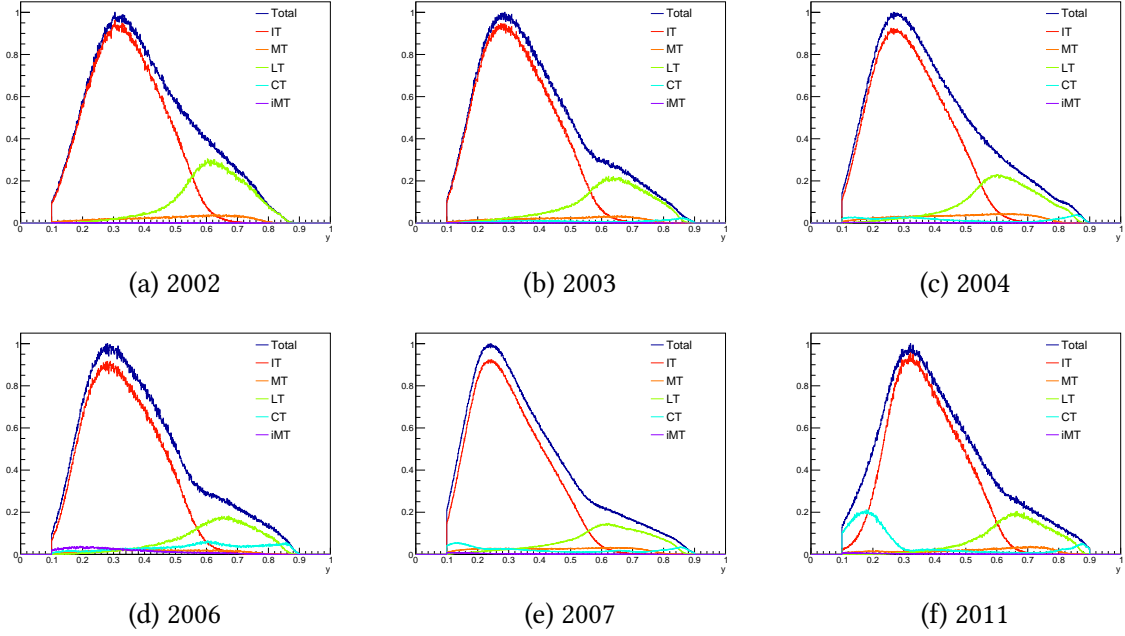


Figure 4.3: Trigger by trigger y distribution for each year.

A muon track candidate requires that the total amount of radiation lengths (X/X_0), which is stored on the mDST file, should be larger than 15. When a hadron track crosses in the solenoid magnet surrounding the target cells, there are possibilities to interact with materials or deposit energy. The inner radius of the solenoid magnet at the end depends on magnet type: at $Z = 118.4$ cm with the SMC magnet, the radius should be smaller than 14 cm. For the OD magnet, the radius should be smaller than 35 cm at $Z = 130.5$ cm.

In the JSV framework, the lower limit of the transverse momentum of the hadron is $1.0 \text{ GeV}/c^2$. To investigate systematic effects and compare asymmetries with previous ones [16, 18, 19, 23], the selection $p_T > 0.7 \text{ GeV}/c$ is employed.

The energy fraction of hadron to virtual photon z is $0.2 < z < 0.8$. By the lower limit, the target fragmentation region is removed. On the other hand, with the higher limit, the contribution from diffractive scattering can be suppressed where a lepton and a nucleon interacts inelastically and creates hadrons in the final state.

A selection for a hadron angle with respect to a virtual photon in the laboratory frame (see Fig. 2.8b) is done by $0.01 < \theta_{\text{hadron}} < 0.12$ to guarantee a common rapidity for the deuteron and the proton target. This θ_{hadron} range corresponds to the one for the rapidity at the muon-nucleon centre of mass system as $2.4 > \eta_{\text{CMS}} > -0.1$. Here η and η_{CMS} are defined as follows:

$$\eta = -\ln \tan \left(\frac{\theta_{\text{hadron}}}{2} \right), \quad (4.4)$$

$$\eta_{\text{CMS}} = \eta - \frac{1}{2} \ln \frac{2E_\mu}{M_N}, \quad (4.5)$$

where the incident muon energy E_μ and the nucleon mass M_N .

The particle identification is done by using the likelihood \mathcal{L} for mass hypotheses. The estimation of likelihood is done at the stage of the data reconstruction using “RICHONE” package

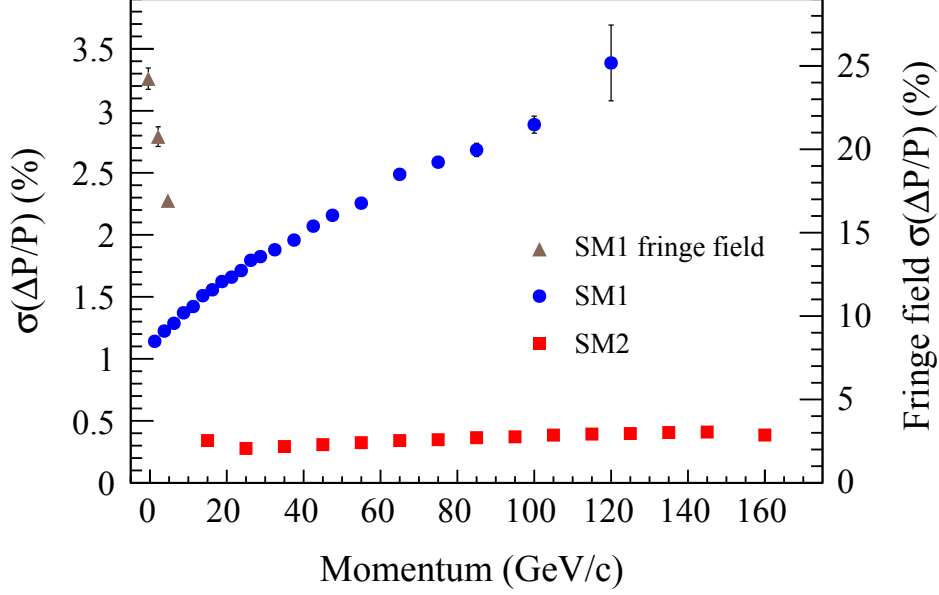


Figure 4.4: Relative momentum resolution as a function of track momentum, taken from Ref. [70]. The uncertainties of momentum determined by SM1 fringe field are quite larger than ones determined by SM1 or SM2.

(see Sec. 3.10). In order to reject electrons, it is required that the ratio $\mathcal{L}_e/\mathcal{L}_\pi$ should be smaller than 1.8.

The final detector hit position on the Z -axis should be larger than 350 cm since the momentum of the hadron detected $Z_{\text{last}} < 350$ cm is determined by the fringe field of the SM1, resulting in a larger momentum uncertainty (shown in Fig. 4.4). In the past COMPASS analyses, Z_{last} cut was required in order to reject hadrons having large momentum uncertainty. In this analysis, such hadrons are already rejected by the other selection criteria.

In Ref. [45], it was shown that the sensitivity of ΔG lost if the asymmetries were calculated with hadrons having larger θ_{hadron} domain ($0.01 < \theta_{\text{hadron}} < 0.18$) comparing to the ones having smaller θ_{hadron} domain ($0.01 < \theta_{\text{hadron}} < 0.07$). Until 2004, the SMC magnet that have smaller acceptance than the OD magnet used from 2006 was used (see Sec. 3.2). Therefore, $\eta_{\text{CMS}} > 0.45$ is applied only for 2002, 2003, and 2004 data not for the other years in order to study the sensitivity of ΔG with respect to η_{CMS} . For the upper limit, $\eta_{\text{CMS}} < 2.4$ is applied that corresponds to $\theta_{\text{hadron}} > 0.01$. The summary table of event and hadron statistics on each selection are shown in Tabs. 4.2 and 4.3.

Table 4.2: Statistics of event selection

(a) the number of events: 2002			(b) the number of events: 2003		
Cut	Events $\times 10^6$	Ratio %	Cut	Events $\times 10^6$	Ratio %
All events	850.4	100.0	All events	1446.0	100.0
Has BPV	723.4	85.1	Has BPV	1327.6	91.8
Has μ and μ'	476.5	56.0	Has μ and μ'	837.9	57.9
Has 2 or more particles	318.2	37.4	Has 2 or more particles	556.6	38.5
Vertex is in target region	219.1	25.8	Vertex is in target region	381.4	26.4
Crossed all target cells	203.6	23.9	Crossed all target cells	362.0	25.0
Beam momentum cut	203.4	23.9	Beam momentum cut	361.2	25.0
$0.1 < y < 0.9$	198.8	23.4	$0.1 < y < 0.9$	350.4	24.2
$Q^2 < 1 \text{ GeV}^2$	186.8	22.0	$Q^2 < 1 \text{ GeV}^2$	322.9	22.3
$\max(p_T) > 0.7$	26.9	3.2	$\max(p_T) > 0.7$	45.4	3.1

(c) the number of events: 2004			(d) the number of events: 2006		
Cut	Events $\times 10^6$	Ratio %	Cut	Events $\times 10^6$	Ratio %
All events	2804.1	100.0	All events	2367.6	100.0
Has BPV	2577.3	91.9	Has BPV	2199.7	92.9
Has μ and μ'	1368.5	48.8	Has μ and μ'	1218.4	51.5
Has 2 or more particles	911.4	32.5	Has 2 or more particles	711.2	30.0
Vertex is in target region	635.7	22.7	Vertex is in target region	478.1	20.2
Crossed all target cells	608.3	21.7	Crossed all target cells	469.7	19.8
Beam momentum cut	606.9	21.6	Beam momentum cut	467.8	19.8
$0.1 < y < 0.9$	587.3	20.9	$0.1 < y < 0.9$	447.3	18.9
$Q^2 < 1 \text{ GeV}^2$	532.1	19.0	$Q^2 < 1 \text{ GeV}^2$	407.1	17.2
$\max(p_T) > 0.7$	79.3	2.8	$\max(p_T) > 0.7$	67.5	2.8

(e) the number of events: 2007			(f) the number of events: 2011		
Cut	Events $\times 10^6$	Ratio %	Cut	Events $\times 10^6$	Ratio %
All events	5644.0	100.0	All events	10100.3	100.0
Has BPV	5525.0	97.9	Has BPV	6343.4	62.8
Has μ and μ'	1913.6	33.9	Has μ and μ'	1478.2	14.6
Has 2 or more particles	1193.8	21.2	Has 2 or more particles	815.4	8.1
Vertex is in target region	983.6	17.4	Vertex is in target region	615.8	6.1
Crossed all target cells	972.6	17.2	Crossed all target cells	611.7	6.1
Beam momentum cut	911.8	16.2	Beam momentum cut	604.1	6.0
$0.1 < y < 0.9$	815.1	14.4	$0.1 < y < 0.9$	564.8	5.6
$Q^2 < 1 \text{ GeV}^2$	735.7	13.0	$Q^2 < 1 \text{ GeV}^2$	500.8	5.0
$\max(p_T) > 0.7$	135.8	2.4	$\max(p_T) > 0.7$	92.9	0.9

Table 4.3: Statistics of hadron selection

(a) hadron selection: 2002			(b) hadron selection: 2003		
Cut	Tracks $\times 10^6$	Ratio %	Cut	Tracks $\times 10^6$	Ratio %
All tracks	80.4	100.0	All tracks	148.2	100.0
triggered	79.6	99.1	triggered	146.9	99.1
don't cross solenoid	76.0	94.5	don't cross solenoid	140.0	94.4
not muon	75.5	94.0	not muon	139.1	93.9
$p_T > 0.7$	25.8	32.0	$p_T > 0.7$	45.7	30.8
$0.2 < z < 0.8$	17.6	21.9	$0.2 < z < 0.8$	31.6	21.3
$0.01 < \theta < 0.12$	17.4	21.7	$0.01 < \theta < 0.12$	31.3	21.1
not electron	16.4	20.4	not electron	31.0	20.9
$Z_{\text{last}} < 350$	16.4	20.4	$Z_{\text{last}} < 350$	31.0	20.9
$0.45 < \eta_{\text{CMS}} < 2.4$	13.6	16.9	$0.45 < \eta_{\text{CMS}} < 2.4$	25.4	17.1

(c) hadron selection: 2004			(d) hadron selection: 2006		
Cut	Tracks $\times 10^6$	Ratio %	Cut	Tracks $\times 10^6$	Ratio %
All tracks	243.7	100.0	All tracks	267.2	100.0
triggered	243.3	99.8	triggered	266.0	99.5
don't cross solenoid	231.5	95.0	don't cross solenoid	265.3	99.3
not muon	230.3	94.5	not muon	264.4	99.0
$p_T > 0.7$	79.6	32.7	$p_T > 0.7$	73.4	27.5
$0.2 < z < 0.8$	55.3	22.7	$0.2 < z < 0.8$	37.1	13.9
$0.01 < \theta < 0.12$	54.5	22.4	$0.01 < \theta < 0.12$	35.5	13.3
not electron	53.4	21.9	not electron	34.6	13.0
$Z_{\text{last}} < 350$	53.4	21.9	$Z_{\text{last}} < 350$	34.6	13.0
$0.45 < \eta_{\text{CMS}} < 2.4$	43.0	17.7	$-0.1 < \eta_{\text{CMS}} < 2.4$	34.6	12.9

(e) hadron selection: 2007			(f) hadron selection: 2011		
Cut	Tracks $\times 10^6$	Ratio %	Cut	Tracks $\times 10^6$	Ratio %
All tracks	576.3	100.0	All tracks	454.7	100.0
triggered	575.5	99.9	triggered	454.2	99.9
don't cross solenoid	573.8	99.6	don't cross solenoid	453.1	99.7
not muon	572.2	99.3	not muon	451.7	99.4
$p_T > 0.7$	155.7	27.0	$p_T > 0.7$	108.6	23.9
$0.2 < z < 0.8$	76.4	13.3	$0.2 < z < 0.8$	42.0	9.2
$0.01 < \theta < 0.12$	68.7	11.9	$0.01 < \theta < 0.12$	40.6	8.9
not electron	66.1	11.5	not electron	40.0	8.8
$Z_{\text{last}} < 350$	66.1	11.5	$Z_{\text{last}} < 350$	40.0	8.8
$-0.1 < \eta_{\text{CMS}} < 2.4$	65.9	11.4	$-0.1 < \eta_{\text{CMS}} < 2.4$	39.5	8.7

4.3. Method for asymmetry calculation

Now one has data for asymmetry calculations. In the simplest method, A_{LL} is calculated by replacing σ with the number of hadrons in Eq. (4.1). However, in this case its statistical uncertainty is larger than other methods described in the following section.

Several methods had been developed in the COMPASS collaboration to minimise the statistical uncertainties: the first order standard method (see Sec. 4.3.1), the first order weighted method (see Sec. 4.3.2), the second order standard method (see Sec. 4.3.3), and the second order weighted method (see Sec. 4.3.4). The second order weighted method gives minimum statistical uncertainties and is employed for all asymmetry calculations.

In the following subsections, they are described in detail. Note that in this section for the simplicity, the subscript LL in A_{LL} is dropped off; A means A_{LL} unless otherwise noted.

4.3.1. The first order method

The number of events measured in the upstream and downstream cells are

$$N_u = \Phi a_u n_u \sigma_0 (1 - w P_{t,u} A), \quad (4.6)$$

$$N_d = \Phi a_d n_d \sigma_0 (1 - w P_{t,d} A) \quad (4.7)$$

where Φ is a flux of an incoming beam, a_u (a_d) is acceptance for the upstream (downstream) cell, n_u (n_d) is the number of the target nucleons, $P_{t,u}$ ($P_{t,d}$) is an absolute value of the polarisation of the upstream (downstream) cell, σ_0 is the unpolarised cross section, and $w = f \times P_b$ is the weight.

Then a counting rate asymmetry is

$$\Delta = \frac{N_u - N_d}{N_u + N_d} = \frac{r - 1 + wA(rP_{t,u} + P_{t,d})}{r + 1 + wA(rP_{t,u} - P_{t,d})} \quad (4.8)$$

where $r = a_u n_u / a_d n_d$. In general $r \neq 1$ and Δ provides a measurement of A that is biased by a term $(r - 1)/(r + 1)$, which is called the apparatus asymmetry.

In order to eliminate this bias the orientations of the spins in the two target cells are reverted by rotating the magnetic field. Note that before the field rotation, the polarisations of the beam and the target are anti-parallel, whereas they are parallel after the rotation.

$$N_{u'} = \Phi' a_{u'} n_u \sigma_0 (1 - w P_{t,u'} A), \quad (4.9)$$

$$N_{d'} = \Phi' a_{d'} n_d \sigma_0 (1 - w P_{t,d'} A), \quad (4.10)$$

$$\Delta' = -\frac{N_{u'} - N_{d'}}{N_{u'} + N_{d'}} = \frac{-(r' - 1) + wA(r'P_{t,u'} + P_{t,d'})}{r' + 1 - wA(r'P_{t,u'} - P_{t,d'})}. \quad (4.11)$$

Thus the spin configuration of $N_{u'}$ is same as N_d , resulting in the sign change in Eq. (4.11).

Adding Eqs. (4.8) and (4.11), one can have the following equation with assumptions (see App. A.1):

$$\frac{\Delta + \Delta'}{2} = \frac{4r}{(1+r)^2} \frac{P_{t,u} + P_{t,d} + P_{t,u'} + P_{t,d'}}{4} wA. \quad (4.12)$$

Thus the first order method for asymmetry extraction is defined by

$$A_{1s} = \frac{1}{1 - \alpha^2} \frac{1}{P_t w} \frac{\Delta + \Delta'}{2}, \quad (4.13)$$

$$\delta A_{1s} = \frac{1}{2P_t \langle w \rangle \sqrt{1 - \alpha^2}} \sqrt{\frac{1}{(N_u + N_d)} + \frac{1}{(N_{u'} + N_{d'})}}, \quad (4.14)$$

$$P_t = \frac{P_{t,u} + P_{t,d} + P_{t,u'} + P_{t,d'}}{4}, \quad (4.15)$$

$$\alpha = \frac{n_u a_u - n_d a_d}{n_u a_u + n_d a_d}. \quad (4.16)$$

The correction factor $1 - \alpha^2$, which is due to $n_u a_u \neq n_d a_d$, is quadratic in α . Thus if $\alpha \approx 0$, one does not need to know it accurately. Typically we have $|r - 1| < 0.1$ and $\alpha^2 < 0.0025$, one can even approximate $1 - \alpha^2 \approx 1$.

One can write δA_{1s} as

$$\delta A_{1s} = \frac{1}{P_t \langle w \rangle \sqrt{(1 - \alpha^2)(1 - \beta^2)(N + N')}} \quad (4.17)$$

where $N = N_u + N_d$, $N' = N_{u'} + N_{d'}$, and $\beta = (N - N')(N + N')$, which is the asymmetry in the amount of data before and after field rotation. The loss in statistics is equivalent to a factor $(1 - \alpha^2)(1 - \beta^2)$ in terms of number of events.

When the double ratio r is different between before and after the rotation, the apparatus asymmetry does not cancel perfectly in $\Delta + \Delta'$ and a false asymmetry appears which biases the measurement:

$$A_f = \frac{1}{1 - \alpha^2} \frac{1}{2P_t w} \left(\frac{1 - r}{1 + r} - \frac{1 - r'}{1 + r'} \right). \quad (4.18)$$

4.3.2. The first order weighted method

The standard method is not optimal from a statistical point of view. It gives the same weight to all events independently of the value of w , whereas it is clear that when w is very small the event carries hardly any information on the physical asymmetry.

Let's consider small bins according to the value of w . Here w means a general weight and an actual value is specified by a calculation. w_i represents the weight at i -th kinematic bin such as y . By using the i -th asymmetry $A_i = \frac{1}{w_i} \frac{N_{u,i} - N_{d,i}}{N_{u,i} + N_{d,i}}$, one can calculate a weighted mean of all A_i :

$$A_w = \frac{\sum_i \frac{A_i}{(\delta A_i)^2}}{\frac{1}{(\delta A_i)^2}} = \frac{\sum_i A_i w_i^2 N_i}{\sum_i w_i^2 N_i} = \frac{\sum_i N_{u,i} w_i - \sum_i N_{d,i} w_i}{\sum_i N_{u,i} w_i^2 + \sum_i N_{d,i} w_i^2}. \quad (4.19)$$

where $1/(\delta A_i)^2 = w_i^2 N_i$. As $\sum_i N_{u,i} w_i$ is identical to the sum of w for all i bins in the upstream cell, it can be replaced with $\sum_u w$:

$$A_w = \frac{\sum_u w - \sum_d w}{\sum_u w^2 + \sum_d w^2}, \quad (4.20)$$

$$(\delta A_w)^2 = \frac{1}{\sum_i \frac{1}{(\delta A_i)^2}} = \frac{1}{\sum_u w^2 + \sum_d w^2} = \frac{1}{\langle w^2 \rangle (N_u + N_d)} \quad (4.21)$$

where $\sum_u w^2 = \langle w^2 \rangle N_u$ is used.

Comparing uncertainty ratio, the weighted method gives a smaller uncertainty:

$$\left(\frac{\delta A_w}{\delta A_s} \right) = \frac{\langle w \rangle^2}{\langle w^2 \rangle} = 1 - \frac{\sigma_w^2}{\langle w^2 \rangle}, \quad (4.22)$$

where σ_w^2 is the variance of the weight w . The larger $\sigma_w^2 / \langle w^2 \rangle$, the larger gain in statistical uncertainty with weighted method.

One can derive the first order weighted method from Eq. (4.13) in the same way described in Sec. 4.3.1:

$$A_{1w} = \frac{1}{2P_t(1-\alpha^2)} \left[\frac{\sum_u w - \sum_d w}{\sum_u w^2 + \sum_d w^2} + \frac{\sum_{u'} w - \sum_{d'} w}{\sum_{u'} w^2 + \sum_{d'} w^2} \right], \quad (4.23)$$

$$P_t = \frac{1}{4} (P_{t,u} + P_{t,d} + P_{t,u'} + P_{t,d'}), \quad (4.24)$$

$$\delta A_{1w} = \frac{1}{2P_t \sqrt{1-\alpha^2}} \sqrt{\frac{1}{\sum_u w^2 + \sum_d w^2} + \frac{1}{\sum_{u'} w^2 + \sum_{d'} w^2}}. \quad (4.25)$$

4.3.3. The second order method

The second order method of the asymmetry extraction is introduced in this section. This method was introduced by the SMC experiment [110] then adapted to the COMPASS experiment.

Let's start the expression of the number of events in a given target cell:

$$N = a\Phi n\sigma(1 + P_b P_t f A) \quad (4.26)$$

For each cell,

$$N_u = a_u \Phi n_u \sigma_0 (1 + P_b P_{t,u} f_u A) = \alpha_u (1 + \beta_u A), \quad (4.27)$$

$$N_d = a_d \Phi n_d \sigma_0 (1 + P_b P_{t,d} f_d A) = \alpha_d (1 + \beta_d A), \quad (4.28)$$

$$N_{u'} = a_{u'} \Phi' n_{u'} \sigma_0 (1 + P_b P_{t,u'} f_{u'} A) = \alpha_{u'} (1 + \beta_{u'} A), \quad (4.29)$$

$$N_{d'} = a_{d'} \Phi' n_{d'} \sigma_0 (1 + P_b P_{t,d'} f_{d'} A) = \alpha_{d'} (1 + \beta_{d'} A). \quad (4.30)$$

The number of events N can be considered as a function of x_{Bj} , Q^2 , vertex position \vec{v} , time t , etc. Integrating N over all variables except x_{Bj} , one obtains

$$N(x_{Bj}) \equiv \int N(x_{Bj}, Q^2, \vec{\nu}, t, \dots) dQ^2 d\vec{\nu} dt \dots \quad (4.31)$$

and one assumes that A does NOT depend on all integration variables. One can combine all integration variables in $d\vec{x} = dQ^2 d\vec{\nu} dt \dots$. This leads to

$$N_u(x_{Bj}) = \left(\int \Phi n_u \sigma_u d\vec{x} \right) \langle a_u \rangle (1 + \langle \beta_u \rangle A) \quad (4.32)$$

with the average acceptance

$$\langle a_u \rangle = \frac{\int a_u \Phi n_u \sigma_u d\vec{x}}{\int \Phi n_u \sigma_u d\vec{x}}, \quad (4.33)$$

and the average β

$$\langle \beta_u \rangle = \frac{\int \alpha_u \beta_u d\vec{x}}{\int \alpha_u d\vec{x}}. \quad (4.34)$$

Now the double ratio of the number of events, δ , is defined as follow:

$$\delta \equiv \frac{N_u N_{d'}}{N_{u'} N_d} \quad (4.35)$$

$$= \frac{\langle a_u \rangle \langle a_{d'} \rangle}{\langle a_{u'} \rangle \langle a_d \rangle} \frac{\int \Phi n_u \sigma_u d\vec{x} \int \Phi n_{d'} \sigma_{d'} d\vec{x}}{\int \Phi n_{u'} \sigma_{u'} d\vec{x} \int \Phi n_d \sigma_d d\vec{x}} \times \frac{(1 + \langle \beta_u \rangle A) (1 + \langle \beta_{d'} \rangle A)}{(1 + \langle \beta_{u'} \rangle A) (1 + \langle \beta_d \rangle A)}. \quad (4.36)$$

$\int \Phi n_u \sigma_u d\vec{x}$ can approximately be written as $\int \Phi d\vec{x}_1 \cdot \int n_u \sigma_u d\vec{x}_2$ with $d\vec{x}_1 = d\vec{\nu} dt$ and $d\vec{x}_2 =$ "all other integration variables" since Φ depends only on the integration variables $\vec{\nu}$ and t whereas $n_u \sigma_u$ depends only weakly on $\vec{\nu}$ if the target is homogeneously filled and does not depend on the time t if the target does not move between field rotation. Thus,

$$\frac{\int \Phi n_u \sigma_u d\vec{x} \int \Phi' n_{d'} \sigma_{d'} d\vec{x}}{\int \Phi' n_{u'} \sigma_{u'} d\vec{x} \int \Phi n_d \sigma_d d\vec{x}} = \frac{\int \Phi d\vec{x}_1 \cdot \int n_u \sigma_u d\vec{x}_2 \int \Phi' d\vec{x}_1 \cdot \int n_{d'} \sigma_{d'} d\vec{x}_2}{\int \Phi' d\vec{x}_1 \cdot \int n_{u'} \sigma_{u'} d\vec{x}_2 \int \Phi d\vec{x}_1 \cdot \int n_d \sigma_d d\vec{x}_2} = 1 \quad (4.37)$$

since n and σ does not change before and after field rotation.

Assuming that the beam position does not change between the filed rotation, the double ratio of $\frac{\langle a_u \rangle \langle a_{d'} \rangle}{\langle a_{u'} \rangle \langle a_d \rangle}$ becomes unity. Eq. (4.36) can be rewritten in the second order equation of A ¹³.

$$aA^2 + bA + c = 0 \quad (4.38)$$

with

¹³This is the origin for the name of this method.

$$a = \delta \langle \beta_{u'} \rangle \langle \beta_d \rangle - \langle \beta_u \rangle \langle \beta_{d'} \rangle , \quad (4.39)$$

$$b = \delta (\langle \beta_{u'} \rangle + \langle \beta_d \rangle) - (\langle \beta_u \rangle + \langle \beta_{d'} \rangle) , \quad (4.40)$$

$$c = \delta - 1 . \quad (4.41)$$

Thus

$$A = \begin{cases} \frac{-b \pm \sqrt{b^2 - 4ac}}{2a} & a \neq 0 \\ -\frac{c}{b} & a = 0 \end{cases} . \quad (4.42)$$

The sign in Eq. (4.42) depends on the sign of $P_{t,u}$.
 $\langle \beta \rangle$ can be calculated as follows

$$\langle \beta \rangle = \frac{\int \alpha \beta d\vec{x}}{\int \alpha d\vec{x}} \stackrel{N \text{ is large}}{\approx} \frac{\sum_{i=1}^N \beta_i}{N} . \quad (4.43)$$

The uncertainty of asymmetry is given by

$$(\sigma_A)^2 = \left(\frac{\partial A}{\partial \delta} \sigma_\delta \right)^2 = \frac{1}{\langle \beta \rangle^2 N_{tot}} \quad (4.44)$$

where $N_{tot} = N_u + N_d + N_{u'} + N_{d'}$, assuming $N_{tot}/4 \equiv N_u \approx N_d \approx N_{u'} \approx N_{d'}$ and $\langle \beta \rangle \equiv \langle \beta_u \rangle = \langle \beta_{d'} \rangle = -\langle \beta_{u'} \rangle = -\langle \beta_d \rangle$.

4.3.4. The second order weighted method

Similarly to the first order weighted method, one can optimise the second order method. In this approach, the values of f , P_b , and P_t are calculated on the event-by-event basis and then they are used as weight. To introduce the weight into the second order method, a few modifications of the formalism are necessary. Here one can define p as follows

$$\begin{aligned} p &\equiv \int w(\vec{x}) N(\vec{x}) d\vec{x} \approx \sum_i^N w_i \\ &= \int \alpha(\vec{x}) w(\vec{x}) d\vec{x} + \int \alpha(\vec{x}) w(\vec{x}) d\vec{x} \frac{A \int \alpha(\vec{x}) w(\vec{x}) \beta(\vec{x}) d\vec{x}}{\int \alpha(\vec{x}) w(\vec{x}) d\vec{x}} \\ &= \int \alpha(\vec{x}) w(\vec{x}) (1 + A \langle \beta \rangle_w) d\vec{x} \\ &= \int d\vec{x} \Phi n \sigma \frac{\int d\vec{x} \Phi n \sigma w a}{\int d\vec{x} \Phi n \sigma w} (1 + A \langle \beta \rangle_w) \\ &= \int d\vec{x} \Phi n \sigma \langle a \rangle_w (1 + A \langle \beta \rangle_w) \end{aligned} \quad (4.45)$$

where

$$\langle \beta \rangle_w = \frac{\int \alpha(\vec{x}) w(\vec{x}) \beta(\vec{x}) d\vec{x}}{\int \alpha(\vec{x}) w(\vec{x}) d\vec{x}} \stackrel{N \text{ is large}}{\approx} \frac{\sum_i^N w_i \beta_i}{\sum_i^N w_i}. \quad (4.46)$$

And the uncertainty on p is

$$\sigma_p^2 = \int w^2(\vec{x}) N(\vec{x}) d\vec{x} \approx \sum_i^N w_i^2. \quad (4.47)$$

Assuming that there is no acceptance difference before and after field rotations, the following equation is derived:

$$\delta = \frac{p_u p_{d'}}{p_d p_{u'}} = \frac{\sum w_u \cdot \sum w_{d'}}{\sum w_d \cdot \sum w_{u'}} = \frac{(1 + \langle \beta_u \rangle_w A)(1 + \langle \beta_{d'} \rangle_w A)}{(1 + \langle \beta_d \rangle_w A)(1 + \langle \beta_{u'} \rangle_w A)}. \quad (4.48)$$

Solving for A , one can have equations:

$$aA^2 + bA + c = 0 \quad (4.49)$$

with

$$a = \delta \langle \beta_{u'} \rangle_w \langle \beta_d \rangle_w - \langle \beta_u \rangle_w \langle \beta_{d'} \rangle_w, \quad (4.50)$$

$$b = \delta (\langle \beta_{u'} \rangle_w + \langle \beta_d \rangle_w) - (\langle \beta_u \rangle_w + \langle \beta_{d'} \rangle_w), \quad (4.51)$$

$$c = \delta - 1. \quad (4.52)$$

Thus

$$A = \begin{cases} \frac{-b \pm \sqrt{b^2 - 4ac}}{2a} & a \neq 0 \\ -\frac{c}{b} & a = 0 \end{cases}, \quad (4.53)$$

which is same as Eq. (4.42). The statistical uncertainty is

$$\begin{aligned} \sigma_A &= \left(\frac{\partial A}{\partial \delta} \sigma_\delta \right)^2 \\ &= \frac{\langle w^2 \rangle}{\langle w\beta \rangle^2} \frac{1}{N_{tot}} \end{aligned} \quad (4.54)$$

with assumptions that are used to derive the uncertainty for the second order non-weighted method Eq. (4.44). The exact expression for the uncertainty is explained in App. A.2.

Here the reason that the weighted method is better than the standard method is explained. The statistical uncertainty on the second order weighted method is reduced to $w = \beta$:

$$\sigma_A^2 = \frac{1}{\langle \beta^2 \rangle} \frac{1}{N}. \quad (4.55)$$

Thus the ratio of uncertainties is

$$\frac{\sigma_{A_{2w}}}{\sigma_{A_{2s}}} = \frac{\frac{1}{\langle \beta^2 \rangle} \frac{1}{N}}{\frac{1}{\langle \beta \rangle^2} \frac{1}{N}} = \frac{\langle \beta \rangle^2}{\langle \beta^2 \rangle} = \frac{\langle \beta^2 \rangle - \sigma_\beta^2}{\langle \beta^2 \rangle} = 1 - \frac{\sigma_\beta^2}{\langle \beta^2 \rangle}. \quad (4.56)$$

$\langle \beta^2 \rangle$ and an uncertainty for β , σ_β , are always positive, so the uncertainty for the weighted method is smaller than the non-weighted method.

The statistically optimal weight would be $w = \beta = fP_bP_t$. However the condition for no false asymmetry is in general not fulfilled even if spectrometers are perfectly stable in time $\partial a/\partial t = 0$. P_t is often different between the spin reversals. Thus the weight $w = fP_b$ is preferable.

Comparison of the uncertainties with Toy Monte Carlo The ratios of statistical uncertainties on four methods are tested by toy Monte Carlo simulation. Parameters used are summarised in Tab. 4.4. The distribution of parameters is the Gaussian function. The uncertainties are calculated with Eqs. (4.17), (4.25), (4.44), and (4.54). The ratios of uncertainties to the one of the first order method converge and summarised in Tab. 4.5. Therefore, the second order method gives the minimum statistical uncertainty.

Table 4.4: The parameters for Monte Carlo simulation of the uncertainties

Parameter	Value
$N_u, N_d, N_{u'}, N_{d'}$	100 000
$\langle P_b \rangle$	0.9
$\langle P_t \rangle$	0.9
$\langle f \rangle$	0.2
$\sigma_{P_b}, \sigma_{P_t}$	0.045
σ_f	0.004

Table 4.5: The ratios of uncertainties to the one of the first order method

Ratio	Value
σ_{1w}/σ_{1s}	0.9986
σ_{2s}/σ_{1s}	1.0000
σ_{2w}/σ_{1s}	0.9973

4.4. Dilution factor

The naïve dilution factor is defined as

$$f = \frac{\text{the number of polarisable nucleons}}{\text{the number of all nucleons}}. \quad (4.57)$$

For example, the ammonia (NH₃) target has three protons that can be polarised and a nitrogen. Thus, the dilution factor for the ammonia is $3/(3 + 14) = 0.18$. For ⁶LiD the dilution factor is $4/8 = 0.5$ [111]¹⁴.

The dilution factor for a nucleus type i , which is either deuteron or proton, is also defined as

$$f_i = \frac{n_i \sigma_i}{\sum_A n_A \sigma_A} \quad (4.58)$$

where n_i is the number of nuclei of type i in the target and σ_i is the muon-nucleus with type i scattering cross section. The sum runs over all the nuclei A .

Eq. (4.58) can be rewritten as

$$f_i = \frac{n_i}{\sum_A n_A \left(\frac{\sigma_A}{\sigma_i}\right)}. \quad (4.59)$$

The ratio σ_A/σ_i is proportional to the one of the unpolarised structure functions F_2^A/F_2^i . These values are measured by the NMC and EMC experiments, and parameterised [112].

Furthermore, the effective dilution factor $f_{\text{eff},i}$ is defined with correction factors:

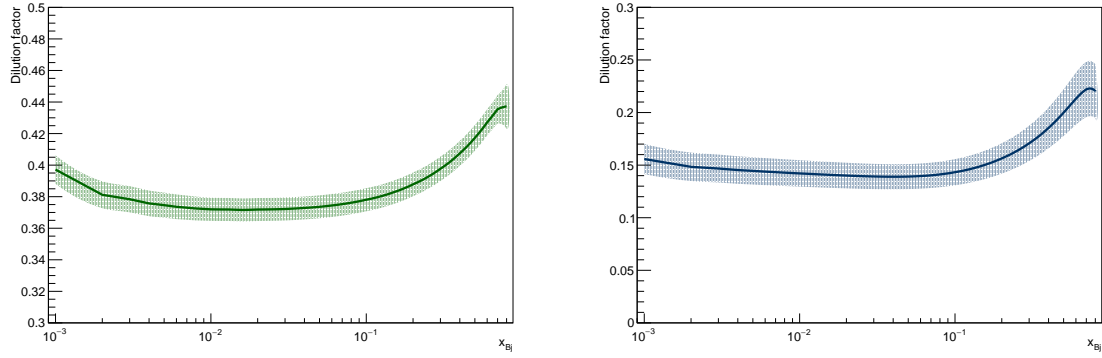
$$f_{\text{eff},i} = C \times \rho \times f_i. \quad (4.60)$$

The factor C (≈ 1.9 for deuteron and ≈ 1.1 for proton) takes into account the facts that there are isotopes of the target materials. In addition to that, in the deuteron case C includes the D state correction [113]. The factor ρ represents the unpolarised radiative corrections, which are calculated by the TERAD program [114].

A calculation of the effective dilution factor depends on the energy fraction y , a target cell position¹⁵, and x_{Bj} . Dilution factors for the deuteron and proton target at the upstream cell with $y = 0.5$ are illustrated in Fig. 4.5 as a function of x_{Bj} . The mean values are 0.41 and 0.18 for deuteron and proton, respectively. The relative uncertainty of the dilution factor in the COMPASS kinematics is estimated to be $\sim 2\%$. The main contributions to this uncertainty are the cross section ratios and the target mass measurement [115].

¹⁴The ⁶LiD is well described as a three-body $\alpha + p + n$ system, and the unpaired nucleons p and n are aligned with the nuclear spin 86.6% of the time. Thus there are four polarisable nucleons (two protons and two neutrons) out of eight nucleons in ⁶LiD.

¹⁵Weights of the target and other materials differ between cells. This difference is corrected by the factor C .

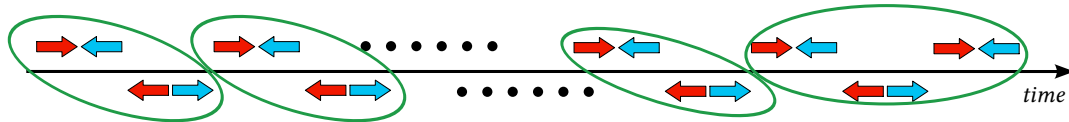


(a) The ${}^6\text{LiD}$ polarised target for hadron trigger. (b) The NH_3 polarised target for hadron trigger.

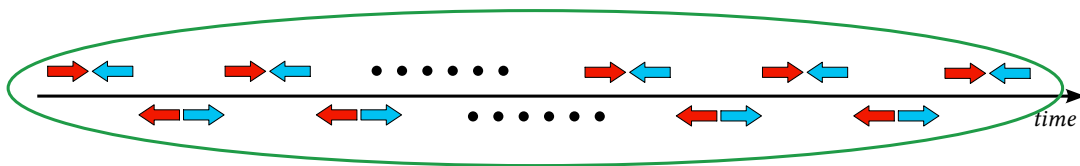
Figure 4.5: Dilution factors for ${}^6\text{LiD}$ and NH_3 as a function of x_{Bj} . Uncertainties are denoted by hashed areas.

4.5. Data grouping

Runs in a period are gathered into a group, in which at least one field rotation occurs. There are two possible data grouping shown in Fig. 4.6. In the consecutive grouping, there are runs with before the field rotation and ones with after the rotation. The detectors are not perfectly stable, even within the period. This allows asymmetries to reduce any systematic biases and is used for the final asymmetry. Whereas, in the global grouping, all the runs in the period are gathered. The global grouping has the advantage of utilisation of larger statistics thus requirement of the 2nd order method that N is large can be safely assumed to be fulfilled. The global grouping is used for the consistency check of the asymmetries calculated by the consecutive grouping and the systematic studies.



(a) Consecutive grouping



(b) Global grouping

Figure 4.6: Schematic pictures of the consecutive and the global grouping. A pair of red and blue arrows, which express the direction of the target polarisation, represents one run. The green circle indicates the group. In case of the unbalanced number of runs for the consecutive grouping, the last run is include in the previous group.

4.6. Asymmetry calculation

A_{LL} is calculated as a function of p_T , η_{CMS} , and hadron charge, *i.e.* positive or negative (2 bins). The binning for p_T is [0.7, 0.75, 0.8, 0.9, 1.0, 1.25, 1.5, 2.0, 2.5, 4.0] (9 bins). The one for η_{CMS} is [-0.1, 0.45, 0.9, 2.4] (3 bins). This η_{CMS} range corresponds to $0.12 < \theta_{\text{hadron}} < 0.70$.

The asymmetry is calculated for each group in the period with the second order weighted method. Next, the group-by-group asymmetries are combined by taking the weighted mean in the period:

$$A^{\text{period}} = \frac{\sum_{\text{group} \in \text{period}} w^{\text{group}} A^{\text{group}}}{\sum_{\text{group} \in \text{period}} w^{\text{group}}} . \quad (4.61)$$

Here the weight w is the inverse of the root of the statistical uncertainty. The period-by-period ones are also combined by taking the weighted mean with respect to the microwave configuration. The asymmetries with the positive and negative microwave configuration are denoted as A_+ and A_- , respectively.

$$A_+^{\text{year}} = \frac{\sum_{\text{period} \in \text{year}} w_+^{\text{group}} A_+^{\text{group}}}{\sum_{\text{period} \in \text{year}} w_+^{\text{group}}} , \quad A_-^{\text{year}} = \frac{\sum_{\text{period} \in \text{year}} w_-^{\text{group}} A_-^{\text{group}}}{\sum_{\text{period} \in \text{year}} w_-^{\text{group}}} \quad (4.62)$$

The microwave configurations for all the periods are shown in Tab. 4.6.

Table 4.6: Microwave configurations for all the periods

Year	Microwave+	Microwave-
2002	P2D, P2E, P2F, P2G+	P1C, P2A, P2G-
2003	P1A, P1B, P1C, P1D, P1I	P1E, P1F, P1J
2004	W22, W23, W37, W38	W26, W27, W28, W29, W30, W31, W32, W39, W40
2006	W32, W33, W34, W35, W36, W37	W40, W41, W42, W43, W44, W45, W46
2007	W35, W36, W37, W38	W32, W33, W34, W44, W45
2011	W25, W27, W30, W31, W32, W33, W34	W36, W38, W39, W41, W43

The year-by-year asymmetry is calculated by taking the arithmetic mean of A_+ and A_- in order to eliminate a systematic uncertainty due to the microwave reversal.

$$A^{\text{year}} = \frac{1}{2} (A_+^{\text{year}} + A_-^{\text{year}}) \quad (4.63)$$

The target-by-target asymmetry is also calculated in the same way to year-by-year one.

$$A_+^{\text{target}} = \frac{\sum_{\text{year} \in \text{target}} w_+^{\text{year}} A_+^{\text{year}}}{\sum_{\text{year} \in \text{target}} w_+^{\text{period}}} , \quad A_-^{\text{target}} = \frac{\sum_{\text{year} \in \text{target}} w_-^{\text{year}} A_-^{\text{year}}}{\sum_{\text{year} \in \text{target}} w_-^{\text{period}}} \quad (4.64)$$

$$A^{\text{target}} = \frac{1}{2} (A_+^{\text{target}} + A_-^{\text{target}}) . \quad (4.65)$$

The statistical uncertainties are calculated as follows. In the case of the weighted mean,

$$\sigma^2 = \frac{1}{\sum_i \frac{1}{\sigma_i^2}} . \quad (4.66)$$

On the other hand, in the case of the arithmetic mean,

$$\sigma^2 = \frac{1}{4} (\sigma_+^2 + \sigma_-^2) . \quad (4.67)$$

Asymmetries integrated over η_{CMS} and hadron charge are calculated by taking the weighted mean.

The beam momentum in 2011 was 200 GeV/ c , whereas the ones in the other years were 160 GeV/ c . It was observed that the distributions of kinematic variables, *e.g.* x_{Bj} , Q^2 , p_T , etc. had no significant differences among the years (see App. B). Thus, the merging 2007 and 2011 data includes any bias as same as the merging for the deuteron target.

5. Results and discussion

In Chapt. 4, a calculation flow from reconstructed data to A_{LL} is shown. In this section, associated systematic uncertainties are discussed.

5.1. Systematic studies

The following sources of systematic uncertainty are considered:

- uncertainties of the beam polarisation, the target polarisation, and the dilution factor,
- reproducible false asymmetry,
- misconfiguration false asymmetry,
- Top-Bottom and Left-Right asymmetry, and
- random false asymmetry via time stability studies (, namely *pulls*).

5.1.1. Multiplicative uncertainties

Uncertainties in the multiplicative factors in A_{LL} are regarded as “Multiplicative uncertainties”. These values vary according to year, *i.e.* the experimental setup, and are summarised in Tab. 5.1.

Table 5.1: Summary of the multiplicative systematic uncertainties. These are relative uncertainties, and the units are given by percentage

	2002	2003	2004	2006	2007	2011
Beam polarisation $\left(\frac{dP_b}{P_b}\right)$	5	5	5	5	5	5
Target polarisation $\left(\frac{dP_t}{P_t}\right)$	5	5	5	5	2	3.5
Dilution factor $\left(\frac{df}{f}\right)$	2	2	2	3	1	1

The uncertainties of them are caused by the following sources:

The beam polarisation

As described in Sec. 3.1, the beam polarisation depends on the ratio of the muon momentum to the pion momentum. Thus it can be computed analytically. However, as the beam contains hadrons (pions and kaons) which are also polarised and decay into muon and muon neutrino, the beam polarisation is evaluated by comparing to Monte Carlo simulation. This gives the 4 % uncertainty [73]. In the actual analyses, a conservative value of 5 % is practically taken.

The target polarisation

As described in Sec. 3.2, the main source to the polarisation uncertainty is the fitting uncertainty to the area unit at TE with the inverse of the temperature [81]. The others are the field polarity due to the field rotation, the NMR signal shifting, etc. The uncertainty in total vary in year, and is about 2 % to 5 %.

The dilution factor

As discussed in Sec. 4.4, the dilution factor is calculated by the total cross section and the factor that takes the contamination in the target material into account. Thus the uncertainty on the dilution factor comes from the contamination in the target material and the uncertainties on the total cross sections. Similarly to the uncertainty of the target polarisation, the value fluctuates year-by-year.

The multiplicative uncertainty for the year-by-year asymmetry is evaluated by the following equation:

$$\sigma_{\text{multi.}}^{\text{year}} = A_{LL}^{\text{year}} \sqrt{\left(\frac{dP_b}{P_b}\right)^2 + \left(\frac{dP_t}{P_t}\right)^2 + \left(\frac{df}{f}\right)^2} = A_{LL}^{\text{year}} \times C^{\text{year}} \quad (5.1)$$

In the case of the target-by-target asymmetry, the uncertainty is calculated as

$$\sigma_{\text{multi.}}^{\text{target}} = \frac{\sum_{\text{year} \in \text{target}} w^{\text{year}} C^{\text{year}} A_{LL}^{\text{year}}}{\sum_{\text{year} \in \text{target}} w^{\text{year}}}, \quad (5.2)$$

$$w^{\text{year}} = \frac{1}{(\sigma^{\text{year}})^2}. \quad (5.3)$$

5.1.2. Reproducible false asymmetry

As described in Sec. 3.2, the microwave reversal takes place once or twice during the data taking in year to suppress a correlation between the direction of the solenoid field and the acceptance. As mentioned in Sec. 4.6, this systematic effect is subtracted by taking the arithmetic mean of the asymmetries with the positive microwave configuration and the ones with the negative configuration.

The actual value subtracted from A_{LL} , denoted as A_R , is written as

$$A_R = \frac{\sigma_+^2 - \sigma_-^2}{\sigma_+^2 + \sigma_-^2} \cdot \frac{1}{2} (A_+ - A_-), \quad (5.4)$$

and is shown in Fig. C.1. By this procedure, A_{LL} has no systematic effect coming from the field rotation and the microwave reversal.

5.1.3. Fake configuration asymmetry

The runs are grouped according to the spectrometer conditions (see Sec. 4.5). To investigate the behaviour of the spectrometer in time, e.g. a continuous decrease of the efficiency of some detectors, the fake configuration asymmetry is calculated, which is shown in Fig. 5.1. There are two kinds of asymmetries according to the polarisation directions: fake configuration + and fake configuration –, which are combined at the end. The sign of polarisation after the field rotation should be flipped to compute correctly as both spin states are same.

The fake configuration false asymmetries are shown in Fig. C.2 and are compatible with zero within the statistical uncertainties. At the second largest p_T bin for proton target, asymmetry deviates from zero about 2.7σ . This is taken into account as *pull* (see Sec. 5.1.5).

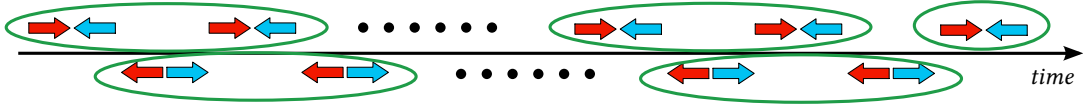


Figure 5.1: Fake configuration grouping. Arrows indicate the direction of the target polarisation. By picking up same polarisation state, fake asymmetries are calculated. The group having single polarisation state is excluded.

5.1.4. Top-Bottom and Left-Right asymmetry

The COMPASS spectrometer does not have a *symmetric* structure with respect to particles detected. Basically, there is no false asymmetry if symmetric structure of the spectrometer is used. False asymmetries, namely Top-Bottom asymmetry and Left-Right asymmetry, are evaluated in this section.

Top asymmetry is calculated only using hadrons that are detected in upper region, *i.e.* $Y > 0$ ¹⁶ in the COMPASS reference system. This Y range corresponds to $0 < \phi < \pi$. In a similar way, Bottom asymmetry is calculated using the hadrons having $Y < 0$, *i.e.* $-\pi < \phi < 0$. Top-Bottom asymmetry is the difference of Top and Bottom asymmetries: $\Delta A_{TB} = A_{Top} - A_{Bottom}$.

Left (Right) asymmetry¹⁷ is calculated with hadrons detected in the left (right) region, *i.e.* $X > 0$ ($X < 0$) in the COMPASS reference system. $X > 0$ ($X < 0$) corresponds to $-\pi/2 < \phi < \pi/2$ ($-\pi < \phi < -\pi/2$ or $\pi/2 < \phi < \pi$). The Left-Right asymmetry is defined as $\Delta A_{LR} = A_{Left} - A_{Right}$.

The Top-Bottom asymmetries are shown in Fig. C.3 and Left-Right asymmetries are shown in Fig. C.4. Both of them are found to be equal within statistical uncertainties. Therefore, systematic uncertainties associated with the geometrical asymmetry in the COMPASS spectrometer can be regarded as 0.

5.1.5. The estimation of the systematic uncertainty via a *pulls* method

The distribution of asymmetries in some periods centred by the weighted mean and normalised by the statistical uncertainty, called *pulls* distribution, must follow a normal distribution:

$$\Delta r_i = \frac{A_{LL,i} - \langle A_{LL} \rangle_w}{\sqrt{(\delta A_{LL,i})^2 - (\delta \langle A_{LL} \rangle_w)^2}} \quad (5.5)$$

where $\langle A_{LL} \rangle_w$ is the weighted mean of $A_{LL,i}$ of the i -th group, $\delta A_{LL,i}$ is the statistical uncertainty of $A_{LL,i}$, and $\delta \langle A_{LL} \rangle_w$ is the uncertainty of $\langle A \rangle_w$. A broadening of the distribution would appear in case of instabilities of the spectrometers. The upper limit for the systematic uncertainty is estimated with the *pulls* distribution in a practical approach having used in other COMPASS analyses, which is called *pulls* method.

¹⁶Axes in Euclidean space are denoted by the small capitals in practice. Here the large capital letters are used in order to avoid confusions with the Bjorken variable x_{Bj} , the energy fraction of a virtual photon to an incident beam y , and the energy fraction of a hadron to the virtual photon z .

¹⁷Left-Right asymmetry is customarily called Jura-Salève asymmetry since the left (right) side of the spectrometer faces to Jura (Salève) mountains.

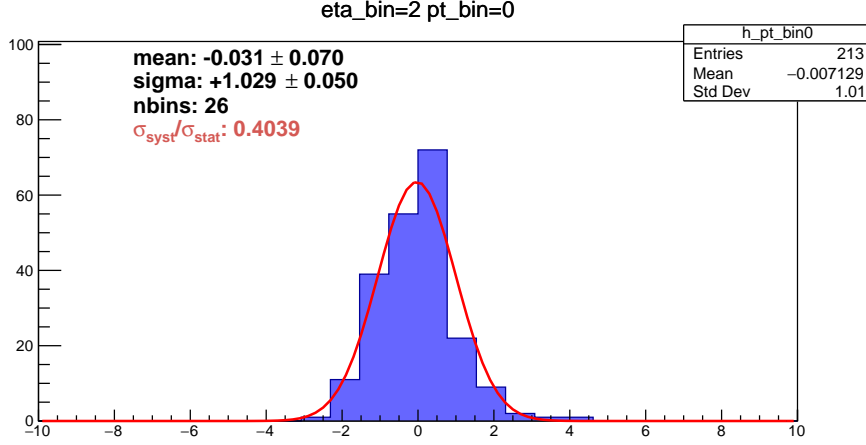


Figure 5.2: The *pulls* distribution for hadron charge integrated asymmetries for the deuteron at a single bin. The Gaussian function fitted is drawn in red.

The variance of the *pulls* distribution can be written as $\sigma_{\text{total}}^2 = \sigma_{\text{stat.}}^2 + \sigma_{\text{syst.}}^2$, where $\sigma_{\text{stat.}}$ is expected to be equal to 1. Here σ_{total} can be written as $\sigma_{\text{total}} = \max\{1, \sigma_{\Delta r}\} + \delta\sigma_{\Delta r}$, where $\max\{1, \sigma_{\Delta r}\}$ denotes choosing a maximum value among $\sigma_{\Delta r}$ and 1, $\sigma_{\Delta r}$ is the width of a Gaussian function fitting the *pulls* distribution by means of the likelihood method, and $\delta\sigma_{\Delta r}$ is its uncertainty. This gives $\sigma_{\text{syst.}}^2 = (\max\{1, \sigma_{\Delta r}\} + \delta\sigma_{\Delta r})^2 - 1$, meaning the upper limit of a ratio between the systematic uncertainty and the statistical one.

The *pulls* distributions of hadron charge integrated asymmetry for the deuteron at $[0.9, 2.4] \in \eta$ bin and $[0.70, 0.75] \in p_T$ bin is shown in Fig. 5.2. The histogram binning is optimised by the method [116], which is described in App. A.3. The number of bins is denoted as nbins on the figure. The *pulls* distribution is fitted with the Gaussian function by means of the likelihood method. The mean and sigma values of the Gaussian function with corresponding uncertainties, and the upper limit of the ratio $\sigma_{\text{syst.}}/\sigma_{\text{stat.}}$ are shown on the figure. Therefore, in this kinematic bin, the systematic uncertainty is evaluated as about 45 % of the statistical uncertainty of the asymmetry.

All the ratio $\sigma_{\text{syst.}}/\sigma_{\text{stat.}}$ are shown in Tabs. C.1 and C.2.

5.1.6. Summary of systematic study

As previous subsections, systematic studies have been performed. The total systematic uncertainty is defined as follows:

$$\sigma_{\text{syst.}} = \sqrt{(\sigma_{\text{multi.}})^2 + (\sigma_{\text{add.}})^2} \quad (5.6)$$

where

$$\sigma_{\text{multi.}} = A_{LL} \sqrt{\left(\frac{dP_b}{P_b}\right)^2 + \left(\frac{dP_t}{P_t}\right)^2 + \left(\frac{df}{f}\right)^2}, \quad (5.7)$$

$$\sigma_{\text{add.}} = \sqrt{(\max\{1, \sigma_{\Delta r}\} + \delta\sigma_{\Delta r})^2 - 1} \times \sigma_{\text{stat.}}. \quad (5.8)$$

Systematic uncertainties at higher p_T bins where false asymmetries are slightly observed appear in the *pulls* distributions. Thus, no further contribution to the systematics is considered. The values of A_{LL} with uncertainties for the deuteron and proton targets in each p_T and η bins are summarised in Tabs. C.3 and C.4. The sizes of the systematic uncertainties are always smaller than the statistical ones.

5.2. Results

The numbers of hadrons used for the calculation are 116 million for deuteron target and 105 million for proton target, respectively. Kinematics' distributions used for asymmetry calculations are shown in App. B. The asymmetries for year-by-year, deuteron, and proton are shown in Figs. C.5, C.6a, and C.6b and are summarised in Tabs. C.3 and C.4. In the plots, error bars at data points contain only statistical uncertainties. The systematic uncertainties are represented by the bands at the bottom.

Comparison with theoretical calculations The asymmetries are then compared with calculated ones based on the JSV framework described in Chapt. 2. Input parameters for the calculation are listed as follows [46, 117]:

Fragmentation function D_c^h
DSS14 [44]

unpolarised photon-parton distributions f_a^γ
GRS [53] with the parametrisation that reproduces photoproduction well

unpolarised PDFs f_b^N
CTEQ65 [118]

For the polarised PDFs, following different sets are used:

- the latest set of DSSV [11] (denoted as DSSV14¹⁸ in plots)
- GRSV with the standard value of ΔG [119] denoted by GRSV_{std}
- GRSV with the minimal value of ΔG [119] denoted by GRSV_{min}
- GRSV with the maximal value of ΔG [119] denoted by GRSV_{max}

In addition to the data used in the original DSSV [120] analysis, the RHIC results [68, 121], inclusive- and semi-inclusive DIS results from COMPASS [32, 43] were added in the DSSV14 analysis. The smaller uncertainties of new RHIC results allow to put tighter constraints on $\Delta g(x_g)$.

Since in the GRSV analysis, inclusive and semi-inclusive DIS results (SLAC, EMC, SMC, and HERMES) were employed, this is admittedly, the out-of-date. In the calculation of Ref. [45], GRSV sets were used. $\Delta g(x_g)$ of GRSV and DSSV14 at $\mu^2 = 3 (\text{GeV}/c)^2$ is shown in Fig. 5.3.

GRSV with the maximal value of ΔG means $\Delta g(x_g, \mu^2) = +g(x_g, \mu^2)$ at $\mu^2 = 0.4 (\text{GeV}/c)^2$; On the contrary, GRSV with a minimal value of ΔG means $\Delta g(x_g, \mu^2) = -g(x_g, \mu^2)$ at the same μ^2 . Thus integrating them over x_g from 0 to 1 result in $\Delta G/G = +1$ and $\Delta G/G = -1$,

¹⁸Some papers refer as DSSV++.

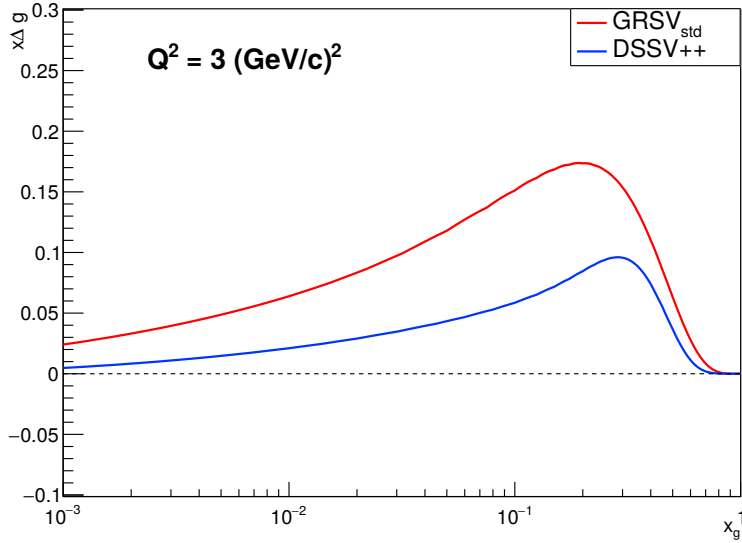


Figure 5.3: $x\Delta g(x_g, \mu^2 = 3)$ of GRSV and DSSV14.

respectively.

GRSV with a standard value of ΔG (denoted by GRSV_{std}) means $\Delta g(x_g, \mu^2)$ is a standard parametrisation of the polarised PDF in GRSV set, which gives $\Delta G = 0.24$ at $\mu^2 = 0.4 (\text{GeV}/c)^2$ integrated over $0 < x_g < 1$. When the QCD scale is $\mu^2 = p_T^2 = 3 (\text{GeV}/c)^2$ and integrating Δg over $0.05 < x_g < 0.2$, $\Delta G_{\text{GRSV}_{\text{min}}} \simeq -0.6$, $\Delta G_{\text{DSSV14}} \simeq 0.1$, $\Delta G_{\text{GRSV}_{\text{std}}} \simeq 0.2$, and $\Delta G_{\text{GRSV}_{\text{max}}} \simeq 0.7$.

DSS14 is a set of updated parton-to-pion fragmentation functions. The set takes account of the latest COMPASS results of pion multiplicity analysis. Comparison of DSS07 and DSS14 FF sets for u, d, c, and g at $\mu^2 = 5 (\text{GeV}/c)^2$ is shown in Fig. 5.4 [117]. As described in Sec. 2.5, z is the ration of the hadron energy to the virtual photon one. The differences among two FF sets are within 90 % C.L. bands of DSS14 for almost regions. As confirming that asymmetries, shown in Fig. 5.5, for hadron and pion production using DSS07 are almost same, it is safe to compare our data with calculated asymmetries with DSS14.

Comparisons between the measured asymmetries and the theoretically calculated ones are shown in Figs. 5.6 and 5.7. The asymmetries are split into sub-asymmetries by hadron charge and the rapidity. As increasing the rapidity, the discriminating power, which is the degree of the separation between asymmetries with different scenario, become large. This effect clearly appears in the negative hadron asymmetries.

In the lowest rapidity bin, the deuteron results for the positive and negative hadrons tend to follow the DSSV14 scenario. Whereas the proton ones for the positive hadron indicate the quite high ΔG scenario and the ones for the negative hadron follow the GRSV_{std} scenario. However the discriminating power for both targets are small and the uncertainties are larger than the discriminating power, it is hard to determine the best scenario from this rapidity bin.

In the middle rapidity bin, the discriminating power is more improved comparing to the lowest bin. The deuteron and proton data points for negative hadron lie on the DSSV14 scenario, whereas the deuteron data for the positive hadron clearly follow the GRSV_{max} scenario. The proton ones for the positive hadron are in favour of GRSV_{max} .

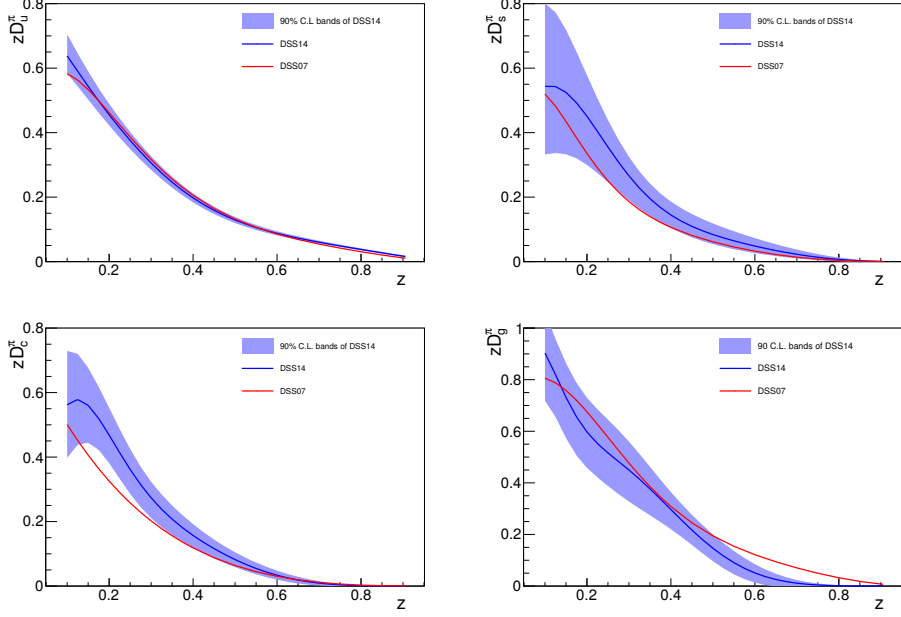
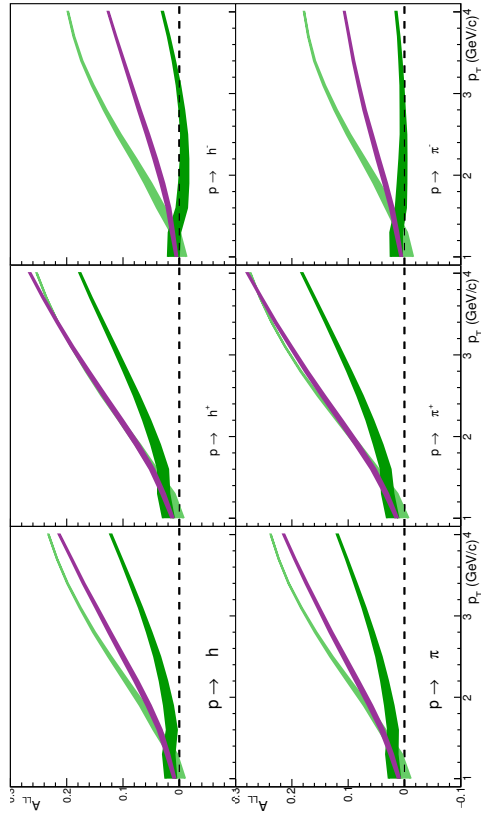


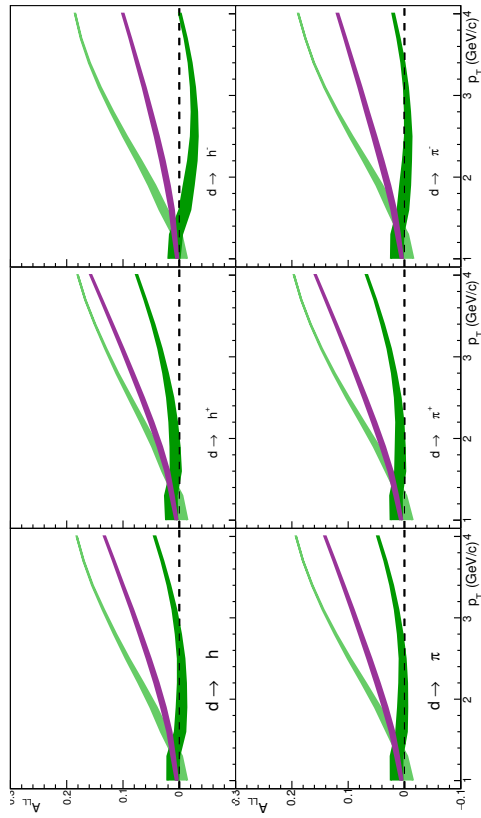
Figure 5.4: Comparison of DSS07 and DSS14 FF sets for u , d , c , and g at $\mu^2 = 5 \text{ (GeV}/c)^2$ [117]. 90 % C.L. bands of DSS14 is shown.

In the highest rapidity bin, larger discriminating power (1σ or more for the statistical uncertainty, say) is observed except for the proton data for the positive hadron. All data tend to follow the GRSV_{max} or DSSV14 scenario.

The results are in favour of the most recent polarised PDF and FF sets: a positive ΔG in $0.05 < x_g < 0.2$. However, they must be taken with care since the theoretical calculations are limited to the NLO accuracy WITHOUT the threshold resummation, which is required to explain the unpolarised cross section data obtained as discussed in Sec. 2.5. Thus, it is quite premature to draw any conclusion on ΔG before implementing the threshold resummation. At least, however, it can be said that ΔG is positive and sizeable in the measured range of x_g since most of the data tend to follow GRSV_{max} or DSSV14 scenario where both of them have positive gluon polarisation at the measured range.



(a) $\mu + d \rightarrow \mu' + h + X$



(b) $\mu + p \rightarrow \mu' + h + X$

Figure 5.5: Comparison between theoretical asymmetries for hadron and pion production using DSS07 fragmentation functions. The three columns shows different rapidity binning: from left to right, $-0.1 < \eta < 0.45$, $0.45 < \eta < 0.9$, and $0.9 < \eta < 2.4$, respectively.

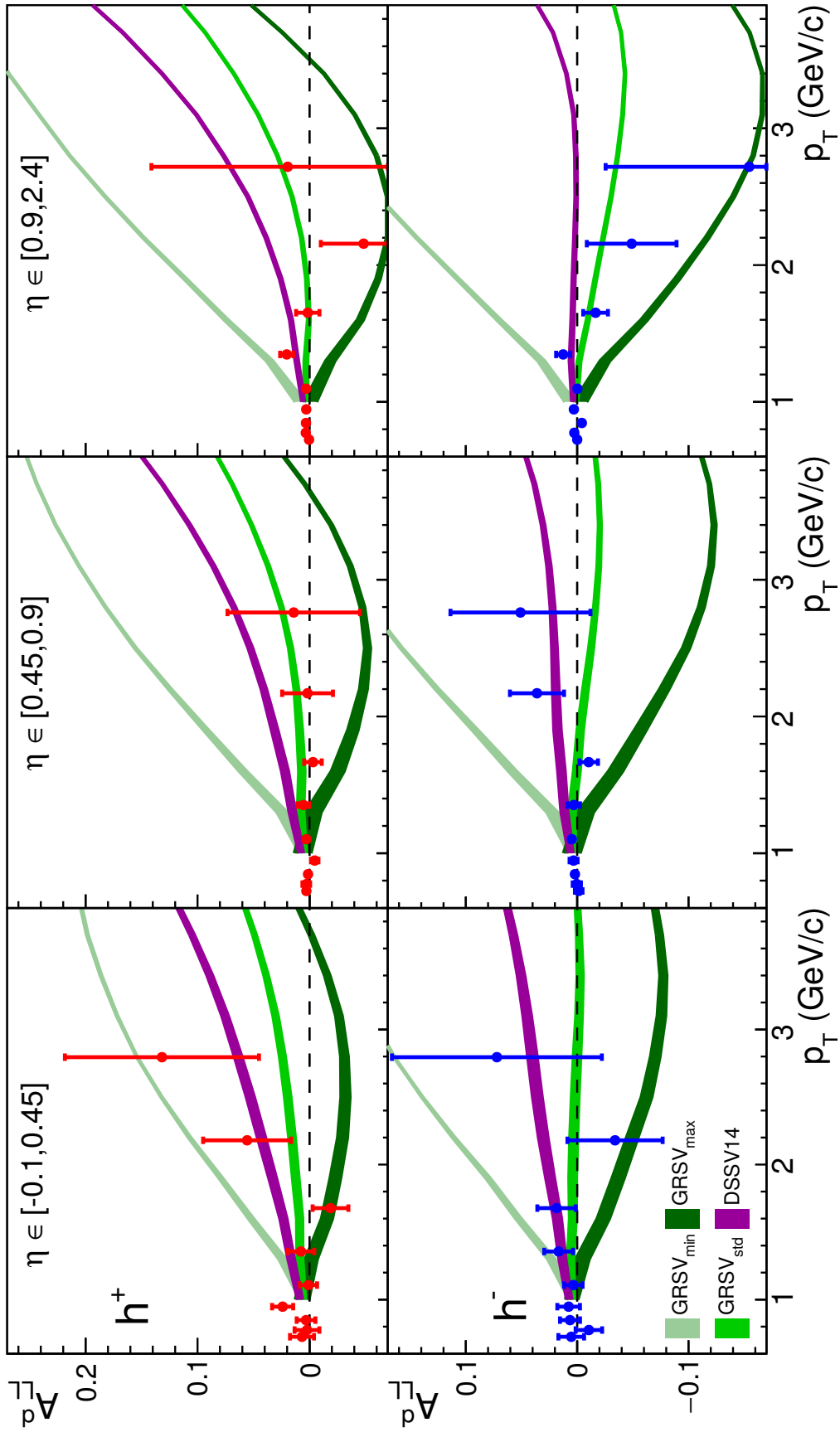


Figure 5.6: Comparison with measured asymmetries and calculated ones for deuteron target.

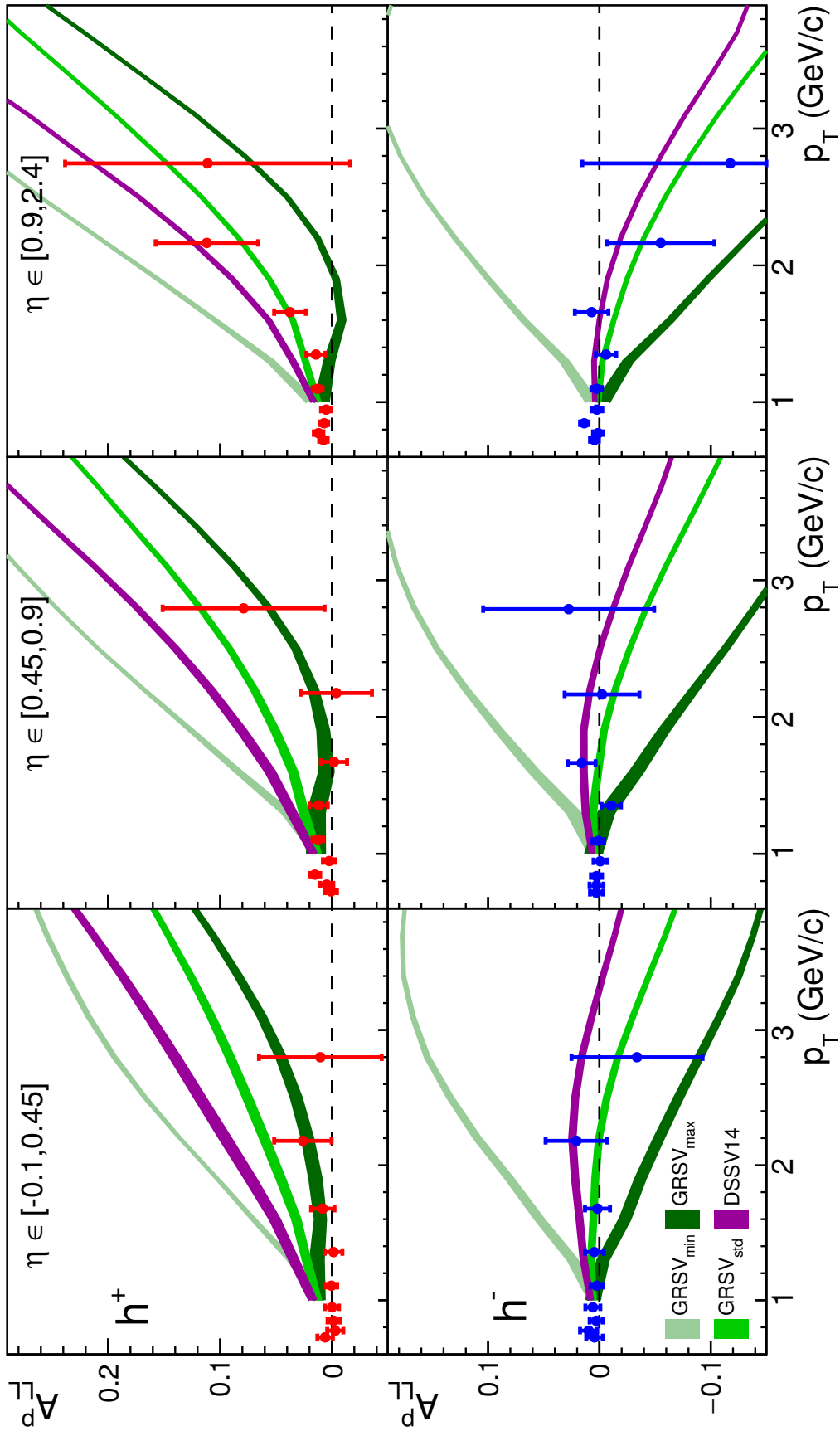


Figure 5.7: Comparison with measured asymmetries and calculated ones for proton target.

6. Conclusion

The study of gluon polarisation has provided vital hints for the spin structure of the nucleon. When it was found that the contribution of quarks to the nucleon spin is only one-third, it was thought that gluon may give sizeable contribution. Many experiments in the world had measured the gluon polarisation; they had found that it could be almost zero, negative, or positive since uncertainties were large. Recent RHIC data have shown that it is non-zero, or even slightly positive rather than negative at some x_{Bj} regime [68, 69].

The COMPASS experiment, one of the experiments to measure gluon polarisation, is performed at CERN. Its purposes are the studies of hadron physics and nucleon structure. It is a fixed target experiments with lepton or hadron beams supplied from Super Proton Synchrotron (SPS). Using highly polarised targets, it can study the nucleon spin structures. COMPASS begun data taking in 2011 and terminated its phase-I program in 2012. Since 2014 phase-II programme has been performed in which GPD and Drell-Yan measurements have been carried out.

I joined the COMPASS collaboration in 2010 and had activities such as the target preparations, DAQ shifts, etc. since that.

The data taken in COMPASS were collected in 2002, 2003, 2004, 2006, 2007, and 2011. Different polarised materials were used: ${}^6\text{LiD}$ as deuteron target was used in 2002, 2003, 2004, and 2006, whereas NH_3 2007 and 2011 as proton target. Polarised muon beam with momentum of 160 GeV/c or 200 GeV/c (only in 2011) has been employed.

The longitudinal double spin asymmetries A_{LL} for deuteron and proton targets are calculated by the second order method that brings a minimal uncertainty comparing to other methods. Systematic uncertainties study shows that there is no significant systematics and the size of them is always smaller than statistical uncertainties. The deuteron data show almost no asymmetry within statistical and systematic uncertainties except a high- p_T bin. The proton data also show no deviation from zero and a tendency to go to negative direction as increasing p_T . They are subdivided based on the charge and the rapidity of hadrons produced: positive or negative and three rapidity bins. Though dividing kinematic regimes, asymmetries are still compatible with zero ($\leq 1.5\sigma$).

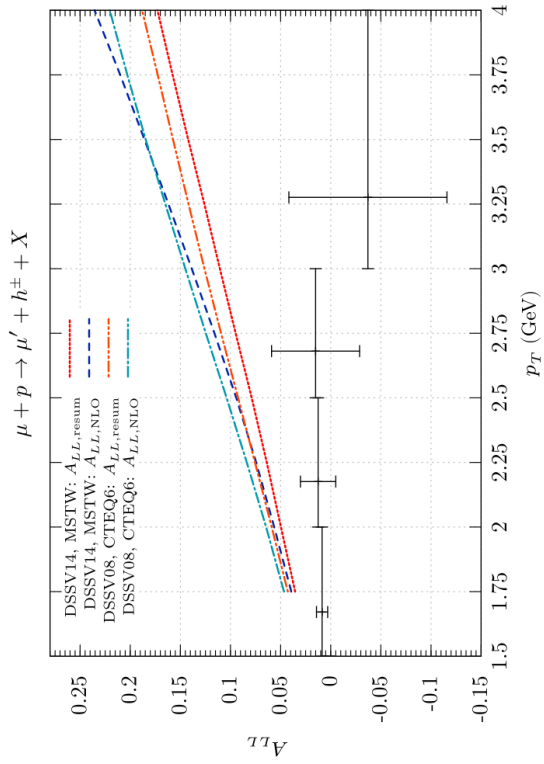
Finally, measured asymmetries are compared with calculated ones based on JSV framework, which have four different parametrisations with respect to a ΔG scenario. The calculation shows that in COMPASS kinematics regime Photon Gluon Fusion process largely dominates. Most of the asymmetries tend to follow DSSV14 scenario and some of them follow GRSV_{max} . This tendency indicates that ΔG is positive and sizeable in COMPASS kinematics regime. However, the technique *threshold resummation*, which reproduces the unpolarised cross section for single hadron photoproduction within theoretical uncertainties, is NOT included yet so that one could not firmly insist the size of ΔG . Once this technique implemented in calculation, one can discuss it quantitatively in the COMPASS kinematic range.

7. Future prospects

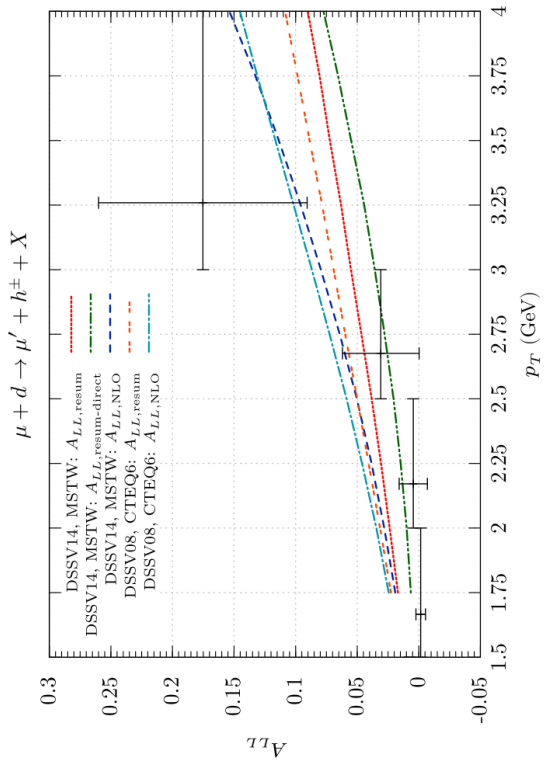
Resummation Recently, the authors of Ref. [122] have presented the theoretical calculation of the polarised cross section for the photo production $\gamma N \rightarrow hX$ with threshold resummation at next-to-leading logarithm (NLL) level at the COMPASS kinematics. However, at the moment they only address the “direct” part of the cross section, where the virtual photon “directly” interacts with the parton coming from the nucleon.

The authors found that the polarised cross section receives much smaller enhancements by resummation than the unpolarised one. Thus the COMPASS results and their calculations for the longitudinal double spin asymmetries are in marginal agreement for the deuteron case and are incompatible for the proton case, shown in Fig. 7.1. Nonetheless, as the resolved contribution for the polarised cross section is not implemented, one can draw a definite conclusion only when the resummation for the resolved component has been carried out.

The calculation of the cross section for the process $H_1 H_2 \rightarrow h_1 h_2 X$ at high invariant mass of the produced hadron pair at next-to-next-to leading logarithmic (NNLL) level improved the agreement to data [123]. Thus the extension of resummation to NNLL level may be necessary to improve the theoretical calculations.



(a) A_{LL} for a deuteron target. The asymmetry with latest data set (denoted as “DSSV14, MSTW: $A_{LL, \text{resum}}^{\text{b}}$ ”) are poorly agreed. $A_{LL, \text{resum-direct}}$ denotes the resummed asymmetry without the resolved contributions of the polarised and unpolarised cases.



(b) A_{LL} for a proton target. No theoretical calculation reproduce the COMPASS result.

Figure 7.1: The theoretical calculations for the longitudinal double spin asymmetry in COMPASS kinematics, taken from Ref. [122]. The preliminary COMPASS results are also shown.

A. Derivations

A.1. The derivation of the first order method

The derivation of $\Delta + \Delta'$ is presented (see Sec. 4.3.1). Their definitions are shown below:

$$\Delta = \frac{(r-1) + wA(rP_u + P_d)}{(r+1) + wA(rP_u - P_d)} = \frac{T_1}{T_2}, \quad (\text{A.1})$$

$$\Delta' = \frac{-(r'-1) + wA(r'P_{u'} + P_{d'})}{(r'+1) - wA(r'P_{u'} - P_{d'})} = \frac{T_3}{T_4}. \quad (\text{A.2})$$

One obtains

$$\Delta + \Delta' = \frac{T_1}{T_2} + \frac{T_3}{T_4} = \frac{T_1 \cdot T_4 + T_2 \cdot T_3}{T_2 \cdot T_4}. \quad (\text{A.3})$$

Before starting the calculation, one assume $r = r'$; no acceptance change before and after the field rotation.

Let's start each term derivation! The denominator:

$$\begin{aligned} T_2 \cdot T_4 &= \left[(r+1) + wA(rP_u - P_d) \right] \left[(r+1) - wA(rP_{u'} - P_{d'}) \right] \\ &= (1+r)^2 + (1+r)wA \left[r(P_u - P_{u'}) - (P_d - P_{d'}) \right] - w^2 A^2 (rP_u - P_d)(rP_{u'} - P_{d'}). \end{aligned} \quad (\text{A.4})$$

The first part of the numerator:

$$\begin{aligned} T_1 \cdot T_4 &= \left[(r-1) + wA(rP_u + P_d) \right] \left[(r+1) - wA(rP_{u'} - P_{d'}) \right] \\ &= (r-1)(r+1) - wA(r-1)(rP_{u'} - P_{d'}) + wA(r+1)(rP_u + P_d) \\ &\quad - w^2 A^2 (rP_u + P_d)(rP_{u'} - P_{d'}) \\ &= (r^2 - 1) + wA(1+r) \left[r^2 P_u + rP_d + rP_u + P_d - (r^2 P_{u'} - rP_{d'} - rP_{u'} + P_{d'}) \right] \\ &\quad - w^2 A^2 (rP_u + P_d)(rP_{u'} - P_{d'}). \end{aligned} \quad (\text{A.5})$$

The second part of the numerator:

$$\begin{aligned} T_2 \cdot T_3 &= \left[(1+r) + wA(rP_u - P_d) \right] \left[-(r-1) + wA(rP_{u'} + P_{d'}) \right] \\ &= -(r^2 - 1) + wA \left[r^2 P_{u'} + rP_{d'} + rP_{u'} + P_{d'} - (r^2 P_u - rP_d - rP_u + P_d) \right] \\ &\quad + w^2 A^2 (rP_u - P_d)(rP_{u'} + P_{d'}). \end{aligned} \quad (\text{A.6})$$

Merging them, one obtains:

$$\begin{aligned}
T_1 \cdot T_4 + T_2 \cdot T_3 &= wA \left[r^2 P_u + r P_d + r P_u + P_d - r^2 P_{u'} + r P_{d'} + r P_{u'} - P_{d'} \right. \\
&\quad \left. + r^2 P_{u'} + r P_{d'} + r P_{u'} + P_{d'} - r^2 P_u + r P_d + r P_u - P_d \right] \\
&\quad + w^2 A^2 \left[-(r P_u - P_d)(r P_{u'} + P_{d'}) + (r P_u - P_d)(r P_{u'} + P_{d'}) \right] \\
&= 2wA(P_u + P_d + P_{u'} + P_{d'}) + rw^2 A^2(P_{u'} P_d - P_{u'} P_d). \tag{A.7}
\end{aligned}$$

$\Delta + \Delta'$ can be rewritten as

$$\begin{aligned}
\Delta + \Delta' &= \left\{ (1+r)^2 + (1+r)wA \left[r(P_u - P_{u'}) - (P_d - P_{d'}) \right] - w^2 A^2 (r P_u - P_d)(r P_{u'} - P_{d'}) \right\}^{-1} \\
&\quad \times \left[2wA(P_u + P_d + P_{u'} + P_{d'}) + rw^2 A^2(P_{u'} P_d - P_{u'} P_d) \right]. \tag{A.8}
\end{aligned}$$

Assuming following relations,

$$wA(P_{u'} P_d - P_{u'} P_d) \ll P_u + P_d + P_{u'} + P_{d'}, \tag{A.9}$$

$$wA \left[r(P_u - P_{u'}) - (P_d - P_{d'}) \right] \ll 1+r, \tag{A.10}$$

$$w^2 A^2 (r P_u - P_d)(r P_{u'} - P_{d'}) \ll (1+r)^2. \tag{A.11}$$

one obtains

$$\frac{\Delta + \Delta'}{2} = \frac{4r}{(1+r)^2} \frac{P_u + P_d + P_{u'} + P_{d'}}{4} wA. \tag{A.12}$$

A.2. The derivation of uncertainty in the second order weighted method

The statistical uncertainty of asymmetry with the second order weighted method is derived in this section. The uncertainty of an asymmetry σ_A is denoted by

$$\sigma_A^2 = \left(\frac{\partial A}{\partial \delta} \sigma_\delta \right)^2 \tag{A.13}$$

where A is an asymmetry and δ is defined in Eq. (4.36).

If the number of hadrons equal in all cells, this can be reduced to

$$\sigma_A^2 = \frac{\langle w \rangle^2}{\langle w\beta \rangle^2} \frac{1}{N} \tag{A.14}$$

since $\langle \beta \rangle = \langle \beta_u \rangle = \langle \beta_{d'} \rangle = -\langle \beta_{u'} \rangle = -\langle \beta_d \rangle$.

However in real condition, these assumption are not correct. One has to drive the uncertainty from Eq. (A.13).

δ is a function of $p_u, p_d, p_{u'}$, and $p_{d'}$, where p_x is the sum of $w_{i,x}$ event by event in a cell x : $\sum_i^{N_x} w_{i,x}$ and its uncertainty is defined as $\sum_i^{N_x} w_{i,x}^2$. From propagation of uncertainty, the uncertainty of δ is

$$\sigma_\delta^2 = \left(\frac{\partial \delta}{\partial p_u} \right)^2 \sigma_{p_u}^2 + \left(\frac{\partial \delta}{\partial p_d} \right)^2 \sigma_{p_d}^2 + \left(\frac{\partial \delta}{\partial p_{u'}} \right)^2 \sigma_{p_{u'}}^2 + \left(\frac{\partial \delta}{\partial p_{d'}} \right)^2 \sigma_{p_{d'}}^2. \quad (\text{A.15})$$

δ is defined in Eq. (4.36), Eq. (A.15) becomes

$$\sigma_\delta^2 = \left(\frac{p_{d'}}{p_d p_{u'}} \right)^2 \sigma_{p_u}^2 + \left[\frac{p_u p_{d'}}{p_{u'}} \left(-\frac{1}{p_d^2} \right) \right]^2 \sigma_{p_d}^2 + \left[\frac{p_u p_{d'}}{p_d} \left(-\frac{1}{p_{u'}^2} \right) \right]^2 \sigma_{p_{u'}}^2 + \left(\frac{p_u}{p_d p_{u'}} \right)^2 \sigma_{p_{d'}}^2. \quad (\text{A.16})$$

From Eq. (4.52), one has $\frac{\partial A}{\partial \delta}$:

$$\frac{\partial}{\partial \delta} (aA^2 + bA + c) = 0, \quad (\text{A.17})$$

$$A^2 \frac{\partial a}{\partial \delta} + 2Aa \frac{\partial A}{\partial \delta} + A \frac{\partial b}{\partial \delta} + b \frac{\partial A}{\partial \delta} + \frac{\partial c}{\partial \delta} = 0. \quad (\text{A.18})$$

Differentiating Eq. (4.52) by δ , the following equations are derived:

$$\frac{\partial a}{\partial \delta} = \frac{\partial}{\partial \delta} (\delta \langle \beta_{u'} \rangle_w \langle \beta_d \rangle_w - \langle \beta_u \rangle_w \langle \beta_{d'} \rangle_w) = \langle \beta_{u'} \rangle_w \langle \beta_d \rangle_w, \quad (\text{A.19})$$

$$\frac{\partial b}{\partial \delta} = \frac{\partial}{\partial \delta} [\delta (\langle \beta_{u'} \rangle_w + \langle \beta_d \rangle_w) - (\langle \beta_u \rangle_w + \langle \beta_{d'} \rangle_w)] = \langle \beta_{u'} \rangle_w + \langle \beta_d \rangle_w, \quad (\text{A.20})$$

$$\frac{\partial c}{\partial \delta} = \frac{\partial}{\partial \delta} (\delta - 1) = 1. \quad (\text{A.21})$$

where

$$\langle \beta_x \rangle_w = \frac{\sum_i^{N_x} w_{i,x} \beta_{i,x}}{\sum_i^{N_x} w_{i,x}} \quad (\text{A.22})$$

at the cell x .

Putting them into Eq. (A.16), one has

$$\frac{\partial A}{\partial \delta} = \frac{-1}{2Aa + b} \left[A^2 \langle \beta_{u'} \rangle_w \langle \beta_d \rangle_w + A (\langle \beta_{u'} \rangle_w + \langle \beta_d \rangle_w) + 1 \right]. \quad (\text{A.23})$$

Therefore, σ_δ is written as

$$\sigma_A^2 = \left\{ \frac{-1}{2Aa+b} \left[A^2 \langle \beta_{u'} \rangle_w \langle \beta_d \rangle_w + A (\langle \beta_{u'} \rangle_w + \langle \beta_d \rangle_w) + 1 \right] \right\}^2$$

$$\times \left\{ \left(\frac{p_{d'}}{p_u p_{u'}} \right)^2 \sigma_{p_u}^2 + \left[\frac{p_u p_{d'}}{p_{u'}} \left(\frac{-1}{p_d^2} \right) \right]^2 \sigma_{p_d}^2 + \left[\frac{p_u p_{d'}}{p_d} \left(\frac{-1}{p_{u'}^2} \right) \right]^2 \sigma_{p_{u'}}^2 + \left(\frac{p_u}{p_d p_{u'}} \right)^2 \sigma_{p_{d'}}^2 \right\} .$$

(A.24)

Comparing an uncertainty with assumptions Eq. (4.54), this has more complicated form.

A.3. Optimised histogram bin

Binwidth for the pull distribution is optimised by the method described in Ref. [116]. Though this is developed for a time histogram, it can be also applied to a “normal” histogram to estimate a probability distribution. The procedure is following:

1. divide the data range into N bins of width Δ , and then counts the number of events k_i in the i -th bin.
2. calculate the mean and variance of the number of events as:

$$k \equiv \frac{1}{N} \sum_{i=1}^N k_i \quad \text{and} \quad \nu = \frac{1}{N} \sum_{i=1}^N (k_i - k)^2 .$$

(A.25)

3. compute the value $C(\Delta) = \frac{2k-\nu}{\Delta^2}$
4. iterate above calculation changing Δ , and find Δ' that minimise C .

B. Kinematic distribution

Distributions of variables are presented in this section:

Fig. B.1 the number of events for each period in each year

Fig. B.2 the number of hadrons for each period in each year

Fig. B.3 Q^2 in each year and target

Fig. B.4 x_{Bj} in each year and target

Fig. B.5 y in each year and target

Fig. B.6 W in each year and target

Fig. B.7 Multiplicity in each year and target

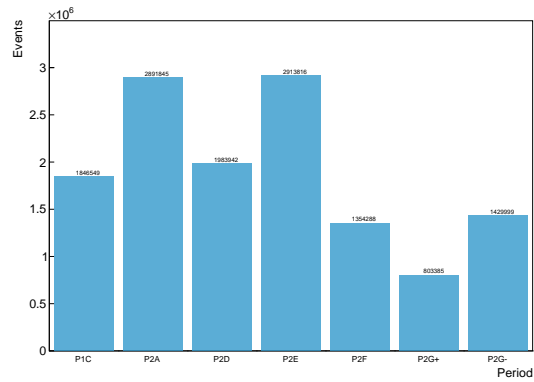
Fig. B.8 z in each year and target

Fig. B.9 p_T in each year and target

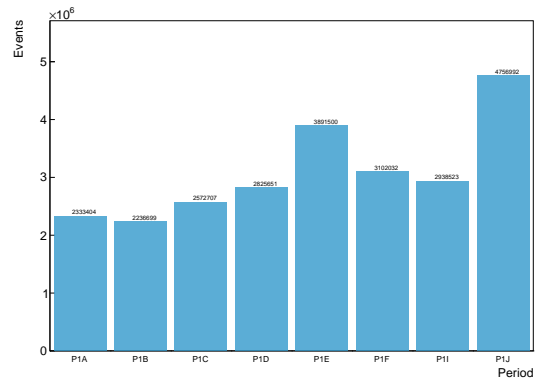
Fig. B.10 θ_{hadron} in each year and target

Fig. B.11 η_{CMS} in each year and target

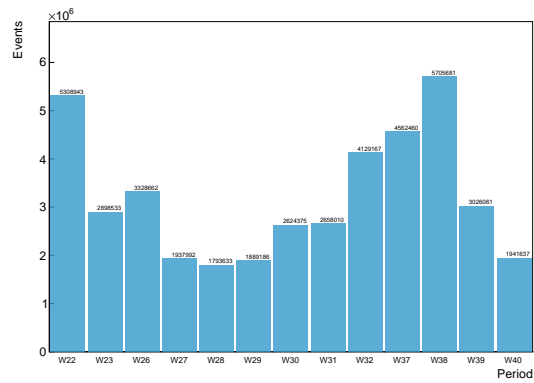
Fig. B.12 Q^2-p_T distributions in each year and target



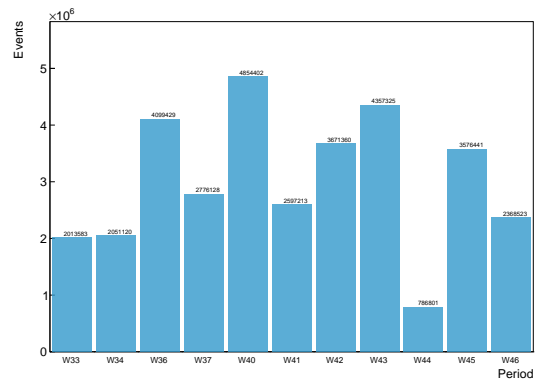
(a) 2002



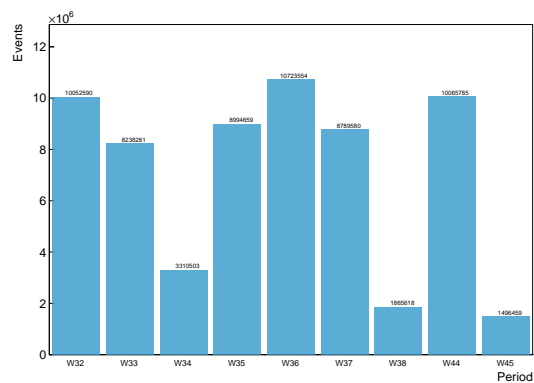
(b) 2003



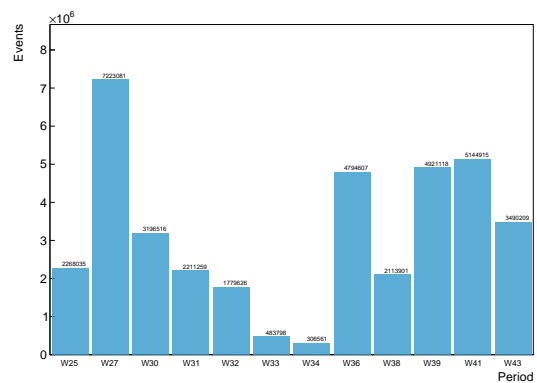
(c) 2004



(d) 2006

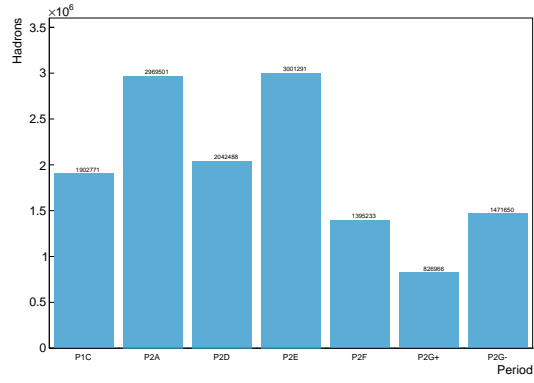


(e) 2007

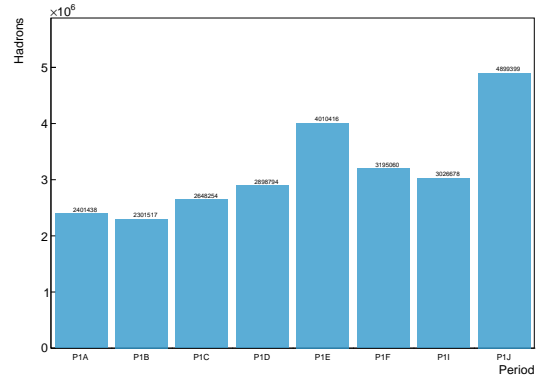


(f) 2011

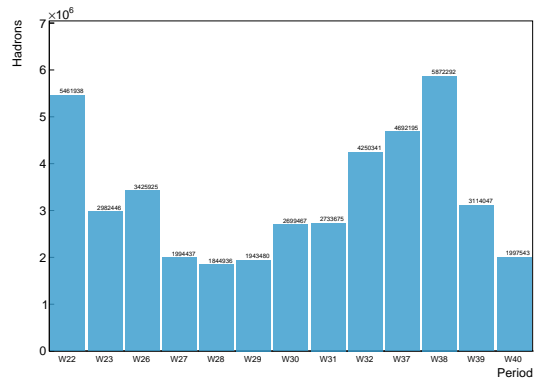
Figure B.1: The number of events period by period in each year. The period W35 in 2006 is removed from analysis, of which statistics is much smaller than other periods.



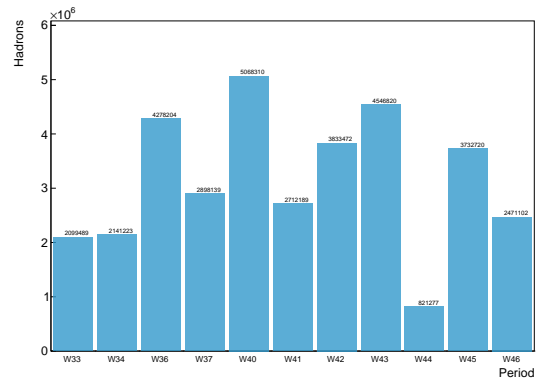
(a) 2002



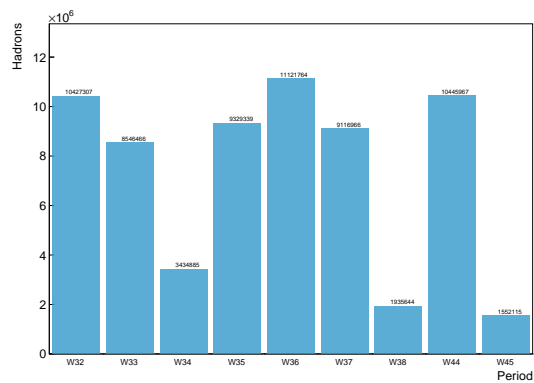
(b) 2003



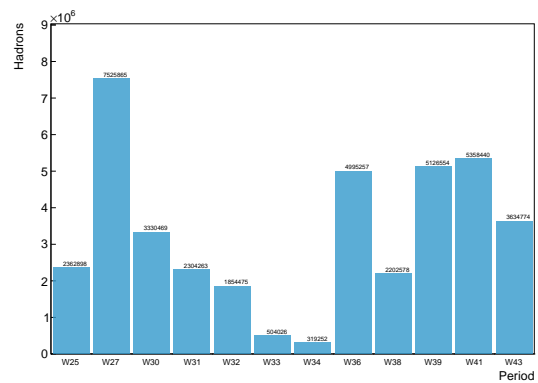
(c) 2004



(d) 2006

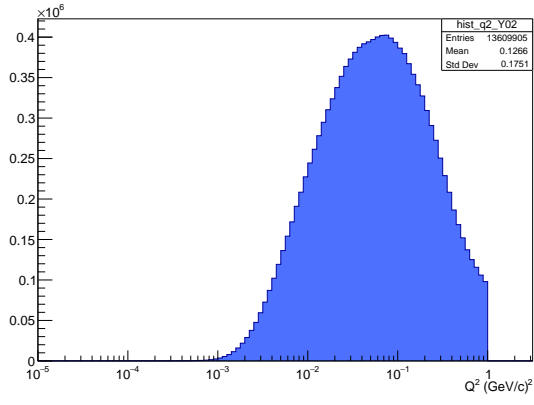


(e) 2007

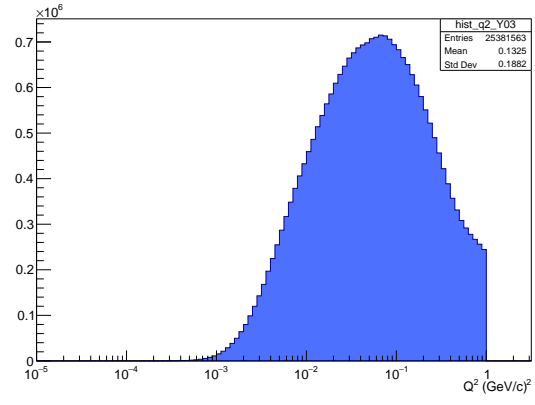


(f) 2011

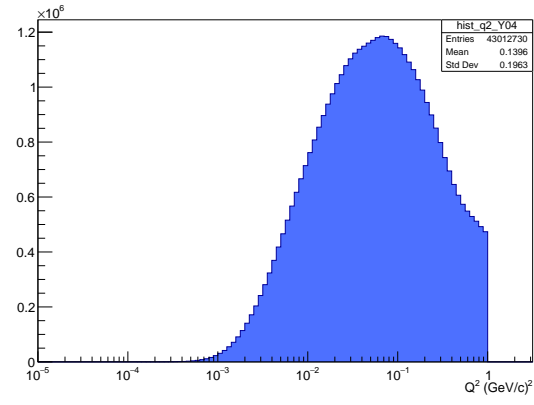
Figure B.2: The number of hadrons period by period in each year.



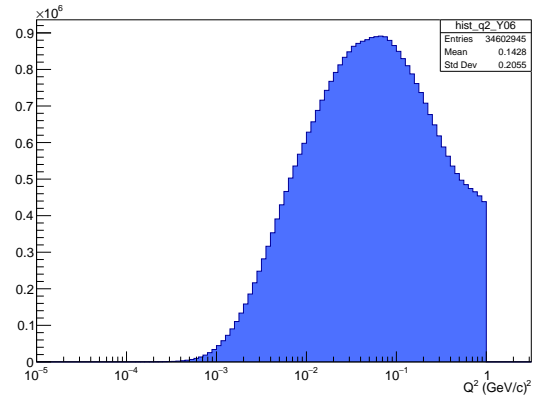
(a) 2002



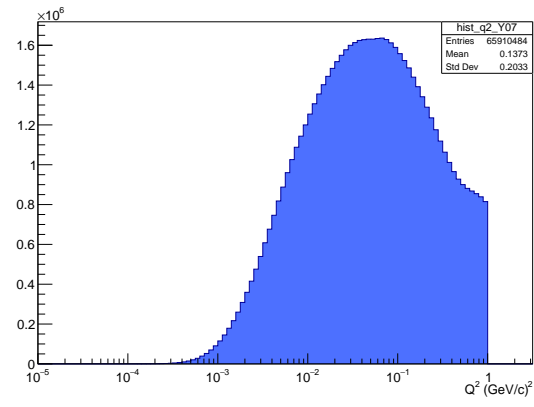
(b) 2003



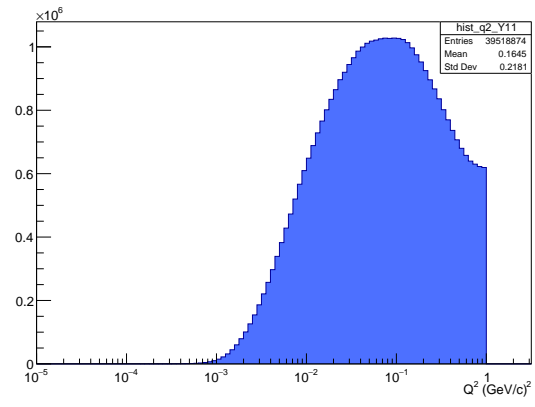
(c) 2004



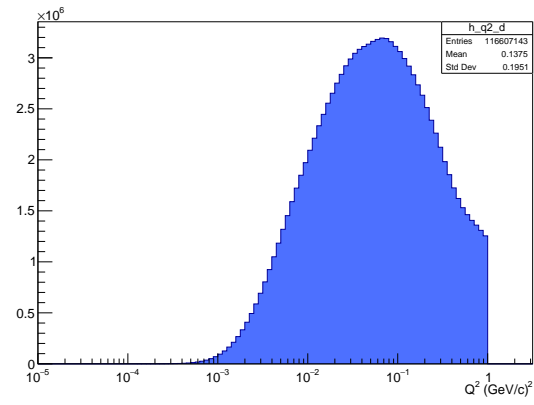
(d) 2006



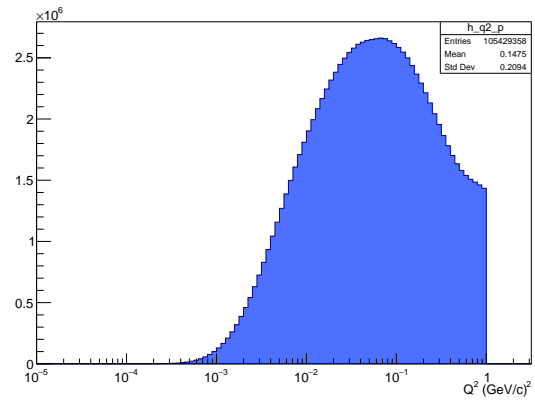
(e) 2007



(f) 2011

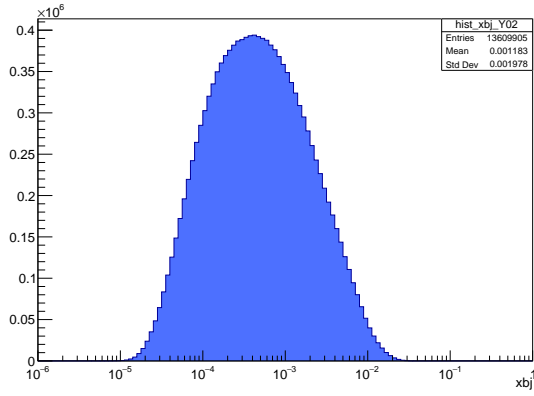


(g) Deuteron

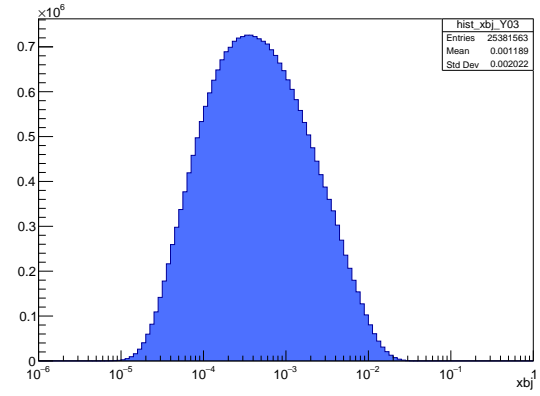


(h) Proton

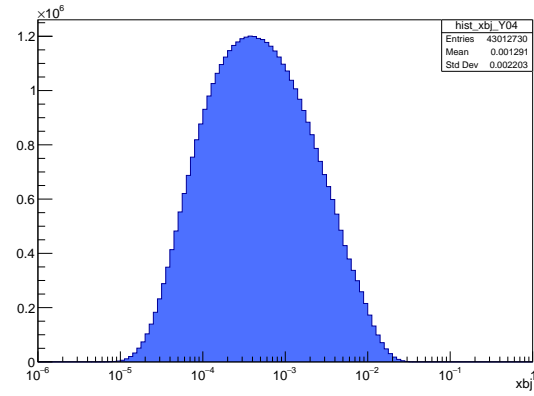
Figure B.3: Q^2 distributions in each year and target.



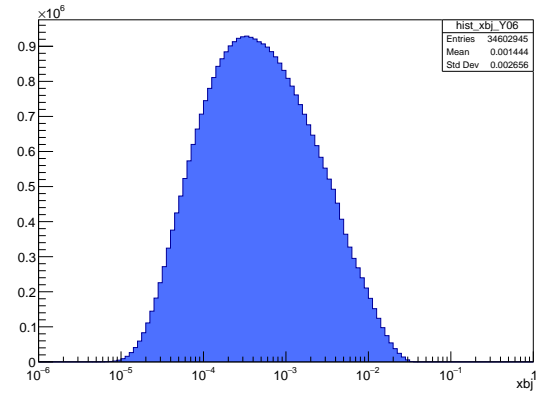
(a) 2002



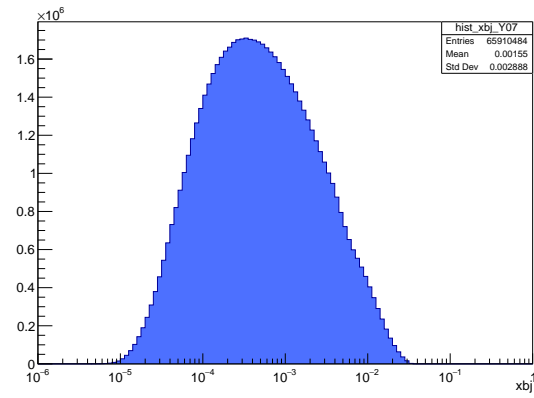
(b) 2003



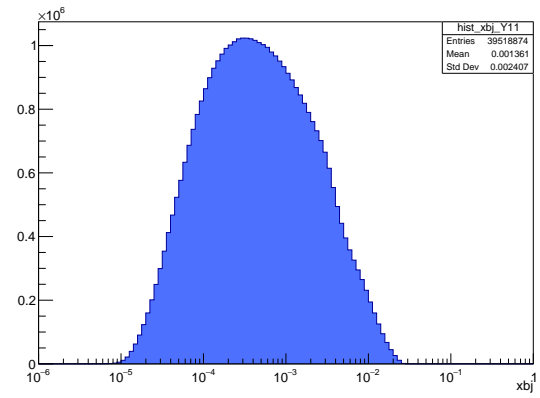
(c) 2004



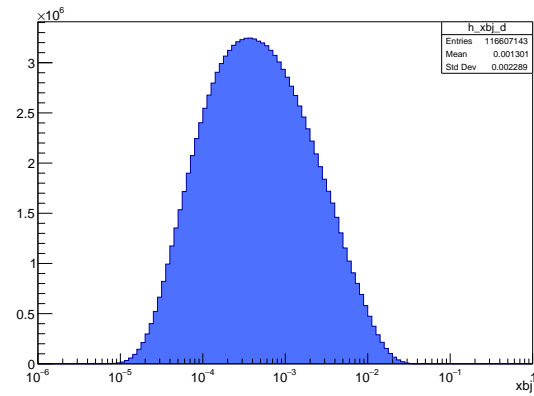
(d) 2006



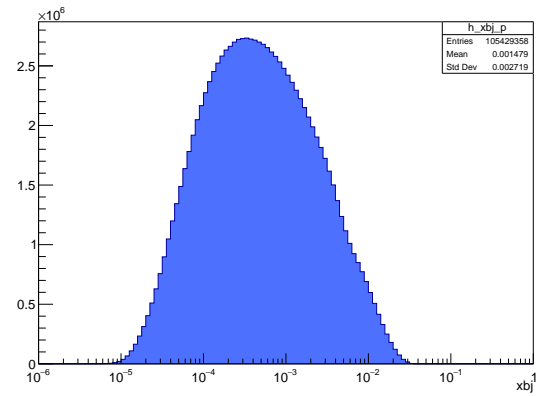
(e) 2007



(f) 2011

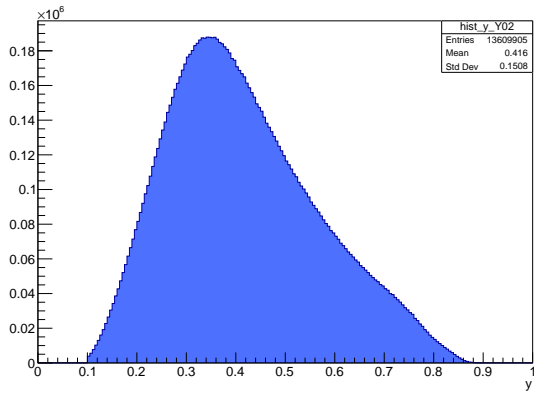


(g) Deuteron

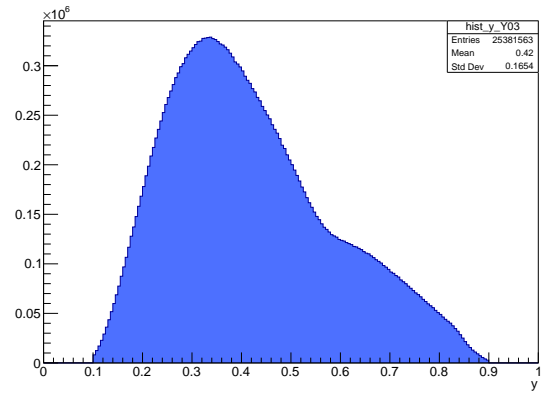


(h) Proton

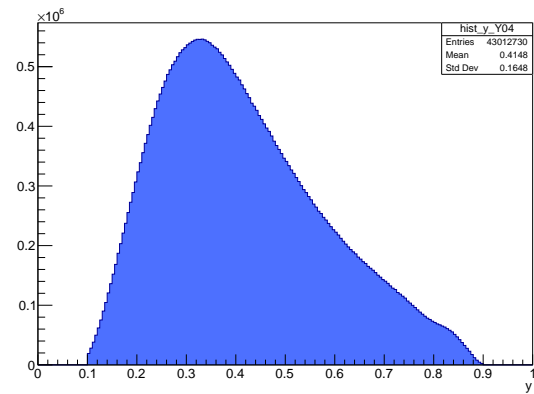
Figure B.4: x_{Bj} distributions in each year and target.



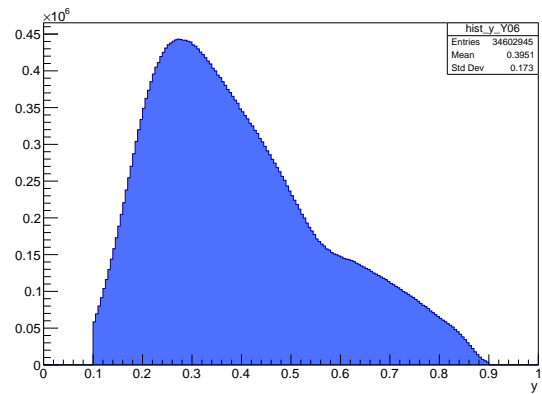
(a) 2002



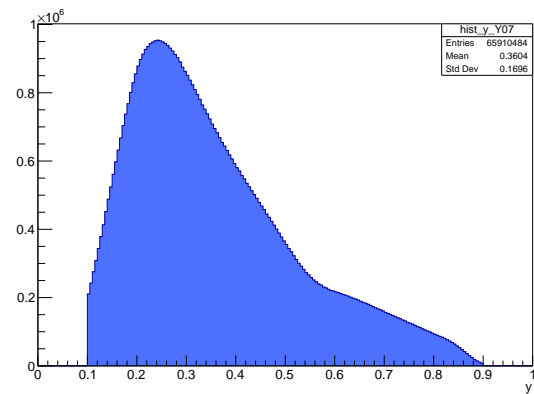
(b) 2003



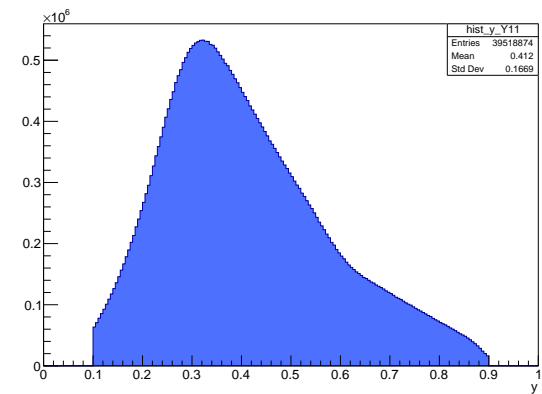
(c) 2004



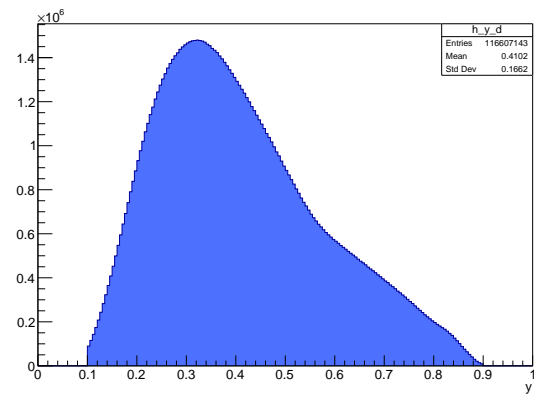
(d) 2006



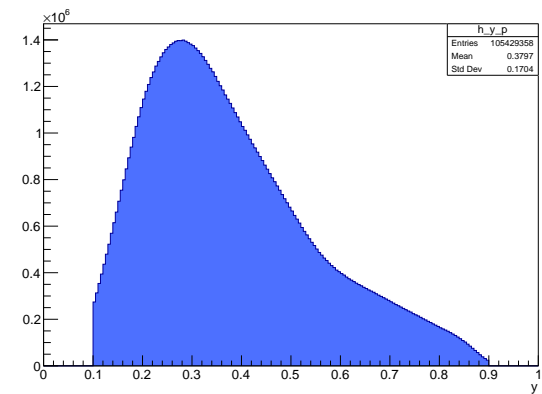
(e) 2007



(f) 2011

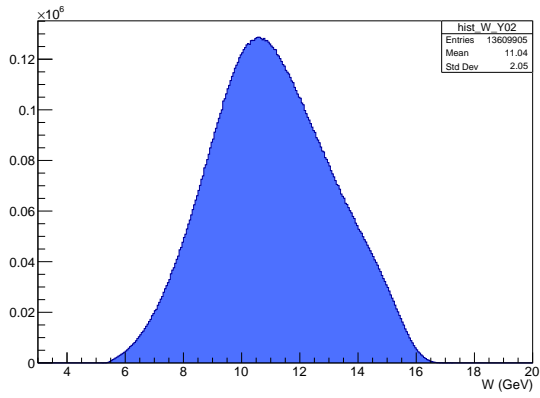


(g) Deuteron

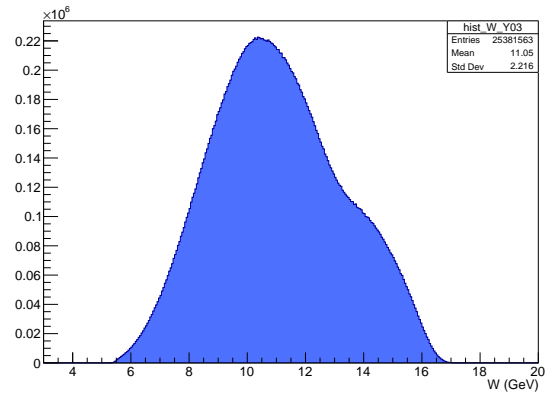


(h) Proton

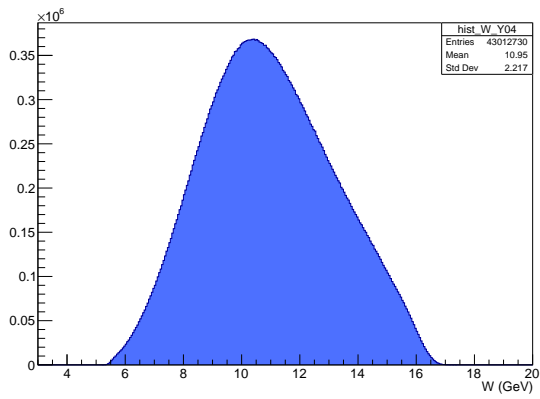
Figure B.5: y distributions in each year and target.



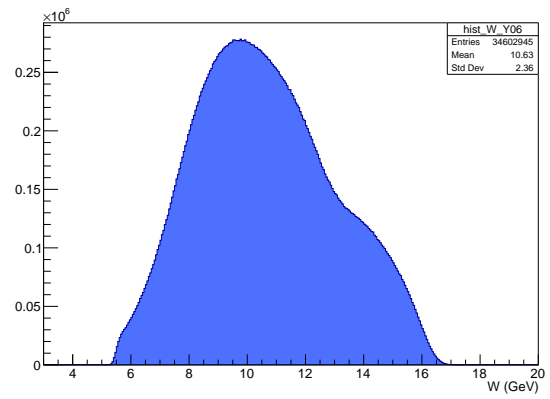
(a) 2002



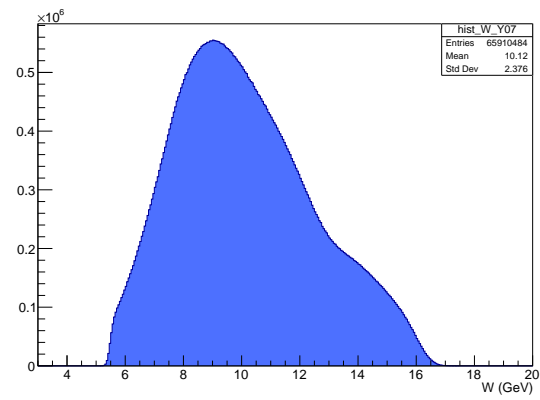
(b) 2003



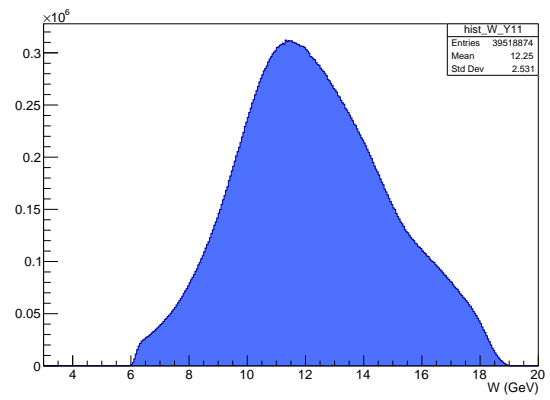
(c) 2004



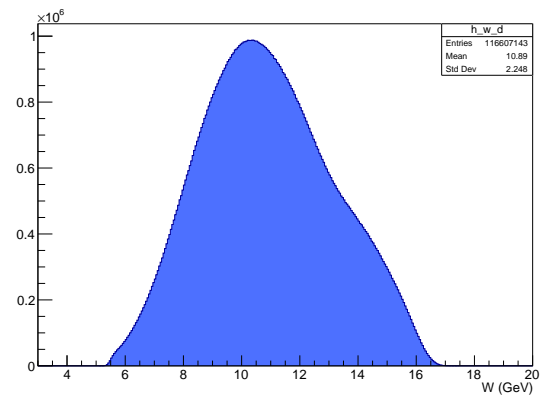
(d) 2006



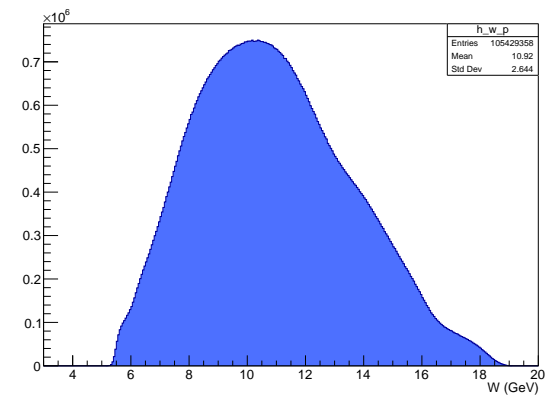
(e) 2007



(f) 2011

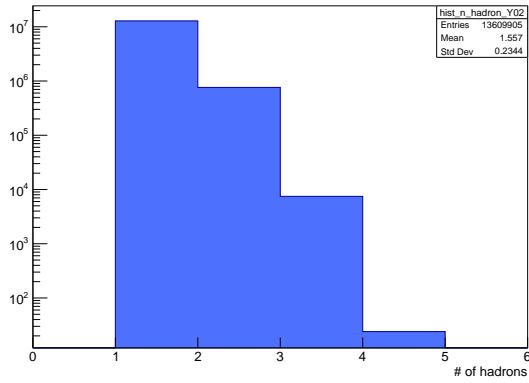


(g) Deuteron

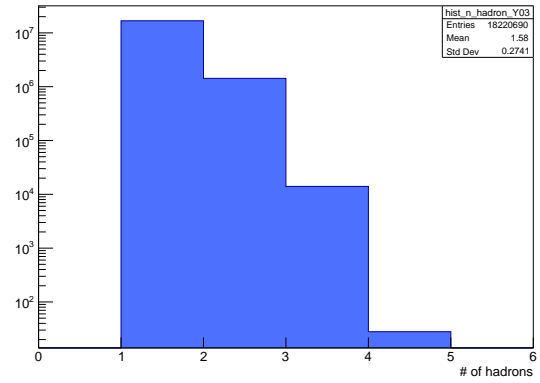


(h) Proton

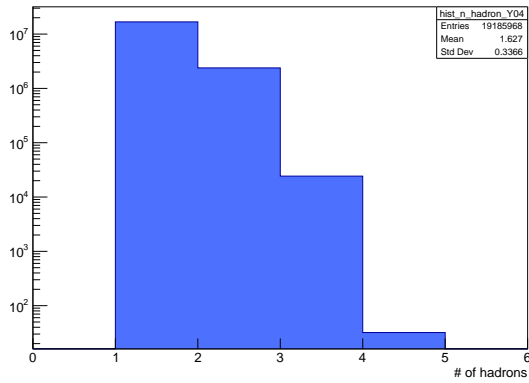
Figure B.6: W distributions in each year.



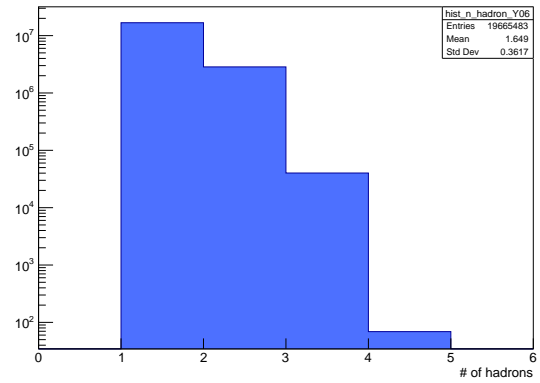
(a) 2002



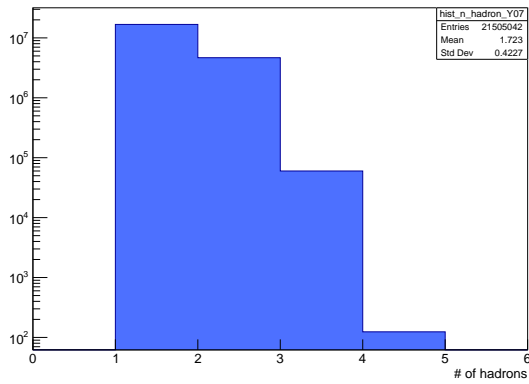
(b) 2003



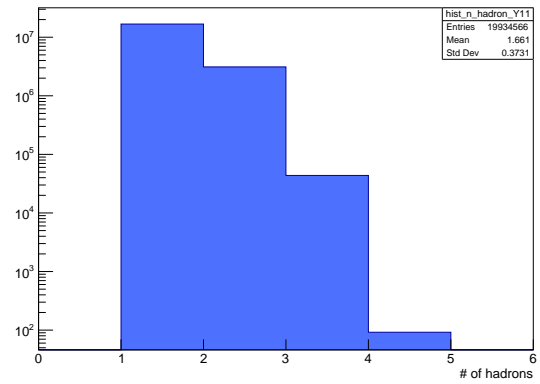
(c) 2004



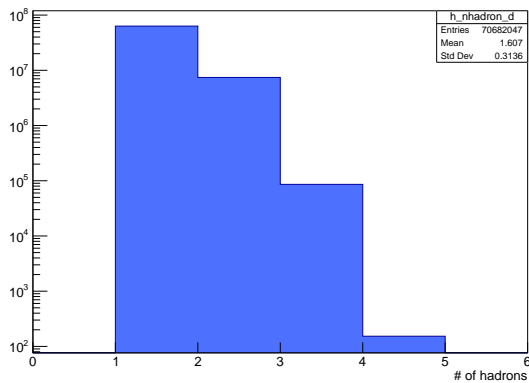
(d) 2006



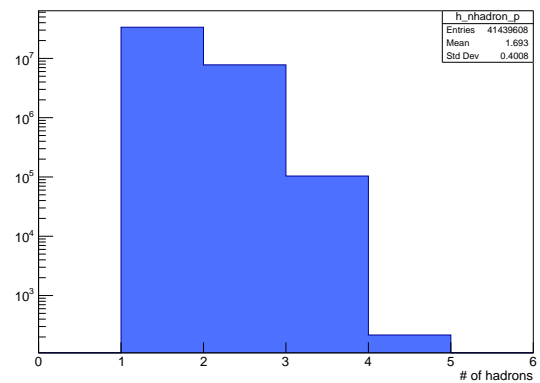
(e) 2007



(f) 2011

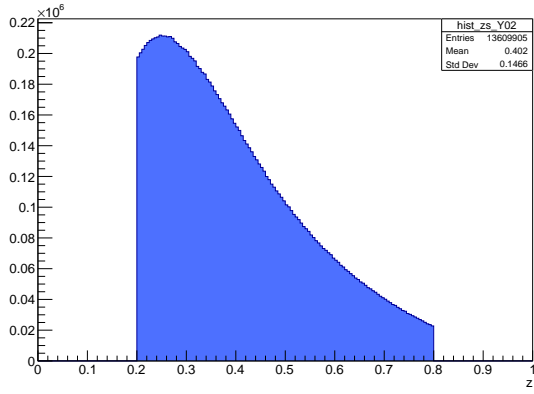


(g) Deuteron

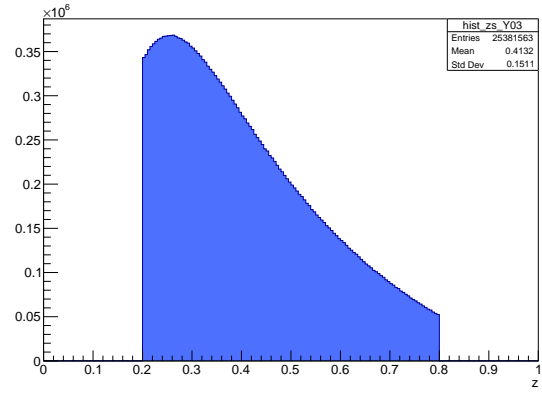


(h) Proton

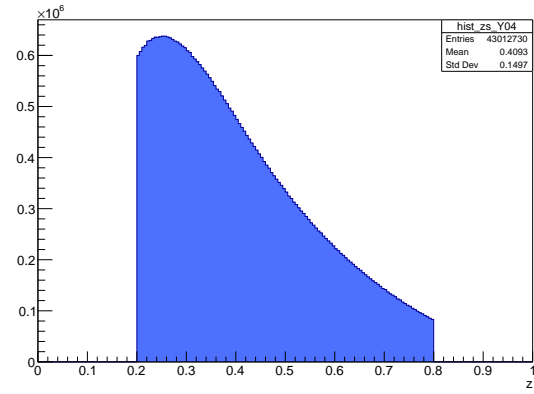
Figure B.7: Multiplicity distributions in each year.



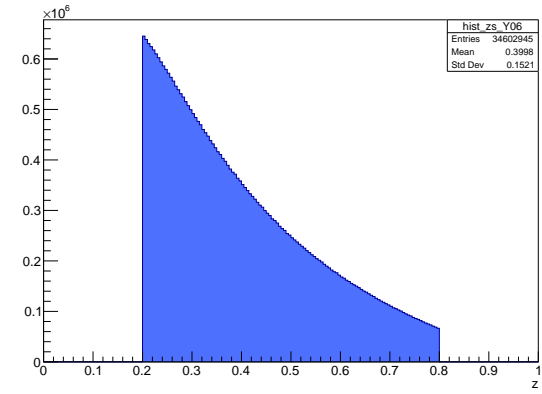
(a) 2002



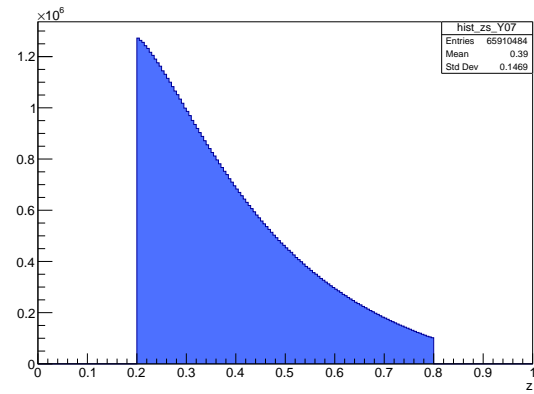
(b) 2003



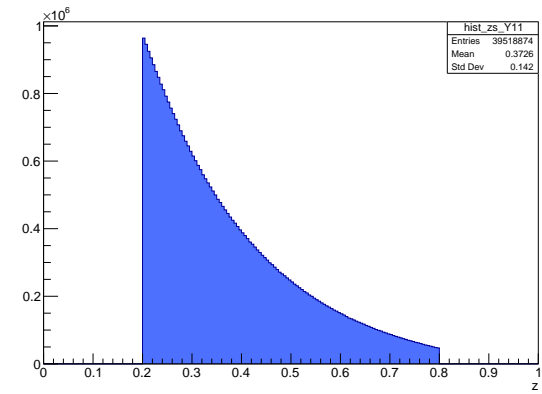
(c) 2004



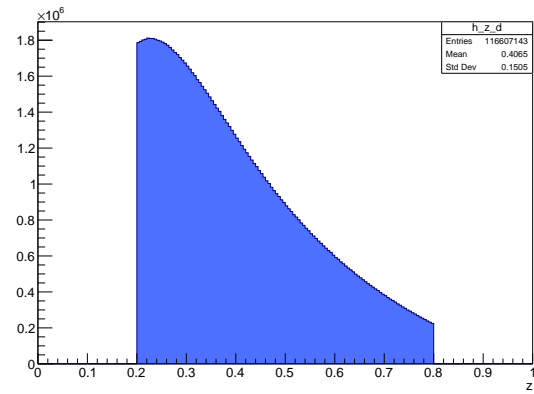
(d) 2006



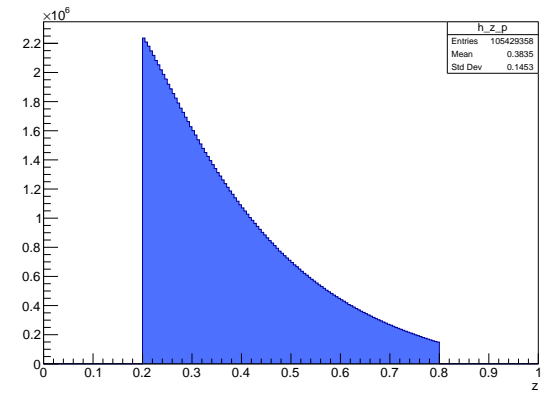
(e) 2007



(f) 2011

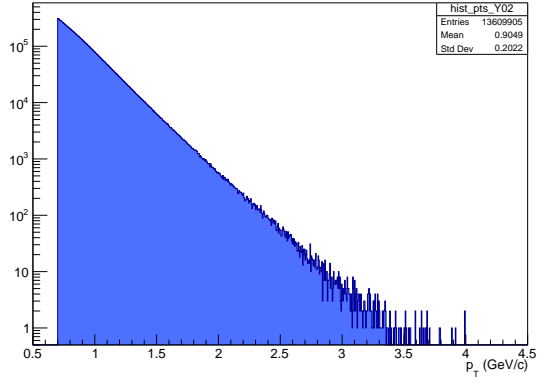


(g) Deuteron

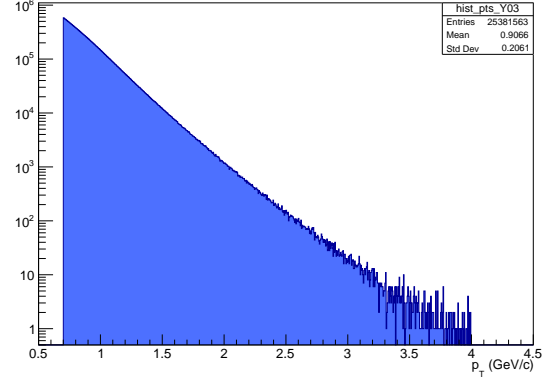


(h) Proton

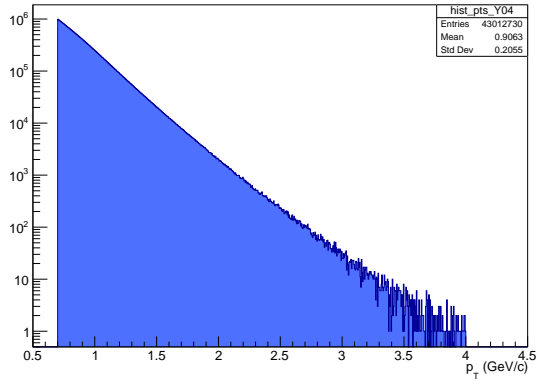
Figure B.8: z distributions in each year and target.



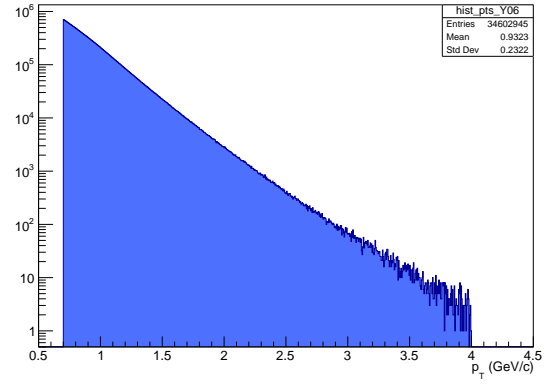
(a) 2002



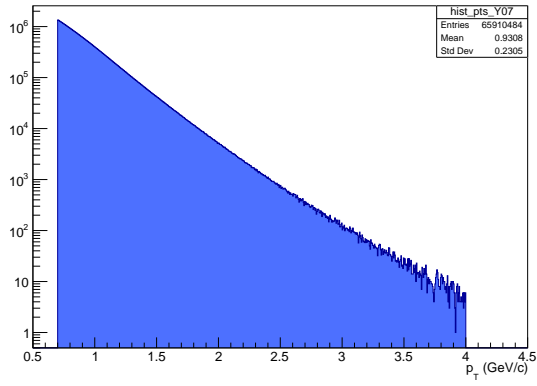
(b) 2003



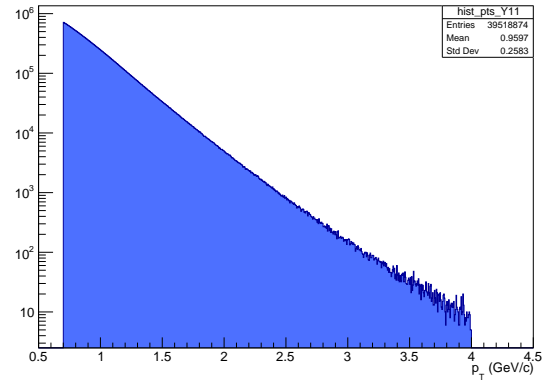
(c) 2004



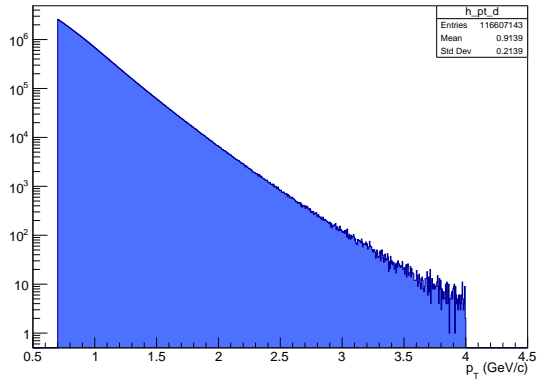
(d) 2006



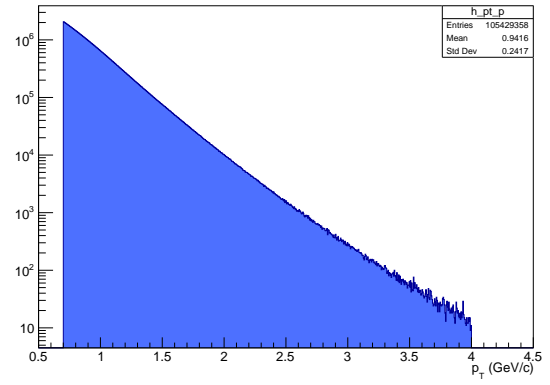
(e) 2007



(f) 2011

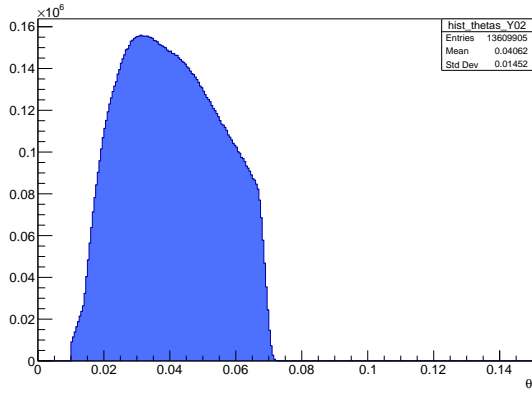


(g) Deuteron

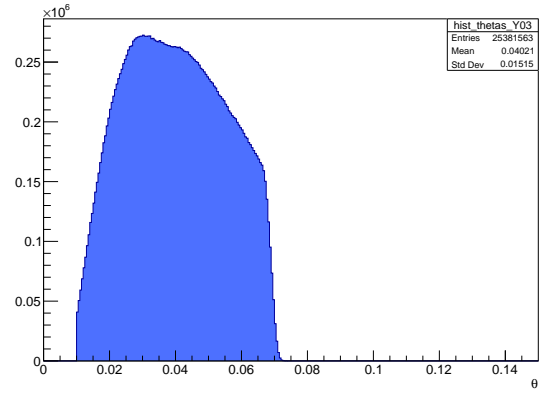


(h) Proton

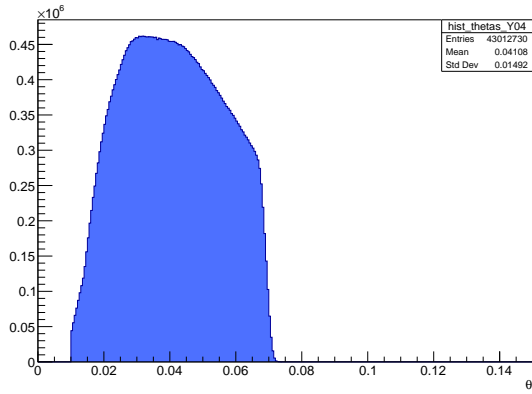
Figure B.9: p_T distributions in each year and target.



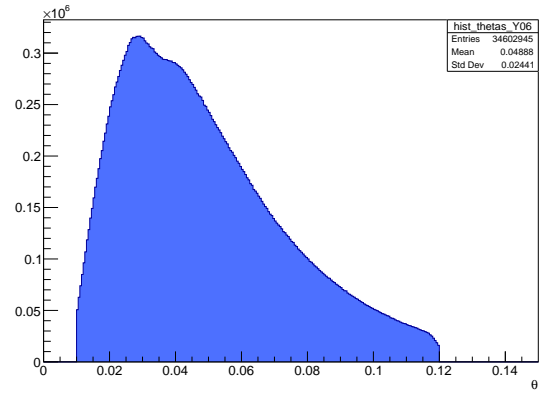
(a) 2002



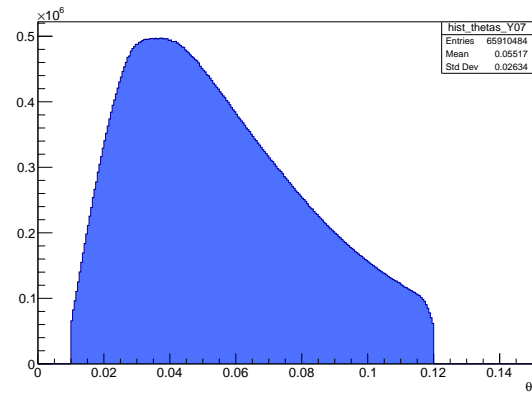
(b) 2003



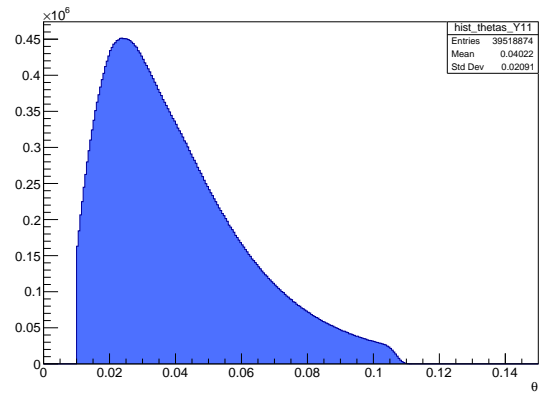
(c) 2004



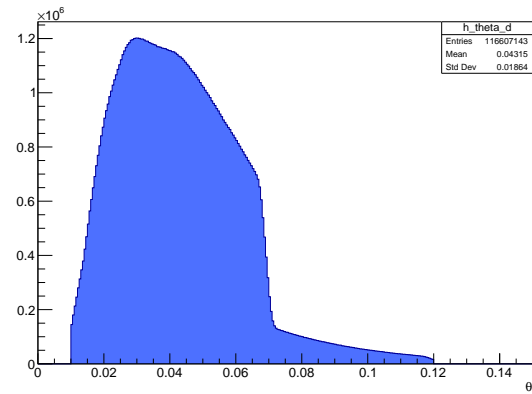
(d) 2006



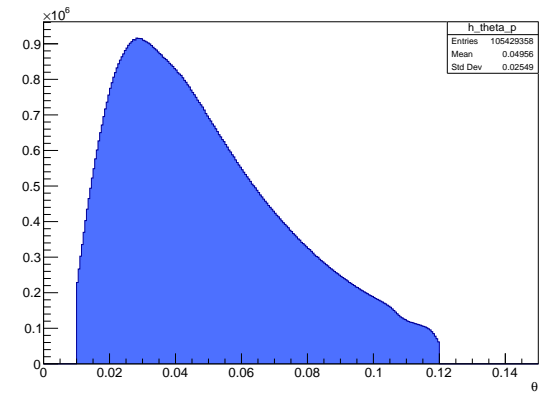
(e) 2007



(f) 2011

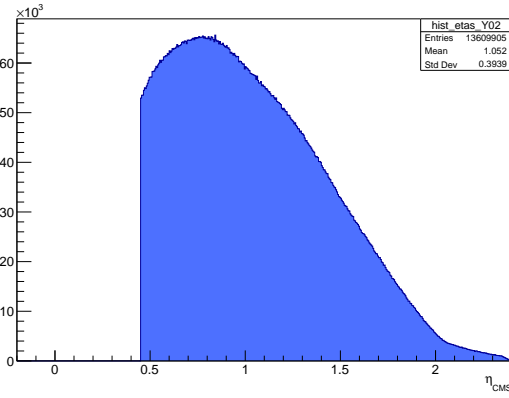


(g) Deuteron

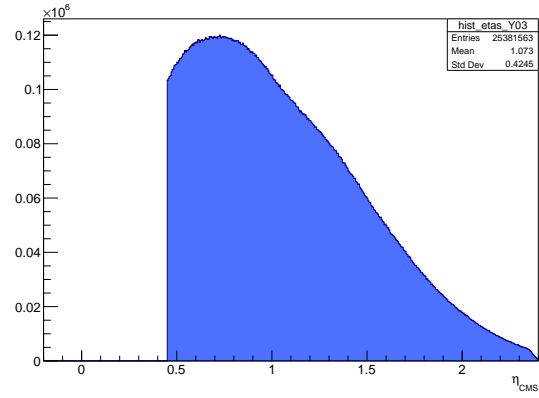


(h) Proton

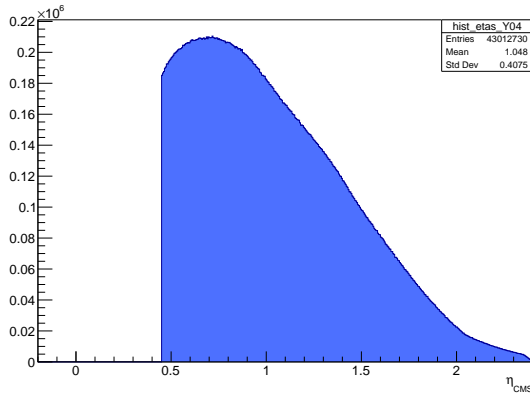
Figure B.10: θ_{hadron} distributions in each year and target. Hadrons with $\theta > 0.07$ are removed until 2004 data. Peak in 2011 shifted lower direction due to high energy beam.



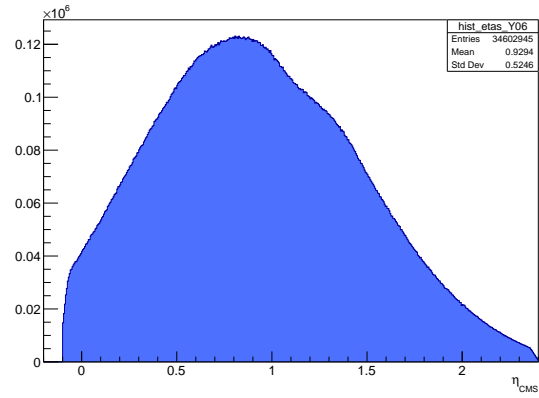
(a) 2002



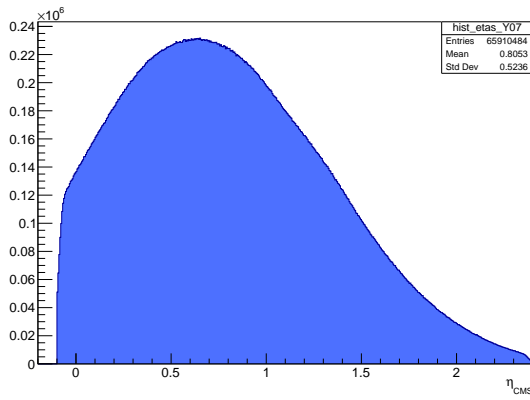
(b) 2003



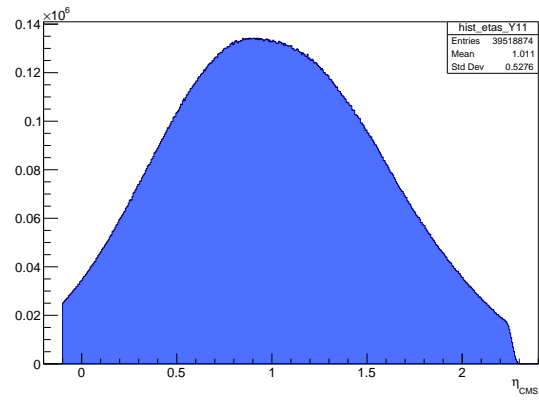
(c) 2004



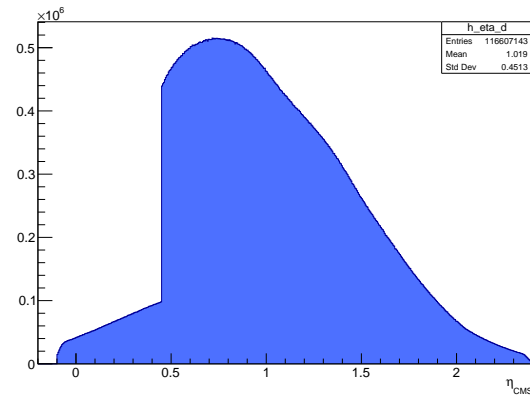
(d) 2006



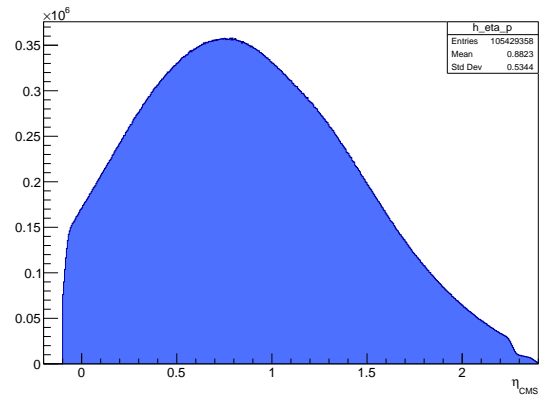
(e) 2007



(f) 2011

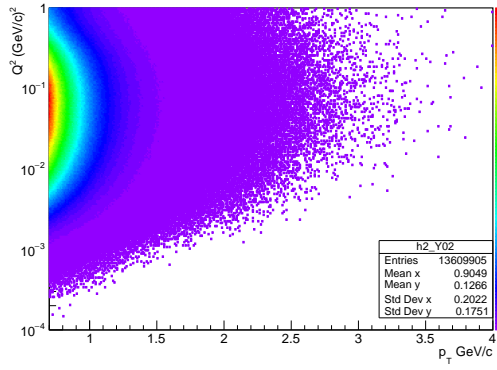


(g) Deuteron

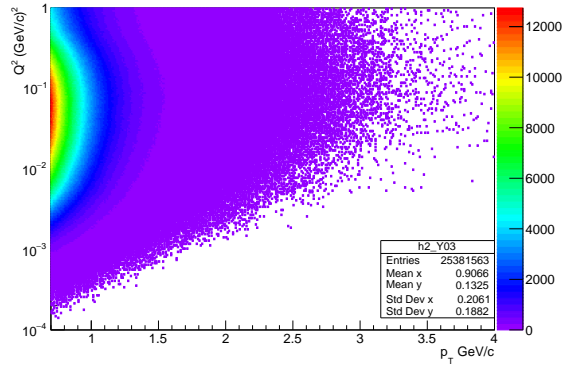


(h) Proton

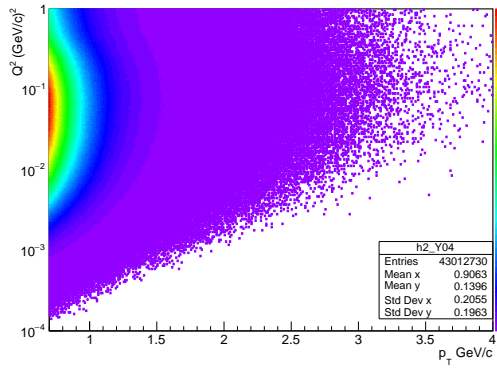
Figure B.11: η_{CMS} distributions in each year and target. $\theta_{\text{hadron}} > 0.07$ corresponds to $\eta_{\text{CMS}} < 0.4$. Hadrons scattering with such angle are removed.



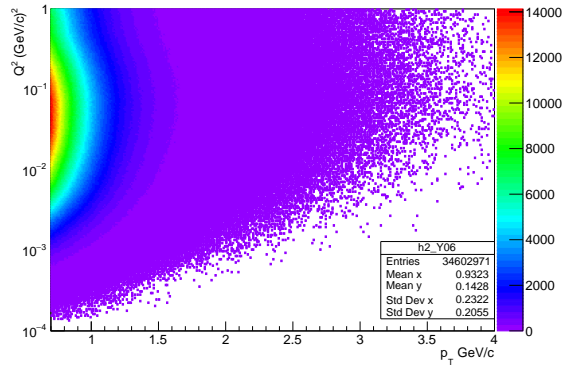
(a) 2002



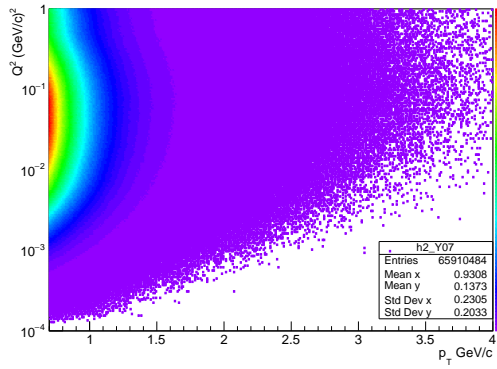
(b) 2003



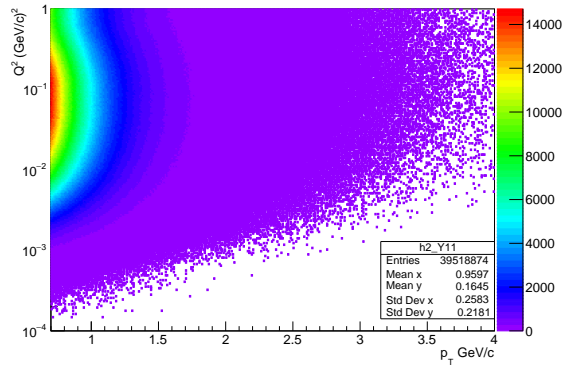
(c) 2004



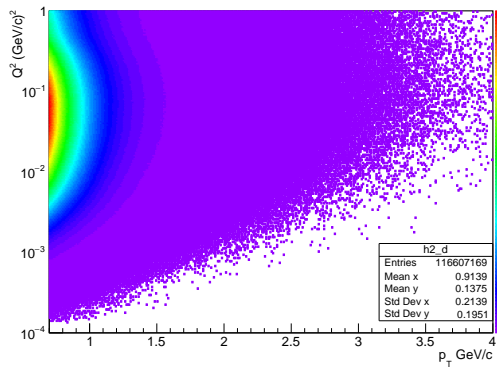
(d) 2006



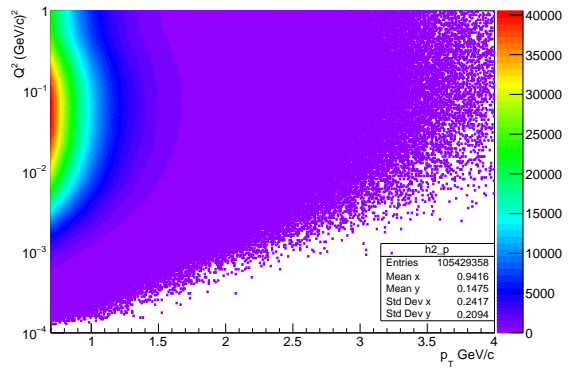
(e) 2007



(f) 2011



(g) Deuteron



(h) Proton

Figure B.12: Q^2 - p_T distributions in each year and target.

C. Tables and plots for asymmetries

C.1. Tables

Table C.1: The ratios of the systematic uncertainty to the statistical one for A_{LL}^d

(a) the positive hadron			(b) the negative hadron		
η_{CMS}	p_T (GeV/c)	$\sigma_{\text{syst.}}/\sigma_{\text{stat.}}$	η_{CMS}	p_T (GeV/c)	$\sigma_{\text{syst.}}/\sigma_{\text{stat.}}$
[-0.1, 0.45]	[0.7, 0.75]	0.513	[-0.1, 0.45]	[0.7, 0.75]	0.517
[-0.1, 0.45]	[0.75, 0.80]	0.363	[-0.1, 0.45]	[0.75, 0.80]	0.554
[-0.1, 0.45]	[0.8, 0.9]	0.490	[-0.1, 0.45]	[0.8, 0.9]	0.452
[-0.1, 0.45]	[0.9, 1.0]	0.491	[-0.1, 0.45]	[0.9, 1.0]	0.485
[-0.1, 0.45]	[1.0, 1.25]	0.746	[-0.1, 0.45]	[1.0, 1.25]	0.518
[-0.1, 0.45]	[1.25, 1.5]	0.490	[-0.1, 0.45]	[1.25, 1.5]	0.495
[-0.1, 0.45]	[1.5, 2.0]	0.495	[-0.1, 0.45]	[1.5, 2.0]	0.460
[-0.1, 0.45]	[2.0, 2.5]	0.582	[-0.1, 0.45]	[2.0, 2.5]	0.439
[-0.1, 0.45]	[2.5, 4.0]	0.664	[-0.1, 0.45]	[2.5, 4.0]	0.510
[0.45, 0.90]	[0.7, 0.75]	0.404	[0.45, 0.90]	[0.7, 0.75]	0.313
[0.45, 0.90]	[0.75, 0.80]	0.408	[0.45, 0.90]	[0.75, 0.80]	0.311
[0.45, 0.90]	[0.8, 0.9]	0.331	[0.45, 0.90]	[0.8, 0.9]	0.312
[0.45, 0.90]	[0.9, 1.0]	0.425	[0.45, 0.90]	[0.9, 1.0]	0.311
[0.45, 0.90]	[1.0, 1.25]	0.568	[0.45, 0.90]	[1.0, 1.25]	0.446
[0.45, 0.90]	[1.25, 1.5]	0.323	[0.45, 0.90]	[1.25, 1.5]	0.383
[0.45, 0.90]	[1.5, 2.0]	0.359	[0.45, 0.90]	[1.5, 2.0]	0.415
[0.45, 0.90]	[2.0, 2.5]	0.383	[0.45, 0.90]	[2.0, 2.5]	0.615
[0.45, 0.90]	[2.5, 4.0]	0.412	[0.45, 0.90]	[2.5, 4.0]	0.435
[0.9, 2.4]	[0.7, 0.75]	0.460	[0.9, 2.4]	[0.7, 0.75]	0.311
[0.9, 2.4]	[0.75, 0.80]	0.349	[0.9, 2.4]	[0.75, 0.80]	0.314
[0.9, 2.4]	[0.8, 0.9]	0.314	[0.9, 2.4]	[0.8, 0.9]	0.358
[0.9, 2.4]	[0.9, 1.0]	0.313	[0.9, 2.4]	[0.9, 1.0]	0.521
[0.9, 2.4]	[1.0, 1.25]	0.332	[0.9, 2.4]	[1.0, 1.25]	0.512
[0.9, 2.4]	[1.25, 1.5]	0.311	[0.9, 2.4]	[1.25, 1.5]	0.360
[0.9, 2.4]	[1.5, 2.0]	0.449	[0.9, 2.4]	[1.5, 2.0]	0.311
[0.9, 2.4]	[2.0, 2.5]	0.318	[0.9, 2.4]	[2.0, 2.5]	0.349
[0.9, 2.4]	[2.5, 4.0]	0.338	[0.9, 2.4]	[2.5, 4.0]	0.401

Table C.2: The ratios of the systematic uncertainty to the statistical one for A_{LL}^p

(a) the positive hadron			(b) the negative hadron		
η_{CMS}	p_T (GeV/c)	$\sigma_{\text{syst.}}/\sigma_{\text{stat.}}$	η_{CMS}	p_T (GeV/c)	$\sigma_{\text{syst.}}/\sigma_{\text{stat.}}$
[-0.1, 0.45]	[0.7, 0.75]	0.402	[-0.1, 0.45]	[0.7, 0.75]	0.402
[-0.1, 0.45]	[0.75, 0.80]	0.605	[-0.1, 0.45]	[0.75, 0.80]	0.494
[-0.1, 0.45]	[0.8, 0.9]	0.414	[-0.1, 0.45]	[0.8, 0.9]	0.525
[-0.1, 0.45]	[0.9, 1.0]	0.395	[-0.1, 0.45]	[0.9, 1.0]	0.838
[-0.1, 0.45]	[1.0, 1.25]	0.418	[-0.1, 0.45]	[1.0, 1.25]	0.401
[-0.1, 0.45]	[1.25, 1.5]	0.610	[-0.1, 0.45]	[1.25, 1.5]	0.430
[-0.1, 0.45]	[1.5, 2.0]	0.385	[-0.1, 0.45]	[1.5, 2.0]	0.430
[-0.1, 0.45]	[2.0, 2.5]	0.402	[-0.1, 0.45]	[2.0, 2.5]	0.996
[-0.1, 0.45]	[2.5, 4.0]	0.425	[-0.1, 0.45]	[2.5, 4.0]	0.579
[0.45, 0.90]	[0.7, 0.75]	0.422	[0.45, 0.90]	[0.7, 0.75]	0.741
[0.45, 0.90]	[0.75, 0.80]	0.412	[0.45, 0.90]	[0.75, 0.80]	0.446
[0.45, 0.90]	[0.8, 0.9]	0.429	[0.45, 0.90]	[0.8, 0.9]	0.420
[0.45, 0.90]	[0.9, 1.0]	0.466	[0.45, 0.90]	[0.9, 1.0]	0.451
[0.45, 0.90]	[1.0, 1.25]	0.520	[0.45, 0.90]	[1.0, 1.25]	0.586
[0.45, 0.90]	[1.25, 1.5]	0.468	[0.45, 0.90]	[1.25, 1.5]	0.694
[0.45, 0.90]	[1.5, 2.0]	0.390	[0.45, 0.90]	[1.5, 2.0]	0.440
[0.45, 0.90]	[2.0, 2.5]	0.415	[0.45, 0.90]	[2.0, 2.5]	0.450
[0.45, 0.90]	[2.5, 4.0]	0.450	[0.45, 0.90]	[2.5, 4.0]	0.410
[0.9, 2.4]	[0.7, 0.75]	0.421	[0.9, 2.4]	[0.7, 0.75]	0.413
[0.9, 2.4]	[0.75, 0.80]	0.788	[0.9, 2.4]	[0.75, 0.80]	0.391
[0.9, 2.4]	[0.8, 0.9]	0.804	[0.9, 2.4]	[0.8, 0.9]	0.509
[0.9, 2.4]	[0.9, 1.0]	0.893	[0.9, 2.4]	[0.9, 1.0]	0.507
[0.9, 2.4]	[1.0, 1.25]	0.672	[0.9, 2.4]	[1.0, 1.25]	0.401
[0.9, 2.4]	[1.25, 1.5]	0.472	[0.9, 2.4]	[1.25, 1.5]	0.450
[0.9, 2.4]	[1.5, 2.0]	0.472	[0.9, 2.4]	[1.5, 2.0]	0.616
[0.9, 2.4]	[2.0, 2.5]	0.420	[0.9, 2.4]	[2.0, 2.5]	0.555
[0.9, 2.4]	[2.5, 4.0]	0.630	[0.9, 2.4]	[2.5, 4.0]	0.741

Table C.3: Values of A_{LL}^d

(a) the positive hadron

η_{CMS}	p_T (GeV/c)	$\langle p_T \rangle$	$\sigma_{(p_T)}$	A_{LL}	$A_{LL}^{\text{stat.}}$	$A_{LL}^{\text{syst.}}$
[-0.1, 0.45]	[0.7, 0.75]	0.725	0.002	6.718E-3	1.073E-2	5.530E-3
[-0.1, 0.45]	[0.75, 0.80]	0.775	0.002	2.246E-3	1.108E-2	4.023E-3
[-0.1, 0.45]	[0.8, 0.9]	0.848	0.001	3.063E-3	8.375E-3	4.109E-3
[-0.1, 0.45]	[0.9, 1.0]	0.948	0.002	2.399E-2	9.433E-3	4.982E-3
[-0.1, 0.45]	[1.0, 1.25]	1.108	0.001	9.545E-4	7.721E-3	5.761E-3
[-0.1, 0.45]	[1.25, 1.5]	1.356	0.002	7.672E-3	1.196E-2	5.896E-3
[-0.1, 0.45]	[1.5, 2.0]	1.678	0.003	-1.877E-2	1.598E-2	8.039E-3
[-0.1, 0.45]	[2.0, 2.5]	2.180	0.006	5.572E-2	3.930E-2	2.326E-2
[-0.1, 0.45]	[2.5, 4.0]	2.794	0.014	1.318E-1	8.668E-2	5.847E-2
[0.45, 0.90]	[0.7, 0.75]	0.724	0.001	2.814E-3	3.190E-3	1.305E-3
[0.45, 0.90]	[0.75, 0.80]	0.774	0.001	2.872E-3	3.465E-3	1.439E-3
[0.45, 0.90]	[0.8, 0.9]	0.847	0.000	1.292E-3	2.791E-3	9.352E-4
[0.45, 0.90]	[0.9, 1.0]	0.947	0.001	-4.653E-3	3.361E-3	1.466E-3
[0.45, 0.90]	[1.0, 1.25]	1.103	0.001	2.831E-3	3.019E-3	1.728E-3
[0.45, 0.90]	[1.25, 1.5]	1.353	0.001	5.455E-3	5.238E-3	1.748E-3
[0.45, 0.90]	[1.5, 2.0]	1.666	0.001	-3.112E-3	7.864E-3	2.825E-3
[0.45, 0.90]	[2.0, 2.5]	2.170	0.004	1.630E-3	2.271E-2	8.708E-3
[0.45, 0.90]	[2.5, 4.0]	2.759	0.009	1.409E-2	5.918E-2	2.447E-2
[0.9, 2.4]	[0.7, 0.75]	0.724	0.000	3.975E-4	2.331E-3	1.073E-3
[0.9, 2.4]	[0.75, 0.80]	0.774	0.000	3.321E-3	2.628E-3	9.403E-4
[0.9, 2.4]	[0.8, 0.9]	0.846	0.000	3.148E-3	2.226E-3	7.320E-4
[0.9, 2.4]	[0.9, 1.0]	0.946	0.001	2.917E-3	2.890E-3	9.307E-4
[0.9, 2.4]	[1.0, 1.25]	1.096	0.001	2.990E-3	2.891E-3	1.001E-3
[0.9, 2.4]	[1.25, 1.5]	1.347	0.001	2.033E-2	5.922E-3	2.375E-3
[0.9, 2.4]	[1.5, 2.0]	1.651	0.002	1.538E-3	1.045E-2	4.695E-3
[0.9, 2.4]	[2.0, 2.5]	2.157	0.006	-4.803E-2	3.825E-2	1.285E-2
[0.9, 2.4]	[2.5, 4.0]	2.716	0.019	1.947E-2	1.217E-1	4.122E-2

(b) the negative hadron

η_{CMS}	p_T (GeV/c)	$\langle p_T \rangle$	$\sigma_{(p_T)}$	A_{LL}	$A_{LL}^{\text{stat.}}$	$A_{LL}^{\text{syst.}}$
[-0.1, 0.45]	[0.7, 0.75]	0.725	0.002	5.290E-3	1.156E-2	5.984E-3
[-0.1, 0.45]	[0.75, 0.80]	0.775	0.002	-1.054E-2	1.189E-2	6.633E-3
[-0.1, 0.45]	[0.8, 0.9]	0.848	0.001	6.415E-3	8.997E-3	4.099E-3
[-0.1, 0.45]	[0.9, 1.0]	0.948	0.002	7.644E-3	1.017E-2	4.963E-3
[-0.1, 0.45]	[1.0, 1.25]	1.108	0.001	3.436E-3	8.328E-3	4.321E-3
[-0.1, 0.45]	[1.25, 1.5]	1.356	0.002	1.659E-2	1.293E-2	6.522E-3
[-0.1, 0.45]	[1.5, 2.0]	1.677	0.003	1.858E-2	1.725E-2	8.070E-3
[-0.1, 0.45]	[2.0, 2.5]	2.180	0.007	-3.403E-2	4.276E-2	1.895E-2
[-0.1, 0.45]	[2.5, 4.0]	2.796	0.015	7.209E-2	9.429E-2	4.841E-2
[0.45, 0.90]	[0.7, 0.75]	0.724	0.001	-1.395E-3	3.424E-3	1.077E-3
[0.45, 0.90]	[0.75, 0.80]	0.774	0.001	3.108E-4	3.701E-3	1.152E-3
[0.45, 0.90]	[0.8, 0.9]	0.847	0.001	2.005E-3	2.979E-3	9.477E-4
[0.45, 0.90]	[0.9, 1.0]	0.947	0.001	3.207E-3	3.613E-3	1.151E-3
[0.45, 0.90]	[1.0, 1.25]	1.103	0.001	4.783E-3	3.242E-3	1.509E-3
[0.45, 0.90]	[1.25, 1.5]	1.353	0.001	3.035E-3	5.590E-3	2.154E-3
[0.45, 0.90]	[1.5, 2.0]	1.666	0.001	-1.038E-2	8.354E-3	3.563E-3
[0.45, 0.90]	[2.0, 2.5]	2.169	0.004	3.607E-2	2.430E-2	1.512E-2
[0.45, 0.90]	[2.5, 4.0]	2.759	0.010	5.091E-2	6.288E-2	2.775E-2
[0.9, 2.4]	[0.7, 0.75]	0.724	0.000	-4.735E-5	2.449E-3	7.615E-4
[0.9, 2.4]	[0.75, 0.80]	0.774	0.000	2.568E-3	2.775E-3	8.908E-4
[0.9, 2.4]	[0.8, 0.9]	0.846	0.000	-4.196E-3	2.372E-3	9.146E-4
[0.9, 2.4]	[0.9, 1.0]	0.945	0.001	2.946E-3	3.106E-3	1.628E-3
[0.9, 2.4]	[1.0, 1.25]	1.096	0.001	-2.381E-4	3.116E-3	1.594E-3
[0.9, 2.4]	[1.25, 1.5]	1.347	0.001	1.255E-2	6.340E-3	2.457E-3
[0.9, 2.4]	[1.5, 2.0]	1.652	0.002	-1.656E-2	1.111E-2	3.647E-3
[0.9, 2.4]	[2.0, 2.5]	2.156	0.006	-4.897E-2	4.029E-2	1.458E-2
[0.9, 2.4]	[2.5, 4.0]	2.722	0.020	-1.545E-1	1.289E-1	5.199E-2

Table C.4: Values of A_{LL}^p

(a) the positive hadron

η_{CMS}	p_T (GeV/c)	$\langle p_T \rangle$	$\sigma_{(p_T)}$	A_{LL}	$A_{LL}^{\text{stat.}}$	$A_{LL}^{\text{syst.}}$
[-0.1, 0.45]	[0.7, 0.75]	0.725	0.001	6.088E-3	6.925E-3	2.808E-3
[-0.1, 0.45]	[0.75, 0.80]	0.775	0.001	-3.013E-3	7.198E-3	4.358E-3
[-0.1, 0.45]	[0.8, 0.9]	0.848	0.001	-1.614E-3	5.504E-3	2.279E-3
[-0.1, 0.45]	[0.9, 1.0]	0.948	0.001	-1.171E-4	6.266E-3	2.476E-3
[-0.1, 0.45]	[1.0, 1.25]	1.108	0.001	4.027E-4	5.138E-3	2.147E-3
[-0.1, 0.45]	[1.25, 1.5]	1.356	0.001	-1.445E-3	7.924E-3	4.832E-3
[-0.1, 0.45]	[1.5, 2.0]	1.678	0.001	8.127E-3	1.046E-2	4.058E-3
[-0.1, 0.45]	[2.0, 2.5]	2.180	0.003	2.591E-2	2.564E-2	1.043E-2
[-0.1, 0.45]	[2.5, 4.0]	2.798	0.006	1.034E-2	5.485E-2	2.333E-2
[0.45, 0.90]	[0.7, 0.75]	0.724	0.001	8.994E-4	5.423E-3	2.290E-3
[0.45, 0.90]	[0.75, 0.80]	0.774	0.001	4.627E-3	5.847E-3	2.420E-3
[0.45, 0.90]	[0.8, 0.9]	0.847	0.001	1.511E-2	4.671E-3	2.176E-3
[0.45, 0.90]	[0.9, 1.0]	0.947	0.001	2.494E-3	5.561E-3	2.593E-3
[0.45, 0.90]	[1.0, 1.25]	1.104	0.001	1.245E-2	4.864E-3	2.620E-3
[0.45, 0.90]	[1.25, 1.5]	1.354	0.001	1.184E-2	8.152E-3	3.867E-3
[0.45, 0.90]	[1.5, 2.0]	1.670	0.001	-1.805E-3	1.174E-2	4.581E-3
[0.45, 0.90]	[2.0, 2.5]	2.174	0.004	-3.888E-3	3.188E-2	1.324E-2
[0.45, 0.90]	[2.5, 4.0]	2.793	0.008	7.887E-2	7.236E-2	3.289E-2
[0.9, 2.4]	[0.7, 0.75]	0.724	0.000	7.561E-3	3.782E-3	1.655E-3
[0.9, 2.4]	[0.75, 0.80]	0.774	0.001	1.190E-2	4.238E-3	3.409E-3
[0.9, 2.4]	[0.8, 0.9]	0.846	0.000	7.006E-3	3.555E-3	2.887E-3
[0.9, 2.4]	[0.9, 1.0]	0.946	0.001	5.491E-3	4.532E-3	4.058E-3
[0.9, 2.4]	[1.0, 1.25]	1.098	0.001	1.267E-2	4.383E-3	3.041E-3
[0.9, 2.4]	[1.25, 1.5]	1.349	0.001	1.394E-2	8.514E-3	4.100E-3
[0.9, 2.4]	[1.5, 2.0]	1.657	0.002	3.730E-2	1.413E-2	6.990E-3
[0.9, 2.4]	[2.0, 2.5]	2.164	0.005	1.118E-1	4.573E-2	2.025E-2
[0.9, 2.4]	[2.5, 4.0]	2.746	0.014	1.111E-1	1.273E-1	8.046E-2

(b) the negative hadron

η_{CMS}	p_T (GeV/c)	$\langle p_T \rangle$	$\sigma_{(p_T)}$	A_{LL}	$A_{LL}^{\text{stat.}}$	$A_{LL}^{\text{syst.}}$
[-0.1, 0.45]	[0.7, 0.75]	0.725	0.001	4.424E-3	7.443E-3	2.999E-3
[-0.1, 0.45]	[0.75, 0.80]	0.775	0.001	9.688E-3	7.724E-3	3.858E-3
[-0.1, 0.45]	[0.8, 0.9]	0.848	0.001	2.911E-3	5.904E-3	3.102E-3
[-0.1, 0.45]	[0.9, 1.0]	0.948	0.001	5.892E-3	6.725E-3	5.649E-3
[-0.1, 0.45]	[1.0, 1.25]	1.108	0.001	2.478E-3	5.521E-3	2.216E-3
[-0.1, 0.45]	[1.25, 1.5]	1.357	0.001	4.521E-3	8.520E-3	3.671E-3
[-0.1, 0.45]	[1.5, 2.0]	1.678	0.001	1.702E-3	1.128E-2	4.849E-3
[-0.1, 0.45]	[2.0, 2.5]	2.179	0.003	2.063E-2	2.774E-2	2.765E-2
[-0.1, 0.45]	[2.5, 4.0]	2.798	0.007	-3.379E-2	5.888E-2	3.415E-2
[0.45, 0.90]	[0.7, 0.75]	0.724	0.001	1.562E-3	5.820E-3	4.312E-3
[0.45, 0.90]	[0.75, 0.80]	0.774	0.001	2.300E-3	6.247E-3	2.787E-3
[0.45, 0.90]	[0.8, 0.9]	0.847	0.001	1.069E-3	4.981E-3	2.095E-3
[0.45, 0.90]	[0.9, 1.0]	0.947	0.001	-1.570E-3	5.966E-3	2.695E-3
[0.45, 0.90]	[1.0, 1.25]	1.104	0.001	6.095E-4	5.234E-3	3.066E-3
[0.45, 0.90]	[1.25, 1.5]	1.354	0.001	-1.215E-2	8.739E-3	6.100E-3
[0.45, 0.90]	[1.5, 2.0]	1.671	0.001	1.472E-2	1.247E-2	5.559E-3
[0.45, 0.90]	[2.0, 2.5]	2.175	0.004	-2.765E-3	3.361E-2	1.513E-2
[0.45, 0.90]	[2.5, 4.0]	2.792	0.009	2.702E-2	7.682E-2	3.156E-2
[0.9, 2.4]	[0.7, 0.75]	0.724	0.000	4.256E-3	3.994E-3	1.668E-3
[0.9, 2.4]	[0.75, 0.80]	0.774	0.001	1.089E-3	4.487E-3	1.756E-3
[0.9, 2.4]	[0.8, 0.9]	0.846	0.000	1.367E-2	3.790E-3	2.086E-3
[0.9, 2.4]	[0.9, 1.0]	0.946	0.001	2.450E-3	4.870E-3	2.473E-3
[0.9, 2.4]	[1.0, 1.25]	1.098	0.001	2.627E-3	4.727E-3	1.903E-3
[0.9, 2.4]	[1.25, 1.5]	1.349	0.001	-6.063E-3	9.144E-3	4.132E-3
[0.9, 2.4]	[1.5, 2.0]	1.659	0.002	7.025E-3	1.505E-2	9.281E-3
[0.9, 2.4]	[2.0, 2.5]	2.164	0.005	-5.507E-2	4.824E-2	2.699E-2
[0.9, 2.4]	[2.5, 4.0]	2.743	0.015	-1.176E-1	1.329E-1	9.872E-2

C.2. Plots

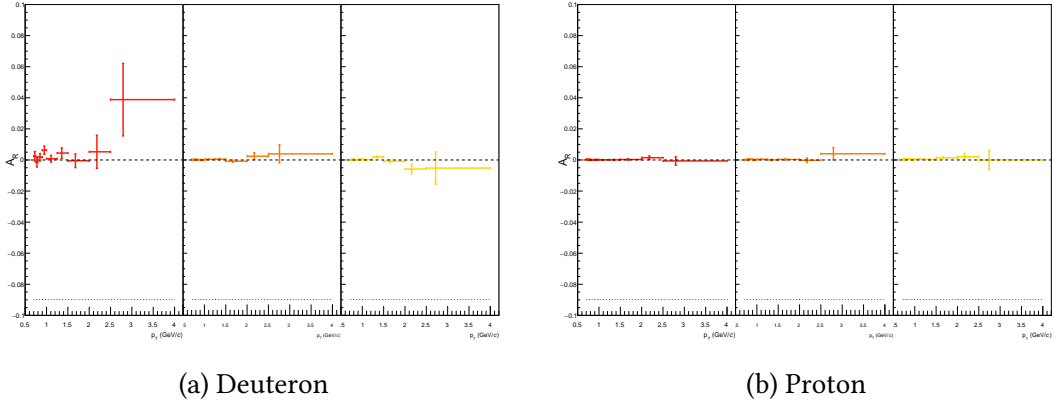


Figure C.1: A_R for deuteron and proton targets. From left to right, A_R is split into η : $[-0.1, 0.45]$, $[0.45, 0.9]$, and $[0.9, 2.4]$.

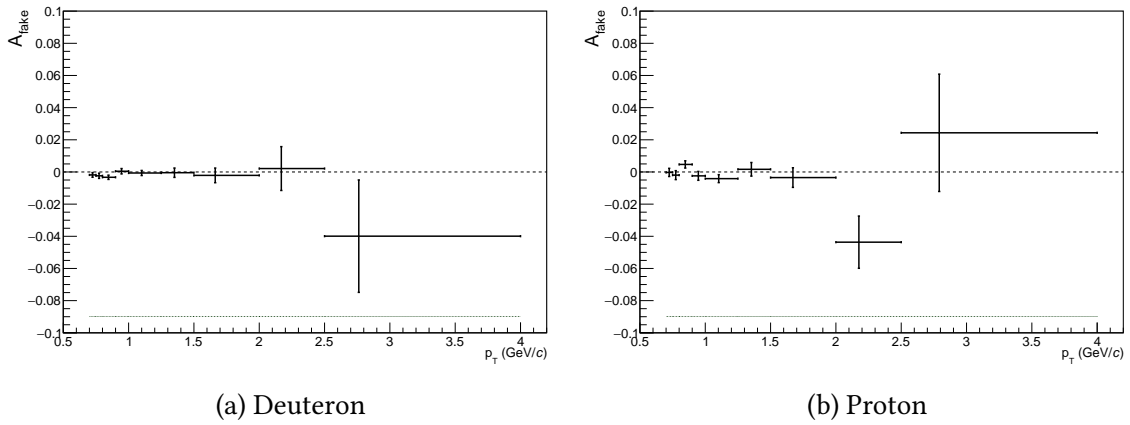
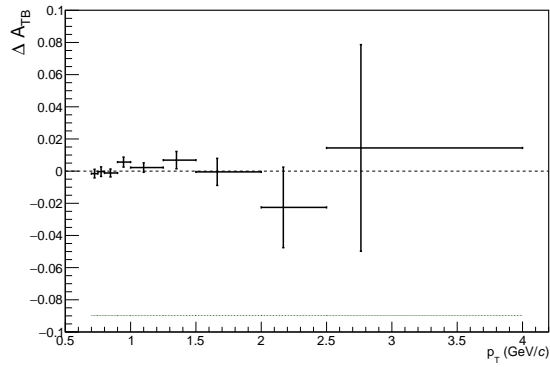
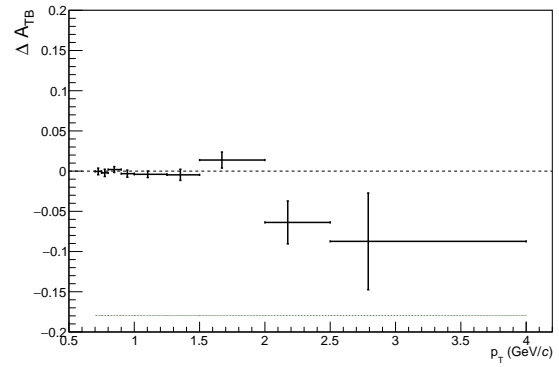


Figure C.2: Fake configuration asymmetries for deuteron and proton. Almost all values are consistent with zero. Few outliers are taken into account as *pull*.

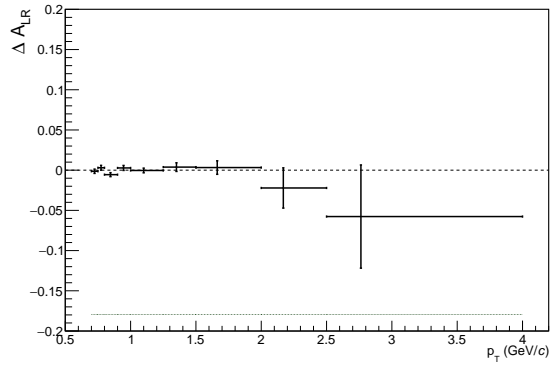


(a) Deuteron

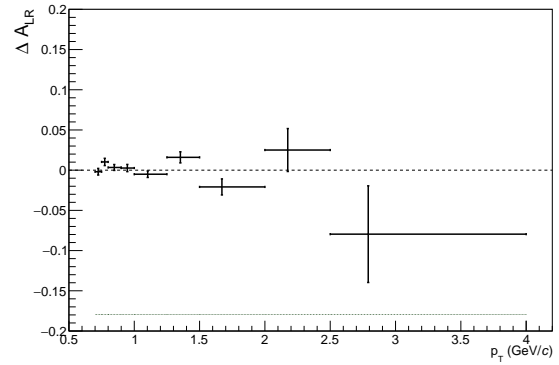


(b) Proton

Figure C.3: Top-Bottom asymmetries for the deuteron and the proton. Almost all values are consistent with zero.

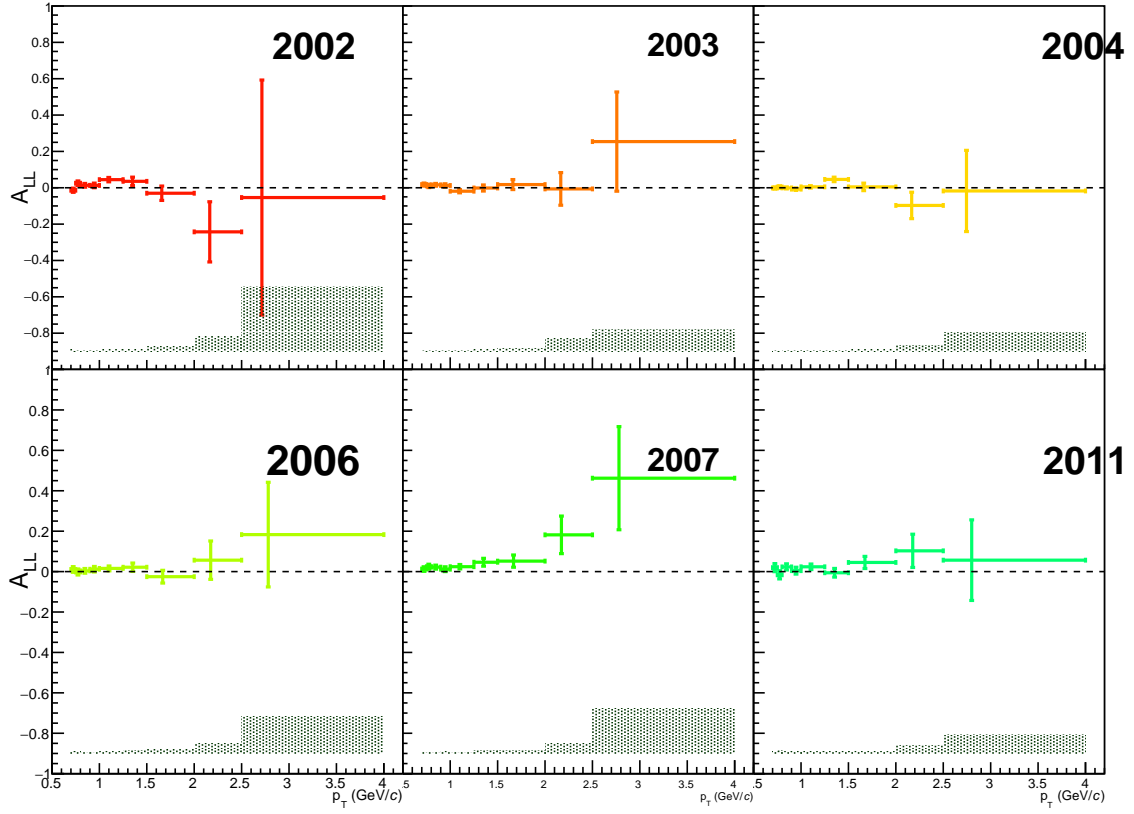


(a) Deuteron

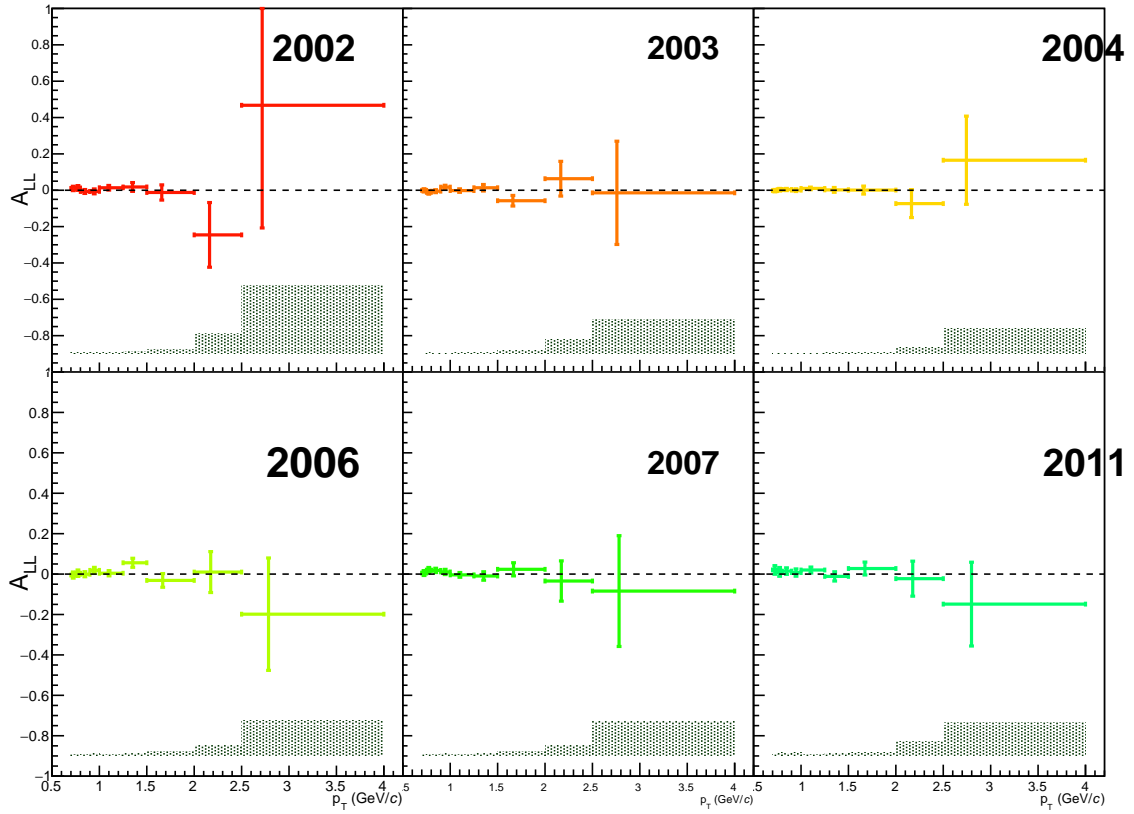


(b) Proton

Figure C.4: Left-Right asymmetries for the deuteron and the proton. Almost all values are consistent with zero.

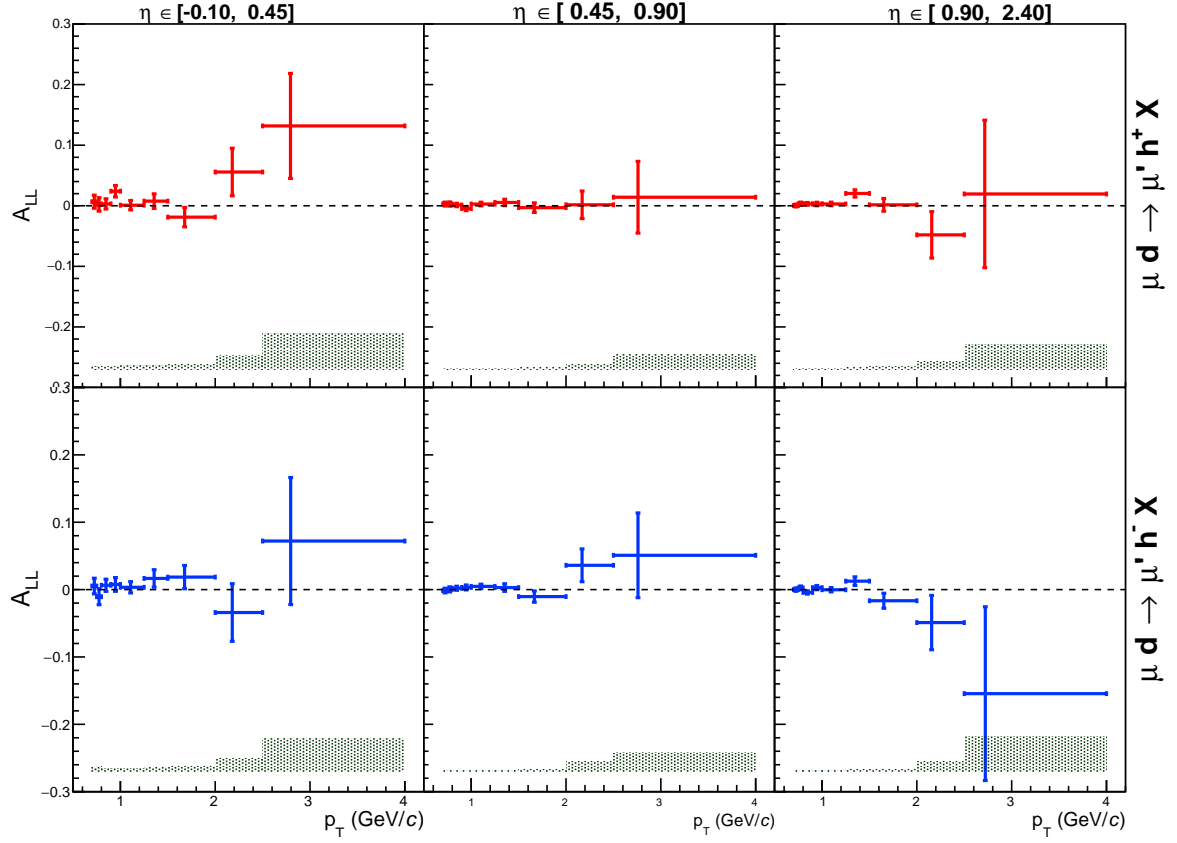


(a) The positive hadron

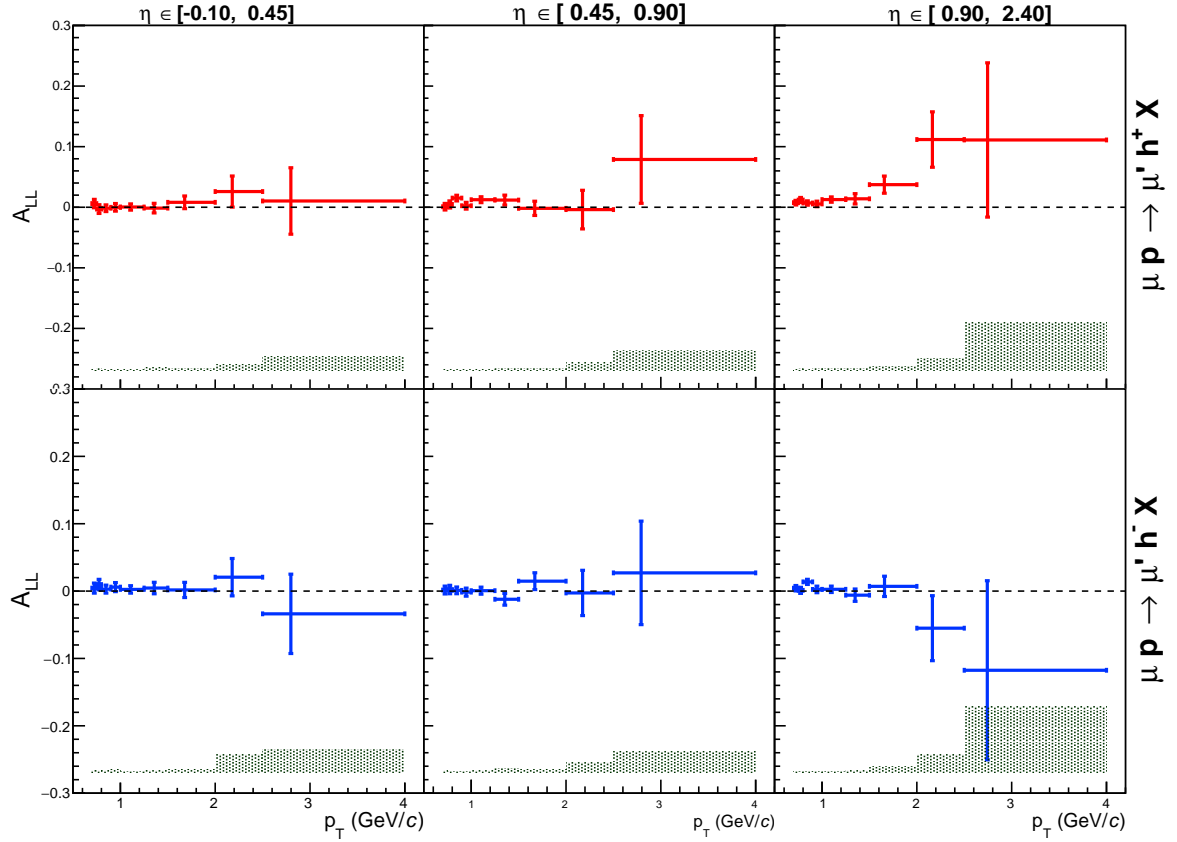


(b) The negative hadron

Figure C.5: Asymmetries for the positive and negative hadron in each year, integrated over the rapidity bin.



(a) Deuteron



(b) Proton

Figure C.6: Asymmetries for deuteron and proton.

Bibliography

- [1] J. D. Bjorken, Asymptotic Sum Rules at Infinite Momentum, [Phys. Rev. **179**, 1547 \(1969\)](#).
cited in 1 and 3.
- [2] J. Cole, *High Energy Collisions: Third International Conference at Stony Brook, N.Y.* (G + B Science Publishers, 1969), [ISBN: 978-067-713-950-0](#).
cited in 1.
- [3] M. Gell-Mann, A Schematic Model of Baryons and Mesons, [Phys. Lett. **8**, 214 \(1964\)](#).
cited in 1.
- [4] G. Zweig, An SU_3 Model for Strong Interaction Symmetry and Its Breaking, in [DEVELOPMENTS IN THE QUARK THEORY OF HADRONS](#), edited by D. Lichtenberg and S. P. Rosen Vol. 1, pp. 22–101, CERN, 1964.
cited in 1.
- [5] European Muon Collaboration, J. Ashman *et al.*, A Measurement of the Spin Asymmetry and Determination of the Structure Function g_1 in Deep Inelastic Muon-Proton Scattering, [Phys. Lett. **B206**, 364 \(1988\)](#).
cited in 1.
- [6] European Muon Collaboration, J. Ashman *et al.*, An Investigation of the Spin Structure of the Proton in Deep Inelastic Scattering of Polarized Muons on Polarized Protons, [Nucl. Phys. **B328**, 1 \(1989\)](#).
cited in 1.
- [7] S. D. Bass, *The Spin Structure of the Proton*, 1 ed. (World Scientific, 2008), [ISBN: 978-981-270-947-9](#).
cited in 1, 6, and 14.
- [8] C. A. Aidala *et al.*, The Spin Structure of the Nucleon, [Rev. Mod. Phys. **85**, 655 \(2013\)](#).
cited in 1.
- [9] E. Leader and C. Lorcé, The Angular Momentum Controversy: What's It All About and Does It Matter?, [Phys. Rept. **541**, 163 \(2014\)](#).
cited in 1 and 2.
- [10] G. Altarelli and G. Ross, The Anomalous Gluon Contribution to Polarized Leptoproduction, [Phys. Lett. **B212**, 391 \(1988\)](#).
cited in 1 and 33.
- [11] D. De Florian *et al.*, Evidence for Polarization of Gluons in the Proton, [Phys. Rev. Lett. **113**, 012001 \(2014\)](#).
cited in 1 and 89.
- [12] R. L. Jaffe and A. Manohar, The g_1 Problem: Deep Inelastic Electron Scattering and the Spin of the Proton, [Nucl. Phys. **B337**, 509 \(1990\)](#).
cited in 1.

- [13] X. Ji, Gauge-Invariant Decomposition of Nucleon Spin, [Phys. Rev. Lett.](#) **78**, 610 (1997).
cited in 1.
- [14] 若松正志, 原子核研究 Vol.60 No.1, [原子核研究](#) **60**, 139 (2015).
cited in 2.
- [15] COMPASS Collaboration, P. Abbon *et al.*, The COMPASS Experiment at CERN, [Nucl. Instrum. Meth.](#) **A577**, 455 (2007).
cited in 2, 36, 42, 43, 44, 45, 45, 45, 46, 47, 50, 51, 52, 53, 54, 58, 60, 61, 62, and 63.
- [16] COMPASS Collaboration, E. S. Ageev *et al.*, Gluon Polarization in the Nucleon from Quasi-real Photoproduction of High- p_T Hadron Pairs, [Phys. Lett.](#) **B633**, 25 (2006).
cited in 2, 27, and 70.
- [17] COMPASS Collaboration, C. Adolph *et al.*, Leading Order Determination of the Gluon Polarisation from DIS Events with High- p_T Hadron Pairs, [Phys. Lett.](#) **B718**, 922 (2013).
cited in 2 and 29.
- [18] COMPASS Collaboration, M. Alekseev *et al.*, Gluon Polarisation in the Nucleon and Longitudinal Double Spin Asymmetries from Open Charm Muoproduction, [Phys. Lett.](#) **B676**, 31 (2009).
cited in 2 and 70.
- [19] COMPASS Collaboration, C. Adolph *et al.*, Leading and Next-to-leading Order Gluon Polarization in the Nucleon and Longitudinal Double Spin Asymmetries from Open Charm Muoproduction, [Phys. Rev.](#) **D87**, 052018 (2013).
cited in 2, 26, 28, 29, and 70.
- [20] S. Procureur, *Determination de la Polarisation des Gluons dans le Nucléon par la Production de Hadrons à Grande Impulsion Transverse à COMPASS*, [PhD thesis](#), Université Paris-Sud, 2006.
cited in 2.
- [21] R. Kuhn, *A Measurement of Spin Asymmetries in Quasi-Real Photo-Production of Hadrons with High Transverse Momentum at COMPASS*, [PhD thesis](#), Technische Universität München, 2007.
cited in 2.
- [22] C. Höppner, *First Measurement of the Cross Section for the Production of Hadrons with High Transverse Momenta at COMPASS and Developments for Particle Tracking in High-Rate Experiments*, [PhD thesis](#), Technische Universität München, 2012.
cited in 2.
- [23] COMPASS Collaboration, C. Adolph *et al.*, Measurement of the Cross Section for High- p_T Hadron Production in the Scattering of 160-GeV/ c Muons off Nucleons, [Phys. Rev.](#) **D88**, 091101 (2013).
cited in 2, 23, and 70.
- [24] G. Mallot, *The Spin from Structure of the Nucleon*, [Hab. thesis](#), Johannes Gutenberg-Universität in Mainz, 1996.
cited in 5.

- [25] L. N. Hand, Experimental Investigation of Pion Electroproduction, [Phys. Rev. **129**, 1834 \(1963\)](#).
cited in 6.
- [26] A. V. Manohar, An Introduction to Spin Dependent Deep Inelastic Scattering, in *Lake Louise Winter Institute: Symmetry and Spin in the Standard Model Lake Louise, Alberta, Canada, February 23-29, 1992, 1992*, [arXiv:hep-ph/9204208](#).
cited in 6.
- [27] 熊野俊三, *KEK 物理学シリーズ 2 原子核物理学*, 1 版 (共立出版, 2015), ISBN: 978-4-320-03485-3.
cited in 6.
- [28] Spin Muon Collaboration, D. Adams *et al.*, Spin Asymmetry in Muon-proton Deep Inelastic Scattering on a Transversely Polarized Target, [Phys. Lett. **B336**, 125 \(1994\)](#).
cited in 8.
- [29] E143 Collaboration, K. Abe *et al.*, Measurements of the Proton and Deuteron Spin Structure Functions g_1 and g_2 , [Phys. Rev. **D58**, 112003 \(1998\)](#).
cited in 8.
- [30] K. A. Olive *et al.*, Review of Particle Physics, [Chin. Phys. **C38**, 090001 \(2014\)](#).
cited in 9, 9, and .
- [31] COMPASS Collaboration, E. S. Ageev *et al.*, Spin Asymmetry A_1^d and the Spin-dependent Structure Function g_1^d of the Deuteron at Low Values of x and Q^2 , [Phys. Lett. **B647**, 330 \(2007\)](#).
cited in 10.
- [32] COMPASS Collaboration, M. G. Alekseev *et al.*, The Spin-dependent Structure Function of the Proton g_1^p and a Test of the Bjorken Sum Rule, [Phys. Lett. **B690**, 466 \(2010\)](#).
cited in 10 and 89.
- [33] COMPASS Collaboration, C. Adolph *et al.*, The Spin Structure Function g_1^p of the Proton and a Test of the Bjorken Sum Rule, [Phys. Lett. **B753**, 18 \(2016\)](#).
cited in 10, 11, 12, and .
- [34] COMPASS Collaboration, V. Yu. Alexakhin *et al.*, The Deuteron Spin-dependent Structure Function g_1^d and its First Moment, [Phys. Lett. **B647**, 8 \(2007\)](#).
cited in 11.
- [35] V. Andrieux, *Polarisation of Quarks and Gluons Inside the Nucleon*, [PhD thesis](#), Université Paris-Sud, 2014.
cited in 12, 35, and 60.
- [36] G. Altarelli and G. Parisi, Asymptotic Freedom in Parton Language, [Nucl. Phys. **B126**, 298 \(1977\)](#).
cited in 10.
- [37] G. Altarelli, Partons in Quantum Chromodynamics, [Phys. Rept. **81**, 1 \(1982\)](#).
cited in 10.

- [38] V. Gribov and L. Lipatov, Deep Inelastic ep Scattering in Perturbation Theory, *Sov.J.Nucl.Phys.* **15**, 438 (1972).
cited in 10.
- [39] Y. L. Dokshitzer, Calculation of the Structure Functions for Deep Inelastic Scattering and e^+e^- Annihilation by Perturbation Theory in Quantum Chromodynamics., *Sov.Phys.JETP* **46**, 641 (1977).
cited in 10.
- [40] J. R. Ellis and R. L. Jaffe, A Sum Rule for Deep Inelastic Electroproduction from Polarized Protons, *Phys. Rev.* **D9**, 1444 (1974), [Erratum: *Phys. Rev.***D10**,1669(1974)].
cited in 14.
- [41] S. A. Larin *et al.*, The α_s^3 Approximation of Quantum Chromodynamics to the Ellis-Jaffe Sum Rule, *Phys. Lett.* **B404**, 153 (1997).
cited in 15.
- [42] W. A. Bardeen *et al.*, Deep-inelastic Scattering Beyond the Leading Order in Asymptotically Free Gauge Theories, *Phys. Rev.* **D18**, 3998 (1978).
cited in 15.
- [43] COMPASS Collaboration, M. G. Alekseev *et al.*, Quark Helicity Distributions from Longitudinal Spin Asymmetries in Muon-proton and Muon-deuteron Scattering, *Phys. Lett.* **B693**, 227 (2010).
cited in 15 and 89.
- [44] D. de Florian *et al.*, Parton-to-pion Fragmentation Reloaded, *Phys. Rev.* **D91**, 014035 (2015).
cited in 16 and 89.
- [45] B. Jäger *et al.*, Longitudinally Polarized Photoproduction of Inclusive Hadrons at Fixed-target Experiments, *Eur. Phys. J.* **C44**, 533 (2005).
cited in 16, 19, 19, 71, and 89.
- [46] COMPASS Collaboration, C. Adolph *et al.*, Longitudinal Double Spin Asymmetries in Single Hadron Quasi-real Photoproduction at High p_T , *Phys. Lett.* **B753**, 573 (2016).
cited in 17 and 89.
- [47] A. Bravar *et al.*, Large Gluon Polarization from Correlated High- p_T Hadron Pairs in Polarized Electro-production, *Phys. Lett.* **B421**, 349 (1998).
cited in 18.
- [48] D. de Florian and S. Frixione, Jet Cross Sections in Polarized Photon-hadron Collisions, *Phys. Lett.* **B457**, 236 (1999).
cited in 19 and 20.
- [49] D. de Florian *et al.*, Soft-gluon Resummation for High- p_T Inclusive-hadron Production at COMPASS, *Phys. Rev.* **D88**, 014024 (2013).
cited in 19, 23, and 24.

- [50] D. de Florian and W. Vogelsang, Threshold Resummation for the Inclusive-hadron Cross Section in pp Collisions, *Phys. Rev.* **D71**, 114004 (2005).
cited in 19.
- [51] L. G. Almeida *et al.*, Threshold Resummation for Dihadron Production in Hadronic Collisions, *Phys. Rev.* **D80**, 074016 (2009).
cited in 19.
- [52] W. K. Tung *et al.*, Heavy Quark Mass Effects in Deep Inelastic Scattering and Global QCD Analysis, *JHEP* **02**, 053 (2007).
cited in 23.
- [53] M. Glück *et al.*, Radiatively Generated Parton Distributions of Real and Virtual Photons, *Phys. Rev. D* **60**, 054019 (1999), [Erratum: *Phys. Rev. D* **62**, 019902(2000)].
cited in 23 and 89.
- [54] D. de Florian *et al.*, Global Analysis of Fragmentation Functions for Pions and Kaons and Their Uncertainties, *Phys. Rev. D* **75**, 114010 (2007).
cited in 23.
- [55] A. Bravar *et al.*, POLDIS: A Monte Carlo for POLarized (semi-inclusive) Deep Inelastic Scattering, *Comput. Phys. Commun.* **105**, 42 (1997).
cited in 25.
- [56] C. Franco, *Measurement of the Gluon Polarisation from Open-charm Production at COMPASS*, *PhD thesis*, Universidade de Lisboa, 2011.
cited in 25 and 26.
- [57] S. Koblitz, *Determination of the Gluon Polarisation from Open Charm Production at COMPASS*, *PhD thesis*, Johannes Gutenberg-Universität Mainz, 2008.
cited in 26.
- [58] L. Silva, *Measurement of The Gluon Polarisation Through High p_T Hadron Production in COMPASS*, *PhD thesis*, Universidade de Lisboa, 2011.
cited in 28.
- [59] COMPASS Collaboration, M. Stolarski, A New LO Extraction of Gluon Polarisation from COMPASS DIS Data, in *22nd International Workshop on Deep-Inelastic Scattering and Related Subjects (DIS2014)*, p. 211, 2014.
cited in 28 and 29.
- [60] COMPASS Collaboration, C. Adolph *et al.*, Leading-order Determination of the Gluon Polarisation Using a Novel Method, [arXiv:1512.05053](https://arxiv.org/abs/1512.05053).
cited in 28.
- [61] Spin Muon Collaboration, B. Adeva *et al.*, Spin Asymmetries for Events with High p_T Hadrons in DIS and an Evaluation of the Gluon Polarization, *Phys. Rev. D* **70**, 012002 (2004).
cited in 29.

- [62] HERMES Collaboration, A. Airapetian *et al.*, Leading-order Determination of the Gluon Polarization from High-pT Hadron Electroproduction, [JHEP **08**, 130 \(2010\)](#).
cited in 29.
- [63] M. Harrison *et al.*, RHIC Project Overview, [Nucl. Instrum. Meth. **A499**, 235 \(2003\)](#).
cited in 30.
- [64] STAR Collaboration, K. H. Ackermann *et al.*, STAR Detector Overview, [Nucl. Instrum. Meth. **A499**, 624 \(2003\)](#).
cited in 30.
- [65] PHENIX Collaboration, K. Adcox *et al.*, PHENIX Detector Overview, [Nucl. Instrum. Meth. **A499**, 469 \(2003\)](#).
cited in 30.
- [66] K. Klimaszewski, *Determination of Gluon Polarisation in the Nucleon from Events with High-p_T Hadron Pairs in COMPASS Experiment*, [PhD thesis](#), Instytut Problemów Jądrowych im. Andrzeja Sołtana (Narodowe Centrum Badań Jądrowych), 2010.
cited in 30.
- [67] S. R. Mane *et al.*, Siberian Snakes in High-energy Accelerators, [J. Phys. **G31**, R151 \(2005\)](#).
cited in 30.
- [68] PHENIX Collaboration, A. Adare *et al.*, Inclusive Double-helicity Asymmetries in Neutral-pion and Eta-meson Production in $\vec{p} + \vec{p}$ Collisions at $\sqrt{s} = 200$ GeV, [Phys. Rev. **D90**, 012007 \(2014\)](#).
cited in 31, 32, 89, and 95.
- [69] STAR Collaboration, L. Adamczyk *et al.*, Precision Measurement of the Longitudinal Double-spin Asymmetry for Inclusive Jet Production in Polarized Proton Collisions at $\sqrt{s} = 200$ GeV, [Phys. Rev. Lett. **115**, 092002 \(2015\)](#).
cited in 31, 32, and 95.
- [70] COMPASS Collaboration, P. Abbon *et al.*, The COMPASS Setup for Physics with Hadron Beams, [Nucl. Instrum. Meth. **A779**, 69 \(2015\)](#).
cited in 33, 36, 37, 37, 43, 49, 50, 56, 56, 57, 61, 71, and .
- [71] COMPASS Collaboration, G. Baum *et al.*, COMPASS: A Proposal for a Common Muon and Proton Apparatus for Structure and Spectroscopy, [CERN-SPSLC-96-14. SPSLC-P-297 \(1996\)](#).
cited in 33.
- [72] COMPASS Collaboration, F. Gautheron *et al.*, COMPASS-II Proposal, [CERN-SPSC-2010-014 SPSC-P-340 \(2010\)](#).
cited in 34.
- [73] N. Doble *et al.*, The Upgraded Muon Beam at the SPS, [Nucl. Instrum. Meth. **A343**, 351 \(1994\)](#).
cited in 35 and 85.

- [74] C. Bovet *et al.*, *The CEDAR Counters for Particle Identification in the SPS Secondary Beams: a Description and an Operation Manual* (CERN, Geneva, 1982), [doi:10.5170/CERN-1982-013](https://doi.org/10.5170/CERN-1982-013).
cited in 37.
- [75] A. Abragam, The Principles of Nuclear Magnetism, *Am. J. Phys.* **29**, 860 (1961).
cited in 38.
- [76] N. Doshita *et al.*, Performance of the COMPASS Polarized Target Dilution Refrigerator, *Nucl. Instrum. Meth.* **A526**, 138 (2004).
cited in 38.
- [77] A. Dael *et al.*, A Superconducting 2.5 T High Accuracy Solenoid and a Large 0.5 T Dipole Magnet for the SMC Target, *IEEE Trans. Magnetics* **28**, 560 (1992).
cited in 39.
- [78] J. Balla *et al.*, On the Large COMPASS Polarized Deuteron Target, *Czech. J. Phys.* **56**, F295 (2006).
cited in 39.
- [79] J. Ball *et al.*, First Results of the Large COMPASS ^6LiD Polarized Target, *Nucl. Instrum. Meth.* **A498**, 101 (2003).
cited in 40.
- [80] J. Koivuniemi *et al.*, Polarization of the Large COMPASS $^{14}\text{NH}_3$ Target, *Journal of Physics: Conference Series* **150**, 012023 (2009).
cited in 40.
- [81] K. Kondo *et al.*, Polarization Measurement in the COMPASS Polarized Target, *Nucl. Instrum. Meth.* **A526**, 70 (2004).
cited in 41, 41, and 85.
- [82] S. Horikawa *et al.*, Development of a Scintillating-fibre Detector with Position-sensitive Photomultipliers for High-rate Experiments, *Nucl. Instrum. Meth.* **A516**, 34 (2004).
cited in 44.
- [83] M. J. French *et al.*, Design and Results from the APV25, a Deep Sub-micron CMOS Front-end Chip for the CMS Tracker, *Nucl. Instrum. Meth.* **A466**, 359 (2001).
cited in 45.
- [84] H. Angerer *et al.*, Present Status of Silicon Detectors in COMPASS, *Nucl. Instrum. Meth.* **A512**, 229 (2003).
cited in 45.
- [85] D. Thers *et al.*, Micromegas as a Large Microstrip Detector for the COMPASS experiment, *Nucl. Instrum. Meth.* **A469**, 133 (2001).
cited in 45.
- [86] F. Kunne *et al.*, The Gaseous Microstrip Detector Micromegas for the COMPASS Experiment at CERN, *Nucl. Phys.* **A721**, 1087 (2003).
cited in 45.

- [87] C. Bernet *et al.*, The $40 \times 40 \text{ cm}^2$ Gaseous Microstrip Detector Micromegas for the High-luminosity COMPASS Experiment at CERN, [Nucl. Instrum. Meth. A536](#), 61 (2005).
cited in 45.
- [88] F. Sauli, GEM: A New Concept for Electron Amplification in Gas Detectors, [Nucl. Instrum. Meth. A386](#), 531 (1997).
cited in 45.
- [89] V. Bychkov *et al.*, The Large Size Straw Drift Chambers of the COMPASS Experiment, [Nucl. Instrum. Meth. A556](#), 66 (2006).
cited in 47 and 48.
- [90] K. Platzter *et al.*, Mapping the Large Area Straw Detectors of the COMPASS Experiment with X-rays, [IEEE Trans. Nucl. Sci. 52](#), 793 (2005).
cited in 48.
- [91] E. Albrecht *et al.*, Status and Characterisation of COMPASS RICH-1, [Nucl. Instrum. Meth. A553](#), 215 (2005).
cited in 49.
- [92] S. Beole *et al.*, Technical Design Report of the High Momentum Particle Identification Detector, [CERN/LHCC 98-19](#) (1998).
cited in 49.
- [93] E. Albrecht *et al.*, The Mirror System of COMPASS RICH-1, [Nucl. Instrum. Meth. A502](#), 236 (2003).
cited in 49.
- [94] P. Abbon *et al.*, Fast Readout of the COMPASS RICH CsI-MWPC Photon Chambers, [Nucl. Instrum. Meth. A567](#), 104 (2006).
cited in 51.
- [95] P. Abbon *et al.*, Fast Photon Detection for Particle Identification with COMPASS RICH-1, [Nucl. Instrum. Meth. A580](#), 906 (2007).
cited in 51.
- [96] P. Abbon *et al.*, Design and Construction of the Fast Photon Detection System for COMPASS RICH-1, [Nucl. Instrum. Meth. A616](#), 21 (2010).
cited in 51 and 52.
- [97] E. Iarocci, Plastic Streamer Tubes and Their Applications in High Energy Physics, [Nucl. Instrum. Meth. 217](#), 30 (1983).
cited in 51.
- [98] W. Busza, Experience with Iarocci Tubes Produced on a Large Scale, [Nucl. Instrum. Meth. A265](#), 210 (1988).
cited in 51.
- [99] DØ Collaboration, C. Brown *et al.*, DØ Muon System with Proportional Drift Tube Chambers, [Nucl. Instrum. Meth. A279](#), 331 (1989).
cited in 53.

- [100] J.-P. Stroot, GAMS at IHEP and at CERN, in *Meeting of the Division of Particles and Fields of the APS*, pp. 498–502, 1984, [CERN-EP/85-01](#).
cited in 54.
- [101] Serpukhov-Brussels-Annecy (LAPP) Collaboration, F. G. Binon *et al.*, Modular Hadron Calorimeter, [Nucl. Instrum. Meth. A256, 444 \(1987\)](#).
cited in 57.
- [102] IHEP - IISN - LANL - LAPP Collaboration, D. Alde *et al.*, Production of G(1590) and Other Mesons Decaying Into η Pairs by 100 GeV/c π^- on Protons, [Nucl. Phys. B269, 485 \(1986\)](#).
cited in 57.
- [103] E. van der Bij *et al.*, S-LINK, a Data Link Interface Specification for the LHC Era, [IEEE Trans. Nucl. Sci. 44, 398 \(1997\)](#).
cited in 61.
- [104] M. Lammna, Tech. report, CASTOR Name Space Analysis, 2014, [PDF document](#).
cited in 63.
- [105] COMPASS Collaboration, CORAL, [COMPASS Internal Wiki](#), accessed: 2015-02-22, access restricted.
cited in 63.
- [106] G. Baum *et al.*, RICHONE: A Software Package for the Analysis of COMPASS RICH-1 Data, [Nucl. Instrum. Meth. A502, 315 \(2003\)](#).
cited in 63.
- [107] R. Barlow, Extended Maximum Likelihood, [Nucl. Instrum. Meth. A297, 496 \(1990\)](#).
cited in 63.
- [108] P. Abbon *et al.*, Particle Identification with COMPASS RICH-1, [Nucl. Instrum. Meth. A631, 26 \(2011\)](#).
cited in 63.
- [109] CERN, The CERN Advanced STORage manager, <http://castor.web.cern.ch/>, accessed: 2015-02-17.
cited in 66.
- [110] L. Klostermann, *The Spin Dependent Structure Function g_1 of the Deuteron and the Proton*, [PhD thesis](#), Technische Universiteit Delft, 1995.
cited in 76.
- [111] O. A. Rondon, Corrections to Nucleon Spin Structure Asymmetries Measured on Nuclear Polarized Targets, [Phys. Rev. C60, 035201 \(1999\)](#).
cited in 81.
- [112] New Muon Collaboration, P. Amaudruz *et al.*, The Ratio F_2^n/F_2^p in Deep Inelastic Muon Scattering, [Nucl. Phys. B371, 3 \(1992\)](#).
cited in 81.

- [113] R. Windmolders, An Introduction to the Evaluation of Spin Structure Functions from Experimental Data, in *10th Rhodanien Seminar: The Spin in Physics Turin*, 2002, [arXiv:0211350](#).
cited in 81.
- [114] A. A. Akhundov *et al.*, Contribution of Electromagnetic Production of Lepton Pairs to Inclusive Cross-section of Deep Inelastic μp Scattering, *Sov. J. Nucl. Phys.* **32**, 234 (1980), [*Yad. Fiz.*32,452(1980)].
cited in 81.
- [115] S. Neliba *et al.*, Weight and Volume Measurement of the Large COMPASS Target, *Nucl. Instrum. Meth.* **A526**, 144 (2004).
cited in 81.
- [116] H. Shimazaki and S. Shinomoto, Kernel Bandwidth Optimization in Spike Rate Estimation, *J. Comput. Neurosci.* **29**, 171 (2010).
cited in 88 and 101.
- [117] M. Levillain, *Double Longitudinal Spin Asymmetries in Single Hadron Photoproduction at High p_T at COMPASS*, [PhD thesis](#), Université Paris-Saclay, 2015.
cited in 89, 90, and 91.
- [118] J. Pumplin *et al.*, New Generation of Parton Distributions with Uncertainties from Global QCD Analysis, *JHEP* **07**, 012 (2002).
cited in 89.
- [119] M. Glück *et al.*, Models for the Polarized Parton Distributions of the Nucleon, *Phys. Rev.* **D63**, 094005 (2001).
cited in 89.
- [120] D. de Florian *et al.*, Global Analysis of Helicity Parton Densities and their Uncertainties, *Phys. Rev. Lett.* **101**, 072001 (2008).
cited in 89.
- [121] STAR Collaboration, P. Djawotho, Gluon polarization and jet production at STAR, *Nuovo Cim.* **C036**, 35 (2013).
cited in 89.
- [122] C. Uebler *et al.*, Threshold Resummation for Polarized High- p_T Hadron Production at COMPASS, *Phys. Rev. D* **92**, 094029 (2015).
cited in 96 and 97.
- [123] P. Hinderer *et al.*, Toward NNLL Threshold Resummation for Hadron Pair Production in Hadronic Collisions, *Phys. Rev.* **D91**, 014016 (2015).
cited in 96.
- [124] PHENIX Collaboration, A. Adare *et al.*, Inclusive Cross Section and Double Helicity Asymmetry for π^0 Production in $p + p$ Collisions at $\sqrt{s} = 200$ GeV: Implications for the Polarized Gluon Distribution in the Proton, *Phys. Rev. D* **76**, 051106 (2007).

- [125] W. L. van Neerven, Review of Higher Order QCD Corrections to Structure Functions, in *Future physics with light and heavy nuclei at HERMES. Contributions to the proceedings of the '95-'96 Workshop on Future Physics at HERA, working group on light and heavy nuclei at HERA. Part 2*, 1996, [arXiv:9609243](https://arxiv.org/abs/9609243).
- [126] M. Anselmino *et al.*, The Theory and Phenomenology of Polarized Deep Inelastic Scattering, *Phys. Rept.* **261**, 1 (1995), [Erratum: *Phys. Rept.*281,399(1997)].
- [127] J. D. Bjorken, Inelastic Scattering of Polarized Leptons from Polarized Nucleons, *Physical Review D* **1**, 1376 (1970).
- [128] W. Vogelsang, A Rederivation of the Spin Dependent Next-to-leading Order Splitting Functions, *Phys. Rev.* **D54**, 2023 (1996).
- [129] D. A. Dicus, Radiative Corrections to $e^+ + e^- \rightarrow \mu^+ + \mu^+$ and Neutral Currents in Unified Gauge Theories, *Phys. Rev.* **D8**, 890 (1973), [Erratum: *Phys. Rev.*D10,1669(1974)].
- [130] COMPASS Collaboration, S. Gerassimov, PHysics Analysis Software Tools, <http://ges.home.cern.ch/ges/phast/>, accessed: 2015-02-17.
- [131] European Muon Collaboration, J. J. Aubert *et al.*, A Large Magnetic Spectrometer System for High-Energy Muon Physics, *Nucl. Instrum. Meth.* **179**, 445 (1981).
- [132] P. Hoodbhoy *et al.*, Novel Effects in Deep Inelastic Scattering from Spin-one Hadrons, *Nucl. Phys.* **B312**, 571 (1989).
- [133] E. C. Aschenauer *et al.*, Helicity Parton Distributions at a Future Electron-ion Collider: A Quantitative Appraisal, *Phys. Rev.* **D86**, 054020 (2012).
- [134] E. Bielert *et al.*, A 2.5 m Long Liquid Hydrogen Target for COMPASS, *Nucl. Instrum. Meth.* **A746**, 20 (2014).
- [135] B. Kniehl *et al.*, Fragmentation Functions for Pions, Kaons, and Protons at Next-to-leading Order, *Nucl. Phys.* **B582**, 514 (2000).
- [136] 吉澤康和, *新しい誤差論*, 5版 (共立出版, 1998), ISBN: 978-4-320-01424-4.
- [137] W. Vogelsang, The Spin-dependent Two-loop Splitting Functions, *Nucl. Phys.* **B475**, 47 (1996).
- [138] C. Bernet *et al.*, The COMPASS Trigger System for Muon Scattering, *Nucl. Instrum. Meth.* **A550**, 217 (2005).
- [139] Spin Muon Collaboration, D. Adams *et al.*, The Polarized Double Cell Target of the SMC, *Nucl. Instrum. Meth.* **A437**, 23 (1999).
- [140] ROOT TTree Class Reference, <https://root.cern.ch/doc/master/classTTree.html>, accessed: 2015-09-23.
- [141] R. Brun and F. Rademakers, ROOT: An Object Oriented Data Analysis Framework, *Nucl. Instrum. Meth.* **A389**, 81 (1997).

- [142] E. C. Aschenauer *et al.*, The RHIC Spin Program: Achievements and Future Opportunities, [arXiv:1304.0079](#).
- [143] PHENIX Collaboration, A. Adare *et al.*, Gluon-Spin Contribution to the Proton Spin from the Double-Helicity Asymmetry in Inclusive π^0 Production in Polarized $p + p$ Collisions at $\sqrt{s} = 200$ GeV, [Phys. Rev. Lett. **103**, 012003 \(2009\)](#).
- [144] M. Glück *et al.*, Photonic Parton Distributions, [Phys. Rev. D **46**, 1973 \(1992\)](#).
- [145] J. D. Bjorken, Applications of the Chiral $U(6) \otimes U(6)$ Algebra of Current Densities, [Phys. Rev. **148**, 1467 \(1966\)](#).
- [146] Y. Antipov *et al.*, Measurement of π^- -meson Polarizability in Pion Compton Effect, [Phys. Lett. **B121**, 445 \(1983\)](#).
- [147] C. G. Callan and D. J. Gross, High-energy Electroproduction and the Constitution of the Electric Current, [Phys. Rev. Lett. **22**, 156 \(1969\)](#).
- [148] European Muon Collaboration, J. Ashman *et al.*, A Measurement of the Ratio of the Nucleon Structure Function in Copper and Deuterium, [Z. Phys. **C57**, 211 \(1993\)](#).
- [149] FNAL E581/704 Collaboration, D. L. Adams *et al.*, Measurement of the Double Spin Asymmetry A_{LL} for Inclusive Multi- γ Pair Production with 200 GeV/c Polarized Proton Beam and Polarized Proton Target, [Phys. Lett. **B336**, 269 \(1994\)](#).
- [150] M. Stolarski, *Spin Structure of the Nucleon at Low x and Q^2 in the COMPASS Experiment at CERN*, [PhD thesis](#), Warsaw University, 2006.
- [151] E. C. Aschenauer *et al.*, Unveiling the Proton Spin Decomposition at a Future Electron-Ion Collider, [Phys. Rev. D **92**, 1 \(2015\)](#).
- [152] Spin Muon Collaboration, B. Adeva *et al.*, Spin Asymmetries A_1 and Structure Functions g_1 of the Proton and the Deuteron from Polarized High-energy Muon Scattering, [Phys. Rev. D **58**, 112001 \(1998\)](#).
- [153] J. Collins, *Foundation of Perturbative QCD*, 1 ed. (Cambridge University Press, 2011), [ISBN: 978-110-764-525-7](#).
- [154] NNPDF Collaboration, E. R. Nocera *et al.*, A First Unbiased Global Determination of Polarized PDFs and Their Uncertainties, [Nucl. Phys. **B887**, 276 \(2014\)](#).
- [155] E. R. Nocera, Unbiased Polarized PDFs Upgraded with New Inclusive DIS Data, in *16th Workshop on High Energy Spin Physics (DSPIN-15) Dubna, Moscow region, Russia, September 8-12, 2015*, 2015, [arXiv:1510.04248](#).
- [156] L. A. Harland-Lang *et al.*, Parton Distributions in the LHC Era: MMHT 2014 PDFs, [Eur. Phys. J. **C75**, 204 \(2015\)](#).

Acknowledgements Remerciements 謝辞

はじめに岩田高広先生に多大なる感謝を申し上げます。学部時代のアドバイザー教官からお世話になり、以来色々と躓いた時的確な助言を与えてくださいました。CERNでのCOMPASS国際共同実験に参加し貴重な経験ができたのも先生がいたからこそです。

宮地義之先生とは山形大学に着任以来、ユニークな視点からアドバイスをいつも与えて下さいました。実験や解析のためのソフトウェア設計などで有意義な議論ができその後の開発で役に立ちました。心よりの御礼厚く申し上げます。

学部、修士、そして博士課程においてCERN滞在中、堂下典弘先生、近藤薫先生には現地の生活などで色々と助けていただきました。それぞれのご家族の方々との食事に誘って頂き話弾ませたことを覚えています。また現地の事務手続きなどで難しい時交渉してくださりその後の手続きが楽に進みました事など含め、全てに対し深く感謝致します。

I would like to thank Mr. Maxime Levillain, Dr. Claude Marchand, Dr. Yann Bedfer, and CEA Saclay Irfu members for co-working this analysis. Mr. Levillain is an intelligent guy and we had fruitful discussions. When I've stayed at Saclay several months in total, Dr. Marchand had not only supported my research but also taught me the life in Paris. Je te remercie très sincèrement!

I also would like to thank all the members of the COMPASS experiment. Their friendly atmosphere greatly helps me everything. I have learned tremendous experiences how to achieve something with people having different backgrounds.

同じ研究室の吉田浩司先生、田島靖久先生には日々の生活や研究でいつもいつも気にかけて頂きました。解析や論文で煮詰まっていた時には本当に励みになりました。また佐々木未来さん、糠塚元気さん、そして後輩諸君には長い間お世話になりました。イベントや普段の生活で楽しく過ごすことができ、よい気分転換になりました。

多くの友人知人にもプライベートではお世話になりました。とりわけ大阪大学の杉山泰之氏には趣味に研究にと日々楽しく過ごすことができました。本当にありがとうございました。

最後になりましたが、両親、妹、さらに叔父・叔母には心から感謝申し上げます。のらりくらしと自分のやりたいことに対して理解して励まして下さいました。CERN滞在中に届いた日本からの品々は心の支えになりました。重ね重ねになりますが、これまで本当にありがとうございました。

また大学生活を通して苦しい時行き詰まっていた時の支えになったのはアイドルマスターシリーズでした。様々なアイドルがいる中でとりわけ水瀬伊織(C.V. 釘宮理恵)さん、島村卯月(C.V. 大橋彩香)さんの歌やキャラクターにいつもいつも励まされてきました。この場を借りて深く感謝を申し上げます。

TERMS AND CONDITIONS

Creative Commons Attribution License

Refs. [30,33,70] are available under the terms of [the Creative Commons Attribution License \(CC BY\)](#). Figures and tables taken from them are used under CC BY.

ELSEVIER LICENSE TERMS AND CONDITIONS

Feb 09, 2016

This is an Agreement between Hiroki Matsuda ("You") and Elsevier ("Elsevier"). It consists of your order details, the terms and conditions provided by Elsevier, and the payment terms and conditions.

All payments must be made in full to CCC. For payment instructions, please see information listed at the bottom of this form.

Supplier	Elsevier Limited The Boulevard, Langford Lane Kidlington, Oxford, OX5 1GB, UK
Registered Company Number	1982084
Customer name	Hiroki Matsuda
Customer address	1-4-12, Kojirakawa-machi Yamagata-shi, Yamagata-ken 990-8560
License number	3804660757572
License date	Feb 09, 2016
Licensed content publisher	Elsevier
Licensed content publication	Physics Letters B
Licensed content title	The deuteron spin-dependent structure function g_{1d} and its first moment
Licensed content author	V.Yu. Alexakhin, Yu. Alexandrov, G.D. Alexeev, M. Alexeev, A. Amoroso, B. Badelek, F. Balestra, J. Ball, J. Barth, G. Baum, M. Becker, Y. Bedfer, C. Bernet, R. Bertini, M. Bettinelli, R. Birsa, J. Bisplinghoff, P. Bordalo, F. Bradamante, A. Bressan, G. Brona, E. Burtin et al.
Licensed content date	29 March 2007
Licensed content volume number	647
Licensed content issue number	1
Number of pages	10
Start Page	8
End Page	17
Type of Use	reuse in a thesis/dissertation
Intended publisher of new work	other
Portion	figures/tables/illustrations
Number of figures/tables/illustrations	2
Format	both print and electronic
Are you the author of this Elsevier article?	No
Will you be translating?	No
Original figure numbers	figures 3, 4
Title of your thesis/dissertation	Measurement of longitudinal double spin asymmetries in the single-inclusive hadron quasi-real photoproduction at high-pT by a muon beam for the study of gluon polarisation in nucleon
Expected completion date	Feb 2016
Estimated size (number of pages)	150

Elsevier VAT number	GB 494 6272 12
Price	0 JPY
VAT/Local Sales Tax	0 JPY / 0.00 GBP
Total	0 JPY
Terms and Conditions	

INTRODUCTION

1. The publisher for this copyrighted material is Elsevier. By clicking "accept" in connection with completing this licensing transaction, you agree that the following terms and conditions apply to this transaction (along with the Billing and Payment terms and conditions established by Copyright Clearance Center, Inc. ("CCC"), at the time that you opened your Rightslink account and that are available at any time at <http://myaccount.copyright.com>).

GENERAL TERMS

2. Elsevier hereby grants you permission to reproduce the aforementioned material subject to the terms and conditions indicated.

3. Acknowledgement: If any part of the material to be used (for example, figures) has appeared in our publication with credit or acknowledgement to another source, permission must also be sought from that source. If such permission is not obtained then that material may not be included in your publication/copies. Suitable acknowledgement to the source must be made, either as a footnote or in a reference list at the end of your publication, as follows:

"Reprinted from Publication title, Vol /edition number, Author(s), Title of article / title of chapter, Pages No., Copyright (Year), with permission from Elsevier [OR APPLICABLE SOCIETY COPYRIGHT OWNER]." Also Lancet special credit - "Reprinted from The Lancet, Vol. number, Author(s), Title of article, Pages No., Copyright (Year), with permission from Elsevier."

4. Reproduction of this material is confined to the purpose and/or media for which permission is hereby given.

5. Altering/Modifying Material: Not Permitted. However figures and illustrations may be altered/adapted minimally to serve your work. Any other abbreviations, additions, deletions and/or any other alterations shall be made only with prior written authorization of Elsevier Ltd. (Please contact Elsevier at permissions@elsevier.com)

6. If the permission fee for the requested use of our material is waived in this instance, please be advised that your future requests for Elsevier materials may attract a fee.

7. Reservation of Rights: Publisher reserves all rights not specifically granted in the combination of (i) the license details provided by you and accepted in the course of this licensing transaction, (ii) these terms and conditions and (iii) CCC's Billing and Payment terms and conditions.

8. License Contingent Upon Payment: While you may exercise the rights licensed immediately upon issuance of the license at the end of the licensing process for the transaction, provided that you have disclosed complete and accurate details of your proposed use, no license is finally effective unless and until full payment is received from you (either by publisher or by CCC) as provided in CCC's Billing and Payment terms and conditions. If full payment is not received on a timely basis, then any license preliminarily granted shall be deemed automatically revoked and shall be void as if never granted. Further, in the event that you breach any of these terms and conditions or any of CCC's Billing and Payment terms and conditions, the license is automatically revoked and shall be void as if never granted. Use of materials as described in a revoked license, as well as any use of the materials beyond the scope of an unrevoked license, may constitute copyright infringement and publisher reserves the right to take any and all action to protect its copyright in the materials.

9. Warranties: Publisher makes no representations or warranties with respect to the licensed material.

10. Indemnity: You hereby indemnify and agree to hold harmless publisher and CCC, and their respective officers, directors, employees and agents, from and against any and all claims arising out of your use of the licensed material other than as specifically authorized pursuant to this license.

11. No Transfer of License: This license is personal to you and may not be sublicensed, assigned, or transferred by you to any other person without publisher's written permission.

12. No Amendment Except in Writing: This license may not be amended except in a writing signed by both parties (or, in the case of publisher, by CCC on publisher's behalf).

13. Objection to Contrary Terms: Publisher hereby objects to any terms contained in any purchase order, acknowledgment, check endorsement or other writing prepared by you, which terms are inconsistent with these terms and conditions or CCC's Billing and Payment terms and conditions. These terms and conditions, together with CCC's Billing and Payment terms and conditions (which are incorporated herein), comprise the entire agreement between you and publisher (and CCC) concerning this licensing transaction. In the event of any conflict between your obligations established by these terms and conditions and those established by CCC's Billing and Payment terms and conditions, these terms and conditions shall control.

14. Revocation: Elsevier or Copyright Clearance Center may deny the permissions described in this License at their sole discretion, for any reason or no reason, with a full refund payable to you. Notice of such denial will be made using the contact information provided by you. Failure to receive such notice will not alter or invalidate the denial. In no event will Elsevier or Copyright Clearance Center be responsible or liable for any costs, expenses or damage incurred by you as a

result of a denial of your permission request, other than a refund of the amount(s) paid by you to Elsevier and/or Copyright Clearance Center for denied permissions.

LIMITED LICENSE

The following terms and conditions apply only to specific license types:

15. **Translation:** This permission is granted for non-exclusive world **English** rights only unless your license was granted for translation rights. If you licensed translation rights you may only translate this content into the languages you requested. A professional translator must perform all translations and reproduce the content word for word preserving the integrity of the article.

16. **Posting licensed content on any Website:** The following terms and conditions apply as follows: Licensing material from an Elsevier journal: All content posted to the web site must maintain the copyright information line on the bottom of each image; A hyper-text must be included to the Homepage of the journal from which you are licensing at <http://www.sciencedirect.com/science/journal/xxxxx> or the Elsevier homepage for books at <http://www.elsevier.com>; Central Storage: This license does not include permission for a scanned version of the material to be stored in a central repository such as that provided by Heron/XanEdu.

Licensing material from an Elsevier book: A hyper-text link must be included to the Elsevier homepage at <http://www.elsevier.com>. All content posted to the web site must maintain the copyright information line on the bottom of each image.

Posting licensed content on Electronic reserve: In addition to the above the following clauses are applicable: The web site must be password-protected and made available only to bona fide students registered on a relevant course. This permission is granted for 1 year only. You may obtain a new license for future website posting.

17. **For journal authors:** the following clauses are applicable in addition to the above:

Preprints:

A preprint is an author's own write-up of research results and analysis, it has not been peer-reviewed, nor has it had any other value added to it by a publisher (such as formatting, copyright, technical enhancement etc.).

Authors can share their preprints anywhere at any time. Preprints should not be added to or enhanced in any way in order to appear more like, or to substitute for, the final versions of articles however authors can update their preprints on arXiv or RePEc with their Accepted Author Manuscript (see below).

If accepted for publication, we encourage authors to link from the preprint to their formal publication via its DOI. Millions of researchers have access to the formal publications on ScienceDirect, and so links will help users to find, access, cite and use the best available version. Please note that Cell Press, The Lancet and some society-owned have different preprint policies. Information on these policies is available on the journal homepage.

Accepted Author Manuscripts: An accepted author manuscript is the manuscript of an article that has been accepted for publication and which typically includes author-incorporated changes suggested during submission, peer review and editor-author communications.

Authors can share their accepted author manuscript:

- immediately
 - via their non-commercial person homepage or blog
 - by updating a preprint in arXiv or RePEc with the accepted manuscript
 - via their research institute or institutional repository for internal institutional uses or as part of an invitation-only research collaboration work-group
 - directly by providing copies to their students or to research collaborators for their personal use
 - for private scholarly sharing as part of an invitation-only work group on commercial sites with which Elsevier has an agreement
- after the embargo period
 - via non-commercial hosting platforms such as their institutional repository
 - via commercial sites with which Elsevier has an agreement

In all cases accepted manuscripts should:

- link to the formal publication via its DOI
- bear a CC-BY-NC-ND license - this is easy to do
- if aggregated with other manuscripts, for example in a repository or other site, be shared in alignment with our hosting policy not be added to or enhanced in any way to appear more like, or to substitute for, the published journal article.

Published journal article (JPA): A published journal article (PJA) is the definitive final record of published research that appears or will appear in the journal and embodies all value-adding publishing activities including peer review co-ordination, copy-editing, formatting, (if relevant) pagination and online enrichment.

Policies for sharing publishing journal articles differ for subscription and gold open access articles:

Subscription Articles: If you are an author, please share a link to your article rather than the full-text. Millions of

researchers have access to the formal publications on ScienceDirect, and so links will help your users to find, access, cite, and use the best available version.

Theses and dissertations which contain embedded PJAs as part of the formal submission can be posted publicly by the awarding institution with DOI links back to the formal publications on ScienceDirect.

If you are affiliated with a library that subscribes to ScienceDirect you have additional private sharing rights for others' research accessed under that agreement. This includes use for classroom teaching and internal training at the institution (including use in course packs and courseware programs), and inclusion of the article for grant funding purposes.

Gold Open Access Articles: May be shared according to the author-selected end-user license and should contain a [CrossMark logo](#), the end user license, and a DOI link to the formal publication on ScienceDirect.

Please refer to Elsevier's [posting policy](#) for further information.

18. **For book authors** the following clauses are applicable in addition to the above: Authors are permitted to place a brief summary of their work online only. You are not allowed to download and post the published electronic version of your chapter, nor may you scan the printed edition to create an electronic version. **Posting to a repository:** Authors are permitted to post a summary of their chapter only in their institution's repository.

19. **Thesis/Dissertation:** If your license is for use in a thesis/dissertation your thesis may be submitted to your institution in either print or electronic form. Should your thesis be published commercially, please reapply for permission. These requirements include permission for the Library and Archives of Canada to supply single copies, on demand, of the complete thesis and include permission for Proquest/UMI to supply single copies, on demand, of the complete thesis. Should your thesis be published commercially, please reapply for permission. Theses and dissertations which contain embedded PJAs as part of the formal submission can be posted publicly by the awarding institution with DOI links back to the formal publications on ScienceDirect.

Elsevier Open Access Terms and Conditions

You can publish open access with Elsevier in hundreds of open access journals or in nearly 2000 established subscription journals that support open access publishing. Permitted third party re-use of these open access articles is defined by the author's choice of Creative Commons user license. See our [open access license policy](#) for more information.

Terms & Conditions applicable to all Open Access articles published with Elsevier:

Any reuse of the article must not represent the author as endorsing the adaptation of the article nor should the article be modified in such a way as to damage the author's honour or reputation. If any changes have been made, such changes must be clearly indicated.

The author(s) must be appropriately credited and we ask that you include the end user license and a DOI link to the formal publication on ScienceDirect.

If any part of the material to be used (for example, figures) has appeared in our publication with credit or acknowledgement to another source it is the responsibility of the user to ensure their reuse complies with the terms and conditions determined by the rights holder.

Additional Terms & Conditions applicable to each Creative Commons user license:

CC BY: The CC-BY license allows users to copy, to create extracts, abstracts and new works from the Article, to alter and revise the Article and to make commercial use of the Article (including reuse and/or resale of the Article by commercial entities), provided the user gives appropriate credit (with a link to the formal publication through the relevant DOI), provides a link to the license, indicates if changes were made and the licensor is not represented as endorsing the use made of the work. The full details of the license are available at <http://creativecommons.org/licenses/by/4.0>.

CC BY NC SA: The CC BY-NC-SA license allows users to copy, to create extracts, abstracts and new works from the Article, to alter and revise the Article, provided this is not done for commercial purposes, and that the user gives appropriate credit (with a link to the formal publication through the relevant DOI), provides a link to the license, indicates if changes were made and the licensor is not represented as endorsing the use made of the work. Further, any new works must be made available on the same conditions. The full details of the license are available at <http://creativecommons.org/licenses/by-nc-sa/4.0>.

CC BY NC ND: The CC BY-NC-ND license allows users to copy and distribute the Article, provided this is not done for commercial purposes and further does not permit distribution of the Article if it is changed or edited in any way, and provided the user gives appropriate credit (with a link to the formal publication through the relevant DOI), provides a link to the license, and that the licensor is not represented as endorsing the use made of the work. The full details of the license are available at <http://creativecommons.org/licenses/by-nc-nd/4.0>. Any commercial reuse of Open Access articles published with a CC BY NC SA or CC BY NC ND license requires permission from Elsevier and will be subject to a fee.

Commercial reuse includes:

- Associating advertising with the full text of the Article
- Charging fees for document delivery or access
- Article aggregation
- Systematic distribution via e-mail lists or share buttons

Posting or linking by commercial companies for use by customers of those companies.

20. **Other Conditions:**

v1.8

Questions? customer@copyright.com or +1-855-239-3415 (toll free in the US) or +1-978-646-2777.

ELSEVIER LICENSE TERMS AND CONDITIONS

Feb 09, 2016

This is an Agreement between Hiroki Matsuda ("You") and Elsevier ("Elsevier"). It consists of your order details, the terms and conditions provided by Elsevier, and the payment terms and conditions.

All payments must be made in full to CCC. For payment instructions, please see information listed at the bottom of this form.

Supplier	Elsevier Limited The Boulevard, Langford Lane Kidlington, Oxford, OX5 1GB, UK
Registered Company Number	1982084
Customer name	Hiroki Matsuda
Customer address	1-4-12, Kojirakawa-machi Yamagata-shi, Yamagata-ken 990-8560
License number	3804661144461
License date	Feb 09, 2016
Licensed content publisher	Elsevier
Licensed content publication	Physics Letters B
Licensed content title	The α S3 approximation of quantum chromodynamics to the Ellis-Jaffe sum rule
Licensed content author	S.A. Larin, T. van Ritbergen, J.A.M. Vermaseren
Licensed content date	3 July 1997
Licensed content volume number	404
Licensed content issue number	1-2
Number of pages	8
Start Page	153
End Page	160
Type of Use	reuse in a thesis/dissertation
Intended publisher of new work	other
Portion	figures/tables/illustrations
Number of figures/tables/illustrations	1
Format	both print and electronic
Are you the author of this Elsevier article?	No
Will you be translating?	No
Original figure numbers	table 1
Title of your thesis/dissertation	Measurement of longitudinal double spin asymmetries in the single-inclusive hadron quasi-real photoproduction at high-pT by a muon beam for the study of gluon polarisation in nucleon
Expected completion date	Feb 2016
Estimated size (number of pages)	150
Elsevier VAT number	GB 494 6272 12

Price	0 JPY
VAT/Local Sales Tax	0 JPY / 0.00 GBP
Total	0 JPY
Terms and Conditions	

INTRODUCTION

1. The publisher for this copyrighted material is Elsevier. By clicking "accept" in connection with completing this licensing transaction, you agree that the following terms and conditions apply to this transaction (along with the Billing and Payment terms and conditions established by Copyright Clearance Center, Inc. ("CCC"), at the time that you opened your Rightslink account and that are available at any time at <http://myaccount.copyright.com>).

GENERAL TERMS

2. Elsevier hereby grants you permission to reproduce the aforementioned material subject to the terms and conditions indicated.

3. Acknowledgement: If any part of the material to be used (for example, figures) has appeared in our publication with credit or acknowledgement to another source, permission must also be sought from that source. If such permission is not obtained then that material may not be included in your publication/copies. Suitable acknowledgement to the source must be made, either as a footnote or in a reference list at the end of your publication, as follows:

"Reprinted from Publication title, Vol /edition number, Author(s), Title of article / title of chapter, Pages No., Copyright (Year), with permission from Elsevier [OR APPLICABLE SOCIETY COPYRIGHT OWNER]." Also Lancet special credit - "Reprinted from The Lancet, Vol. number, Author(s), Title of article, Pages No., Copyright (Year), with permission from Elsevier."

4. Reproduction of this material is confined to the purpose and/or media for which permission is hereby given.

5. Altering/Modifying Material: Not Permitted. However figures and illustrations may be altered/adapted minimally to serve your work. Any other abbreviations, additions, deletions and/or any other alterations shall be made only with prior written authorization of Elsevier Ltd. (Please contact Elsevier at permissions@elsevier.com)

6. If the permission fee for the requested use of our material is waived in this instance, please be advised that your future requests for Elsevier materials may attract a fee.

7. Reservation of Rights: Publisher reserves all rights not specifically granted in the combination of (i) the license details provided by you and accepted in the course of this licensing transaction, (ii) these terms and conditions and (iii) CCC's Billing and Payment terms and conditions.

8. License Contingent Upon Payment: While you may exercise the rights licensed immediately upon issuance of the license at the end of the licensing process for the transaction, provided that you have disclosed complete and accurate details of your proposed use, no license is finally effective unless and until full payment is received from you (either by publisher or by CCC) as provided in CCC's Billing and Payment terms and conditions. If full payment is not received on a timely basis, then any license preliminarily granted shall be deemed automatically revoked and shall be void as if never granted. Further, in the event that you breach any of these terms and conditions or any of CCC's Billing and Payment terms and conditions, the license is automatically revoked and shall be void as if never granted. Use of materials as described in a revoked license, as well as any use of the materials beyond the scope of an unrevoked license, may constitute copyright infringement and publisher reserves the right to take any and all action to protect its copyright in the materials.

9. Warranties: Publisher makes no representations or warranties with respect to the licensed material.

10. Indemnity: You hereby indemnify and agree to hold harmless publisher and CCC, and their respective officers, directors, employees and agents, from and against any and all claims arising out of your use of the licensed material other than as specifically authorized pursuant to this license.

11. No Transfer of License: This license is personal to you and may not be sublicensed, assigned, or transferred by you to any other person without publisher's written permission.

12. No Amendment Except in Writing: This license may not be amended except in a writing signed by both parties (or, in the case of publisher, by CCC on publisher's behalf).

13. Objection to Contrary Terms: Publisher hereby objects to any terms contained in any purchase order, acknowledgment, check endorsement or other writing prepared by you, which terms are inconsistent with these terms and conditions or CCC's Billing and Payment terms and conditions. These terms and conditions, together with CCC's Billing and Payment terms and conditions (which are incorporated herein), comprise the entire agreement between you and publisher (and CCC) concerning this licensing transaction. In the event of any conflict between your obligations established by these terms and conditions and those established by CCC's Billing and Payment terms and conditions, these terms and conditions shall control.

14. Revocation: Elsevier or Copyright Clearance Center may deny the permissions described in this License at their sole discretion, for any reason or no reason, with a full refund payable to you. Notice of such denial will be made using the contact information provided by you. Failure to receive such notice will not alter or invalidate the denial. In no event will Elsevier or Copyright Clearance Center be responsible or liable for any costs, expenses or damage incurred by you as a result of a denial of your permission request, other than a refund of the amount(s) paid by you to Elsevier and/or Copyright Clearance Center for denied permissions.

LIMITED LICENSE

The following terms and conditions apply only to specific license types:

15. **Translation:** This permission is granted for non-exclusive world **English** rights only unless your license was granted for translation rights. If you licensed translation rights you may only translate this content into the languages you requested. A professional translator must perform all translations and reproduce the content word for word preserving the integrity of the article.

16. **Posting licensed content on any Website:** The following terms and conditions apply as follows: Licensing material from an Elsevier journal: All content posted to the web site must maintain the copyright information line on the bottom of each image; A hyper-text must be included to the Homepage of the journal from which you are licensing at <http://www.sciencedirect.com/science/journal/xxxxx> or the Elsevier homepage for books at <http://www.elsevier.com>; Central Storage: This license does not include permission for a scanned version of the material to be stored in a central repository such as that provided by Heron/XanEdu.

Licensing material from an Elsevier book: A hyper-text link must be included to the Elsevier homepage at <http://www.elsevier.com> . All content posted to the web site must maintain the copyright information line on the bottom of each image.

Posting licensed content on Electronic reserve: In addition to the above the following clauses are applicable: The web site must be password-protected and made available only to bona fide students registered on a relevant course. This permission is granted for 1 year only. You may obtain a new license for future website posting.

17. **For journal authors:** the following clauses are applicable in addition to the above:

Preprints:

A preprint is an author's own write-up of research results and analysis, it has not been peer-reviewed, nor has it had any other value added to it by a publisher (such as formatting, copyright, technical enhancement etc.).

Authors can share their preprints anywhere at any time. Preprints should not be added to or enhanced in any way in order to appear more like, or to substitute for, the final versions of articles however authors can update their preprints on arXiv or RePEc with their Accepted Author Manuscript (see below).

If accepted for publication, we encourage authors to link from the preprint to their formal publication via its DOI. Millions of researchers have access to the formal publications on ScienceDirect, and so links will help users to find, access, cite and use the best available version. Please note that Cell Press, The Lancet and some society-owned have different preprint policies. Information on these policies is available on the journal homepage.

Accepted Author Manuscripts: An accepted author manuscript is the manuscript of an article that has been accepted for publication and which typically includes author-incorporated changes suggested during submission, peer review and editor-author communications.

Authors can share their accepted author manuscript:

- immediately
 - via their non-commercial person homepage or blog
 - by updating a preprint in arXiv or RePEc with the accepted manuscript
 - via their research institute or institutional repository for internal institutional uses or as part of an invitation-only research collaboration work-group
 - directly by providing copies to their students or to research collaborators for their personal use
 - for private scholarly sharing as part of an invitation-only work group on commercial sites with which Elsevier has an agreement
- after the embargo period
 - via non-commercial hosting platforms such as their institutional repository
 - via commercial sites with which Elsevier has an agreement

In all cases accepted manuscripts should:

- link to the formal publication via its DOI
- bear a CC-BY-NC-ND license - this is easy to do
- if aggregated with other manuscripts, for example in a repository or other site, be shared in alignment with our hosting policy not be added to or enhanced in any way to appear more like, or to substitute for, the published journal article.

Published journal article (JPA): A published journal article (PJA) is the definitive final record of published research that appears or will appear in the journal and embodies all value-adding publishing activities including peer review co-ordination, copy-editing, formatting, (if relevant) pagination and online enrichment.

Policies for sharing publishing journal articles differ for subscription and gold open access articles:

Subscription Articles: If you are an author, please share a link to your article rather than the full-text. Millions of researchers have access to the formal publications on ScienceDirect, and so links will help your users to find, access, cite, and use the best available version.

Theses and dissertations which contain embedded PJAs as part of the formal submission can be posted publicly by the awarding institution with DOI links back to the formal publications on ScienceDirect.

If you are affiliated with a library that subscribes to ScienceDirect you have additional private sharing rights for others' research accessed under that agreement. This includes use for classroom teaching and internal training at the institution (including use in course packs and courseware programs), and inclusion of the article for grant funding purposes.

Gold Open Access Articles: May be shared according to the author-selected end-user license and should contain a [CrossMark logo](#), the end user license, and a DOI link to the formal publication on ScienceDirect.

Please refer to Elsevier's [posting policy](#) for further information.

18. **For book authors** the following clauses are applicable in addition to the above: Authors are permitted to place a brief summary of their work online only. You are not allowed to download and post the published electronic version of your chapter, nor may you scan the printed edition to create an electronic version. **Posting to a repository:** Authors are permitted to post a summary of their chapter only in their institution's repository.

19. **Thesis/Dissertation:** If your license is for use in a thesis/dissertation your thesis may be submitted to your institution in either print or electronic form. Should your thesis be published commercially, please reapply for permission. These requirements include permission for the Library and Archives of Canada to supply single copies, on demand, of the complete thesis and include permission for Proquest/UMI to supply single copies, on demand, of the complete thesis. Should your thesis be published commercially, please reapply for permission. Theses and dissertations which contain embedded PJAs as part of the formal submission can be posted publicly by the awarding institution with DOI links back to the formal publications on ScienceDirect.

Elsevier Open Access Terms and Conditions

You can publish open access with Elsevier in hundreds of open access journals or in nearly 2000 established subscription journals that support open access publishing. Permitted third party re-use of these open access articles is defined by the author's choice of Creative Commons user license. See our [open access license policy](#) for more information.

Terms & Conditions applicable to all Open Access articles published with Elsevier:

Any reuse of the article must not represent the author as endorsing the adaptation of the article nor should the article be modified in such a way as to damage the author's honour or reputation. If any changes have been made, such changes must be clearly indicated.

The author(s) must be appropriately credited and we ask that you include the end user license and a DOI link to the formal publication on ScienceDirect.

If any part of the material to be used (for example, figures) has appeared in our publication with credit or acknowledgement to another source it is the responsibility of the user to ensure their reuse complies with the terms and conditions determined by the rights holder.

Additional Terms & Conditions applicable to each Creative Commons user license:

CC BY: The CC-BY license allows users to copy, to create extracts, abstracts and new works from the Article, to alter and revise the Article and to make commercial use of the Article (including reuse and/or resale of the Article by commercial entities), provided the user gives appropriate credit (with a link to the formal publication through the relevant DOI), provides a link to the license, indicates if changes were made and the licensor is not represented as endorsing the use made of the work. The full details of the license are available at <http://creativecommons.org/licenses/by/4.0>.

CC BY NC SA: The CC BY-NC-SA license allows users to copy, to create extracts, abstracts and new works from the Article, to alter and revise the Article, provided this is not done for commercial purposes, and that the user gives appropriate credit (with a link to the formal publication through the relevant DOI), provides a link to the license, indicates if changes were made and the licensor is not represented as endorsing the use made of the work. Further, any new works must be made available on the same conditions. The full details of the license are available at <http://creativecommons.org/licenses/by-nc-sa/4.0>.

CC BY NC ND: The CC BY-NC-ND license allows users to copy and distribute the Article, provided this is not done for commercial purposes and further does not permit distribution of the Article if it is changed or edited in any way, and provided the user gives appropriate credit (with a link to the formal publication through the relevant DOI), provides a link to the license, and that the licensor is not represented as endorsing the use made of the work. The full details of the license are available at <http://creativecommons.org/licenses/by-nc-nd/4.0>. Any commercial reuse of Open Access articles published with a CC BY NC SA or CC BY NC ND license requires permission from Elsevier and will be subject to a fee.

Commercial reuse includes:

- Associating advertising with the full text of the Article
- Charging fees for document delivery or access
- Article aggregation
- Systematic distribution via e-mail lists or share buttons

Posting or linking by commercial companies for use by customers of those companies.

20. **Other Conditions:**

v1.8

Questions? customercare@copyright.com or +1-855-239-3415 (toll free in the US) or +1-978-646-2777.

AMERICAN PHYSICAL SOCIETY LICENSE TERMS AND CONDITIONS

Feb 09, 2016

This Agreement between Hiroki Matsuda ("You") and American Physical Society ("American Physical Society") consists of your license details and the terms and conditions provided by American Physical Society and Copyright Clearance Center.

License Number	3804670068440
License date	Feb 09, 2016
Licensed Content Publisher	American Physical Society
Licensed Content Publication	Physical Review D
Licensed Content Title	Soft-gluon resummation for high- p_{\perp} inclusive-hadron production at COMPASS
Licensed Content Author	Daniel de Florian et al.
Licensed Content Date	Jul 16, 2013
Licensed Content Volume Number	88
I would like to...	Thesis/Dissertation
Requestor type	Student
Format	Print, Electronic
Portion	image/photo
Number of images/photos requested	1
Portion description	Figure 4
Rights for	Main product
Duration of use	Life of Current Edition
Creation of copies for the disabled	no
With minor editing privileges	no
For distribution to	Worldwide
In the following language(s)	Original language of publication
With incidental promotional use	no
The lifetime unit quantity of new product	0 to 499
The requesting person/organization is:	Hiroki Matsuda
Order reference number	None
Title of your thesis / dissertation	Measurement of longitudinal double spin asymmetries in the single-inclusive hadron quasi-real photoproduction at high- p_T by a muon beam for the study of gluon polarisation in nucleon
Expected completion date	Feb 2016
Expected size (number of pages)	150
Requestor Location	Hiroki Matsuda 1-4-12, Kojirakawa-machi

	None
	None
	Yamagata-shi, Japan 990-8560
	Attn: Hiroki Matsuda
Billing Type	Invoice
Billing Address	Hiroki Matsuda
	1-4-12, Kojirakawa-machi
	None
	None
	Yamagata-shi, Japan 990-8560
	Attn: Hiroki Matsuda
Total	0 JPY
Terms and Conditions	

Terms and Conditions

The American Physical Society (APS) is pleased to grant the Requestor of this license a non-exclusive, non-transferable permission, limited to **print** and/or **electronic** format, depending on what they chose], provided all criteria outlined below are followed.

1. For electronic format permissions, Requestor agrees to provide a hyperlink from the reprinted APS material using the source material's DOI on the web page where the work appears. The hyperlink should use the standard DOI resolution URL, <http://dx.doi.org/{DOI}>. The hyperlink may be embedded in the copyright credit line.
2. For print format permissions, Requestor agrees to print the required copyright credit line on the first page where the material appears: "Reprinted (abstract/excerpt/figure) with permission from [(FULL REFERENCE CITATION) as follows: Author's Names, APS Journal Title, Volume Number, Page Number and Year of Publication.] Copyright (YEAR) by the American Physical Society."
3. Permission granted in this license is for a one-time use and does not include permission for any future editions, updates, databases, formats or other matters. Permission must be sought for any additional use.
4. Use of the material does not and must not imply any endorsement by APS.
5. Under no circumstance does APS purport or intend to grant permission to reuse materials to which it does not hold copyright. It is the requestors sole responsibility to ensure the licensed material is original to APS and does not contain the copyright of another entity, and that the copyright notice of the figure, photograph, cover or table does not indicate that it was reprinted by APS, with permission from another source.
6. The permission granted herein is personal to the Requestor for the use specified and is not transferable or assignable without express written permission of APS. This license may not be amended except in writing by APS.
7. You may not alter, edit or modify the material in any manner.
8. You may translate the materials only when translation rights have been granted.
9. You may not use the material for promotional, sales, advertising or marketing purposes.
10. The foregoing license shall not take effect unless and until APS or its agent, Copyright Clearance Center (CCC), receives payment in full in accordance with CCC Billing and Payment Terms and Conditions, which are incorporated herein by reference.
11. Should the terms of this license be violated at any time, APS or CCC may revoke the license with no refund to you and seek relief to the fullest extent of the laws of the USA. Official written notice will be made using the contact information provided with the permission request. Failure to receive such notice will not nullify revocation of the permission.
12. APS reserves all rights not specifically granted herein.
13. This document, including the CCC Billing and Payment Terms and Conditions, shall be the entire agreement between the parties relating to the subject matter hereof.

Other Terms and Conditions

Questions? customercare@copyright.com or +1-855-239-3415 (toll free in the US) or +1-978-646-2777.

AMERICAN PHYSICAL SOCIETY LICENSE TERMS AND CONDITIONS

Feb 09, 2016

This Agreement between Hiroki Matsuda ("You") and American Physical Society ("American Physical Society") consists of your license details and the terms and conditions provided by American Physical Society and Copyright Clearance Center.

License Number	3804670425637
License date	Feb 09, 2016
Licensed Content Publisher	American Physical Society
Licensed Content Publication	Physical Review D
Licensed Content Title	Inclusive double-helicity asymmetries in neutral-pion and eta-meson production in $\sqrt{s}=200$ GeV collisions at A. Adare et al. ((PHENIX Collaboration))
Licensed Content Author	A. Adare et al. ((PHENIX Collaboration))
Licensed Content Date	Jul 17, 2014
Licensed Content Volume Number	90
I would like to...	Thesis/Dissertation
Requestor type	Student
Format	Print, Electronic
Portion	image/photo
Number of images/photos requested	2
Portion description	Figures 11, 12
Rights for	Main product
Duration of use	Life of Current Edition
Creation of copies for the disabled	no
With minor editing privileges	no
For distribution to	Worldwide
In the following language(s)	Original language of publication
With incidental promotional use	no
The lifetime unit quantity of new product	0 to 499
The requesting person/organization is:	Hiroki Matsuda
Order reference number	None
Title of your thesis / dissertation	Measurement of longitudinal double spin asymmetries in the single-inclusive hadron quasi-real photoproduction at high-pT by a muon beam for the study of gluon polarisation in nucleon
Expected completion date	Feb 2016
Expected size (number of pages)	150

Requestor Location Hiroki Matsuda
1-4-12, Kojirakawa-machi
None
None
Yamagata-shi, Japan 990-8560
Attn: Hiroki Matsuda

Billing Type Invoice

Billing Address Hiroki Matsuda
1-4-12, Kojirakawa-machi
None
None
Yamagata-shi, Japan 990-8560
Attn: Hiroki Matsuda

Total **0 JPY**

Terms and Conditions

Terms and Conditions

The American Physical Society (APS) is pleased to grant the Requestor of this license a non-exclusive, non-transferable permission, limited to [print and/or electronic format, depending on what they chose], provided all criteria outlined below are followed.

1. For electronic format permissions, Requestor agrees to provide a hyperlink from the reprinted APS material using the source material's DOI on the web page where the work appears. The hyperlink should use the standard DOI resolution URL, <http://dx.doi.org/{DOI}>. The hyperlink may be embedded in the copyright credit line.
2. For print format permissions, Requestor agrees to print the required copyright credit line on the first page where the material appears: "Reprinted (abstract/excerpt/figure) with permission from [(FULL REFERENCE CITATION) as follows: Author's Names, APS Journal Title, Volume Number, Page Number and Year of Publication.] Copyright (YEAR) by the American Physical Society."
3. Permission granted in this license is for a one-time use and does not include permission for any future editions, updates, databases, formats or other matters. Permission must be sought for any additional use.
4. Use of the material does not and must not imply any endorsement by APS.
5. Under no circumstance does APS purport or intend to grant permission to reuse materials to which it does not hold copyright. It is the requestors sole responsibility to ensure the licensed material is original to APS and does not contain the copyright of another entity, and that the copyright notice of the figure, photograph, cover or table does not indicate that it was reprinted by APS, with permission from another source.
6. The permission granted herein is personal to the Requestor for the use specified and is not transferable or assignable without express written permission of APS. This license may not be amended except in writing by APS.
7. You may not alter, edit or modify the material in any manner.
8. You may translate the materials only when translation rights have been granted.
9. You may not use the material for promotional, sales, advertising or marketing purposes.
10. The foregoing license shall not take effect unless and until APS or its agent, Copyright Clearance Center (CCC), receives payment in full in accordance with CCC Billing and Payment Terms and Conditions, which are incorporated herein by reference.
11. Should the terms of this license be violated at any time, APS or CCC may revoke the license with no refund to you and seek relief to the fullest extent of the laws of the USA. Official written notice will be made using the contact information provided with the permission request. Failure to receive such notice will not nullify revocation of the permission.
12. APS reserves all rights not specifically granted herein.
13. This document, including the CCC Billing and Payment Terms and Conditions, shall be the entire agreement between the parties relating to the subject matter hereof.

Other Terms and Conditions

Questions? customercare@copyright.com or +1-855-239-3415 (toll free in the US) or +1-978-646-2777.

AMERICAN PHYSICAL SOCIETY LICENSE TERMS AND CONDITIONS

Feb 09, 2016

This Agreement between Hiroki Matsuda ("You") and American Physical Society ("American Physical Society") consists of your license details and the terms and conditions provided by American Physical Society and Copyright Clearance Center.

License Number	3804671053824
License date	Feb 09, 2016
Licensed Content Publisher	American Physical Society
Licensed Content Publication	Physical Review D
Licensed Content Title	Threshold resummation for polarized high- p_T hadron production at COMPASS
Licensed Content Author	Claudia Uebler, Andreas Schäfer, and Werner Vogelsang
Licensed Content Date	Nov 23, 2015
Licensed Content Volume Number	92
I would like to...	Thesis/Dissertation
Requestor type	Student
Format	Print, Electronic
Portion	image/photo
Number of images/photos requested	1
Portion description	Figure 6
Rights for	Main product
Duration of use	Life of Current Edition
Creation of copies for the disabled	no
With minor editing privileges	no
For distribution to	Worldwide
In the following language(s)	Original language of publication
With incidental promotional use	no
The lifetime unit quantity of new product	0 to 499
The requesting person/organization is:	Hiroki Matsuda
Order reference number	None
Title of your thesis / dissertation	Measurement of longitudinal double spin asymmetries in the single- inclusive hadron quasi-real photonproduction at high- p_T by a muon

ELSEVIER LICENSE TERMS AND CONDITIONS

Feb 09, 2016

This is an Agreement between Hiroki Matsuda ("You") and Elsevier ("Elsevier"). It consists of your order details, the terms and conditions provided by Elsevier, and the payment terms and conditions.

All payments must be made in full to CCC. For payment instructions, please see information listed at the bottom of this form.

Supplier	Elsevier Limited The Boulevard, Langford Lane Kidlington, Oxford, OX5 1GB, UK
Registered Company Number	1982084
Customer name	Hiroki Matsuda
Customer address	1-4-12, Kojirakawa-machi Yamagata-shi, Yamagata-ken 990-8560
License number	3804680896137
License date	Feb 09, 2016
Licensed content publisher	Elsevier
Licensed content publication	Nuclear Instruments and Methods in Physics Research Section A: Accelerators, Spectrometers, Detectors and Associated Equipment
Licensed content title	Design and construction of the fast photon detection system for COMPASS RICH-1
Licensed content author	P. Abbon, M. Alexeev, H. Angerer, R. Birsas, P. Bordalo, F. Bradamante, A. Bressan, M. Chiosso, P. Ciliberti, M. Colantoni, T. Dafni, S. Dalla Torre, E. Delagnes, O. Denisov, H. Deschamps, V. Diaz, N. Dibiase, V. Duic, W. Eyrich, A. Ferrero, M. Finger, M. Finger Jr. et al.
Licensed content date	21 April 2010
Licensed content volume number	616
Licensed content issue number	1
Number of pages	17
Start Page	21
End Page	37
Type of Use	reuse in a thesis/dissertation
Intended publisher of new work	other
Portion	figures/tables/illustrations
Number of figures/tables/illustrations	1
Format	both print and electronic
Are you the author of this Elsevier article?	No
Will you be translating?	No
Original figure numbers	Figure 26
Title of your thesis/dissertation	Measurement of longitudinal double spin asymmetries in the single-inclusive hadron quasi-real photoproduction at high-pT by a muon beam for the study of gluon polarisation in nucleon
Expected completion date	Feb 2016
Estimated size (number	150

of pages)

Elsevier VAT number GB 494 6272 12
Price 0 JPY
VAT/Local Sales Tax 0 JPY / 0.00 GBP
Total 0 JPY

[Terms and Conditions](#)

INTRODUCTION

1. The publisher for this copyrighted material is Elsevier. By clicking "accept" in connection with completing this licensing transaction, you agree that the following terms and conditions apply to this transaction (along with the Billing and Payment terms and conditions established by Copyright Clearance Center, Inc. ("CCC"), at the time that you opened your Rightslink account and that are available at any time at <http://myaccount.copyright.com>).

GENERAL TERMS

2. Elsevier hereby grants you permission to reproduce the aforementioned material subject to the terms and conditions indicated.

3. Acknowledgement: If any part of the material to be used (for example, figures) has appeared in our publication with credit or acknowledgement to another source, permission must also be sought from that source. If such permission is not obtained then that material may not be included in your publication/copies. Suitable acknowledgement to the source must be made, either as a footnote or in a reference list at the end of your publication, as follows:

"Reprinted from Publication title, Vol /edition number, Author(s), Title of article / title of chapter, Pages No., Copyright (Year), with permission from Elsevier [OR APPLICABLE SOCIETY COPYRIGHT OWNER]." Also Lancet special credit - "Reprinted from The Lancet, Vol. number, Author(s), Title of article, Pages No., Copyright (Year), with permission from Elsevier."

4. Reproduction of this material is confined to the purpose and/or media for which permission is hereby given.

5. Altering/Modifying Material: Not Permitted. However figures and illustrations may be altered/adapted minimally to serve your work. Any other abbreviations, additions, deletions and/or any other alterations shall be made only with prior written authorization of Elsevier Ltd. (Please contact Elsevier at permissions@elsevier.com)

6. If the permission fee for the requested use of our material is waived in this instance, please be advised that your future requests for Elsevier materials may attract a fee.

7. Reservation of Rights: Publisher reserves all rights not specifically granted in the combination of (i) the license details provided by you and accepted in the course of this licensing transaction, (ii) these terms and conditions and (iii) CCC's Billing and Payment terms and conditions.

8. License Contingent Upon Payment: While you may exercise the rights licensed immediately upon issuance of the license at the end of the licensing process for the transaction, provided that you have disclosed complete and accurate details of your proposed use, no license is finally effective unless and until full payment is received from you (either by publisher or by CCC) as provided in CCC's Billing and Payment terms and conditions. If full payment is not received on a timely basis, then any license preliminarily granted shall be deemed automatically revoked and shall be void as if never granted. Further, in the event that you breach any of these terms and conditions or any of CCC's Billing and Payment terms and conditions, the license is automatically revoked and shall be void as if never granted. Use of materials as described in a revoked license, as well as any use of the materials beyond the scope of an unrevoked license, may constitute copyright infringement and publisher reserves the right to take any and all action to protect its copyright in the materials.

9. Warranties: Publisher makes no representations or warranties with respect to the licensed material.

10. Indemnity: You hereby indemnify and agree to hold harmless publisher and CCC, and their respective officers, directors, employees and agents, from and against any and all claims arising out of your use of the licensed material other than as specifically authorized pursuant to this license.

11. No Transfer of License: This license is personal to you and may not be sublicensed, assigned, or transferred by you to any other person without publisher's written permission.

12. No Amendment Except in Writing: This license may not be amended except in a writing signed by both parties (or, in the case of publisher, by CCC on publisher's behalf).

13. Objection to Contrary Terms: Publisher hereby objects to any terms contained in any purchase order, acknowledgment, check endorsement or other writing prepared by you, which terms are inconsistent with these terms and conditions or CCC's Billing and Payment terms and conditions. These terms and conditions, together with CCC's Billing and Payment terms and conditions (which are incorporated herein), comprise the entire agreement between you and publisher (and CCC) concerning this licensing transaction. In the event of any conflict between your obligations established by these terms and conditions and those established by CCC's Billing and Payment terms and conditions, these terms and conditions shall control.

14. Revocation: Elsevier or Copyright Clearance Center may deny the permissions described in this License at their sole discretion, for any reason or no reason, with a full refund payable to you. Notice of such denial will be made using the contact information provided by you. Failure to receive such notice will not alter or invalidate the denial. In no event will

Elsevier or Copyright Clearance Center be responsible or liable for any costs, expenses or damage incurred by you as a result of a denial of your permission request, other than a refund of the amount(s) paid by you to Elsevier and/or Copyright Clearance Center for denied permissions.

LIMITED LICENSE

The following terms and conditions apply only to specific license types:

15. **Translation:** This permission is granted for non-exclusive world **English** rights only unless your license was granted for translation rights. If you licensed translation rights you may only translate this content into the languages you requested. A professional translator must perform all translations and reproduce the content word for word preserving the integrity of the article.

16. **Posting licensed content on any Website:** The following terms and conditions apply as follows: Licensing material from an Elsevier journal: All content posted to the web site must maintain the copyright information line on the bottom of each image; A hyper-text must be included to the Homepage of the journal from which you are licensing at <http://www.sciencedirect.com/science/journal/xxxxx> or the Elsevier homepage for books at <http://www.elsevier.com>; Central Storage: This license does not include permission for a scanned version of the material to be stored in a central repository such as that provided by Heron/XanEdu.

Licensing material from an Elsevier book: A hyper-text link must be included to the Elsevier homepage at <http://www.elsevier.com>. All content posted to the web site must maintain the copyright information line on the bottom of each image.

Posting licensed content on Electronic reserve: In addition to the above the following clauses are applicable: The web site must be password-protected and made available only to bona fide students registered on a relevant course. This permission is granted for 1 year only. You may obtain a new license for future website posting.

17. **For journal authors:** the following clauses are applicable in addition to the above:

Preprints:

A preprint is an author's own write-up of research results and analysis, it has not been peer-reviewed, nor has it had any other value added to it by a publisher (such as formatting, copyright, technical enhancement etc.).

Authors can share their preprints anywhere at any time. Preprints should not be added to or enhanced in any way in order to appear more like, or to substitute for, the final versions of articles however authors can update their preprints on arXiv or RePEc with their Accepted Author Manuscript (see below).

If accepted for publication, we encourage authors to link from the preprint to their formal publication via its DOI. Millions of researchers have access to the formal publications on ScienceDirect, and so links will help users to find, access, cite and use the best available version. Please note that Cell Press, The Lancet and some society-owned have different preprint policies. Information on these policies is available on the journal homepage.

Accepted Author Manuscripts: An accepted author manuscript is the manuscript of an article that has been accepted for publication and which typically includes author-incorporated changes suggested during submission, peer review and editor-author communications.

Authors can share their accepted author manuscript:

- immediately
 - via their non-commercial person homepage or blog
 - by updating a preprint in arXiv or RePEc with the accepted manuscript
 - via their research institute or institutional repository for internal institutional uses or as part of an invitation-only research collaboration work-group
 - directly by providing copies to their students or to research collaborators for their personal use
 - for private scholarly sharing as part of an invitation-only work group on commercial sites with which Elsevier has an agreement
- after the embargo period
 - via non-commercial hosting platforms such as their institutional repository
 - via commercial sites with which Elsevier has an agreement

In all cases accepted manuscripts should:

- link to the formal publication via its DOI
- bear a CC-BY-NC-ND license - this is easy to do
- if aggregated with other manuscripts, for example in a repository or other site, be shared in alignment with our hosting policy not be added to or enhanced in any way to appear more like, or to substitute for, the published journal article.

Published journal article (JPA): A published journal article (PJA) is the definitive final record of published research that appears or will appear in the journal and embodies all value-adding publishing activities including peer review co-ordination, copy-editing, formatting, (if relevant) pagination and online enrichment.

Policies for sharing publishing journal articles differ for subscription and gold open access articles:

Subscription Articles: If you are an author, please share a link to your article rather than the full-text. Millions of researchers have access to the formal publications on ScienceDirect, and so links will help your users to find, access, cite, and use the best available version.

Theses and dissertations which contain embedded PJAs as part of the formal submission can be posted publicly by the awarding institution with DOI links back to the formal publications on ScienceDirect.

If you are affiliated with a library that subscribes to ScienceDirect you have additional private sharing rights for others' research accessed under that agreement. This includes use for classroom teaching and internal training at the institution (including use in course packs and courseware programs), and inclusion of the article for grant funding purposes.

Gold Open Access Articles: May be shared according to the author-selected end-user license and should contain a [CrossMark logo](#), the end user license, and a DOI link to the formal publication on ScienceDirect.

Please refer to Elsevier's [posting policy](#) for further information.

18. **For book authors** the following clauses are applicable in addition to the above: Authors are permitted to place a brief summary of their work online only. You are not allowed to download and post the published electronic version of your chapter, nor may you scan the printed edition to create an electronic version. **Posting to a repository:** Authors are permitted to post a summary of their chapter only in their institution's repository.

19. **Thesis/Dissertation:** If your license is for use in a thesis/dissertation your thesis may be submitted to your institution in either print or electronic form. Should your thesis be published commercially, please reapply for permission. These requirements include permission for the Library and Archives of Canada to supply single copies, on demand, of the complete thesis and include permission for Proquest/UMI to supply single copies, on demand, of the complete thesis. Should your thesis be published commercially, please reapply for permission. Theses and dissertations which contain embedded PJAs as part of the formal submission can be posted publicly by the awarding institution with DOI links back to the formal publications on ScienceDirect.

Elsevier Open Access Terms and Conditions

You can publish open access with Elsevier in hundreds of open access journals or in nearly 2000 established subscription journals that support open access publishing. Permitted third party re-use of these open access articles is defined by the author's choice of Creative Commons user license. See our [open access license policy](#) for more information.

Terms & Conditions applicable to all Open Access articles published with Elsevier:

Any reuse of the article must not represent the author as endorsing the adaptation of the article nor should the article be modified in such a way as to damage the author's honour or reputation. If any changes have been made, such changes must be clearly indicated.

The author(s) must be appropriately credited and we ask that you include the end user license and a DOI link to the formal publication on ScienceDirect.

If any part of the material to be used (for example, figures) has appeared in our publication with credit or acknowledgement to another source it is the responsibility of the user to ensure their reuse complies with the terms and conditions determined by the rights holder.

Additional Terms & Conditions applicable to each Creative Commons user license:

CC BY: The CC-BY license allows users to copy, to create extracts, abstracts and new works from the Article, to alter and revise the Article and to make commercial use of the Article (including reuse and/or resale of the Article by commercial entities), provided the user gives appropriate credit (with a link to the formal publication through the relevant DOI), provides a link to the license, indicates if changes were made and the licensor is not represented as endorsing the use made of the work. The full details of the license are available at <http://creativecommons.org/licenses/by/4.0>.

CC BY NC SA: The CC BY-NC-SA license allows users to copy, to create extracts, abstracts and new works from the Article, to alter and revise the Article, provided this is not done for commercial purposes, and that the user gives appropriate credit (with a link to the formal publication through the relevant DOI), provides a link to the license, indicates if changes were made and the licensor is not represented as endorsing the use made of the work. Further, any new works must be made available on the same conditions. The full details of the license are available at <http://creativecommons.org/licenses/by-nc-sa/4.0>.

CC BY NC ND: The CC BY-NC-ND license allows users to copy and distribute the Article, provided this is not done for commercial purposes and further does not permit distribution of the Article if it is changed or edited in any way, and provided the user gives appropriate credit (with a link to the formal publication through the relevant DOI), provides a link to the license, and that the licensor is not represented as endorsing the use made of the work. The full details of the license are available at <http://creativecommons.org/licenses/by-nc-nd/4.0>. Any commercial reuse of Open Access articles published with a CC BY NC SA or CC BY NC ND license requires permission from Elsevier and will be subject to a fee.

Commercial reuse includes:

- Associating advertising with the full text of the Article
- Charging fees for document delivery or access
- Article aggregation

- Systematic distribution via e-mail lists or share buttons

Posting or linking by commercial companies for use by customers of those companies.

20. **Other Conditions:**

v1.8

Questions? customercare@copyright.com or +1-855-239-3415 (toll free in the US) or +1-978-646-2777.

ELSEVIER LICENSE TERMS AND CONDITIONS

Feb 09, 2016

This is an Agreement between Hiroki Matsuda ("You") and Elsevier ("Elsevier"). It consists of your order details, the terms and conditions provided by Elsevier, and the payment terms and conditions.

All payments must be made in full to CCC. For payment instructions, please see information listed at the bottom of this form.

Supplier	Elsevier Limited The Boulevard,Langford Lane Kidlington,Oxford,OX5 1GB,UK
Registered Company Number	1982084
Customer name	Hiroki Matsuda
Customer address	1-4-12, Kojirakawa-machi Yamagata-shi, Yamagata-ken 990-8560
License number	3804690326606
License date	Feb 09, 2016
Licensed content publisher	Elsevier
Licensed content publication	Nuclear Instruments and Methods in Physics Research Section A: Accelerators, Spectrometers, Detectors and Associated Equipment
Licensed content title	The COMPASS experiment at CERN
Licensed content author	P. Abbon,E. Albrecht,V.Yu. Alexakhin,Yu. Alexandrov,G.D. Alexeev,M.G. Alekseev,A. Amoroso,H. Angerer,V.A. Anosov,B. Badelek,F. Balestra,J. Ball,J. Barth,G. Baum,M. Becker,Y. Bedfer,P. Berglund,C. Bernet,R. Bertini,M. Bettinelli,R. Birsa et al.
Licensed content date	11 July 2007
Licensed content volume number	577
Licensed content issue number	3
Number of pages	64
Start Page	455
End Page	518
Type of Use	reuse in a thesis/dissertation
Intended publisher of new work	other
Portion	figures/tables/illustrations
Number of figures/tables /illustrations	10
Format	both print and electronic
Are you the author of this Elsevier article?	No
Will you be translating?	No
Original figure numbers	Figures 1, 5, 34, 37, 43, 44, 46, 54, 55, 58
Title of your thesis/dissertation	Measurement of longitudinal double spin asymmetries in the single-inclusive hadron quasi-real photoproduction at high-pT by a muon beam for the study of gluon polarisation in nucleon
Expected completion date	Feb 2016

Estimated size (number of pages)	150
Elsevier VAT number	GB 494 6272 12
Price	0 JPY
VAT/Local Sales Tax	0 JPY / 0.00 GBP
Total	0 JPY
Terms and Conditions	

INTRODUCTION

1. The publisher for this copyrighted material is Elsevier. By clicking "accept" in connection with completing this licensing transaction, you agree that the following terms and conditions apply to this transaction (along with the Billing and Payment terms and conditions established by Copyright Clearance Center, Inc. ("CCC"), at the time that you opened your Rightslink account and that are available at any time at <http://myaccount.copyright.com>).

GENERAL TERMS

2. Elsevier hereby grants you permission to reproduce the aforementioned material subject to the terms and conditions indicated.
3. Acknowledgement: If any part of the material to be used (for example, figures) has appeared in our publication with credit or acknowledgement to another source, permission must also be sought from that source. If such permission is not obtained then that material may not be included in your publication/copies. Suitable acknowledgement to the source must be made, either as a footnote or in a reference list at the end of your publication, as follows: "Reprinted from Publication title, Vol /edition number, Author(s), Title of article / title of chapter, Pages No., Copyright (Year), with permission from Elsevier [OR APPLICABLE SOCIETY COPYRIGHT OWNER]." Also Lancet special credit - "Reprinted from The Lancet, Vol. number, Author(s), Title of article, Pages No., Copyright (Year), with permission from Elsevier."
4. Reproduction of this material is confined to the purpose and/or media for which permission is hereby given.
5. Altering/Modifying Material: Not Permitted. However figures and illustrations may be altered/adapted minimally to serve your work. Any other abbreviations, additions, deletions and/or any other alterations shall be made only with prior written authorization of Elsevier Ltd. (Please contact Elsevier at permissions@elsevier.com)
6. If the permission fee for the requested use of our material is waived in this instance, please be advised that your future requests for Elsevier materials may attract a fee.
7. Reservation of Rights: Publisher reserves all rights not specifically granted in the combination of (i) the license details provided by you and accepted in the course of this licensing transaction, (ii) these terms and conditions and (iii) CCC's Billing and Payment terms and conditions.
8. License Contingent Upon Payment: While you may exercise the rights licensed immediately upon issuance of the license at the end of the licensing process for the transaction, provided that you have disclosed complete and accurate details of your proposed use, no license is finally effective unless and until full payment is received from you (either by publisher or by CCC) as provided in CCC's Billing and Payment terms and conditions. If full payment is not received on a timely basis, then any license preliminarily granted shall be deemed automatically revoked and shall be void as if never granted. Further, in the event that you breach any of these terms and conditions or any of CCC's Billing and Payment terms and conditions, the license is automatically revoked and shall be void as if never granted. Use of materials as described in a revoked license, as well as any use of the materials beyond the scope of an unrevoked license, may constitute copyright infringement and publisher reserves the right to take any and all action to protect its copyright in the materials.
9. Warranties: Publisher makes no representations or warranties with respect to the licensed material.
10. Indemnity: You hereby indemnify and agree to hold harmless publisher and CCC, and their respective officers, directors, employees and agents, from and against any and all claims arising out of your use of the licensed material other than as specifically authorized pursuant to this license.
11. No Transfer of License: This license is personal to you and may not be sublicensed, assigned, or transferred by you to any other person without publisher's written permission.
12. No Amendment Except in Writing: This license may not be amended except in a writing signed by both parties (or, in the case of publisher, by CCC on publisher's behalf).
13. Objection to Contrary Terms: Publisher hereby objects to any terms contained in any purchase order, acknowledgment, check endorsement or other writing prepared by you, which terms are inconsistent with these terms and conditions or CCC's Billing and Payment terms and conditions. These terms and conditions, together with CCC's Billing and Payment terms and conditions (which are incorporated herein), comprise the entire agreement between you and publisher (and CCC) concerning this licensing transaction. In the event of any conflict between your obligations established by these terms and conditions and those established by CCC's Billing and Payment terms and conditions, these terms and conditions shall control.
14. Revocation: Elsevier or Copyright Clearance Center may deny the permissions described in this License at their sole discretion, for any reason or no reason, with a full refund payable to you. Notice of such denial will be made

using the contact information provided by you. Failure to receive such notice will not alter or invalidate the denial. In no event will Elsevier or Copyright Clearance Center be responsible or liable for any costs, expenses or damage incurred by you as a result of a denial of your permission request, other than a refund of the amount(s) paid by you to Elsevier and/or Copyright Clearance Center for denied permissions.

LIMITED LICENSE

The following terms and conditions apply only to specific license types:

15. **Translation:** This permission is granted for non-exclusive world **English** rights only unless your license was granted for translation rights. If you licensed translation rights you may only translate this content into the languages you requested. A professional translator must perform all translations and reproduce the content word for word preserving the integrity of the article.

16. **Posting licensed content on any Website:** The following terms and conditions apply as follows: Licensing material from an Elsevier journal: All content posted to the web site must maintain the copyright information line on the bottom of each image; A hyper-text must be included to the Homepage of the journal from which you are licensing at <http://www.sciencedirect.com/science/journal/xxxxx> or the Elsevier homepage for books at <http://www.elsevier.com>; Central Storage: This license does not include permission for a scanned version of the material to be stored in a central repository such as that provided by Heron/XanEdu.

Licensing material from an Elsevier book: A hyper-text link must be included to the Elsevier homepage at <http://www.elsevier.com>. All content posted to the web site must maintain the copyright information line on the bottom of each image.

Posting licensed content on Electronic reserve: In addition to the above the following clauses are applicable: The web site must be password-protected and made available only to bona fide students registered on a relevant course. This permission is granted for 1 year only. You may obtain a new license for future website posting.

17. **For journal authors:** the following clauses are applicable in addition to the above:

Preprints:

A preprint is an author's own write-up of research results and analysis, it has not been peer-reviewed, nor has it had any other value added to it by a publisher (such as formatting, copyright, technical enhancement etc.).

Authors can share their preprints anywhere at any time. Preprints should not be added to or enhanced in any way in order to appear more like, or to substitute for, the final versions of articles however authors can update their preprints on arXiv or RePEc with their Accepted Author Manuscript (see below).

If accepted for publication, we encourage authors to link from the preprint to their formal publication via its DOI.

Millions of researchers have access to the formal publications on ScienceDirect, and so links will help users to find, access, cite and use the best available version. Please note that Cell Press, The Lancet and some society-owned have different preprint policies. Information on these policies is available on the journal homepage.

Accepted Author Manuscripts: An accepted author manuscript is the manuscript of an article that has been accepted for publication and which typically includes author-incorporated changes suggested during submission, peer review and editor-author communications.

Authors can share their accepted author manuscript:

- immediately
 - via their non-commercial person homepage or blog
 - by updating a preprint in arXiv or RePEc with the accepted manuscript
 - via their research institute or institutional repository for internal institutional uses or as part of an invitation-only research collaboration work-group
 - directly by providing copies to their students or to research collaborators for their personal use
 - for private scholarly sharing as part of an invitation-only work group on commercial sites with which Elsevier has an agreement
- after the embargo period
 - via non-commercial hosting platforms such as their institutional repository
 - via commercial sites with which Elsevier has an agreement

In all cases accepted manuscripts should:

- link to the formal publication via its DOI
- bear a CC-BY-NC-ND license - this is easy to do
- if aggregated with other manuscripts, for example in a repository or other site, be shared in alignment with our hosting policy not be added to or enhanced in any way to appear more like, or to substitute for, the published journal article.

Published journal article (JPA): A published journal article (PJA) is the definitive final record of published research that appears or will appear in the journal and embodies all value-adding publishing activities including peer review co-ordination, copy-editing, formatting, (if relevant) pagination and online enrichment.

Policies for sharing publishing journal articles differ for subscription and gold open access articles:

Subscription Articles: If you are an author, please share a link to your article rather than the full-text. Millions of researchers have access to the formal publications on ScienceDirect, and so links will help your users to find, access, cite, and use the best available version.

Theses and dissertations which contain embedded PJAs as part of the formal submission can be posted publicly by the awarding institution with DOI links back to the formal publications on ScienceDirect.

If you are affiliated with a library that subscribes to ScienceDirect you have additional private sharing rights for others' research accessed under that agreement. This includes use for classroom teaching and internal training at the institution (including use in course packs and courseware programs), and inclusion of the article for grant funding purposes.

Gold Open Access Articles: May be shared according to the author-selected end-user license and should contain a [CrossMark logo](#), the end user license, and a DOI link to the formal publication on ScienceDirect.

Please refer to Elsevier's [posting policy](#) for further information.

18. **For book authors** the following clauses are applicable in addition to the above: Authors are permitted to place a brief summary of their work online only. You are not allowed to download and post the published electronic version of your chapter, nor may you scan the printed edition to create an electronic version. **Posting to a repository:** Authors are permitted to post a summary of their chapter only in their institution's repository.

19. **Thesis/Dissertation:** If your license is for use in a thesis/dissertation your thesis may be submitted to your institution in either print or electronic form. Should your thesis be published commercially, please reapply for permission. These requirements include permission for the Library and Archives of Canada to supply single copies, on demand, of the complete thesis and include permission for Proquest/UMI to supply single copies, on demand, of the complete thesis. Should your thesis be published commercially, please reapply for permission. Theses and dissertations which contain embedded PJAs as part of the formal submission can be posted publicly by the awarding institution with DOI links back to the formal publications on ScienceDirect.

Elsevier Open Access Terms and Conditions

You can publish open access with Elsevier in hundreds of open access journals or in nearly 2000 established subscription journals that support open access publishing. Permitted third party re-use of these open access articles is defined by the author's choice of Creative Commons user license. See our [open access license policy](#) for more information.

Terms & Conditions applicable to all Open Access articles published with Elsevier:

Any reuse of the article must not represent the author as endorsing the adaptation of the article nor should the article be modified in such a way as to damage the author's honour or reputation. If any changes have been made, such changes must be clearly indicated.

The author(s) must be appropriately credited and we ask that you include the end user license and a DOI link to the formal publication on ScienceDirect.

If any part of the material to be used (for example, figures) has appeared in our publication with credit or acknowledgement to another source it is the responsibility of the user to ensure their reuse complies with the terms and conditions determined by the rights holder.

Additional Terms & Conditions applicable to each Creative Commons user license:

CC BY: The CC-BY license allows users to copy, to create extracts, abstracts and new works from the Article, to alter and revise the Article and to make commercial use of the Article (including reuse and/or resale of the Article by commercial entities), provided the user gives appropriate credit (with a link to the formal publication through the relevant DOI), provides a link to the license, indicates if changes were made and the licensor is not represented as endorsing the use made of the work. The full details of the license are available at <http://creativecommons.org/licenses/by/4.0>.

CC BY NC SA: The CC BY-NC-SA license allows users to copy, to create extracts, abstracts and new works from the Article, to alter and revise the Article, provided this is not done for commercial purposes, and that the user gives appropriate credit (with a link to the formal publication through the relevant DOI), provides a link to the license, indicates if changes were made and the licensor is not represented as endorsing the use made of the work. Further, any new works must be made available on the same conditions. The full details of the license are available at <http://creativecommons.org/licenses/by-nc-sa/4.0>.

CC BY NC ND: The CC BY-NC-ND license allows users to copy and distribute the Article, provided this is not done for commercial purposes and further does not permit distribution of the Article if it is changed or edited in any way, and provided the user gives appropriate credit (with a link to the formal publication through the relevant DOI), provides a link to the license, and that the licensor is not represented as endorsing the use made of the work. The full details of the license are available at <http://creativecommons.org/licenses/by-nc-nd/4.0>. Any commercial reuse of Open Access articles published with a CC BY NC SA or CC BY NC ND license requires permission from Elsevier and will be subject to a fee.

Commercial reuse includes:

- Associating advertising with the full text of the Article
- Charging fees for document delivery or access
- Article aggregation
- Systematic distribution via e-mail lists or share buttons

Posting or linking by commercial companies for use by customers of those companies.

20. Other Conditions:

v1.8

Questions? customercare@copyright.com or +1-855-239-3415 (toll free in the US) or +1-978-646-2777.

ELSEVIER LICENSE TERMS AND CONDITIONS

Feb 09, 2016

This is an Agreement between Hiroki Matsuda ("You") and Elsevier ("Elsevier"). It consists of your order details, the terms and conditions provided by Elsevier, and the payment terms and conditions.

All payments must be made in full to CCC. For payment instructions, please see information listed at the bottom of this form.

Supplier	Elsevier Limited The Boulevard, Langford Lane Kidlington, Oxford, OX5 1GB, UK
Registered Company Number	1982084
Customer name	Hiroki Matsuda
Customer address	1-4-12, Kojirakawa-machi Yamagata-shi, Yamagata-ken 990-8560
License number	3804690752870
License date	Feb 09, 2016
Licensed content publisher	Elsevier
Licensed content publication	Nuclear Instruments and Methods in Physics Research Section A: Accelerators, Spectrometers, Detectors and Associated Equipment
Licensed content title	The large size straw drift chambers of the COMPASS experiment
Licensed content author	V.N. Bychkov, N. Dedek, W. Dünneberger, M. Faessler, H. Fischer, J. Franz, R. Geyer, Yu.V. Gousakov, A. Grünemaier, F.H. Heinsius, C. Ilgner, I.M. Ivanchenko, G.D. Kekelidze, K. Königsmann, V.V. Livinski, V.M. Lysan, J. Marzec, D.A. Matveev, S.V. Mishin et al.
Licensed content date	1 January 2006
Licensed content volume number	556
Licensed content issue number	1
Number of pages	14
Start Page	66
End Page	79
Type of Use	reuse in a thesis/dissertation
Intended publisher of new work	other
Portion	figures/tables/illustrations
Number of figures/tables/illustrations	1
Format	both print and electronic
Are you the author of this Elsevier article?	No
Will you be translating?	No
Original figure numbers	Figure 2
Title of your thesis/dissertation	Measurement of longitudinal double spin asymmetries in the single-inclusive hadron quasi-real photoproduction at high-pT by a muon beam for the study of gluon polarisation in nucleon
Expected completion date	Feb 2016
Estimated size (number	150

of pages)

Elsevier VAT number	GB 494 6272 12
Price	0 JPY
VAT/Local Sales Tax	0 JPY / 0.00 GBP
Total	0 JPY
Terms and Conditions	

INTRODUCTION

1. The publisher for this copyrighted material is Elsevier. By clicking "accept" in connection with completing this licensing transaction, you agree that the following terms and conditions apply to this transaction (along with the Billing and Payment terms and conditions established by Copyright Clearance Center, Inc. ("CCC"), at the time that you opened your Rightslink account and that are available at any time at <http://myaccount.copyright.com>).

GENERAL TERMS

2. Elsevier hereby grants you permission to reproduce the aforementioned material subject to the terms and conditions indicated.

3. Acknowledgement: If any part of the material to be used (for example, figures) has appeared in our publication with credit or acknowledgement to another source, permission must also be sought from that source. If such permission is not obtained then that material may not be included in your publication/copies. Suitable acknowledgement to the source must be made, either as a footnote or in a reference list at the end of your publication, as follows:

"Reprinted from Publication title, Vol /edition number, Author(s), Title of article / title of chapter, Pages No., Copyright (Year), with permission from Elsevier [OR APPLICABLE SOCIETY COPYRIGHT OWNER]." Also Lancet special credit - "Reprinted from The Lancet, Vol. number, Author(s), Title of article, Pages No., Copyright (Year), with permission from Elsevier."

4. Reproduction of this material is confined to the purpose and/or media for which permission is hereby given.

5. Altering/Modifying Material: Not Permitted. However figures and illustrations may be altered/adapted minimally to serve your work. Any other abbreviations, additions, deletions and/or any other alterations shall be made only with prior written authorization of Elsevier Ltd. (Please contact Elsevier at permissions@elsevier.com)

6. If the permission fee for the requested use of our material is waived in this instance, please be advised that your future requests for Elsevier materials may attract a fee.

7. Reservation of Rights: Publisher reserves all rights not specifically granted in the combination of (i) the license details provided by you and accepted in the course of this licensing transaction, (ii) these terms and conditions and (iii) CCC's Billing and Payment terms and conditions.

8. License Contingent Upon Payment: While you may exercise the rights licensed immediately upon issuance of the license at the end of the licensing process for the transaction, provided that you have disclosed complete and accurate details of your proposed use, no license is finally effective unless and until full payment is received from you (either by publisher or by CCC) as provided in CCC's Billing and Payment terms and conditions. If full payment is not received on a timely basis, then any license preliminarily granted shall be deemed automatically revoked and shall be void as if never granted. Further, in the event that you breach any of these terms and conditions or any of CCC's Billing and Payment terms and conditions, the license is automatically revoked and shall be void as if never granted. Use of materials as described in a revoked license, as well as any use of the materials beyond the scope of an unrevoked license, may constitute copyright infringement and publisher reserves the right to take any and all action to protect its copyright in the materials.

9. Warranties: Publisher makes no representations or warranties with respect to the licensed material.

10. Indemnity: You hereby indemnify and agree to hold harmless publisher and CCC, and their respective officers, directors, employees and agents, from and against any and all claims arising out of your use of the licensed material other than as specifically authorized pursuant to this license.

11. No Transfer of License: This license is personal to you and may not be sublicensed, assigned, or transferred by you to any other person without publisher's written permission.

12. No Amendment Except in Writing: This license may not be amended except in a writing signed by both parties (or, in the case of publisher, by CCC on publisher's behalf).

13. Objection to Contrary Terms: Publisher hereby objects to any terms contained in any purchase order, acknowledgment, check endorsement or other writing prepared by you, which terms are inconsistent with these terms and conditions or CCC's Billing and Payment terms and conditions. These terms and conditions, together with CCC's Billing and Payment terms and conditions (which are incorporated herein), comprise the entire agreement between you and publisher (and CCC) concerning this licensing transaction. In the event of any conflict between your obligations established by these terms and conditions and those established by CCC's Billing and Payment terms and conditions, these terms and conditions shall control.

14. Revocation: Elsevier or Copyright Clearance Center may deny the permissions described in this License at their sole discretion, for any reason or no reason, with a full refund payable to you. Notice of such denial will be made using the contact information provided by you. Failure to receive such notice will not alter or invalidate the denial. In no event will

Elsevier or Copyright Clearance Center be responsible or liable for any costs, expenses or damage incurred by you as a result of a denial of your permission request, other than a refund of the amount(s) paid by you to Elsevier and/or Copyright Clearance Center for denied permissions.

LIMITED LICENSE

The following terms and conditions apply only to specific license types:

15. **Translation:** This permission is granted for non-exclusive world **English** rights only unless your license was granted for translation rights. If you licensed translation rights you may only translate this content into the languages you requested. A professional translator must perform all translations and reproduce the content word for word preserving the integrity of the article.

16. **Posting licensed content on any Website:** The following terms and conditions apply as follows: Licensing material from an Elsevier journal: All content posted to the web site must maintain the copyright information line on the bottom of each image; A hyper-text must be included to the Homepage of the journal from which you are licensing at <http://www.sciencedirect.com/science/journal/xxxxx> or the Elsevier homepage for books at <http://www.elsevier.com>; Central Storage: This license does not include permission for a scanned version of the material to be stored in a central repository such as that provided by Heron/XanEdu.

Licensing material from an Elsevier book: A hyper-text link must be included to the Elsevier homepage at <http://www.elsevier.com>. All content posted to the web site must maintain the copyright information line on the bottom of each image.

Posting licensed content on Electronic reserve: In addition to the above the following clauses are applicable: The web site must be password-protected and made available only to bona fide students registered on a relevant course. This permission is granted for 1 year only. You may obtain a new license for future website posting.

17. **For journal authors:** the following clauses are applicable in addition to the above:

Preprints:

A preprint is an author's own write-up of research results and analysis, it has not been peer-reviewed, nor has it had any other value added to it by a publisher (such as formatting, copyright, technical enhancement etc.).

Authors can share their preprints anywhere at any time. Preprints should not be added to or enhanced in any way in order to appear more like, or to substitute for, the final versions of articles however authors can update their preprints on arXiv or RePEc with their Accepted Author Manuscript (see below).

If accepted for publication, we encourage authors to link from the preprint to their formal publication via its DOI. Millions of researchers have access to the formal publications on ScienceDirect, and so links will help users to find, access, cite and use the best available version. Please note that Cell Press, The Lancet and some society-owned have different preprint policies. Information on these policies is available on the journal homepage.

Accepted Author Manuscripts: An accepted author manuscript is the manuscript of an article that has been accepted for publication and which typically includes author-incorporated changes suggested during submission, peer review and editor-author communications.

Authors can share their accepted author manuscript:

- immediately
 - via their non-commercial person homepage or blog
 - by updating a preprint in arXiv or RePEc with the accepted manuscript
 - via their research institute or institutional repository for internal institutional uses or as part of an invitation-only research collaboration work-group
 - directly by providing copies to their students or to research collaborators for their personal use
 - for private scholarly sharing as part of an invitation-only work group on commercial sites with which Elsevier has an agreement
- after the embargo period
 - via non-commercial hosting platforms such as their institutional repository
 - via commercial sites with which Elsevier has an agreement

In all cases accepted manuscripts should:

- link to the formal publication via its DOI
- bear a CC-BY-NC-ND license - this is easy to do
- if aggregated with other manuscripts, for example in a repository or other site, be shared in alignment with our hosting policy not be added to or enhanced in any way to appear more like, or to substitute for, the published journal article.

Published journal article (JPA): A published journal article (PJA) is the definitive final record of published research that appears or will appear in the journal and embodies all value-adding publishing activities including peer review co-ordination, copy-editing, formatting, (if relevant) pagination and online enrichment.

Policies for sharing publishing journal articles differ for subscription and gold open access articles:

Subscription Articles: If you are an author, please share a link to your article rather than the full-text. Millions of researchers have access to the formal publications on ScienceDirect, and so links will help your users to find, access, cite, and use the best available version.

Theses and dissertations which contain embedded PJAs as part of the formal submission can be posted publicly by the awarding institution with DOI links back to the formal publications on ScienceDirect.

If you are affiliated with a library that subscribes to ScienceDirect you have additional private sharing rights for others' research accessed under that agreement. This includes use for classroom teaching and internal training at the institution (including use in course packs and courseware programs), and inclusion of the article for grant funding purposes.

Gold Open Access Articles: May be shared according to the author-selected end-user license and should contain a [CrossMark logo](#), the end user license, and a DOI link to the formal publication on ScienceDirect.

Please refer to Elsevier's [posting policy](#) for further information.

18. **For book authors** the following clauses are applicable in addition to the above: Authors are permitted to place a brief summary of their work online only. You are not allowed to download and post the published electronic version of your chapter, nor may you scan the printed edition to create an electronic version. **Posting to a repository:** Authors are permitted to post a summary of their chapter only in their institution's repository.

19. **Thesis/Dissertation:** If your license is for use in a thesis/dissertation your thesis may be submitted to your institution in either print or electronic form. Should your thesis be published commercially, please reapply for permission. These requirements include permission for the Library and Archives of Canada to supply single copies, on demand, of the complete thesis and include permission for Proquest/UMI to supply single copies, on demand, of the complete thesis. Should your thesis be published commercially, please reapply for permission. Theses and dissertations which contain embedded PJAs as part of the formal submission can be posted publicly by the awarding institution with DOI links back to the formal publications on ScienceDirect.

Elsevier Open Access Terms and Conditions

You can publish open access with Elsevier in hundreds of open access journals or in nearly 2000 established subscription journals that support open access publishing. Permitted third party re-use of these open access articles is defined by the author's choice of Creative Commons user license. See our [open access license policy](#) for more information.

Terms & Conditions applicable to all Open Access articles published with Elsevier:

Any reuse of the article must not represent the author as endorsing the adaptation of the article nor should the article be modified in such a way as to damage the author's honour or reputation. If any changes have been made, such changes must be clearly indicated.

The author(s) must be appropriately credited and we ask that you include the end user license and a DOI link to the formal publication on ScienceDirect.

If any part of the material to be used (for example, figures) has appeared in our publication with credit or acknowledgement to another source it is the responsibility of the user to ensure their reuse complies with the terms and conditions determined by the rights holder.

Additional Terms & Conditions applicable to each Creative Commons user license:

CC BY: The CC-BY license allows users to copy, to create extracts, abstracts and new works from the Article, to alter and revise the Article and to make commercial use of the Article (including reuse and/or resale of the Article by commercial entities), provided the user gives appropriate credit (with a link to the formal publication through the relevant DOI), provides a link to the license, indicates if changes were made and the licensor is not represented as endorsing the use made of the work. The full details of the license are available at <http://creativecommons.org/licenses/by/4.0>.

CC BY NC SA: The CC BY-NC-SA license allows users to copy, to create extracts, abstracts and new works from the Article, to alter and revise the Article, provided this is not done for commercial purposes, and that the user gives appropriate credit (with a link to the formal publication through the relevant DOI), provides a link to the license, indicates if changes were made and the licensor is not represented as endorsing the use made of the work. Further, any new works must be made available on the same conditions. The full details of the license are available at <http://creativecommons.org/licenses/by-nc-sa/4.0>.

CC BY NC ND: The CC BY-NC-ND license allows users to copy and distribute the Article, provided this is not done for commercial purposes and further does not permit distribution of the Article if it is changed or edited in any way, and provided the user gives appropriate credit (with a link to the formal publication through the relevant DOI), provides a link to the license, and that the licensor is not represented as endorsing the use made of the work. The full details of the license are available at <http://creativecommons.org/licenses/by-nc-nd/4.0>. Any commercial reuse of Open Access articles published with a CC BY NC SA or CC BY NC ND license requires permission from Elsevier and will be subject to a fee.

Commercial reuse includes:

- Associating advertising with the full text of the Article
- Charging fees for document delivery or access
- Article aggregation

- Systematic distribution via e-mail lists or share buttons

Posting or linking by commercial companies for use by customers of those companies.

20. **Other Conditions:**

v1.8

Questions? customercare@copyright.com or +1-855-239-3415 (toll free in the US) or +1-978-646-2777.

ELSEVIER LICENSE TERMS AND CONDITIONS

Feb 09, 2016

This is an Agreement between Hiroki Matsuda ("You") and Elsevier ("Elsevier"). It consists of your order details, the terms and conditions provided by Elsevier, and the payment terms and conditions.

All payments must be made in full to CCC. For payment instructions, please see information listed at the bottom of this form.

Supplier	Elsevier Limited The Boulevard,Langford Lane Kidlington,Oxford,OX5 1GB,UK
Registered Company Number	1982084
Customer name	Hiroki Matsuda
Customer address	1-4-12, Kojirakawa-machi Yamagata-shi, Yamagata-ken 990-8560
License number	3804731045333
License date	Feb 09, 2016
Licensed content publisher	Elsevier
Licensed content publication	Nuclear Instruments and Methods in Physics Research Section A: Accelerators, Spectrometers, Detectors and Associated Equipment
Licensed content title	First results of the large COMPASS 6LiD polarized target
Licensed content author	J Ball,G Baum,P Berglund,I Daito,N Doshita,F Gautheron,St Goertz,J Harmsen,T Hasegawa,J Heckmann,N Horikawa,T Iwata,Yu Kisselev,J Koivuniemi,K Kondo,J.M Le Goff,A Magnon,A Meier,W Meyer,E Radtke,G Reicherz,N Takabayashi
Licensed content date	11 February 2003
Licensed content volume number	498
Licensed content issue number	1-3
Number of pages	11
Start Page	101
End Page	111
Type of Use	reuse in a thesis/dissertation
Portion	figures/tables/illustrations
Number of figures/tables /illustrations	1
Format	both print and electronic
Are you the author of this Elsevier article?	No
Will you be translating?	No
Original figure numbers	Figure 1
Title of your thesis/dissertation	Measurement of longitudinal double spin asymmetries in the single-inclusive hadron quasi-real photoproduction at high-pT by a muon beam for the study of gluon polarisation in nucleon
Expected completion date	Feb 2016
Estimated size (number of pages)	150
Elsevier VAT number	GB 494 6272 12

Price	0 JPY
VAT/Local Sales Tax	0 JPY / 0.00 GBP
Total	0 JPY
Terms and Conditions	

INTRODUCTION

1. The publisher for this copyrighted material is Elsevier. By clicking "accept" in connection with completing this licensing transaction, you agree that the following terms and conditions apply to this transaction (along with the Billing and Payment terms and conditions established by Copyright Clearance Center, Inc. ("CCC"), at the time that you opened your Rightslink account and that are available at any time at <http://myaccount.copyright.com>).

GENERAL TERMS

2. Elsevier hereby grants you permission to reproduce the aforementioned material subject to the terms and conditions indicated.
3. Acknowledgement: If any part of the material to be used (for example, figures) has appeared in our publication with credit or acknowledgement to another source, permission must also be sought from that source. If such permission is not obtained then that material may not be included in your publication/copies. Suitable acknowledgement to the source must be made, either as a footnote or in a reference list at the end of your publication, as follows:
"Reprinted from Publication title, Vol /edition number, Author(s), Title of article / title of chapter, Pages No., Copyright (Year), with permission from Elsevier [OR APPLICABLE SOCIETY COPYRIGHT OWNER]." Also Lancet special credit - "Reprinted from The Lancet, Vol. number, Author(s), Title of article, Pages No., Copyright (Year), with permission from Elsevier."
4. Reproduction of this material is confined to the purpose and/or media for which permission is hereby given.
5. Altering/Modifying Material: Not Permitted. However figures and illustrations may be altered/adapted minimally to serve your work. Any other abbreviations, additions, deletions and/or any other alterations shall be made only with prior written authorization of Elsevier Ltd. (Please contact Elsevier at permissions@elsevier.com)
6. If the permission fee for the requested use of our material is waived in this instance, please be advised that your future requests for Elsevier materials may attract a fee.
7. Reservation of Rights: Publisher reserves all rights not specifically granted in the combination of (i) the license details provided by you and accepted in the course of this licensing transaction, (ii) these terms and conditions and (iii) CCC's Billing and Payment terms and conditions.
8. License Contingent Upon Payment: While you may exercise the rights licensed immediately upon issuance of the license at the end of the licensing process for the transaction, provided that you have disclosed complete and accurate details of your proposed use, no license is finally effective unless and until full payment is received from you (either by publisher or by CCC) as provided in CCC's Billing and Payment terms and conditions. If full payment is not received on a timely basis, then any license preliminarily granted shall be deemed automatically revoked and shall be void as if never granted. Further, in the event that you breach any of these terms and conditions or any of CCC's Billing and Payment terms and conditions, the license is automatically revoked and shall be void as if never granted. Use of materials as described in a revoked license, as well as any use of the materials beyond the scope of an unrevoked license, may constitute copyright infringement and publisher reserves the right to take any and all action to protect its copyright in the materials.
9. Warranties: Publisher makes no representations or warranties with respect to the licensed material.
10. Indemnity: You hereby indemnify and agree to hold harmless publisher and CCC, and their respective officers, directors, employees and agents, from and against any and all claims arising out of your use of the licensed material other than as specifically authorized pursuant to this license.
11. No Transfer of License: This license is personal to you and may not be sublicensed, assigned, or transferred by you to any other person without publisher's written permission.
12. No Amendment Except in Writing: This license may not be amended except in a writing signed by both parties (or, in the case of publisher, by CCC on publisher's behalf).
13. Objection to Contrary Terms: Publisher hereby objects to any terms contained in any purchase order, acknowledgment, check endorsement or other writing prepared by you, which terms are inconsistent with these terms and conditions or CCC's Billing and Payment terms and conditions. These terms and conditions, together with CCC's Billing and Payment terms and conditions (which are incorporated herein), comprise the entire agreement between you and publisher (and CCC) concerning this licensing transaction. In the event of any conflict between your obligations established by these terms and conditions and those established by CCC's Billing and Payment terms and conditions, these terms and conditions shall control.
14. Revocation: Elsevier or Copyright Clearance Center may deny the permissions described in this License at their sole discretion, for any reason or no reason, with a full refund payable to you. Notice of such denial will be made using the contact information provided by you. Failure to receive such notice will not alter or invalidate the denial. In no event will Elsevier or Copyright Clearance Center be responsible or liable for any costs, expenses or damage incurred by you as a result of a denial of your permission request, other than a refund of the amount(s) paid by you to Elsevier and/or Copyright Clearance Center for denied permissions.

LIMITED LICENSE

The following terms and conditions apply only to specific license types:

15. **Translation:** This permission is granted for non-exclusive world **English** rights only unless your license was granted for translation rights. If you licensed translation rights you may only translate this content into the languages you requested. A professional translator must perform all translations and reproduce the content word for word preserving the integrity of the article.

16. **Posting licensed content on any Website:** The following terms and conditions apply as follows: Licensing material from an Elsevier journal: All content posted to the web site must maintain the copyright information line on the bottom of each image; A hyper-text must be included to the Homepage of the journal from which you are licensing at <http://www.sciencedirect.com/science/journal/xxxxx> or the Elsevier homepage for books at <http://www.elsevier.com>; Central Storage: This license does not include permission for a scanned version of the material to be stored in a central repository such as that provided by Heron/XanEdu.

Licensing material from an Elsevier book: A hyper-text link must be included to the Elsevier homepage at <http://www.elsevier.com>. All content posted to the web site must maintain the copyright information line on the bottom of each image.

Posting licensed content on Electronic reserve: In addition to the above the following clauses are applicable: The web site must be password-protected and made available only to bona fide students registered on a relevant course. This permission is granted for 1 year only. You may obtain a new license for future website posting.

17. **For journal authors:** the following clauses are applicable in addition to the above:

Preprints:

A preprint is an author's own write-up of research results and analysis, it has not been peer-reviewed, nor has it had any other value added to it by a publisher (such as formatting, copyright, technical enhancement etc.).

Authors can share their preprints anywhere at any time. Preprints should not be added to or enhanced in any way in order to appear more like, or to substitute for, the final versions of articles however authors can update their preprints on arXiv or RePEc with their Accepted Author Manuscript (see below).

If accepted for publication, we encourage authors to link from the preprint to their formal publication via its DOI.

Millions of researchers have access to the formal publications on ScienceDirect, and so links will help users to find, access, cite and use the best available version. Please note that Cell Press, The Lancet and some society-owned have different preprint policies. Information on these policies is available on the journal homepage.

Accepted Author Manuscripts: An accepted author manuscript is the manuscript of an article that has been accepted for publication and which typically includes author-incorporated changes suggested during submission, peer review and editor-author communications.

Authors can share their accepted author manuscript:

- immediately
 - via their non-commercial person homepage or blog
 - by updating a preprint in arXiv or RePEc with the accepted manuscript
 - via their research institute or institutional repository for internal institutional uses or as part of an invitation-only research collaboration work-group
 - directly by providing copies to their students or to research collaborators for their personal use
 - for private scholarly sharing as part of an invitation-only work group on commercial sites with which Elsevier has an agreement
- after the embargo period
 - via non-commercial hosting platforms such as their institutional repository
 - via commercial sites with which Elsevier has an agreement

In all cases accepted manuscripts should:

- link to the formal publication via its DOI
- bear a CC-BY-NC-ND license - this is easy to do
- if aggregated with other manuscripts, for example in a repository or other site, be shared in alignment with our hosting policy not be added to or enhanced in any way to appear more like, or to substitute for, the published journal article.

Published journal article (JPA): A published journal article (PJA) is the definitive final record of published research that appears or will appear in the journal and embodies all value-adding publishing activities including peer review co-ordination, copy-editing, formatting, (if relevant) pagination and online enrichment.

Policies for sharing publishing journal articles differ for subscription and gold open access articles:

Subscription Articles: If you are an author, please share a link to your article rather than the full-text. Millions of researchers have access to the formal publications on ScienceDirect, and so links will help your users to find, access, cite, and use the best available version.

Theses and dissertations which contain embedded PJAs as part of the formal submission can be posted publicly by the awarding institution with DOI links back to the formal publications on ScienceDirect.

If you are affiliated with a library that subscribes to ScienceDirect you have additional private sharing rights for others' research accessed under that agreement. This includes use for classroom teaching and internal training at the institution (including use in course packs and courseware programs), and inclusion of the article for grant funding purposes.

Gold Open Access Articles: May be shared according to the author-selected end-user license and should contain a [CrossMark logo](#), the end user license, and a DOI link to the formal publication on ScienceDirect.

Please refer to Elsevier's [posting policy](#) for further information.

18. **For book authors** the following clauses are applicable in addition to the above: Authors are permitted to place a brief summary of their work online only. You are not allowed to download and post the published electronic version of your chapter, nor may you scan the printed edition to create an electronic version. **Posting to a repository:** Authors are permitted to post a summary of their chapter only in their institution's repository.

19. **Thesis/Dissertation:** If your license is for use in a thesis/dissertation your thesis may be submitted to your institution in either print or electronic form. Should your thesis be published commercially, please reapply for permission. These requirements include permission for the Library and Archives of Canada to supply single copies, on demand, of the complete thesis and include permission for Proquest/UMI to supply single copies, on demand, of the complete thesis. Should your thesis be published commercially, please reapply for permission. Theses and dissertations which contain embedded PJAs as part of the formal submission can be posted publicly by the awarding institution with DOI links back to the formal publications on ScienceDirect.

Elsevier Open Access Terms and Conditions

You can publish open access with Elsevier in hundreds of open access journals or in nearly 2000 established subscription journals that support open access publishing. Permitted third party re-use of these open access articles is defined by the author's choice of Creative Commons user license. See our [open access license policy](#) for more information.

Terms & Conditions applicable to all Open Access articles published with Elsevier:

Any reuse of the article must not represent the author as endorsing the adaptation of the article nor should the article be modified in such a way as to damage the author's honour or reputation. If any changes have been made, such changes must be clearly indicated.

The author(s) must be appropriately credited and we ask that you include the end user license and a DOI link to the formal publication on ScienceDirect.

If any part of the material to be used (for example, figures) has appeared in our publication with credit or acknowledgement to another source it is the responsibility of the user to ensure their reuse complies with the terms and conditions determined by the rights holder.

Additional Terms & Conditions applicable to each Creative Commons user license:

CC BY: The CC-BY license allows users to copy, to create extracts, abstracts and new works from the Article, to alter and revise the Article and to make commercial use of the Article (including reuse and/or resale of the Article by commercial entities), provided the user gives appropriate credit (with a link to the formal publication through the relevant DOI), provides a link to the license, indicates if changes were made and the licensor is not represented as endorsing the use made of the work. The full details of the license are available at <http://creativecommons.org/licenses/by/4.0>.

CC BY NC SA: The CC BY-NC-SA license allows users to copy, to create extracts, abstracts and new works from the Article, to alter and revise the Article, provided this is not done for commercial purposes, and that the user gives appropriate credit (with a link to the formal publication through the relevant DOI), provides a link to the license, indicates if changes were made and the licensor is not represented as endorsing the use made of the work. Further, any new works must be made available on the same conditions. The full details of the license are available at <http://creativecommons.org/licenses/by-nc-sa/4.0>.

CC BY NC ND: The CC BY-NC-ND license allows users to copy and distribute the Article, provided this is not done for commercial purposes and further does not permit distribution of the Article if it is changed or edited in any way, and provided the user gives appropriate credit (with a link to the formal publication through the relevant DOI), provides a link to the license, and that the licensor is not represented as endorsing the use made of the work. The full details of the license are available at <http://creativecommons.org/licenses/by-nc-nd/4.0>. Any commercial reuse of Open Access articles published with a CC BY NC SA or CC BY NC ND license requires permission from Elsevier and will be subject to a fee.

Commercial reuse includes:

- Associating advertising with the full text of the Article
- Charging fees for document delivery or access
- Article aggregation
- Systematic distribution via e-mail lists or share buttons

Posting or linking by commercial companies for use by customers of those companies.

20. Other Conditions:

v1.8

Questions? customer care@copyright.com or +1-855-239-3415 (toll free in the US) or +1-978-646-2777.
